UNIVERSITY OF SOUTHAMPTON

FACULTY OF ENGINEERING AND APPLIED SCIENCE
MECHANICAL ENGINEERING DEPARTMENT

"NUMERICAL METHODS FOR STRESS ANALYSIS USING KNOWN ELASTICITY SOLUTIONS"

by

A.R. Carmichael

Being a thesis submitted for the degree of
Doctor of Philosophy

April 1983

To Sarah

CONTENTS

	Page
ABSTRACT	iv.
ACKNOWLEDGEMENTS	v.
NOTATION: (Part I)	vi.
(Part II)	x.
LIST OF FIGURES	xiv.
LIST OF TABLES	xvi.
CHAPTER 1. GENERAL INTRODUCTION	
1.1 Background to the work	1
1.2 Review of theoretical methods and solutions	4
1.2.1 Exact analytical methods	4
1.2.2 Approximate analytical methods	5
1.2.3 Numerical methods	7
1.3 Layout of thesis	11
PART I Finite Element Superposition Method	
CHAPTER 2. FINITE ELEMENT FORMULATION	
2.1 Introduction	13
2.2 Notation for the boundaries	14
2.3 Displacement and stress fields	16
2.4 The variational principle	19
2.5 Determination of correction stress field $\underline{\sigma}_i^c$	22
2.6 Determination of the nodal displacements $\underline{q}_i^F$	24
2.7 Determination of the trial function coefficients	26
2.8 Determination of the stress at any point	29
2.9 Summary	30
CHAPTER 3. TRIAL FUNCTIONS AND LOADING FUNCTION	
3.1 Introduction	31
3.2 Trial functions for elliptical holes	31

Page

3.3 Trial functions for circular holes 33

3.4 Loading function for circular holes 39

CHAPTER 4. IMPLEMENTATION OF FINITE ELEMENT METHOD

4.1 Introduction 42

4.2 Structure of Program 42

4.2.1 Data input 44
4.2.2 Areas of elements 44
4.2.3 Stiffness matrix 45
4.2.4 Trial and loading functions 45
4.2.5 Stress fields $\underline{\sigma}^{\dagger}_{1}$ 45
4.2.6 Boundary conditions 46
4.2.7 Strain energy term 46
4.2.8 Correction to matrix $\underline{D}_{s}$ 46
4.2.9 Solution of the equations 48
4.2.10 Trial function coefficients 48
4.2.11 Displacements and stresses 48

4.3 Using the Program 48

CHAPTER 5. FINITE ELEMENT RESULTS

5.1 Introduction 50

5.2 Rectangular plate with central traction-free hole 51

5.2.1 Effect of mesh refinement 53
5.2.2 Effect of hole size 54
5.2.3 Effect of hole aspect ratio 56
5.2.4 Effect of special region size and additional trial functions 60
5.2.5 Effect of local mesh refinement 67

5.3 Square plate with central traction-free hole 69

5.3.1 Circular hole 69
5.3.2 Elliptical hole 72

5.4 Configurations with loaded circular holes 76

5.4.1 Various loadings on a circular hole 77
5.4.2 Pressurized hole in annulus or large plate 92
5.4.3 Symmetrical rectangular lug 93
5.4.4 Rectangular lugs 98

PART II Modified Boundary Element Method

CHAPTER 6. BOUNDARY ELEMENT FORMULATION

6.1 Introduction 105

6.2 Notation 107

Page

6.3 Basis of the boundary element method 109
6.4 Discretization of the equations 111
6.5 Solution of the equations 113
6.6 Interior points 113
6.7 Modified kernel function 115
6.8 Implementation 117

CHAPTER 7. BOUNDARY ELEMENT RESULTS

7.1 Configurations analysed 119
7.2 Comparison between modified and standard kernel functions 120
7.3 Annuli with various sizes of hole 123
7.4 Square plates with various sizes of hole 125

* * *

CHAPTER 8. GENERAL CONCLUSIONS

8.1 The finite element superposition method 128
8.2 The modified boundary element method 131
8.3 Comparison of the methods 132
8.4 Future work 133

REFERENCES 136

APPENDIX A. Derivation of the variational principle 154

APPENDIX B. Listings of selected program segments (FESM) 157

APPENDIX C. Data preparation for finite element program 174

APPENDIX D. Running the finite element program 181

APPENDIX E. Finite element meshes 196

APPENDIX F. Modified fundamental solution 202

APPENDIX G. Running the boundary element program 205

UNIVERSITY OF SOUTHAMPTON

ABSTRACT

FACULTY OF ENGINEERING AND APPLIED SCIENCE

MECHANICAL ENGINEERING

Doctor of Philosophy

NUMERICAL METHODS FOR STRESS ANALYSIS USING KNOWN ELASTICITY SOLUTIONS

by Andrew Robert Carmichael

Two methods for the determination of the stress concentration near holes in two dimensional elastic components are developed. One, which is based on the finite element method extends a superposition technique originally developed for crack problems; the other uses the boundary element method. Both methods involve using analytical solutions which satisfy conditions on the hole boundary exactly thereby reducing or, in the case of boundary elements avoiding entirely, the need for elements modelling the hole.

The first method uses a modified complementary energy functional to determine the coefficients of the superimposed functions and the finite element nodal displacements, from which the estimates of stress are obtained. Tractions on the hole boundary are represented accurately using Fourier series, and the formulation is modified by the inclusion of a "loading function" which is the solution for an infinite region containing the hole under the specified loading. Representing the tractions on the hole in this way avoids inaccuracies due to approximate modelling of the load, for example as point forces, close to the point where the stress concentration factor is required. The loading function is incorporated into the formulation without requiring numerical integration of the tractions over the curved boundary of the hole. Accuracy of the method for use on traction-free circular or elliptical holes and loaded circular holes is systematically examined. For quite coarse finite element meshes (typically 70 degrees of freedom with four-fold symmetry) 3% accuracy or better may be expected, an improvement by a factor of between 5 and 10 over conventional elements. The effect on accuracy of such parameters as the mesh refinement, the size and shape of the hole and outer boundaries, the extent of the region of superposition and the type of loading is investigated. Fourier series are derived for different distributions of tractions occurring at a hole boundary due to a pin-load, and these are used to determine stress concentration factors for rectangular lugs of various dimensions.

The formulation of the boundary element method for plane elastic problems is presented and is modified by introducing a kernel function which satisfies the traction-free conditions on a hole boundary. It is shown that with this formulation no elements are required to model the hole, thus stresses at or near the hole may be evaluated without being affected by the proximity of elements on this boundary. Results for externally pressurized annuli and square plates with circular holes are obtained with the method, which show a marked improvement in accuracy over the boundary element method with an unmodified kernel function. From these results it appears that the constant shape function of the elements is a limitation for the application of the method to more general configurations and higher order elements are recommnded.

ACKNOWLEDGEMENTS

The author wishes to acknolwedge the receipt of support by MOD(PE) under Agreement No. 2040/0202 STR. The assistance given by members of the Royal Aircraft Establishment (RAE), Farnborough, during the course of the work is gratefully acknowledged. In particular the author wishes to thank Dr P. Bartholomew of the Structures Department RAE for his valuable assistance and cooperation with parts of the finite element work, and Mr D.P. Rooke of the Materials Department RAE and members of the Sub-department Engineering Materials and the Mechanical Engineering Department at the University of Southampton for many useful discussions and suggestions. Thanks are also due to Jan Ward for her care in typing the manuscript and to Michelle Smith for her help with some of the figures.

Above all my sincere gratitude and thanks goes to Dr D.J. Cartwright for the guidance and encouragement he has given as my supervisor in this work. It has been most appreciated.

NOTATION

Notation for PART I (including Appendix A)

The following symbols are used to represent vectors of the type shown:

$\underline{\sigma}$	stress
$\underline{\epsilon}$	strain
$\underline{T}$	tractions
$\underline{u}$	displacements
$\underline{p}$	nodal loads
$\underline{q}$	nodal displacements

The following superscripts specify the particular field:

*	trial functions derived from exact elasticity solutions
†	an approximation to the trial function fields having linear displacements between nodes
^{F}	finite element field
$^-$	(bar) prescribed quantities on boundaries
$^\sim$	(tilde) displacement field defined on element boundaries
^{I}	stress field defined in the interior of elements
^{c}	additional stresses, constant within elements, arising from compatibility constraints
(1),(2)or(3)	associated with a particular node
a or b	referring to an element denoted a or b

The following subscripts may also be used:

0,1,2...i,j	associated with the particular trial function or, if equal to zero, the loading function
N	associated with the N'th element

Components of the above vectors are not underlined and may have the following additional subscripts:

X,Y	Cartesian coordinates referred to global axes
x,y	Cartesian coordinates referred to trial function axes
r,θ	Polar coordinates referred to trial function axes
n,s	directions normal and tangential to boundary

Boundaries are denoted by S with the following subscripts:

none	complete boundary
K	kinematic boundary (displacements specified)
T	traction boundary
R	interface boundary between the external and special regions
E	inter-element boundary
N	complete boundary of N'th element

The boundaries may be further specified by the following qualifiers:

'	(prime) denotes that part of the boundary adjacent to the special region
N	(subscript) denotes that part of the boundary adjacent to the N'th element
e	(superscript) denotes that part of the boundary adjacent to the external region only

Other symbols:

a	radius of circular holes or semi-major axis length of elliptical hole
a_n, a'_n	arbitrary constants in Airy stress function
$\underline{A}$	strain/stress compliance matrix
A_n	coefficients of Fourier series specifying the normal tractions on the hole
b	semi-minor axis length of elliptical hole
b_n, b'_n	arbitrary constants in Airy stress function
$\underline{B}_N$	element strain matrix for N'th element
$\underline{\bar{B}}_{(n)}$	submatrix of $\underline{B}_N$ where n = 1, 2 or 3
c	arbitrary constant
c_n, c'_n	arbitrary constants in Airy stress function
$\underline{C}_i$	matrix defined by equation (2.21)
$\underline{D}$	matrix of coefficients of $\underline{\alpha}$ in equation (2.45)
d_{ij}	element of the matrix $\underline{D}$
$\underline{D}'$	matrix of coefficients in equation (2.44)
d'_{ij}	element of the matrix $\underline{D}'$
$\underline{D}_S$	matrix of coefficients arising from integral on S'
d^S_{ij}	element of the matrix $\underline{D}_S$

D_n	coefficients of Fourier series specifying the shear tractions on the hole
d_n, d'_n	arbitrary constants in Airy stress function
e	exponential constant
E	Young's modulus of elasticity
$\underline{F}$	vector of right-hand sides in equation (2.45)
f_i	element of the vector $\underline{F}$
$\underline{F}'$	vector of coefficients in equation (2.44)
f'_i	element of the vector $\underline{F}'$
G	shear modulus
i	$\sqrt{-1}$
i	integer specifying number of trial function
j	integer specifying number of trial function
k	total number of trial functions
K_t	stress concentration factor
K_∞	stress concentration factor in infinite region
$\underline{K}$	finite element stiffness matrix
ℓ	half length of symmetrical plate
ℓ_1	distance from centre of hole to top of lug
ℓ_2	distance from centre of hole to bottom of lug
$\underline{L}$	traction/stress matrix
L_n, K_n	constants defined by equations (3.23) and (3.26)
m	limit of Fourier series in Φ_A (equal to k/2)
m_1	limit of Fourier series defining normal tractions on hole
m_2	limit of Fourier series defining tangential tractions on hole
m_3	limit of Fourier series equal to the maximum of m_1 and m_2
n	integer (or integer subscript)
N	element number
N_o	mesh size parameter
O	origin of global coordinates
O'	origin of trial function coordinates
$\underline{p}$	nodal loads (see above)
P	magnitude of resultant force on the hole
P_s	magnitude of resultant force due to shear tractions on the hole
p_o	internal pressure on annulus
$\underline{q}$	nodal displacements (see above)
Q	parameter defined as K_t/K_∞

r	radial polar coordinate
R	$= \frac{a+b}{2}$ for an elliptical hole
R_A	ratio of special region area to area of hole
s	distance along an element side measured from node (1)
s_o	length of element side
S	boundary of region (see above)
t	thickness of finite elements in the special region
$\underline{T}$	tractions (see above)
$\underline{u}$	displacements (see above)
U	strain energy function
$U_{Sp.R}$	strain energy function evaluated in the special region
V	complete region
w	half width of plate
X,Y	Cartesian coordinates referred to global axes
x,y	Cartesian coordinates referred to trial function axes
z	complex number = x + i y
α_i	coefficient of trial function or, if i=0, of the loading function
$\underline{\alpha}$	vector of trial function coefficients α_i (i=1 to k)
$\underline{\alpha}'$	vector of coefficients α_i (i=0 to k)
β	half angle subtended by arc of pressure
γ	angle between OX and O'x axes
γ	shear strain component (see above for qualifiers)
δ_o	typical linear dimension of elements near hole
Δ	area of triangular element
$\underline{\varepsilon}$	strain vector (see above)
ε_{ref}	percentage difference term for comparing two values of maximum stress see equation (5.1) for definition
ζ	complex function of z
θ	angular polar coordinate
Θ	arbitrary angle
κ	$= \frac{3-\nu}{1+\nu}$ (for plane stress)
$\underline{\lambda}$	Lagrange multiplier
μ	$= \frac{a-b}{a+b}$ for an elliptical hole
ν	Poisson's ratio
ξ	complex function of z
π	pi $\simeq$ 3.1415927
Π	functional (complementary energy)
Π_c	modified functional
$\underline{\sigma}$	stress (see above)

σ_o	nominal applied stress
σ_{max}	maximum tensile stress
σ_{com}	maximum compressive stress
σ_{ref}	value of stress for comparison
τ	shear stress component (see above for qualifiers)
ϕ	angle between X axis and outward normal to boundary
ϕ_i	complex stress function for trial function
Φ_A	Airy stress function
ψ_i	complex stress function for trial function
∞	infinity

Other notation:

log	natural logarithm
Im	denotes imaginary part of complex number
Re	denotes real part of complex number
$\bar{}$	(bar) unless referred to above denotes complex conjugate
$'$	(prime) } unless referred to above denotes
$''$	(double prime) } differentiation
$\delta\{\ \}$	denotes the variation of a functional
$\sum$	denotes summation
$\propto$	denotes proportional to
$(\ )^T$	denotes the transpose of a vector
$\underline{\ }$	underlined symbols denote vectors or matrices

Notation for PART II (including Appendix F)

In Part II tensor notation is used whereby subscripts - for example i, j or k - denote the direction of components. The following tensor variables are used:

b_i	body force
ℓ_i	cosine of the angle between the boundary normal and i coordinate axis
T_i	traction
u_i	displacement
x_i	position of the point force in kernel function

ε_{ij}	strain
σ_{ij}	stress
ξ_i	position of the point at which the kernel function is evaluated

Tensors referring to the kernel function are denoted by the superscript * and have an additional subscript (before other subscripts) which indicates the direction of the point force.

A subscript preceded by a comma (e.g. $u_{i,j}$) means partial differentiation with respect to the coordinate component x_j. A repeated suffix implies summation.

The following superscripts may also be used:

K	corresponding to the Kelvin solution
c	complementary part of the kernel function (added to Kelvin solution yields the kernel function)
m or n	pertaining to the m'th or n'th node or element
P	pertaining to an internal point

Boundaries are denoted by S with the following qualifiers:

none	complete boundary of the problem
n	(subscript) n'th boundary element
*	(superscript) boundary included in the kernel function
H	(subscript) part of the boundary of the problem coinciding with S*
'	(prime) remainder of the boundary of the problem

Other symbols:

a	radius of circular hole
b_i	(see above)
$\underline{A}$	matrix of the coefficients of the unknown tractions or displacements
$c_{k\ell}$	coefficient of displacement in Somigliana's identity (6.17). A superscript may denote the coefficient for a particular element.
$D_{\ell ij}$	(italic) function defined by equation (6.32)
E	Young's modulus of elasticity

f	arbitrary function
$\underline{F}$	vector of right-hand sides in the simultaneous equations
$g_{k\ell mn}$	coefficient of the tractions defined by equation (6.24)
G	shear modulus
$\underline{G}$	matrix of the traction coefficients
$h_{k\ell mn}$	coefficient of the displacements defined by equations (6.22) and (6.23)
$\underline{H}$	matrix of the displacement coefficients
i	$\sqrt{-1}$
i,j,k,ℓ	integers defining coordinate directions
K	number of dimensions of the problem (2 or 3)
K_t	stress concentration factor
L	complex number = $\ell_1 + i\ell_2$
ℓ_i	(see above)
m	element (or node) number
n	node (or element) number
N	number of elements and nodes
r	radial polar coordinate
S	boundary (see above)
$S_{\ell ij}$	(italic) function defined by equation (6.33)
T_i	(see above)
V	region of the problem
u_i	(see above)
w	radius of annulus or half width of square plate
x_i	(see above)
z	complex number defining position of point in plane (= $\xi_1 + i\xi_2$)
z_o	complex number defining position of the point force (= $x_1 + ix_2$)
δ_{ij}	Kronecker delta. See equation (6.5)
$\delta(x-\xi)$	Dirac delta function. See equations (6.13)-(6.15)
ε_{ij}	(see above)
ε_{ref}	percentage difference term for comparing two values of stress. See equation (5.1) for definition
θ	angular polar coordinate
κ	$= \frac{3-\nu}{1+\nu}$ (for plane stress) $= 3-4\nu$ (for plane strain)
ν	Poisson's ratio
λ	Lamé constant given by equation (6.3)
λ'	equivalent constant for plane stress applications see equation (6.8)

ξ_i	(see above)
π	pi $\simeq$ 3.1415927
σ_{ij}	(see above)
σ_o	externally applied stress
σ_r, σ_θ	radial and tangential components of stress
χ_k	complex number = $\delta_{1k} + i\delta_{2k}$
ϕ_k, ψ_k	complex potential for the kernel function with the point force in the k direction
∞	infinity

Other notation:

ℓn	natural logarithm
Im	denotes imaginary part of complex number
Re	denotes real part of complex number
-	(bar) denotes complex conjugate
'	(prime)
''	(double prime) — unless referred to above denotes differentiation with respect to z
$\sum$	denotes summation
$,j$	(subscript) denotes partial differentiation with respect to x_j
ϵ	denotes "is included in..."
$\int_V \{\}dV(\xi)$	denotes integration over V with respect to the variable ξ
$\underline{\ }$	underlined symbols denote matrices

LIST OF FIGURES

Figure		Page
2.1	Two dimensional body with loaded hole	15
2.2	Two dimensional body showing special region	15
4.1	Structure of the FESM program	43
4.2	Areas of element on hole boundary	44
4.3	Boundary conditions subroutine	47
5.1	Rectangular plate with a central elliptical (or circular) hole	52
5.2	Effect of mesh refinement on the accuracy of the stress concentration factor	55
5.3	Effect of hole size on the accuracy of the stress concentration factor	57
5.4	Effect of hole aspect ratio on the accuracy of the stress concentration factor	59
5.5	Effect of special region size on accuracy for mesh A	65
5.6	Effect of special region size on accuracy for mesh B	66
5.7	Square plate with circular hole	69
5.8	Stress concentration results for square plate with elliptical holes of varying aspect ratios	74
5.9	Stress concentration results for square plate with elliptical holes of varying size	75
5.10	Use of a superposition principle to derive the stress concentration factor for the loaded lug (ii) from the configuration (i)	78
5.11	Stresses around boundary of hole in infinite sheet. Loading a) Pressure $\propto[\cos\theta+1]\ (-\pi<\theta\leqslant\pi)$	79
5.12	Stresses around boundary of hole in infinite sheet. Loading b) Pressure $\propto \cos\theta\ (-\pi/2\leqslant\theta\leqslant\pi/2)$	81
5.13	Stresses around boundary of hole in infinite sheet. Loading c) Pressure $\propto \cos^2\theta\ (-\pi/2\leqslant\theta\leqslant\pi/2)$	82
5.14	Stresses around boundary of hole in infinite sheet. Loading d) Constant pressure over ½ of the boundary $(-\pi/2\leqslant\theta\leqslant\pi/2)$	83
5.15	Stresses around boundary of hole in infinite sheet. Loading d) Constant pressure over 1/6 of the boundary $(-\pi/6\leqslant\theta\leqslant\pi/6)$	83
5.16	Stresses around boundary of hole in infinite sheet. Loading e) Constant pressure $(-\pi<\theta\leqslant\pi)$	84
5.17	Stresses around boundary of hole in infinite sheet. Loading f) Pressure $\propto \cos^2\theta\ (-\pi<\theta\leqslant\pi)$	85
5.18	Stresses around boundary of hole in infinite sheet. i) Loading b) + g) $\cos\theta$ normal pressure & $\sin\theta$shear	87

Figure		Page
5.19	Stresses around boundary of hole in infinite sheet. ii) Loading b) + h) $\cos\theta$ normal pressure & $\sin 2\theta$ shear	88
5.20	Stresses around boundary of hole in infinite sheet. iii) Loading b) + j) $\cos\theta$ normal pressure & $\sin^3\theta\cos\theta$ shear	88
5.21	Stresses around boundary of hole in infinite sheet. iv) Loading c) + g) $\cos^2\theta$normal pressure & $\sin\theta$ shear	90
5.22	Stresses around boundary of hole in infinite sheet. v) Loading c) + h) $\cos^2\theta$normal pressure & $\sin\theta$ shear	90
5.23	Stresses around boundary of hole in infinite sheet. vi) Loading c) + j) $\cos^2\theta$normal pressure & $\sin^3\theta\ \cos\theta$ shear	91
5.24	Pressurized annulus	92
5.25	Symmetrical lug (pin-loaded)	94
5.26	Rectangular lug (pin-loaded)	98
5.27	Stress concentration factors for symmetrical/ asymmetrical loaded lugs	100
5.28	Stress concentration factors for loaded lugs	101
5.29	Lug with rounded end	103
5.30	Comparison of stress concentration factors for rectangular lugs (FESM) with rounded lugs	103
6.1	Boundaries with the modified kernel function	115
7.1	Externally loaded annulus	119
7.2	Square plate with central circular hole in biaxial tension	120
7.3	Comparison of results for σ_θ in externally loaded annulus	121
7.4	Comparison of results for σ_r in externally loaded annulus	123
7.5	Accuracy of the modified BEM solution for annuli with various sizes of hole	124
7.6	Accuracy of the modified BEM solution for square plates with various sizes of hole	126

(Appendices)

E1-E29	Finite element meshes	197
G1	Boundary grid specified using the macro DRAWBEL	209

LIST OF TABLES

Table		Page
5.1	The stress concentration factor for rectangular plate in tension (a/w = 0.5) for different meshes	54
5.2	The stress concentration factor for rectangular plate in tension with various sizes of circular hole	56
5.3	The stress concentration factor for rectangular plate in tension with elliptical hole of varying aspect ratio (a/w = 0.25)	58
5.4	The stress concentration factor for rectangular plate in tension with elliptical hole of varying aspect ratio (a/w = 0.5)	58
5.5	Reference values of stress at the edge of a circular hole in an infinite strip in tension (a/w = 0.5)	61
5.6	The stress concentration factors for different special regions. Mesh A.	62
5.7	The stress concentration factors for different special regions. Mesh B.	63
5.8	Stress concentration factors for plate with circular hole (a/w = 0.5) using different finite element meshes	68
5.9	Stress concentration factors given by reference [5.5] for square plate in tension with circular hole.	70
5.10	Stress concentration factors for square plate with circular hole (a/w = 0.5) by FESM	71
5.11	Stress concentration factors for square plate with circular hole (a/w = 0.5) by other finite element methods	71
5.12	Stress concentration factors for square plate in tension with elliptical hole	73
5.13	Tractions and Fourier coefficients for various distributions of radial load	80
5.14	Tractions and Fourier coefficients for various distributions of shear	86
5.15	Results for pressurized hole	93
5.16	Stress concentrations for symmetrical lug with different distributions of load	95
5.17	Stress concentration factor for rectangular pin-loaded lugs	99
5.18	Stress concentration factors for a lug with rounded ends from reference [5.9].	102

Table		Page
(Appendices)		
B.1	Programs segments listed in this appendix (B)	157
B.2	Other program segments used by FESM program	158
C.1	Information stored in the direct access file	179
C.2	Variables in the direct access file	180
D.1	Macros used with the FESM program	181

CHAPTER 1

GENERAL INTRODUCTION

1.1 Background to the work

The presence of holes or notches in structural components increases the nominal stress in these components by a factor, K_t, known as the stress concentration factor [1.1]. The aim of this work has been the development of accurate methods for determining K_t in a wide variety of configurations.

The need for accurate estimates of stress concentration factors has arisen in particular from studies in fracture mechanics. Fatigue damage may be caused by the initiation and growth of cracks near stress concentrations when the structure is subject to cyclic loading. Since these cracks may appear early in the life of the structure, or indeed may occur in manufacture, the fatigue life depends on the rate at which the crack grows, and to determine crack growth rates the stress *intensity* factor for the crack must be known. Stress *intensity* factors characterise the stress field near to a crack tip and values for most simple configurations have been collected in reference manuals [1.2-1.4]. For short cracks - and for most of the life of a component the crack will be short- simple methods of determining the stress *intensity* factor [1.5,1.6] may be used even for complex geometries, provided that data is available for the stress concentration factor or, in the case of weight function methods, the stress distribution over the crack site in the absence of the crack. The recent compounding method for determining stress *intensity* factors [1.7-1.9] also requires knowledge of the stress concentration factor at the site of the crack if there is significant interaction between the boundaries of the configuration [1.10], (e.g. when the hole is close to the edge of the component). Furthermore since the crack growth rate depends on the stress *intensity* factor raised to a power (typically 4) the stress concentration factor must be known accurately (1%-3%) for these methods to be of use. In fact there are many classes of problem (e.g. finite plates with holes, pin-loaded lugs) for which stress concentration factors of the required accuracy are known for relatively few and only the simplest geometries. Even where they are known the stress distribution, which is required by some methods for evaluating the stress intensity factors of cracks, may not have been

included. Hence there is a need for an accurate, versatile and convenient method for determining stress concentration factors and the stress distribution near to holes and notches.

For methods to be applicable to a variety of complex structures with several interacting boundaries and varied loading conditions, a numerical method of stress analysis is required. Broadly these may be divided into three main types: finite difference methods, finite element methods and boundary element methods. The finite difference method is perhaps the most straight forward and historically was developed first [1.11]. By dividing the region of the problem with equally spaced nodes throughout,the governing differential equation may be solved in terms of values of stress or displacement at the nodal points. However the method is not suited to problems where there are high stress gradients, such as occur at holes or notches, since the nodes must be closely spaced to model the region of stress concentration, and consequently the total number required for an accurate representation of the solution becomes very large. For this reason finite difference methods have been largely superseded by finite elements [1.12-1.13] for all but specialized applications, and the two methods developed in the present work are based on the finite element and boundary element methods.

The finite element method is widely used in all branches of continuum mechanics and since its inception for stress analysis [1.14] it has been developed to include many variants. The basis of the method is that the region of the problem is divided into small elements of simple shape (in two dimensions usually triangles or quadrilaterals) which are assumed to be interconnected only at a discrete number of nodes. A "shape function", for example a polynomial, is used to represent the stresses or displacements within the elements in terms of the nodal values of either displacements, stresses or both, depending on the particular formulation. An approximate solution for these nodal unknowns is obtained by applying a weighted residual technique or variational principle (for example minimizing energy) to give a set of symmetric banded simultaneous equations [1.15, 1.16]. The technique is extremely powerful and has been applied successfully to many different problems including three-dimensional, anisotropic and non-linear cases.

Some of the considerable amount of work done with finite elements for two dimensional elastic problems with high stress gradients is reviewed, along with other methods, in section 1.2. In developing a new method for stress concentrations near holes, as described in Part I of this work, certain drawbacks of the finite element method are avoided. Firstly in areas of steep stress gradient, such as found at stress concentrations, the finite element method usually requires a very fine mesh to obtain acceptable accuracy. This is expensive in both data preparation time and run time on the computer. Furthermore the simplest finite element methods used constant strain triangular elements with nodal displacements as unknowns. This means that to estimate the stress at any boundary (the edge of a hole for example) the value must be extrapolated from the average stress in the elements near to the boundary, introducing a further source of error. By incorporating into the finite element scheme known elasticity solutions, such as that for an infinite sheet with a hole, the new method proposed and developed in this thesis increases the effectiveness of finite elements for stress concentration problems.

In recent years boundary element techniques have gained considerable acceptance as a preferred alternative to finite elements [1.17, 1.18]. As the name suggests these methods require elements on the boundary of the region only and thus the dimensionality of the elements is reduced by one. The simultaneous equations, which must be solved to give the unknowns on the boundary, are derived from integral equations (hence the alternative name, "boundary integral equation" methods), and although the matrix formed is not banded as in finite element methods, it is much smaller than would arise with finite elements for most problems. Once the equations are solved the values of stress or displacement at any interior points may be calculated. However a disadvantage of the method for stress concentrations, where stresses must be evaluated at boundaries, is that this is usually more difficult and less accurate than for interior points. In Part II of this work a boundary element method is formulated incorporating modified "fundamental solutions" (elasticity solutions for a point force in a given region). These fundamental solutions become the "kernel functions" in the integral equations. The boundary conditions on the part of the boundary where the stress concentration factor is required are satisfied exactly in these new fundamental solutions and

this enables this part of the boundary to be included without using boundary elements. Thus the required stresses may be determined as accurately as at interior points and the number of elements needed is reduced.

1.2 Review of theoretical methods and solutions

The existence of high stress near geometrical discontinuities has been appreciated for many years and investigations of stress concentrations, both experimental and theoretical, were begun during the last century [1.19-1.21]. Since that time an immense volume of work has been published on the subject and this review is aimed at highlighting some of the more important work. Reviews of general methods of obtaining stress concentrations [1.22] and of analytical methods in particular, [1.23, 1.24] have appeared in the literature and several collections of the solutions obtained have been made [1.1, 1.25-1.31] . The aim of the present survey is to consider the various theoretical methods available for obtaining stress concentration factors and to compare them with the finite element superposition method (FESM) and the modified boundary element method (BEM) which are developed in Parts I and II respectively. The review is limited to methods applied to *two dimensional* configurations of elastic, isotropic and homogeneous materials with in-plane loadings. An assessment is made of the relative merits of the methods, the accuracy (where known), whether the methods may be extended to more complex geometries or materials (e.g. three-dimensional configurations, anisotropic materials, etc.) and, in general terms, their theoretical basis.

1.2.1 Exact Analytical Methods

The solution by Lamé [1.19] to the case of a hollow cylinder subjected to uniform pressure on the inner and outer surfaces, was the precursor of many of the analytical solutions to stress concentration problems. It was based on the mathematical theory of elasticity which was formulated, in a systematic way, during the first part of the last century by Navier [1.32], Cauchy [1.33] and others. The introduction by Airy [1.34] of a formulation using stress functions led to important solutions, including those for an infinite sheet in tension containing a traction-free circular hole [1.20], a traction-free elliptical hole [1.35] and a loaded circular hole [1.36]. The configuration of an elliptical hole in an infinite sheet in tension was first solved by Kolosov [1.37] who introduced two most important concepts, complex

potentials and conformal mapping. This led to the development of a most powerful analytical method for elasticity problems and much more work was done using this approach by the Russian school, notably Muskhelishvili [1.38-1.40] and co-workers. The technique remained unknown outside Russia for many years and was later used independently by Stevenson [1.41, 1.42] and others [1.43, 1.44] for stress concentration problems. Examples of other solutions obtained using Muskhelishvili's method are: infinite or semi-infinite plates in tension containing deep hyperbolic or shallow semi-elliptical notches [1.31], and point forces acting in an infinite plate containing a circular [1.45] or elliptical [1.46] cut-out. In spite of the powerful nature of the method and the usefulness of the solutions so obtained, only a few configurations have been solved in closed form, and general solutions not in closed form (e.g. [1.47]) require much analysis to obtain a particular solution, even assuming that the series involved converge. For this reason approximate methods for calculating the stresses have been developed and applied to a much wider range of problems than is possible using an exact analytical technique. However the exact methods are most important in the development of approximate techniques and in the present work exact analytical solutions based on the methods of Airy [1.34] or Muskhelishvili [1.38] are incorporated into numerical methods to improve their efficiency.

1.2.2 Approximate Analytical Methods

Approximate methods such as the "alternating technique" have been used to determine Airy stress functions from a series representation, and hence to obtain the stress in, for example, an infinite strip with a central circular hole [1.48]. The basis of this method was that separate parts of the boundary (e.g. the hole and the straight edges of the strip) were considered alternatively. At each iteration of the method residual stresses occurred on the other part of the boundary, which were then cancelled by the next iteration, leaving smaller residuals on the first part of the boundary. This was continued until an acceptable accuracy was obtained. Approximate solutions for plates and strips with circular holes [1.49-1.52] and for loaded holes in strips [1.53-1.55] have been produced by Howland and others in a similar manner. The method was extended for a strip with an asymmetrical hole by Ling [1.56] who also obtained the solution for an infinite sheet loaded in tension, perforated by two equal holes [1.57, 1.58].

Isida [1.59-1.65] solved several strip configurations using a "perturbation" method based on the alternating technique used by Howland. the solutions included those for strips containing an eccentric circular hole [1.59,1.61], elliptical hole [1.62, 1.63] and symmetrical notches [1.60]. The solution by Shibuya et al [1.66] for a plate with a conical hole is based on a similar principle but extended to 3 dimensions by using a least-squares approximation to satisfy the boundary conditions.

Approximate solutions for plates with different shaped holes have also been obtained based on Muskhelishvili's complex variable approach with conformal mapping. Many variants of the method exist, but generally the hole or notch is mapped on to a unit circle, the complex potentials are determined from the boundary conditions, usually in a series form, and truncation of the series yields an approximate solution. Savin [1.26, 1.27] and many other authors have obtained solutions for plates perforated by circular holes [1.67-1.69], square, rectangular or triangular holes [1.70-1.74], reinforced holes [1.75-1.77] and multiple holes [1.78-1.80], and many of these solutions are collected in the two monographs [1.26, 1.27] where many anisotropic and elastic/plastic problems are also treated. The same approach has also been used for some edge notch problems [1.81-1.83].

Results from these approximate analytical methods are generally accurate to within 2% but each problem must be formulated individually and particular mapping functions must be found for each configuration. This may not be possible especially if there are discontinuities in the curvature of the notch. Often there are problems of convergence also, such that an appreciable improvement of accuracy can only be achieved by including a great many more terms in the series representation of the potentials, and this is particularly true when the configurations are of finite size, rather than infinite planes or strips. The importance of the methods to the present work therefore, is not that they offer an alternative to more general numerical techniques, but that several accurate solutions have already been obtained that may be used for comparisons in confirming the accuracy of any new method. In particular solutions by Howland [1.48], Hengst [1.52], Knight [1.54] and Isida [1.62] have been used in the present work for this purpose.

1.2.3 Numerical Methods

The advent of powerful digital computers meant that the emphasis in stress analysis moved from analytical methods to numerical methods. Of these, mention has already been made of the finite difference, finite element and boundary element methods. The "collocation method" however is another important technique.

The collocation method [1.84] consists of using stress functions or complex potentials in series form, the coefficients of the series being unknown. The series are truncated and the coefficients determined by matching the boundary conditions at a finite number of points on the boundary. Hooke [1.85, 1.86] used this method for two-dimensional and axisymmetric three-dimensional notch problems under tension and bending loads.

The collocation method has been combined with conformal mapping by Bowie and others [1.87, 1.88] and further improved by partitioning the region of the problem into separate sub-regions [1.89]. Solutions for various shapes of edge notches in semi-infinite plates and holes in infinite plates have been obtained using this method [1.90]. The collocation method may also be combined with other numerical techniques, such as the finite element method [1.91], which gives added flexibility in its use. Typical accuracy for the method is generally in the region of 1% [1.92] but problems with convergence, ill-conditioning or sensitivity to the number and distribution of the boundary points may increase the error. Consequently the collocation method is not as versatile as some other numerical methods and it has received relatively little attention compared to finite or boundary elements. Some work is continuing on the collocation method for the evaluation of stress intensity factors, at the University of Southampton [1.93].

A drawback of the analytical methods, and to an extent the collocation and finite difference methods, is a lack of versatility in analysing a wide variety of different geometries. It is in this respect particularly that the finite element method and boundary element method are so effective and this explains the large amount of work which has been done in the last twenty years, especially on the finite element method.

General reviews of work in finite elements have been presented, for example, in several of the standard texts [1.12, 1.13, 1.94]. Here, however, having mentioned some of the problems of conventional finite elements, particular attention is paid to the development of methods combining both finite element and continuum concepts, of which the finite element superposition method formulated in the present work is an example.

In applying conventional finite element methods to configurations with steep stress gradients, several difficulties occur. Many elements are required to model the stress field accurately and consequently it is expensive for data preparation, computer processing and post-processing of the results. In addition to obtain a value of stress at the boundary some sort of interpolation from interior points may be required. Even higher order elements are not always an advantage since although the number of elements would be reduced (or the accuracy increased) more nodes are introduced per element and this may lead to a similar number of unknowns in the problem. Much work has been done in proposing modifications to the finite element scheme to overcome these problems, particularly for crack problems [1.95]. Isoparametric elements [1.96], different variational principles [1.97], and hybrid methods [1.98] have all been used to improve the method for cracked configurations. The forerunners of the present work, also using methods formulated for crack problems, superimposed analytical trial functions, corresponding to the singular stress field around a crack tip, over a region of the configuration. This region varied from a special crack-tip element [1.99-1.103] to the whole region of the problem [1.104-1.108] or, as in the present formulation, a "special region" including several elements around the notch or crack [1.109-1.111]. A superposition approach was proposed for stress concentrations at smooth cut-outs by Rao [1.103] using large "primary" elements in the region of the notch, and by Schnack [1.111] who combined the use of augmenting functions with six-node hybrid elements. The aim of these methods is to incorporate known solutions for the stress field near to a crack or notch in an *infinite* region, into the finite element scheme. Thus the finite elements model only the difference between the infinite region solution, scaled by arbitrary coefficients, and the exact solution for the configuration being analysed.

Since this difference will be relatively small in the region of interest if the trial functions are appropriate to the particular problem, the errors introduced by modelling the region with a coarse finite element mesh and interpolating values of stress on the boundary, will also be small.

The finite element superposition method presented in Part I is a development of this work in that trial functions, derived from known elasticity solutions to appropriate configurations, are combined with constant strain triangular finite elements. Loading on a hole boundary is incorporated into the method using similar elasticity solutions, known as loading functions, which remove the need to represent loadings as a series of nodal forces - often a further source of error in conventional finite element analysis. The trial functions for configurations with circular holes are based on the general Airy stress functions, rather than solutions for infinite regions, which means that the effects of the other parts of the boundary may also be included in the trial functions to some extent. The accuracy and small number of degrees of freedom that result from well chosen trial and loading functions, and the versatility of the finite element method in general combine to make this a powerful method for the solution of stress concentration problems.

The boundary element method was proposed not long after the finite element method, but the first practical applications of the method by Jaswon and Symm [1.112, 1.113] appeared in 1963 and initial development was much less rapid than finite elements. This may possibly be due to the slightly greater mathematical complexity of the formulation, and the fact that it is less easily understood intuitively. However the method has several advantages over finite elements, the most important being that since only the boundary of the region need be divided into elements the dimensions of the elements are reduced by one, e.g. from a three-dimensional volume to a two dimensional surface. The method was first used for elastostatic problems by Cruse and Rizzo [1.114, 1.115] and in recent years an upsurge in interest in the method has taken place due to its claimed superiority over the finite element method for many applications [1.116, 1.117]. Broadly the method may be divided into two main types: direct formulations [1.118-1.121] where the unknown functions

in the boundary integral equations are the physical variables of the problem (e.g. tractions and displacements), and indirect formulations [1.122-1.125] in which the integral equations are expressed in terms of a "density function", which in itself has no physical significance but from which the physical parameters may be derived at any point in the body. A form of indirect method, called the "body force method" developed by Nisitani [1.126] has been used for many notch and crack problems [1.46, 1.127-1.129] . These include an infinite sheet containing one or two rows of elliptical holes, a semi-infinite plate containing variously shaped notches, a row of elliptical holes or a row of notches, and an infinite strip containing two symmetrical semi-elliptical notches.

Much of the recent interest in boundary elements, as with finite elements, centred on improving the method for configurations with cracks. Cruse [1.130] proposed including the crack explicitly in the fundamental solution from which the integral equations are derived so that the crack need not be modelled by boundary elements, and this proved most successful. In the case of the body force method a similar approach was adopted by Murakami and Nisitani for elliptical holes [1.131, 1.132] and, using a direct boundary element method, Telles and Brebbia [1.133-1.134] used the approach for configurations containing a long straight boundary. The success of these methods suggested that a similar approach could be used for a direct boundary element formulation with a fundamental solution which satisfied the boundary conditions of a circular hole. This idea is the basis of the work presented in part II of this thesis. Not only does this approach reduce the number of elements required but also the stresses at the hole may be calculated directly and with greater accuracy than would be possible with standard boundary elements.

1.3 Layout of the thesis

The main body of the thesis is divided into two parts: Part I comprising Chapters 2 to 5 is concerned with the work on finite elements and Part II comprising Chapters 6 and 7 concerns the boundary element work. Chapters 1 and 8 are general to both aspects of the work.

CHAPTER 2 presents the formulation of the finite element superposition method. The concept of trial functions derived from known elasticity solutions is introduced for configurations with loaded or traction-free holes. In addition to the trial functions the new loading function is incorporated into the method which is the (known) solution for an infinite sheet with the specified loading on the hole. A variational principle is used to determine the arbitrary coefficients of the trial functions, the finite element unknowns (nodal displacements) and certain correction stresses which arise in elements near boundaries.

CHAPTER 3 deals with the analytical elasticity solutions which are required by the finite element superposition method, i.e. the trial functions and loading function. Two trial functions are given for elliptical holes based on an analytical solution using complex stress functions and a conformal mapping function. For circular holes the generalised solution for the Airy stress function in two dimensional polar coordinates is used to specify a general set of trial functions. The generalised solution is also used to give the loading function, with a distribution of tractions round the hole boundary specified using a Fourier expansion.

In CHAPTER 4 the way in which the method is implemented on the computer is explained. The structure and the main processes occurring in the program are discussed and a brief resume is given of how the program and its peripheral facilities may be used in practice.

The results obtained using the finite element superposition method are presented in CHAPTER 5. Confirmation of the accuracy of the method for traction-free holes is carried out by comparison with other estimates for stress concentration factors in rectangular plates with holes. The

effect on accuracy of such parameters as the finite element mesh size, number of trial functions and size of the hole is determined and new results for the stress concentration factors of elliptical traction-free holes in square plates are given. Various distributions for the tractions on loaded holes are suggested and compared. Estimates for stress concentration factors for loaded holes determined by the finite element superposition method are compared with some known values and finally new results are obtained for rectangular lugs with loaded holes.

In CHAPTER 6 the formulation of the boundary element method is presented and the modification to the method, by using fundamental solutions which include the boundary near the stress concentration, is explained. The implementation of these modifications in the computer program is also discussed.

The results given in CHAPTER 7 were obtained using the modified boundary element method. The advantages and limitations of the modified method are shown by comparing the results from the two methods for an externally pressurized annulus. The accuracy of the modified method for annuli and square plates with various sizes of circular hole is shown by comparing the estimates for stress concentration factors from the boundary element program with known values.

CHAPTER 8, the final chapter, contains a summary of the conclusions from both the finite element and boundary element work. Comparison between the methods and their relative merits is made and some possible directions for future work are suggested.

PART I

THE FINITE ELEMENT SUPERPOSITION METHOD

CHAPTER 2

FINITE ELEMENT FORMULATION

2.1 Introduction

The finite element superposition method (FESM) used in this work is based on a method originated by Morley [2.1] and extended by Bartholomew [2.2, 2.3]. The basis of the method is that the piece-wise linear displacement field of constant strain finite elements may be augmented by the superposition of one or more known elasticity solutions, referred to as the "trial functions", which are weighted by arbitrary coefficients.* The trial functions are elasticity solutions which satisfy exactly conditions of equilibrium and compatibility but not all the boundary conditions of the problem. They are chosen such that they give rise to stresses and displacements closely matching those in the region of the stress concentration. For example the known solution for a uniformly stressed infinite sheet containing a circular hole may be used as a trial function for a finite plate loaded in some manner with a similar hole.

Bartholomew has formulated this method for traction-free cracks. In the present work the method is extended to apply to configurations with circular or elliptical holes which may be traction-free or subjected to specified tractions. To deal with loaded holes another known elasticity solution referred to as the "loading function" has been introduced. The use of this function removes the need to represent the tractions at the hole in the piece-wise constant form usually employed by the finite element method, thus avoiding the introduction of inaccuracies at the very point where the stress concentration factor is to be determined.

The loading function corresponds to the elasticity solution in which the hole is subjected to the tractions for which a solution is

---

* The term "trial function" may be used of any function used to approximate the exact solution. In this sense the piece-wise linear displacement field is also a trial function, however here the term is used of the known elasticity solutions with which the constant strain finite element field is augmented.

required but the extent of the sheet is assumed to be infinite. The trial functions, on the other hand, are elasticity solutions for a plate with a *stress-free* hole under various different remote boundary conditions which need not necessarily correspond to an infinite region. The superposition of the loading function and these trial functions therefore, results in the traction boundary conditions on the hole being satisfied exactly and leaves residuals remote from the hole which are corrected by the constant strain finite elements.

It has been shown [2.3] that in the case of cracked configurations it is advantageous to limit the superposition to a "special region" which is larger than a single special element but smaller than the complete region of the problem. For this reason the present formulation continues the use of a special region over which the trial functions and loading function are superimposed, constant strain elements alone being used in the exterior region.

The trial functions and loading function for specific classes of problem are determined in Chapter 3. The details of how the method is formulated are outlined in the remainder of this chapter, with additional material in Appendix A.

2.2 Notation for the boundaries

The configuration to be analysed by FESM may be represented diagramatically as in figure 2.1. The two dimensional body containing a hole is denoted V and the boundary, including the hole boundary, is denoted by S. The boundary S is made up of S_T, where traction boundary conditions are applied, and S_K, where kinematic boundary conditions are applied. Since a superposition principle is to be used in the representation of load on the hole boundary, it is assumed that the hole forms part of S_T. The geometry of the configuration is defined relative to Cartesian coordinates (X,Y) with an origin at O.

The variational principle, from which the finite element solution is derived, will be represented in terms of volume and boundary integrals over various parts of the configuration. Since a special region is introduced, over which the trial functions are to be superimposed, further subdivision of the boundary S is required (see figure 2.2).

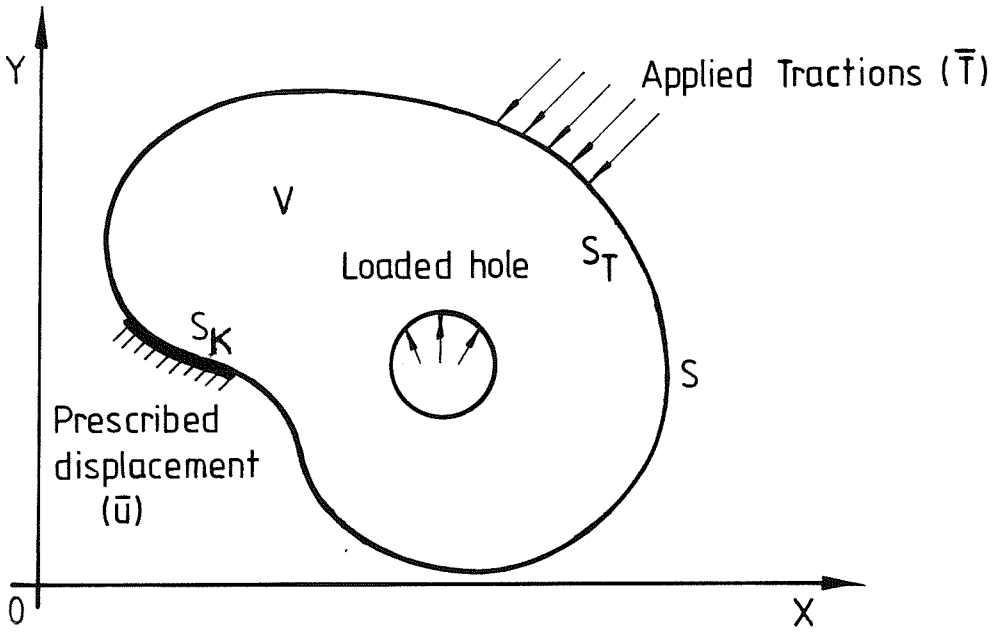

Figure 2.1 Two dimensional body with loaded hole

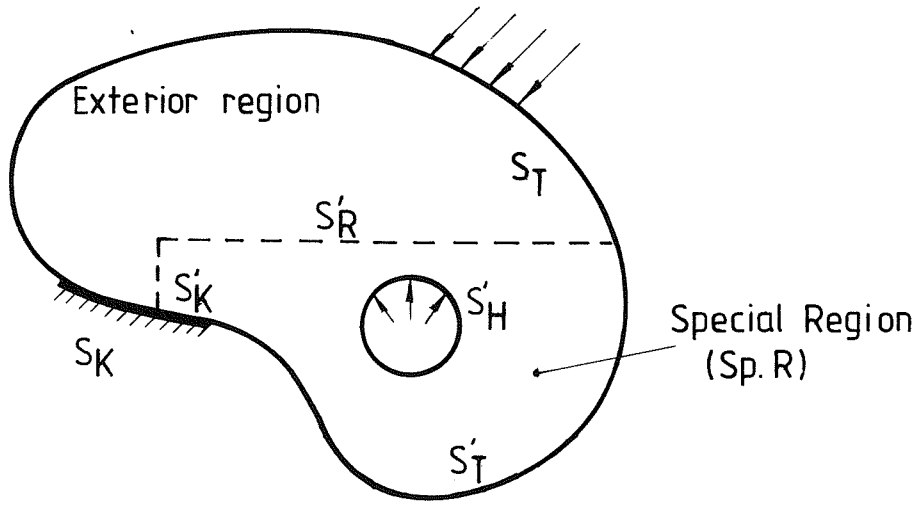

Figure 2.2 Two dimensional body showing special region

Boundaries adjacent to the special region are denoted with a prime ('), hence S'_K for example. The traction boundary adjacent to the special region is divided into two parts, S'_H the hole boundary and S'_T the remaining traction boundaries. This distinction is necessary in the present work due to the introduction of the loading function to represent the loading on the hole. The "interface boundary" between the special region and exterior region is denoted S'_R. The notation for the boundaries may be summarized therefore as follows:

$$\left.\begin{aligned} S &= S_K + S_T \\ S' &= S'_K + S'_T + S'_H + S'_R \\ \text{and} \quad S_T &= S^e_T + S'_T + S'_H \end{aligned}\right\} \qquad (2.1)$$

where S^e_T denotes that part of the traction boundary in the exterior region. The complete region V is divided into triangular elements.

2.3 Displacement and stress fields

The basis of FESM is that the displacements, $\underline{\tilde{u}}$, and stresses, $\underline{\sigma}^I$, of the approximate solution are a superposition of a constant strain finite element field and a set of known elasticity solutions with displacements and stresses denoted $\underline{u}^*_i$ and $\underline{\sigma}^*_i$ respectively. The integer i takes the values 1 to k for the trial functions, k being the number of trial functions, and i=0 for the loading function. (Underlined symbols are used throughout the text to define both vector fields and matrices).

The assumed form of the displacement field $\underline{\tilde{u}}$ on the boundaries of the finite elements may therefore be expressed as follows:

$$\left.\begin{aligned} \underline{\tilde{u}} &= \underline{u}^F + \sum_{i=0}^{k} \alpha_i (\underline{u}^*_i - \underline{u}^\dagger_i) && \text{within the special region, on } S'_T \text{ and } S'_H \\ \underline{\tilde{u}} &= \underline{u}^F && \text{in the external region, on } S'_R \text{ and } S'_K \\ \underline{\tilde{u}} &= \underline{u}^F = \underline{\bar{u}} && \text{on } S_K \end{aligned}\right\} \qquad (2.2)$$

where α_i is the coefficient of the i'th trial function,

$\bar{\underline{u}}$ are the prescribed displacements on S_K,

and $\underline{u}_i^{\dagger}$ are constant strain finite element fields which take the same values as $\underline{u}_i^{*}$ at the finite element nodes and are linear between nodes. The reason for introducing these fields, $\underline{u}_i^{\dagger}$, is that $(\underline{u}_i^{*} - \underline{u}_i^{\dagger})$ is zero at the nodes thus nodal displacements are given simply by $\underline{u}^F$ in both the exterior and special regions and the displacement field, as defined by equation (2.2) is compatible across all element boundaries.

As is usual in the development of finite element methods the piecewise linear displacement fields $\underline{u}^F$ and $\underline{u}_i^{\dagger}$ are expressed in terms of vectors, $\underline{q}^F$ and $\underline{q}_i^{\dagger}$ respectively, containing the components of displacement at the nodes. The strain within an element is constant from these fields and thus may be expressed in terms of the nodal displacements as:

$$\left.\begin{aligned} \underline{B}_N \, \underline{q}_N^F &= \underline{\varepsilon}_N^F \\ \text{and} \qquad \underline{B}_N \, \underline{q}_{N_i}^{\dagger} &= \underline{\varepsilon}_{N_i}^{\dagger} \end{aligned}\right\} \tag{2.3}$$

where $\underline{q}_N^F$ and $\underline{q}_{N_i}^{\dagger}$ contain displacement components for the N'th element only, $\underline{B}_N$ is the "element strain matrix" and $\underline{\varepsilon}_N^F$ and $\underline{\varepsilon}_{N_i}^{\dagger}$ are the constant strain vectors (three components in plane stress) for the respective fields. The matrix $\underline{B}_N$ is obtained from the geometry of the element and is given ; as in reference [2.4], by:

$$\underline{B}_N = [\bar{\underline{B}}_{(1)}, \bar{\underline{B}}_{(2)}, \bar{\underline{B}}_{(3)}] \tag{2.4}$$

where a typical sub-matrix, $\bar{\underline{B}}_{(1)}$ say, is:

$$\bar{\underline{B}}_{(1)} = \frac{1}{2\Delta} \begin{bmatrix} (Y_2-Y_3) & 0 \\ 0 & (X_3-X_2) \\ (X_3-X_2) & (Y_2-Y_3) \end{bmatrix} \tag{2.5}$$

and Δ is the area of the element, X_n, Y_n are the coordinates of the n'th node and the nodes are numbered anti-clockwise round the element.

The stress field $\underline{\sigma}^I$ may now be defined in the *interior* of each element as follows:

$$\left.\begin{aligned} \underline{\sigma}^I &= \underline{\sigma}^F + \sum_{i=0}^{k} \alpha_i \, (\underline{\sigma}_i^* - \underline{\sigma}_i^\dagger + \underline{\sigma}_i^c) \qquad \text{In the special region} \\ \underline{\sigma}^I &= \underline{\sigma}^F \qquad\qquad\qquad\qquad\qquad\qquad\quad \text{In the external region} \end{aligned}\right\} \quad (2.6)$$

The stress fields $\underline{\sigma}^F$, $\underline{\sigma}_i^*$ and $\underline{\sigma}_i^\dagger$ correspond to exact solutions for the displacement fields $\underline{u}^F$, $\underline{u}_i^*$ and $\underline{u}_i^\dagger$ respectively. The terms $\underline{\sigma}_i^c$ constant within elements, must be included in the special region due to linear displacements being defined on the boundaries S_K' and S_R' to ensure compatibility. The terms $\underline{\sigma}_i^c$ therefore are non-zero only in special region elements adjacent to kinematic or interface boundaries. In spite of the many terms in equation (2.6a) it may be seen that it is simply the superposition of constant finite element fields, $\underline{\sigma}^F$, $\underline{\sigma}_i^\dagger$ and $\underline{\sigma}_i^c$, with the trial function fields $\underline{\sigma}_i^*$.

Again following standard finite element methods, the constant stress fields for an element may be expressed in terms of strain. Thus:

$$\left.\begin{aligned} \underline{A}\,\underline{\sigma}_N^F &= \underline{\varepsilon}_N^F \\ \underline{A}\,\underline{\sigma}_{N_i}^\dagger &= \underline{\varepsilon}_{N_i}^\dagger \\ \text{and} \qquad \underline{A}\,\underline{\sigma}_{N_i}^c &= \underline{\varepsilon}_{N_i}^c \end{aligned}\right\} \quad (2.7)$$

where $\underline{\sigma}_N^F$, $\underline{\sigma}_{N_i}^\dagger$, $\underline{\sigma}_{N_i}^c$ and $\underline{\varepsilon}_N^F$, $\underline{\varepsilon}_{N_i}^\dagger$, $\underline{\varepsilon}_{N_i}^c$ contain the stress and strain components respectively for the N'th element, and

$$\underline{A} = \frac{1}{E} \begin{bmatrix} 1 & -\nu & 0 \\ -\nu & 1 & 0 \\ 0 & 0 & 2(1+\nu) \end{bmatrix} \quad (2.8)$$

for plane stress. E is Young's modulus and ν is Poisson's ratio.

In order to determine displacements and stresses from the equations (2.2) and (2.6), the nodal displacements, $\underline{q}^F$, the trial function coefficients, α_i, and the correction stress fields, $\underline{\sigma}_i^c$, must be known. These are determined using a variational principle.

2.4 The variational principle

A variational principle uses a scalar quantity (a "functional") which may be defined in terms of integrals of the unknown parameters in a continuum problem - in this case displacement and stress. The functions of the parameters which make the functional stationary is the solution to the problem. By limiting the possible functions of displacement and stress to a set of trial functions (as above) with finite degrees of freedom the problem may be reduced to a set of simultaneous equations.

The specification of both displacements and stresses by equations (2.2) and (2.6) means that the variational principle must allow for trial functions to be specified for both parameters. Such a variational principle derived from a modified principle of minimum complementary energy (see Appendix A) was given by Pian and Tong [2.5]:

$$\Pi_c = \sum_N \{ -U_N(\underline{\sigma}^I) + \int_{S_N} (\underline{\tilde{u}})^T \underline{T}^I \, dS - \int_{S_{T_N}} (\underline{\tilde{u}})^T \underline{\bar{T}} \, dS \} \qquad (2.9)$$

where $U_N(\underline{\sigma}^I)$ is the strain energy of the specified field for the N'th element, $\underline{\sigma}^I$ and $\underline{T}^I$ are respectively the interior stress and corresponding tractions for the element, $\underline{\tilde{u}}$ is the displacement on the complete element boundary, which is denoted by S_N, and $\underline{\bar{T}}$ are the prescribed tractions on the element traction boundary S_{T_N}. The superscript $(\ )^T$ denotes the the transpose of a vector or matrix. The summation is carried out over all the elements.

In general the function $U(\underline{\sigma}_1, \underline{\sigma}_2)$ is defined as the strain energy, in the region V bounded by the surface S, due to two stress fields $\underline{\sigma}_1$ and $\underline{\sigma}_2$. Thus:

$$U(\underline{\sigma}_1, \underline{\sigma}_2) = \frac{1}{2} \int_V (\underline{\sigma}_1)^T \underline{\varepsilon}_2 \, dV \qquad (2.10)$$

where $\underline{\varepsilon}_2$ is the strain due to the stress field $\underline{\sigma}_2$.

If only one parameter is specified to the function the two fields in equation (2.10) are understood to be the same. Similarly the function may be written with displacement rather than stress fields as the variables. Provided that for one field, $\underline{\sigma}_1$ say, the stresses are in equilibrium over V and for the other the strain field is compatible over V, the volume integral may be reduced to a surface integral using the divergence theorem:

$$U(\underline{\sigma}_1,\underline{\sigma}_2) = \frac{1}{2}\int_S (\underline{T}_1)^T \underline{u}_2 \, dS \tag{2.11}$$

where $\underline{T}_1$ and $\underline{u}_2$ are the tractions and displacements respectively of the two fields and there are no body forces. Using these properties of the strain energy function and substituting equations (2.2) and (2.6) into equation (2.9) the following form of the functional is obtained:

$$\begin{aligned}
\Pi_c = {} & U(\underline{u}^F) - \int_{S_T} (\underline{u}^F)^T \bar{\underline{T}} \, dS \\
& - 2\sum_{i=0}^{k} \alpha_i U_{Sp.R}(\underline{u}^F,\underline{u}_i^\dagger) + \sum_{i=0}^{k}\sum_{j=0}^{k} \alpha_i\alpha_j \left[U_{Sp.R}(\underline{u}_i^\dagger,\underline{u}_j^\dagger) - U_{Sp.R}(\underline{u}_i^c,\underline{u}_j^c)\right] \\
& + \sum_{i=0}^{k} \alpha_i \left[\int_{S_T'+S_H'} (\underline{u}^F)^T \underline{T}_i^* \, dS - \int_{S_T'+S_H'} (\underline{u}_i^* - \underline{u}_i^\dagger)^T \bar{\underline{T}} \, dS\right] \\
& + \frac{1}{2}\sum_{i=0}^{k}\sum_{j=0}^{k} \alpha_i\alpha_j \int_{S_T'+S_H'} (\underline{u}_i^* - 2\underline{u}_i^\dagger)^T \underline{T}_j^* \, dS \\
& + \sum_{i=0}^{k} \alpha_i \left[\int_{S_K'} (\bar{\underline{u}})^T \underline{T}_i^* \, dS + \int_{S_R'} (\underline{u}^F)^T \underline{T}_i^* \, dS - \int_{S_R'+S_K'} (\underline{u}_i^* - \underline{u}_i^\dagger)^T \underline{T}^F dS\right] \\
& + \sum_{i=0}^{k}\sum_{j=0}^{k} \alpha_i\alpha_j \left[-\frac{1}{2}\int_{S_R'+S_K'} (\underline{u}_i^*)^T \underline{T}_j^* \, dS + \int_{S_R'+S_K'} (\underline{u}_i^* - \underline{u}_i^\dagger)^T \underline{T}_j^\dagger \, dS \right. \\
& \left. - \int_{S_R'+S_K'} (\underline{u}_i^* - \underline{u}_i^\dagger)^T \underline{T}_j^c \, dS \right]
\end{aligned} \tag{2.12}$$

where $\underline{T}$, with the appropriate subscripts and superscripts, denotes the tractions on a boundary due to the corresponding stress field and $U_{Sp.R}$ is the strain energy function evaluated in the special region only.

The prescribed tractions on the hole boundary S'_H are applied explicitly using the loading function. This function is defined such that:

$$\alpha_0 \underline{T}^*_0 = \underline{\bar{T}} \qquad \text{(on the hole boundary } S'_H) \tag{2.13}$$

Since α_0, the coefficient of the loading function, is constant it is not a trial function. It is included in the functional with the trial functions but the coefficient is determined by the magnitude of the loading on the hole and thus it does not appear as an unknown in the final system of equations.

The trial functions are chosen to satisfy zero traction conditions on the hole boundary, i.e.:

$$\underline{T}^*_i = 0 \qquad \text{(on } S'_H, \text{ for i=1 to k)} \tag{2.14}$$

By substituting equation (2.13) in the functional, equation (2.12), the terms which relate to the traction boundaries may be rewritten as:

$$- \int_{S^e_T+S'_T} (\underline{u}^F)^T \underline{\bar{T}}\, dS - \alpha_0 \int_{S'_H} (\underline{u}^F)^T \underline{T}^*_0\, dS + \alpha_0 \int_{S'_H} (\underline{u}^F)^T \underline{T}^*_0\, dS$$

$$+ \sum_{i=1}^{k} \alpha_i \int_{S'_H} (\underline{u}^F)^T \underline{T}^*_i\, dS + \sum_{i=0}^{k} \alpha_i \left[\int_{S'_T} (\underline{u}^F)^T \underline{T}^*_i - \int_{S'_T} (\underline{u}^*_i - \underline{u}^\dagger_i)^T \underline{\bar{T}}\, dS \right]$$

$$- \sum_{i=0}^{k} \alpha_0 \alpha_i \int_{S'_H} (\underline{u}^*_i - \underline{u}^\dagger_i)^T \underline{T}^*_0\, dS + \sum_{i=0}^{k} \sum_{j=0}^{k} \alpha_i \alpha_j \int_{S'_H} (\underline{u}^*_i - \underline{u}^\dagger_i)^T \underline{T}^*_j\, dS$$

$$+ \sum_{i=0}^{k} \sum_{j=0}^{k} \alpha_i \alpha_j \left[\int_{S'_T} (\underline{u}^*_i - \underline{u}^\dagger_i)^T \underline{T}^*_j\, dS - \frac{1}{2} \int_{S'_T+S'_H} (\underline{u}^*_i)^T \underline{T}^*_j\, dS \right] \tag{2.15}$$

Further substituting equation (2.14) in the above expression eliminates all but the five underlined terms and thus the functional may be written:

$$\Pi_c = U(\underline{u}^F) - 2\sum_{i=0}^{k} \alpha_i U_{Sp.R}(\underline{u}^F, \underline{u}_i^\dagger) + \sum_{i=0}^{k}\sum_{j=0}^{k} \alpha_i\alpha_j [U_{Sp.R}(\underline{u}_i^\dagger, \underline{u}_j^\dagger) - U_{Sp.R}(\underline{\sigma}_i^c, \underline{\sigma}_j^c)]$$

$$- \int_{S_T^e+S_T'} (\underline{u}^F)^T \bar{\underline{T}}\, dS + \sum_{i=0}^{k} \alpha_i \left[\int_{S_T'} (\underline{u}^F)^T \underline{T}_i^* - \int_{S_T'} (\underline{u}_i^* - \underline{u}_i^\dagger)^T \bar{\underline{T}}\, dS\right]$$

$$+ \sum_{i=0}^{k}\sum_{j=0}^{k} \alpha_i\alpha_j \left[\int_{S_T'} (\underline{u}_i^* - \underline{u}_i^\dagger)^T \underline{T}_j^*\, dS - \frac{1}{2} \int_{S'} (\underline{u}_i^*)^T \underline{T}_j^*\, dS\right]$$

$$+ \sum_{i=0}^{k} \alpha_i \left[\int_{S_K'} (\bar{\underline{u}})^T \underline{T}_i^*\, dS + \int_{S_R'} (\underline{u}^F)^T \underline{T}_i^*\, dS - \int_{S_R'+S_K'} (\underline{u}_i^* - \underline{u}_i^\dagger)^T \underline{T}^F\, dS\right]$$

$$+ \sum_{i=0}^{k}\sum_{j=0}^{k} \alpha_i\alpha_j \left[\int_{S_R'+S_K'} (\underline{u}_i^* - \underline{u}_i^\dagger)^T \underline{T}_j\, dS - \int_{S_R'+S_K'} (\underline{u}_i^* - \underline{u}_i^\dagger)^T \underline{T}_j^c\, dS\right] \qquad (2.16)$$

2.5 Determination of the correction stress fields $\underline{\sigma}_i^c$

The correction stress fields are determined by variation of the functional equation (2.16), with respect to $\underline{\sigma}_i^c$. The terms which depend on $\underline{\sigma}_i^c$ are:

$$\sum_{i=0}^{k}\sum_{j=0}^{k} \alpha_i\alpha_j \left[-U_{Sp.R}(\underline{\sigma}_i^c, \underline{\sigma}_j^c) - \int_{S_R'-S_K'} (\underline{u}_i^* - \underline{u}_i^\dagger)^T \underline{T}_j^c\, dS\right] \qquad (2.17)$$

Since the stresses $\underline{\sigma}_i^c$ are constant over each element, the expression (2.17) may be expressed:

$$\sum_{N}^{(Sp.R)} \left\{ \sum_{i=0}^{k}\sum_{j=0}^{k} \alpha_i\alpha_j \left[-\frac{1}{2} t\, \Delta\, (\underline{\sigma}_{Ni}^c)^T \underline{A}\, \underline{\sigma}_{Nj}^c - (\underline{\sigma}_{Nj}^c)^T \underline{L}\, \underline{C}_i\right] \right\} \qquad (2.18)$$

where the summation is carried out over all elements in the special region, t is the thickness of the elements in the special region and $\underline{\sigma}_{Ni}^c$ is the vector of components of the correction stress field in the X and Y coordinate directions for the N'th element.

Thus:

$$\underline{\sigma}_{Ni}^{c} = \begin{bmatrix} \sigma_{Xi}^{c} \\ \sigma_{Yi}^{c} \\ \tau_{XYi}^{c} \end{bmatrix}_{N} \tag{2.19}$$

τ_{XYi}^{c} being the shear component. $\underline{L}$ is the matrix which when pre-multiplied by the vector $(\sigma_{Ni}^{c})^{T}$ gives the tractions on the part of the boundary $S'_R+S'_K$ adjacent to the element. i.e.

$$\underline{L} = \begin{bmatrix} \cos\phi & 0 \\ 0 & \sin\phi \\ \sin\phi & \cos\phi \end{bmatrix} \tag{2.20}$$

where ϕ is the angle between the X axis and the normal to the boundary. Finally $\underline{C}_i$ is defined by:

$$\underline{C}_i = \begin{bmatrix} \int_{S'_{R_N}+S'_{K_N}} (u^{*}_{Xi} - u^{\dagger}_{Xi})\, dS \\ \int_{S'_{R_N}+S'_{K_N}} (u^{*}_{Yi} - u^{\dagger}_{Yi})\, dS \end{bmatrix} \tag{2.21}$$

when the subscript N denotes the part of the boundary of the N'th element and the suffices X and Y denote the components in the X and Y coordinate directions respectively. At the stationary point the variation of (2.18) with respect to the variables $\underline{\sigma}_{Ni}^{c}$ (i = 0 to k, N = 1 to the number of elements in the special region) is zero. Thus the components of $\underline{\sigma}_{Ni}^{c}$ may be determined, in terms of integrals of the known fields $\underline{u}_i^{*}$ and $\underline{u}_i^{\dagger}$, by differentiating equation (2.18). They are given by:

$$\underline{\sigma}_{Ni}^{c} = -\frac{1}{t\Delta}\ \underline{A}^{-1}\ \underline{L}\ \underline{C}_i \tag{2.22}$$

where $\underline{A}^{-1}$ is:

$$\underline{A}^{-1} = \frac{E}{1-\nu^2} \begin{bmatrix} 1 & \nu & 0 \\ \nu & 1 & 0 \\ 0 & 0 & \frac{1}{2}(1-\nu) \end{bmatrix} \tag{2.23}$$

The integrals of equation (2.21) are carried out numerically using 6 point Gauss quadrature.

2.6 Determination of the nodal displacements $\underline{q}^F$

The constant strain finite element part of the displacement field, $\underline{u}^F$, is defined by the vector $\underline{q}^F$ of its nodal components. The terms in equation (2.16) which depend on $\underline{u}^F$ are as follows:

$$U(\underline{u}^F) - \int_{S_T+S'_T} (\underline{u}^F)^T \bar{\underline{T}}\, dS + \sum_{i=0}^{k} \alpha_i \{ \int_{S'_T+S'_R} (\underline{u}^F)^T \underline{T}_i^*\, dS$$

$$- \int_{S'_R+S'_K} (\underline{u}_i^* - \underline{u}_i^\dagger)^T \underline{T}^F\, dS - 2\, U_{Sp.R}(\underline{u}^F, \underline{u}_i^\dagger) \} \qquad (2.24)$$

In terms of $\underline{q}^F$ this may be written:

$$\frac{1}{2} (\underline{q}^F)^T \underline{K}\, \underline{q}^F - (\underline{q}^F)^T \underline{p} + \sum_{i=0}^{k} \alpha_i (\underline{q}^F)^T \underline{p}_i \qquad (2.25)$$

where $\underline{K}$ is the stiffness matrix for the constant strain finite element scheme and $\underline{p}$ and $\underline{p}_i$ are vectors which may be considered as equivalent nodal loads. $\underline{K}$ is assembled from the stiffness matrices of individual elements as for conventional finite element methods. Thus the first term of equation (2.24) may be written:

$$\sum_N t\Delta (\underline{\varepsilon}_N^F)^T \underline{A}^{-1} \underline{\varepsilon}_N^F \qquad (2.26)$$

or

$$\sum_N t\Delta (\underline{q}_N^F)^T [\, \underline{B}_N^T \underline{A}^{-1} \underline{B}_N \,] \underline{q}_N^F \qquad (2.27)$$

where the summation is over all elements. The element stiffness matrix therefore is given by $t\Delta\, [\underline{B}_N^T \underline{A}^{-1} \underline{B}_N]$ and by summing the contributions from each element the stiffness matrix $\underline{K}$ is obtained.

The vector $\underline{p}$ is determined simply from the prescribed tractions $\bar{\underline{T}}$ (excluding the tractions on the hole boundary S'_H). A uniform load on an element traction boundary is distributed equally between the 2 nodes on the element side.

Contributions to the vector $\underline{p}_i$ however arise from the last three terms in expression (2.24). From the first of these terms the following equivalent nodal loads arise in an element with a part of the boundary S'_T or S'_R between two of its nodes, node (1) and node (2) say:

$$\left.\begin{aligned} \underline{p}_i^{(1)} &= t \int_{(1)}^{(2)} \left(1 - \frac{s}{s_o}\right) \underline{T}_i^* \, dS \\ \underline{p}_i^{(2)} &= t \int_{(1)}^{(2)} \frac{s}{s_o} \underline{T}_i^* \, dS \end{aligned}\right\} \quad \text{on } S_T' \text{ or } S_R' \qquad (2.28)$$

where s is the distance along the element side measured from node (1), s_o is the length of the element side and the suffix to $\underline{p}_i^{(\ )}$ denotes the node at which the equivalent load is considered to act. The integral is of a known function and may be carried out numerically. The remaining two terms of equation (2.24) may be written:

$$\sum_{N}^{Sp.R} \{ - (\underline{\sigma}_N^F)^T \ \underline{L} \ \underline{C}_i - t\Delta \ (\underline{\varepsilon}_N^F)^T \ \underline{\sigma}_{Ni}^\dagger \} \qquad (2.29)$$

where the summation is carried out for elements in the special region and the vector $\underline{\sigma}_{Ni}^\dagger$ contains the components of $\underline{\sigma}_i^\dagger$ for the N'th element. The expression (2.29) may be rearranged, using equation (2.22) and the definition of the matrix $\underline{B}_N$ (equations (2.3) to (2.5)), as:

$$\sum_{N}^{Sp.R} \{ - t\Delta \ (\underline{\sigma}_{Ni}^c + \underline{\sigma}_{Ni}^\dagger)^T \ \underline{B}_N \ \underline{q}_N^F \} \qquad (2.30)$$

Thus the contributions to the nodal loads $\underline{p}_i$ in the N'th element from these terms are given by:

$$\left.\begin{aligned} & - t\Delta \ (\underline{\sigma}_{Ni}^c)^T \ \underline{B}_N \\ \text{and} \quad & - t\Delta \ (\underline{\sigma}_{Ni}^\dagger)^T \ \underline{B}_N \end{aligned}\right\} \qquad (2.31)$$

which may be evaluated when the stresses $\underline{\sigma}_{Ni}^c$ and $\underline{\sigma}_{Ni}^\dagger$ are calculated for each element in the special region.

Since the matrices $\underline{K}$, $\underline{p}$ and $\underline{p}_i$ in the expression (2.25) can be determined, the stationary point may be found by setting the variation of the expression with respect to $\underline{q}^F$ as zero, thus:

$$\underline{K} \ \underline{q}^F = \underline{p} - \sum_{i=0}^{k} \alpha_i \ \underline{p}_i \qquad (2.32)$$

The variables $\underline{q}$ and $\underline{q}_i$ are now defined such that:

$$\underline{q} = \underline{K}^{-1} \underline{p} \tag{2.33}$$

and

$$\underline{q}_i = \underline{K}^{-1} \underline{p}_i \tag{2.34}$$

These simultaneous equations, subject to the kinematic constraints

$$\left.\begin{aligned} \underline{q} &= \bar{\underline{u}} \\ \text{and} \quad \underline{q}_i &= 0 \end{aligned}\right\} \quad \text{on} \quad S_K, \tag{2.35}$$

are solved on the computer using Choleski factorisation of the matrix in banded form, as implemented by Morley [2.6] and others [2.7, 2.8]. The displacements $\underline{q}$, as defined by equations (2.33) are those which would arise from constant strain finite elements if no augmenting trial functions were used. This "basic" solution may be used for comparison in assessing the improvement in the final augmented solution.

The nodal displacements, $\underline{q}^F$, written in terms of $\underline{q}$ and $\underline{q}_i$ follow from equations (2.32) to (2.34) and are given by:

$$\underline{q}^F = \underline{q} - \sum_{i=0}^{k} \alpha_i \underline{q}_i \tag{2.36}$$

2.7 Determination of the trial function coefficients

Equation (2.36) may be substituted back into equation (2.25) and hence into the functional, equation (2.16). Furthermore the following terms from equation (2.16) may also be combined:

$$\sum_{i=0}^{k} \sum_{j=0}^{k} \alpha_i \alpha_j \{ U_{Sp.R}(\underline{u}_i^{\dagger}, \underline{u}_j^{\dagger}) - U_{Sp.R}(\underline{u}_i^{c}, \underline{u}_j^{c}) + \int_{S_R'+S_K'} (\underline{u}_i^{*}-\underline{u}_i^{\dagger})^T \underline{T}_j^{\dagger} \, dS - \int_{S_R'+S_K'} (\underline{u}_i^{*}-\underline{u}_i^{\dagger})^T \underline{T}_j^{c} \, dS \} \tag{2.37}$$

Since the stresses $\underline{\sigma}_i^{\dagger}$ and $\underline{\sigma}_i^{c}$ are constant over each element the final two terms of the expression (2.37) may be written:

$$(\underline{T}_j^{\dagger})^T \int_{S_R'+S_K'} (\underline{u}_i^{*}-\underline{u}_i^{\dagger})\, dS = \sum_{N}^{Sp.R} (\underline{\sigma}_{Nj}^{\dagger})^T \underline{L}\, \underline{C}_i$$

$$\text{and} \quad -(\underline{T}_j^{c})^T \int_{S_R'+S_K'} (\underline{u}_i^{*}-\underline{u}_i^{\dagger})\, dS = -\sum_{N}^{Sp.R} (\underline{\sigma}_{Nj}^{c})^T \underline{L}\, \underline{C}_i \qquad (2.38)$$

Since, from equation (2.22)

$$\underline{L}\, \underline{C}_i = -\, t\Delta\, \underline{A}\, \underline{\sigma}_{Ni}^{c} \qquad (2.39)$$

$$\text{and} \quad U(\underline{\sigma}_{Ni}^{c}, \underline{\sigma}_{Nj}^{\dagger}) = \frac{1}{2}\, t\Delta\, (\underline{\sigma}_{Ni}^{c})^T \underline{A}\, \underline{\sigma}_{Nj}^{\dagger}\ , \qquad (2.40)$$

the expression (2.37) may be written:

$$\sum_{i=0}^{k}\sum_{j\neq 0}^{k} \alpha_i\alpha_j \{U_{Sp.R}(\underline{u}_i^{\dagger},\underline{u}_j^{\dagger}) - 2\, U_{Sp.R}(\underline{\sigma}_i^{c},\underline{\sigma}_j^{\dagger}) + U_{Sp.R}(\underline{\sigma}_i^{c},\underline{\sigma}_j^{c})\} \qquad (2.41)$$

or in terms of the stress fields:

$$\sum_{i=0}^{k}\sum_{j\neq 0}^{k} \alpha_i\alpha_j\, U_{Sp.R}(\underline{\sigma}_i^{\dagger}-\underline{\sigma}_i^{c},\ \underline{\sigma}_j^{\dagger}-\underline{\sigma}_j^{c}) \qquad (2.42)$$

Thus the final form of the functional to be varied with respect to the remaining unknowns α_i (i=1 to k) is as follows:

$$\Pi_c = \frac{1}{2}(\underline{q})^T \underline{K}\, \underline{q} - (\underline{q})^T \underline{p} + \sum_{i=0}^{k} \alpha_i\, [-(\underline{q}_i)^T \underline{K}\, \underline{q} + (\underline{q}_i)^T \underline{p} + (\underline{q})^T \underline{p}_i]$$

$$+ \sum_{i=0}^{k}\sum_{j=0}^{k} \alpha_i\alpha_i\, [\, \frac{1}{2}(\underline{q}_i)^T \underline{K}\, \underline{q}_j - (\underline{q}_i)^T \underline{p}_j\,]$$

$$+ \sum_{i=0}^{k} \alpha_i\, [\, -\int_{S_T'} (\underline{u}_i^{*}-\underline{u}_i^{\dagger})^T \bar{\underline{T}}\, dS + \int_{S_K'} (\bar{\underline{u}})^T \underline{T}_i^{*}\, dS\,]$$

$$+ \sum_{i=0}^{k}\sum_{j=0}^{k} \alpha_i\alpha_j\, [\, \int_{S_T'} (\underline{u}_i^{*}-\underline{u}_i^{\dagger})^T \underline{T}_j^{*}\, dS - \frac{1}{2} \int_{S'} (\underline{u}_i^{*})^T \underline{T}_j^{*}\, dS$$

$$+ U_{Sp.R}(\underline{\sigma}_i^{\dagger}-\underline{\sigma}_i^{c},\ \underline{\sigma}_j^{\dagger}-\underline{\sigma}_j^{c})\,] \qquad (2.43)$$

This is a quadratic expression in α_i which may be written in matrix form:

$$\frac{1}{2}(\underline{\alpha}')^T\underline{D}'\ \underline{\alpha}' - \underline{F}'\ \underline{\alpha}' + c \qquad (2.44)$$

where $\underline{D}'$ is a square matrix, $\underline{F}'$ a vector and $\underline{\alpha}'$ the vector of coefficients, all having (k+1) rows. The final term c does not vary with $\underline{\alpha}'$. Variation with respect to α_i (i = 1 to k) to determine the stationary point yields a set of simultaneous equations:

$$\underline{D}\ \underline{\alpha} = \underline{F} \qquad (2.45)$$

where $\underline{D}$, $\underline{F}$ and $\underline{\alpha}$ in this case have only k rows (omitting the loading function coefficient α_o from $\underline{\alpha}'$). $\underline{D}$ is a symmetric matrix where an element d_{ij}, of the matrix may be given in terms of the elements, d'_{ij}, of $\underline{D}'$, as:

$$d_{ij} = \frac{d'_{ij} + d'_{ji}}{2} \qquad (i, j = 1 \text{ to } k) \qquad (2.46)$$

Equation (2.46) may be verified by expanding the expression (2.44) and differentiating. The coefficients of α_o in $\underline{D}'$, d'_{oi} and d'_{io} (i = 1 to k), contribute to the right hand side of equation (2.45) since α_o is a constant, and thus an element of $\underline{F}$, f_i, in terms of the corresponding element of $\underline{F}'$, f'_i, is given by:

$$f_i = f'_i - \alpha_o\left(\frac{d'_{io} + d'_{oi}}{2}\right) \qquad (i = 1 \text{ to } k) \qquad (2.47)$$

The line integrals in equation (2.43) are carried out using Gauss quadrature over the boundaries S'_T, S'_K and S'_R in order to form the required matrices $\underline{D}$ and $\underline{F}$. A particular advantage of the present formulation of this method, however, is that no approximate integration need be carried out over the hole boundary S'_H, which since it is curved might have introduced either greater complication or inaccuracy. The boundary S'_H appears in equation (2.43) as part of S', but explicit integration may be avoided as follows. Let the relevant terms, denoted d^S_{ij}, be stored in the matrix $\underline{D}_S$, where

$$d^S_{ij} = -\frac{1}{2}\int_{S'_T+S'_R+S'_K} (\underline{u}^*_i)^T\ \underline{T}^*_j\ dS \qquad (i,j = 0 \text{ to } k) \qquad (2.48)$$

Since from equation (2.14)

$$\int_{S'_H} (\underline{u}_i^*)^T \underline{T}_j^* \, dS = 0 \qquad \text{for} \begin{cases} i = 0 \text{ to } k \\ j = 1 \text{ to } k \end{cases} \tag{2.49}$$

then:

$$d_{ij}^S = -\frac{1}{2} \int_{S'} (\underline{u}_i^*)^T \underline{T}_j^* \, dS \qquad \text{for} \begin{cases} i = 0 \text{ to } k \\ j = 1 \text{ to } k \end{cases} \tag{2.50}$$

Thus only the terms d_{io}^S do not give the integral required by equation (2.43). Since $\underline{u}_i^*$ and $\underline{T}_j^*$ are exact elasticity solutions and S' is a closed contour

$$\int_{S'} (\underline{u}_i^*)^T \underline{T}_j^* \, dS = \int_{S'} (\underline{u}_j^*)^T \underline{T}_i^* \, dS \qquad (i,j = 0 \text{ to } k) \tag{2.51}$$

Therefore the terms d_{oi}^S may be substituted for the terms d_{io}^S to give the required integral in the matrix $\underline{D}_S$. The only term which may not be corrected in this way is d_{oo}^S which is a coefficient of α_o^2 in the functional. Since α_o does not vary this term is not required and thus the potentially complicated integration of the trial functions on the curved hole boundary is avoided.

The simultaneous equations (2.45) may now be solved to give the coefficients α_i.

2.8 Determination of the stress at any point

The nodal displacements $\underline{q}^F$, and hence the displacement field $\underline{u}^F$ are determined from equations (2.36). Equation (2.2) gives the displacements, $\tilde{\underline{u}}$, should they be required at intermediate points, and the stresses may then be calculated from equation (2.6). The stress field $\underline{\sigma}^F$ is determined for each element from the nodal displacements $\underline{q}^F$, the trial function stresses $\underline{\sigma}_i^*$ may be evaluated at any point from the known analytical expressions for the trial functions, and the term $(\underline{\sigma}_i^\dagger - \underline{\sigma}_i^c)$, which is constant for each element in the special region would have been calculated previously for each element in order to evaluate the final term of the functional (2.43). All the terms in equation (2.6) therefore are known and are used in evaluating the stresses at the required points.

2.9 Summary

In conclusion, the formulation of this method is based on a variational principle which requires the specification of displacements (on element boundaries) and stresses (within elements) in terms of trial functions which are known elasticity solutions. Tractions on part of the boundary (in this case the hole boundary) may be specified using another elasticity solution, the loading function. Variation of the functional with respect to the unknowns of the problem yields a system of simultaneous equations. Some line integrals of the trial functions and loading functions must be evaluated for the coefficients of these equations but no integrations on the hole boundary are necessary as a result of the loading function. The stress at any point in an element may be determined from the solution to the simultaneous equations, the trial and loading functions and the correction terms for the elements which will have been evaluated in constructing the equation.

CHAPTER 3

TRIAL FUNCTIONS AND LOADING FUNCTION

3.1 Introduction

The trial functions for use with the finite element superposition method (FESM) are derived from two-dimensional elasticity solutions for configurations which identically satisfy zero-traction conditions at the hole or notch where the stress concentration is to be calculated. Boundary conditions remote from the hole are not specified for the trial functions. If the hole is loaded in some manner the tractions on the hole must be represented by a loading function which is the exact elasticity solution for an *infinite* sheet with the same hole and the same loading on the hole as the problem to be solved and zero stress remote from the hole. The superposition of trial functions and loading function therefore satisfies the boundary conditions on the hole exactly. For the method to work well the constant strain finite element field, which ensures that the remote boundary conditions are approximately satisfied, should introduce only small corrections to that part of the solution resulting from the loading and trial functions. Thus an important aspect of the method is the selection of suitable trial functions.

In section 3.2 two trial functions are given for configurations with elliptical (or circular) holes. A more general set of trial functions for configurations with circular holes is given in section 3.3 and the loading function for circular holes is given in section 3.4. The trial functions and loading function are defined either in cartesian coordinates (x,y) or polar coordinates (r,θ) relative to axes with the origin, O', at the centre of the hole. The finite element geometry is defined in cartesian coordinates (X,Y) relative to the "global" axes with a different origin O and different orientation. The position of the hole and the angle, γ, between the OX and O'x axes must therefore be specified in each case.

3.2 Trial functions for elliptical holes

Two satisfactory trial functions may be obtained for configurations with elliptical or circular holes from the known solution for a uniformly stressed infinite sheet containing a traction-free hole [3.1].

The infinite region bounded by the ellipse:

$$\frac{x^2}{a^2} + \frac{y^2}{b^2} = 1 \tag{3.1}$$

where a and b are the semi-major and semi-minor axes of the ellipse respectively, may be transformed to the unit circle, $|\xi| \leq 1$, by the conformal mapping function

$$z = R\left(\frac{1}{\zeta} + \mu\,\zeta\right) \tag{3.2}$$

where $z = x + iy$. The parameters R and μ are given by:

$$R = \frac{a+b}{2}$$

and

$$\mu = \frac{a-b}{a+b} \tag{3.3}$$

For a circular hole R is equal to the radius of the hole a, and $\mu = 0$. The transformation (3.2) is single valued and it is important that its inverse is also single valued. This is given by:

$$\zeta = \frac{1}{2R\mu}\left\{ z - \left(\sqrt{z-2R\sqrt{\mu}}\right)\left(\sqrt{z+2R\sqrt{\mu}}\right)\right\} \tag{3.4}$$

for $\mu \neq 0$, where $\sqrt{\ }$ denotes the complex square root with a positive real part (i.e. the argument of the square root, θ say, lies in the range $-\pi/2 < \theta \leq \pi/2$). When $\mu = 0$ the inverse of the transformation is given by:

$$\zeta = R/z \tag{3.5}$$

The two trial functions are obtained from the solutions for the configuration with different remote loadings: 1) uniform tension at infinity parallel to the x axis, and 2) uniform tension at infinity parallel to the y axis. With coefficients α_1 and α_2 respectively the complex stress functions, ϕ_i and ψ_i, for the i'th trial function are given by:

For trial function i = 1:

$$\phi_1(\zeta) = \frac{\alpha_1 R}{4}\left[\frac{1}{\zeta} + \zeta\,(2-\mu)\right]$$

$$\psi_1(\zeta) = -\frac{\alpha_1 R}{2}\left[\frac{1}{\zeta} + \frac{\zeta}{1-\mu\zeta^2}\,(1 - \mu + \mu^2 - \zeta^2)\right] \tag{3.6}$$

For trial function i = 2:

$$\phi_2(\zeta) = \frac{\alpha_2 R}{4} \left[\frac{1}{\zeta} - \zeta(2 + \mu) \right]$$

$$\psi_2(\zeta) = -\frac{\alpha_2 R}{2} \left[-\frac{1}{\zeta} + \frac{\zeta}{1-\mu\zeta^2}(1 + \mu + \mu^2 + \zeta^2) \right] \qquad (3.7)$$

where the subscript i (i = 1 or 2) denotes the number of the trial function. The components of the trial function stresses (σ^*_{ri}, $\sigma^*_{\theta i}$ and $\tau^*_{r\theta i}$) and displacements (u^*_{ri} and $u^*_{\theta i}$), in polar coordinates (r,θ), are obtained from the following general formulae:

$$u^*_{ri} + i\, u^*_{\theta i} = \frac{e^{i\theta}}{2G} \left[\kappa\phi_i(z) - z\, \overline{\phi_i'(z)} - \overline{\psi_i(z)} \right]$$

$$\sigma^*_{ri} + \sigma^*_{\theta i} = 4\, \mathrm{Re} \left[\phi_i'(z) \right]$$

$$\sigma^*_{\theta i} - \sigma^*_{ri} + 2i\, \tau^*_{r\theta i} = 2\, e^{2i\theta} \left[\bar{z}\, \phi_i''(z) + \psi_i'(z) \right] \qquad (3.8)$$

where the bar ($\bar{}$) here denotes the complex conjugate, prime (') denotes differentiation with respect to z and Re denotes the real part. Also

$$\kappa = \frac{3-\nu}{1+\nu} \quad \text{(for plane stress)}$$

$$\text{and} \qquad G = \frac{E}{2(1+\nu)} \qquad (3.9)$$

where ν is Poisson's ratio, E is Young's modulus and G is the shear modulus.

3.3 Trial functions for circular holes

In section 3.2 a set of two trial functions are given for configurations with traction-free elliptical or circular holes. A more general set of functions may be obtained for circular holes by using the generalised solution for the Airy stress function, Φ_A, for the two-dimensional problem in polar coordinates [3.2]. This is in series form:

$$\Phi_A = a_o \log r + b_o r^2 + c_o r^2 \log r + d_o r^2\theta + a'_o\theta$$

$$+ \frac{a_1}{2} r\,\theta \sin\theta + (b_1 r^3 + a'_1 r^{-1} + b'_1 r \log r) \cos\theta$$

$$- \frac{c_1}{2} r\,\theta \cos\theta + (d_1 r^3 + c'_1 r^{-1} + d'_1 r \log r) \sin\theta$$

$$+ \sum_{n=2}^{\infty} (a_n r^n + b_n r^{n+2} + a'_n r^{-n} + b'_n r^{-n+2}) \cos n\theta$$

$$+ \sum_{n=2}^{\infty} (c_n r^n + d_n r^{n+2} + c'_n r^{-n} + d'_n r^{-n+2}) \sin n\theta \qquad (3.10)$$

where a_n, b_n, c_n, d_n, a'_n, b'_n, c'_n, d'_n ($n = 0$ to ∞) are constants determined by the boundary conditions of the problem. By limiting the problems to be solved to those with at least one axis of symmetry (about $\theta = 0$ say), the following constants may be eliminated:

$$d_o = a'_o = c_n = d_n = c'_n = d'_n = 0 \quad (n = 1 \text{ to } \infty) \qquad (3.11)$$

since these coefficients would give rise to asymmetric stresses and displacements. Furthermore for the displacements to be single-valued it is found that:

$$c_o = 0$$

and

$$b'_1 = -\frac{a_1(1-\nu)}{4} \qquad (3.12)$$

The summation may be truncated to a finite number of terms, m, and thus the stress function is reduced to:

$$\Phi_A = a_o \log r + b_o r^2 + \frac{a_1}{2} r\,\theta \sin\theta + \left(b_1 r^3 + \frac{a'_1}{r} - \frac{a_1(1-\nu)}{4} r \log r\right) \cos\theta$$

$$+ \sum_{n=2}^{m} (a_n r^n + b_n r^{n+2} + a'_n r^{-n} + b'_n r^{-n+2}) \cos n\theta \qquad (3.13)$$

The stresses (σ^*_r, σ^*_θ and $\tau^*_{r\theta}$) are given by:

$$\sigma_r^* = \frac{1}{r}\frac{\partial \Phi_A}{\partial r} + \frac{1}{r^2}\frac{\partial^2 \Phi_A}{\partial \theta^2}$$

$$\sigma_\theta^* = \frac{\partial^2 \Phi_A}{\partial r^2}$$

$$\tau_{r\theta}^* = -\frac{\partial}{\partial r}\left(\frac{1}{r}\frac{\partial \Phi_A}{\partial r}\right) \qquad (3.14)$$

which yield:

$$\sigma_r^* = a_o r^{-2} + 2b_o + \frac{1}{4}\left[a_1(3+\nu)r^{-1} + 8b_1 r - 8a_1' r^{-3}\right] \cos\theta$$

$$- \sum_{n=2}^{m} \{n(n-1)a_n r^{n-2} + (n+1)(n-2)b_n r^n + n(n+1)a_n' r^{n-2} + (n-1)(n+2)b_n' r^{-n}\} \cos n\theta$$

$$\sigma_\theta^* = -a_o r^{-2} + 2b_o + \frac{1}{4}\left[-a_1(1-\nu)r^{-1} + 24b_1 r + 8a_1' r^{-3}\right] \cos\theta$$

$$+ \sum_{n=2}^{m} \{n(n-1)a_n r^{n-2} + (n+1)(n+2)b_n r^n + n(n+1)a_n' r^{-n-2} + (n-1)(n-2)b_n' r^{-n}\} \cos n\theta$$

$$\tau_{r\theta}^* = \frac{1}{4}\left[-a_1(1-\nu)r^{-1} + 8b_1 r - 8a_1' r^{-3}\right] \sin\theta$$

$$+ \sum_{n=2}^{m} \{n(n-1)a_n r^{n-2} + n(n+1)b_n r^n - n(n+1)a_n' r^{-n-2} - n(n-1)b_n' r^{-n}\} \sin n\theta \qquad (3.15)$$

By substituting into the equations (3.15) the zero traction boundary conditions on the hole, but not the remote boundary conditions, half of the unknown coefficients may be determined. The remaining coefficients, scaled to a convenient level, may then be used as the trial function coefficients, denoted α_i, which are determined from the variational principle (see section 2.7). The stress function given by equation (3.13) therefore yields a set of 2m trial functions.

The expressions for displacements are obtained from the stresses using the formula for the strain components (ε_r^*, ε_θ^*, $\gamma_{r\theta}^*$) :

$$\varepsilon_r^* = \frac{1}{E}(\sigma_r^* - \nu\sigma_\theta^*)$$

$$\varepsilon_\theta^* = \frac{1}{E}(\sigma_\theta^* - \nu\sigma_r^*)$$

$$\gamma_{r\theta}^* = \frac{1}{G}\tau_{r\theta} \qquad (3.16)$$

and the strain - displacement relations:

$$\varepsilon_r^* = \frac{\partial u_r^*}{\partial r}$$

$$\varepsilon_\theta^* = \frac{u_r^*}{r} + \frac{\partial u_\theta^*}{r\partial\theta}$$

$$\gamma_{r\theta}^* = \frac{\partial u_r^*}{r\partial\theta} + \frac{\partial u_\theta^*}{\partial r} - \frac{u_\theta^*}{r} \qquad (3.17)$$

For an unloaded circular hole, of radius a, the boundary conditions on the hole are:

$$\sigma_r^*\,(r = a) = 0$$

$$\tau_{r\theta}^*\,(r = a) = 0 \qquad (3.18)$$

These may be substituted into (3.15) to give the following expressions for σ_{ri}^*, $\sigma_{\theta i}^*$, $\tau_{r\theta i}^*$, u_{ri}^* and $u_{\theta i}^*$ where i denotes the variable associated with the i'th trial function.

For trial function i = 1:

$$\sigma_{r1}^* = \frac{\alpha_1}{2}(1 - \frac{a^2}{r^2})$$

$$\sigma_{\theta 1}^* = \frac{\alpha_1}{2}(1 + \frac{a^2}{r^2})$$

$$\tau_{r\theta 1}^* = 0$$

$$u_{r1}^* = \frac{\alpha_1 a}{2E}\left[(1-\nu)\frac{r}{a} + (1+\nu)\frac{a}{r}\right]$$

$$u_{\theta 1}^* = 0 \qquad (3.19)$$

For trial function i = 2:

$$\sigma^*_{r2} = \frac{\alpha_2}{4}\left(\frac{r}{a} - \frac{a^3}{r^3}\right)\cos\theta$$

$$\sigma^*_{\theta 2} = \frac{\alpha_2}{4}\left(\frac{3r}{a} + \frac{a^3}{r^3}\right)\cos\theta$$

$$\tau^*_{r\theta 2} = \frac{\alpha_2}{4}\left(\frac{r}{a} - \frac{a^3}{r^3}\right)\sin\theta$$

$$u^*_{r2} = \frac{\alpha_2 a}{8E}\left[(1-3\nu)\frac{r^2}{a^2} + (1+\nu)\frac{a^2}{r^2} + 2(3+\nu)\right]\cos\theta$$

$$u^*_{\theta 2} = \frac{\alpha_2 a}{8E}\left[(5+\nu)\frac{r^2}{a^2} + (1+\nu)\frac{a^2}{r^2} - 2(3+\nu)\right]\sin\theta \qquad (3.20)$$

For trial function i = [2n-1], n≥2:

$$\sigma^*_{r[2n-1]} = \frac{\alpha_{[2n-1]}}{4}\left[\frac{r^{n-2}}{a^{n-2}}(n-1) - \frac{a^{n+2}}{r^{n+2}} - \frac{r^n}{a^n}(n-2)\right]\cos n\theta$$

$$\sigma^*_{\theta[2n-1]} = -\frac{\alpha_{[2n-1]}}{4}\left[\frac{r^{n-2}}{a^{n-2}}(n-1) - \frac{a^{n+2}}{r^{n+2}} - \frac{r^n}{a^n}(n+2)\right]\cos n\theta$$

$$\tau^*_{r\theta[2n-1]} = -\frac{\alpha_{[2n-1]}}{4}\left[\frac{r^{n-2}}{a^{n-2}}(n-1) + \frac{a^{n+2}}{r^{n+2}} - \frac{nr^n}{a^n}\right]\sin n\theta$$

$$u^*_{r[2n-1]} = \frac{a\alpha_{[2n-1]}}{4E(n+1)}\left\{\left[(1+\nu)\left[\frac{r^{n-1}}{a^{n-1}}(n+1)\frac{a^{n+1}}{r^{n+1}}\right] - [n-2+\nu(n+2)]\frac{r^{n+1}}{a^{n+1}}\right]\cos n\theta - 4L_n\cos\theta\right\}$$

$$u^*_{\theta[2n-1]} = -\frac{a\alpha_{[2n-1]}}{4E(n+1)}\left\{\left[(1+\nu)\left[\frac{r^{n-1}}{a^{n-1}}(n+1) - \frac{a^{n+1}}{r^{n+1}}\right] - [n+4+n\nu]\frac{r^{n+1}}{a^{n+1}}\right]\sin n\theta - 4L_n\sin\theta\right\} \qquad (3.21)$$

For trial function i = [2n], n≥2:

$$\sigma^*_{r[2n]} = -\frac{\alpha_{[2n]}}{4}\left[\frac{r^{n-2}}{a^{n-2}} + \frac{a^{n+2}}{r^{n+2}}(n+1) - \frac{a^n}{r^n}(n+2)\right] \cos n\theta$$

$$\sigma^*_{\theta[2n]} = \frac{\alpha_{[2n]}}{4}\left[\frac{r^{n-2}}{a^{n-2}} + \frac{a^{n+2}}{r^{n+2}}(n+1) - \frac{a^n}{r^n}(n-2)\right] \cos n\theta$$

$$\tau^*_{r\theta[2n]} = \frac{\alpha_{[2n]}}{4}\left[\frac{r^{n-2}}{a^{n-2}} - \frac{a^{n+2}}{r^{n+2}}(n+1) + \frac{na^n}{r^n}\right] \sin n\theta$$

$$u^*_{r[2n]} = -\frac{a\alpha_{[2n]}}{4E(n-1)}\left\{\left[(1+\nu)\left[\frac{r^{n-1}}{a^{n-1}} - \frac{a^{n+1}}{r^{n+1}}(n-1)\right] + [n+2+\nu(n-2)]\frac{a^{n-1}}{r^{n-1}}\right] \cos n\theta + 4\,L_n \cos\theta\right\}$$

$$u^*_{\theta[2n]} = \frac{a\alpha_{[2n]}}{4E(n-1)}\left\{\left[(1+\nu)\left[\frac{r^{n-1}}{a^{n-1}} + \frac{a^{n+1}}{r^{n+1}}(n-1)\right] - [n-4+n\nu]\frac{a^{n-1}}{r^{n-1}}\right] \sin n\theta + 4\,L_n \sin\theta\right\} \qquad (3.22)$$

where $L_n = 0$ when n is even

$L_n = (-1)^{\frac{n+1}{2}}$ when n is odd (3.23)

In the above expressions the trial function coefficients α_i have been scaled such that when α_i is unity the maximum hoop stress at the hole $\sigma^*_{\theta i}$ is also unity. This is useful in assessing the relative importance of the various trial functions in particular solutions. The displacements given by the trial functions are defined such that $u^*_{\theta i}$ is zero when $\theta = 0$ or π and $u^*_{\theta i}$ is zero on the hole boundary when $\theta = \pm \pi/2$.

Physically these trial functions may be understood to be solutions for a sheet or annular region containing a traction-free hole with various boundary conditions remote from the hole. For example the solution for an infinite sheet with a hole, stressed at infinity in two directions, as was used in section 3.2, may be obtained for a

circular hole from a linear combination of the trial functions 1 and 4 of this section. It may be seen from equations (3.19) to (3.22) that these are the only trial functions that do not give large stresses as r tends to infinity. For this reason it is found that these functions have the greater contribution to the solution of configurations with special regions which are large relative to the size of the hole.

3.4 Loading function for circular holes

For configurations with loaded holes, a loading function, must be specified which satisfies the traction boundary conditions on the hole exactly (see equation (2.13), section 2.4). The constant coefficient of the loading function, α_o, is here assumed to be unity and the tractions on the hole are represented as Fourier series. Thus the boundary conditions of the loading function are:

$$\sigma^*_{ro} = \sum_{n=0}^{m_1} A_n \cos n\theta \qquad \text{at } r = a$$

$$\tau^*_{r\theta o} = \sum_{n=1}^{m_2} D_n \sin n\theta \qquad \text{at } r = a \tag{3.24}$$

where m_1 and m_2 are the finite limits of the Fourier series and A_n and D_n are the known coefficients, determined from the specified tractions on the hole. A further requirement of the loading function is that the stresses approach zero remote from the hole, i.e.:

$$\sigma^*_{ro} = \tau^*_{r\theta o} = 0 \qquad \text{as } r \to \infty \tag{3.25}$$

With the boundary conditions (3.24) and (3.25) all the arbitrary constants of equation (3.15) may be determined and thus the loading function is given by:

$$\sigma^*_{ro} = \frac{a^2}{r^2} A_o + \{\frac{a}{4r}(A_1-D_1)(3+\nu) + \frac{a^3}{4r^3}[A_1(1-\nu)+D_1(3+\nu)]\} \cos\theta$$

$$+ \sum_{n=2}^{m_3} \{-\frac{1}{2}[nA_n-(n+2)D_n](\frac{a}{r})^{n+2} + \frac{1}{2}(n+2)(A_n-D_n)(\frac{a}{r})^n\} \cos n\theta$$

$$\sigma^*_{\theta o} = -\frac{a^2}{r^2} A_o + \{-\frac{a}{4r}(A_1-D_1)(1-\nu) - \frac{a^3}{4r^3}[A_1(1-\nu)+D_1(3+\nu)]\} \cos\theta$$

$$+ \sum_{n=2}^{m_3} \{\frac{1}{2}[nA_n-(n+2)D_n](\frac{a}{r})^{n+2} - \frac{1}{2}(n-2)(A_n-D_n)(\frac{a}{r})^n\} \cos n\theta$$

$$\tau^*_{r\theta o} = \{-\frac{a}{4r}(A_1-D_1)(1-\nu) + \frac{a^3}{4r^3}[A_1(1-\nu)+D_1(3+\nu)]\} \sin\theta$$

$$+ \sum_{n=2}^{m_3} \{-\frac{1}{2}[nA_n-(n+2)D_n](\frac{a}{r})^{n+2} + \frac{1}{2}n(A_n-D_n)(\frac{a}{r})^n\} \sin n\theta$$

$$u^*_{ro} = \frac{a}{2E} \{-\frac{2a}{r} A_o(1+\nu) + \frac{(1+\nu)}{4}[2(A_1-D_1)(3-\nu)\log(\frac{r}{a}) - \frac{a^2}{r^2}(A_1(1-\nu)+D_1(3+\nu))$$

$$- A_1(3+\nu) - D_1(1-\nu)] \cos\theta$$

$$+ \sum_{n=2}^{m_3} [\{\frac{(1+\nu)}{(n+1)}(nA_n-(n+2)D_n)[\frac{a}{r}]^{n+1} - \frac{n+2+(n-2)\nu}{(n-1)}(A_n-D_n)[\frac{a}{r}]^{n-1}\} \cos n\theta$$

$$- \frac{2K_n}{(n^2-1)} \cos\theta]\}$$

$$u^*_{\theta o} = \frac{a}{2E} \{-\frac{(1+\nu)}{4}\{2(A_1-D_1)(3-\nu)\log(\frac{r}{a}) + (\frac{a^2}{r^2}-1)(A_1(1-\nu)+D_1(3+\nu))\}] \sin\theta$$

$$+ \sum_{n=2}^{m_3} [\{\frac{(1+\nu)}{(n+1)}(nA_n-(n+2)D_n)[\frac{a}{r}]^{n+1} - \frac{n-4+n\nu}{(n-1)}(A_n-D_n)[\frac{a}{r}]^{n-1}\} \sin n\theta$$

$$+ \frac{2K_n}{(n^2-1)} \sin\theta]\} \qquad (3.26)$$

where $K_n = 0$ where n is even

$K_n = (-1)^{\frac{n+1}{2}} [A_n(n+2-n\nu) - D_n(2n+1+\nu)]$ when n is odd ,

and m_3 , the limit of Fourier series in this case, is equal to the greater of m_1 and m_2 ($A_n = 0$ for $n > m_1$, $D_n = 0$ for $n > m_2$).

The Fourier coefficients A_n and D_n must be specified to give the magnitude and distribution of the loading on the hole and this is discussed in section 5.4.1. For several standard cases (e.g. cosine pressure distribution, constant pressure over an arc, combined cosine pressure and sine shear distributions) calculation of the required Fourier coefficients has been programmed on the computer so that only the magnitude of resultant force need be specified.

CHAPTER 4

IMPLEMENTATION OF FINITE ELEMENT METHOD

4.1 Introduction

The computer program developed from the formulation of the method described in chapter 2, is based on a program developed at the Royal Aircraft Establishment, Farnborough (R.A.E.) [4.1, 4.2], for the determination of stress intensity factors at cracks, which was made available for the present work. The program was implemented on the ICL 2970 computer at Southampton University and has been substantially extended, incorporating the new trial functions and loading function of chapter 3, and the revisions necessary for their use in determining stress concentration factors at traction-free or loaded holes. The modifications include changes in calculating the areas of elements, to allow for the curvature of the hole, and modifications to the contour integrals, as discussed in chapter 2, due to the inclusion of the loading function. Up to 8 trial functions may be used with this version of the program and up to a total of 54 Fourier coefficients may be specified for the loading function. Further extensions to the program enable various additional means of data input and output to be used, including graphical techniques.

Section 4.2 gives an outline of how the method is carried out in the program. Specific reference is made to seven segments of the program which are listed in Appendix B. These are: NOTCH, AREAS, TRLFNS1, TRLFNS2, LOADFN, BCONDS and ALPHAS. A table of the other subroutines used by the program and a summary of their function will also be found in this appendix (table B2). A summary of the method for using the program on the ICL 2970 computer is given in section 4.3 and further details are given in the appendices C and D. Appendix C gives the requirements for the input of data and appendix D explains the use of various commands for running the program and manipulating the data.

4.2 Structure of the program

The block diagram, figure 4.1, shows the manner in which FESM is implemented by the program. These steps are also noted by comments in the listing of the program segment "NOTCH" (see Appendix B). The numbers in each block of diagram 4.1 refer to the paragraphs below.

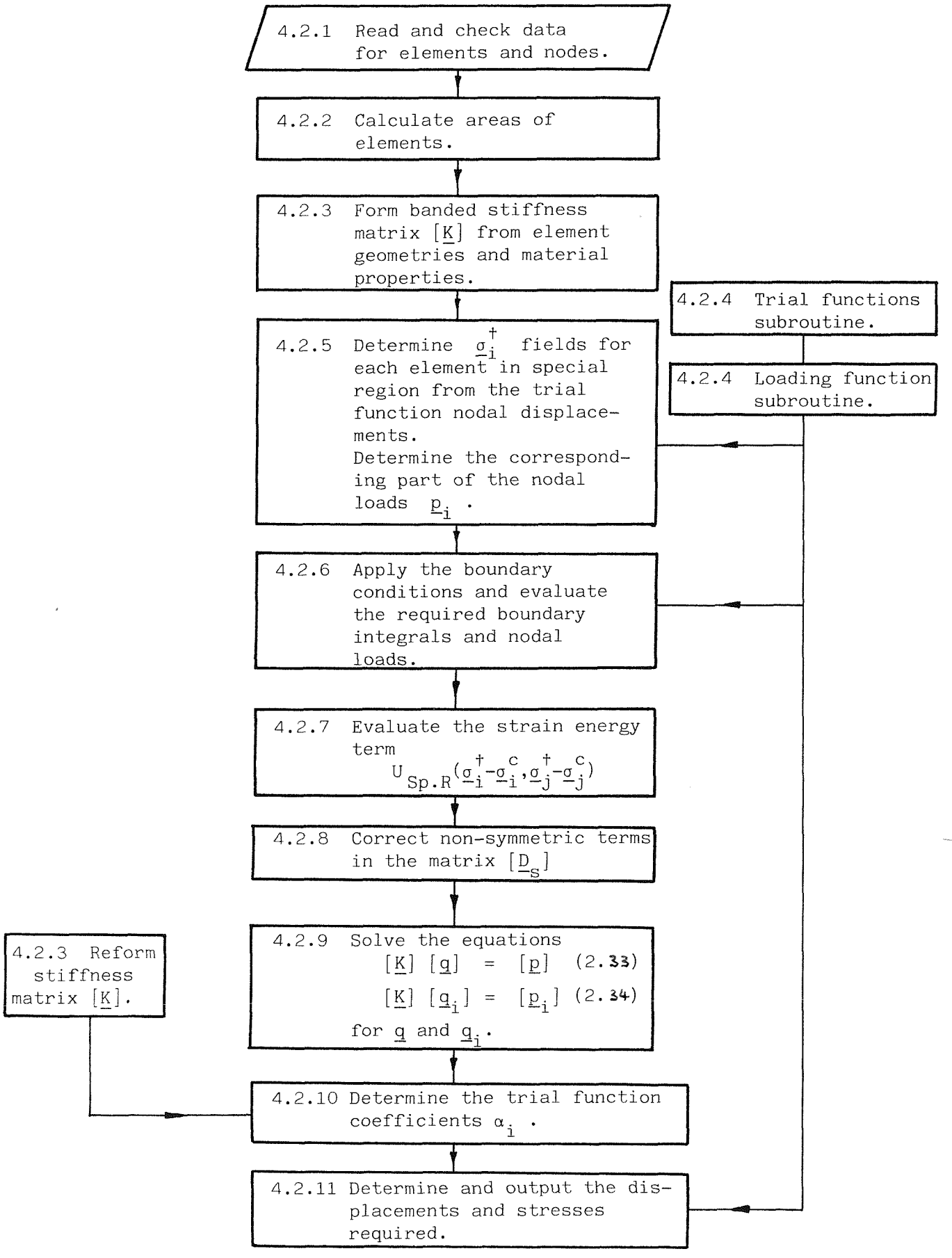

Figure 4.1 Structure of the FESM program.

4.2.1 Data input

The data may be input either from sequential data files (on cards or magnetic tape) or from a direct access file. When the data is read from sequential files it is stored on a direct access file together with the results. The direct access file may then be used to input the results to the graphical facilities or may be modified and re-input to the main program. The data is checked for correct dimensioning, and parameters such as the bandwidth and number of equations are determined. The coordinates of the nodes are transformed to axes which are rotated through an angle γ - i.e. parallel to the ones used by the trial functions. If required the data is printed.

4.2.2 Areas of Elements

The calculation of the areas of the elements is carried out in the subroutine "AREAS" (see appendix B) and is straightforward for the normal triangular elements. On the boundary of elliptical or circular holes however the area of the element will be reduced by the segment of the hole within the triangle of the element (see figure 4.2). The reduction in the area of the element is given by the following formula:

$$\text{Reduction in area} = \frac{1}{2}\{ab\left|\cos^{-1}\left(\frac{x_1}{a}\right) - \cos^{-1}\left(\frac{x_2}{a}\right)\right| - x_2y_1 + x_2y_2\} \qquad (4.1)$$

where (x_1,y_1) and (x_2,y_2) are the coordinates of the nodes on the hole boundary (numbered anti-clockwise round the element) relative to an origin at the centre of the hole.

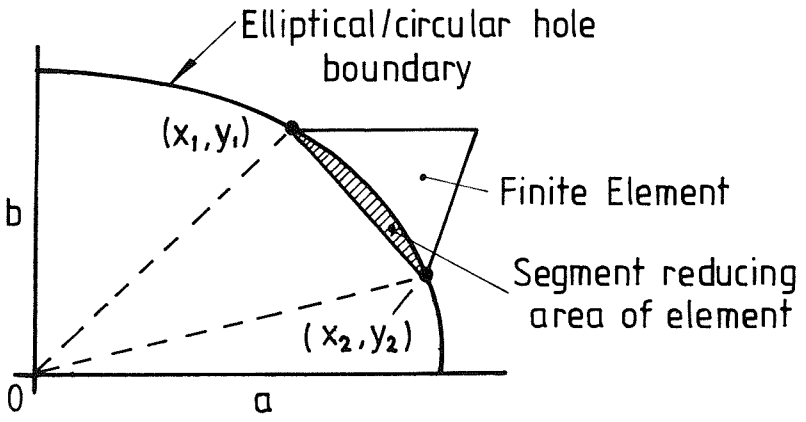

Figure 4.2 Area of element on hole boundary

The effect of reducing the area of these elements in this way is to slightly increase the estimate for the stress. Since no integration is carried out explicitly along the curved part of the boundary no further complications are introduced from having a curved side to the element.

4.2.3 Stiffness matrix

The stiffness matrix $\underline{K}$ is formed from the element geometries and material properties in the normal way for constant strain finite elements (see chapter 2, section 2.6). The subroutines used in this section were developed at R.A.E. [4.3] and have remained unchanged. When the equations are solved (section 4.2.9) $\underline{K}$ is changed and must therefore be re-formed (or it could have been stored) as it is needed to determine the coefficients α_i (section 4.2.10).

4.2.4 Trial and loading functions

The trial functions subroutine gives the stresses and displacements at a point due to a number of trial functions and, where appropriate, the loading function. The subroutine is used at several points in the program. There are three alternative trial function subroutines currently implemented in the program. "TRLFNSØ" is the original routine, used for configurations with a crack. "TRLFNS1" is used for configurations with a circular hole and is based on equations (3.19) to (3.22) with i = 1 to 8. Up to eight trial functions plus the loading function may be used from this subroutine. When the loading function is used a further subroutine "LOADFN" is called, which uses the equations (3.26). "TRLFNS2", based on equation (3.8) with i = 1 and 2, is for configurations with elliptical holes and yields two trial functions. As yet no loading function has been developed for elliptical holes. The subroutines "TRLFNS1", "LOADFN" and "TRLFNS2" are listed in appendix B.

4.2.5 Stress fields $\underline{\sigma}_i^\dagger$

The stress fields $\underline{\sigma}_i^\dagger$ are constant over each element and may therefore be calculated using equations (2.3) and (2.7) from the displacements $\underline{q}_i^\dagger$. These displacements equal $\underline{u}_i^*$ at the element nodes and may be obtained from the trial functions subroutine. The

values of $\underline{\sigma}_i^{\dagger}$ for each element in the special region are stored. The corresponding contribution to the nodal loads vector $\underline{p}_i$ follows from the determination of $\underline{\sigma}_i^{\dagger}$ as shown by equation (2.31b).

4.2.6 Boundary conditions

The boundary condition data is read and the required integrals calculated in the subroutine "BCONDS" (see Appendix B for listing). Figure 4.3 shows the method by which this is carried out.

The boundary conditions are input one by one. On boundaries of the external region or of the hole, no integrations are performed but details of the constraints, for kinematic boundaries, or loads, for traction boundaries, are stored. On the boundaries S_K' or S_T' integrals are evaluated by six point Gauss quadrature to determine the equivalent loads $\underline{p}_i$, the correction stress field $\underline{\sigma}_i^c$, and the integrals of equation 2.43 which are stored in the arrays, DCTR, DCKR, DCT and DS.

When all the boundary conditions have been read and processed, the integrations must be carried out for the interface boundary S_R'. This completes the computation carried out on the boundaries.

4.2.7 Strain energy term

The stresses $(\underline{\sigma}_i^{\dagger}-\underline{\sigma}_i^c)$ have been evaluated for each element in the previous two sections of the program, thus the strain energy term, $U_{Sp.R}(\underline{\sigma}_i^{\dagger}-\underline{\sigma}_i^c,\ \underline{\sigma}_j^{\dagger}-\underline{\sigma}_j^c)$ may be determined using the relationship

$$U(\underline{\sigma}_{Ni}^{\dagger}-\underline{\sigma}_{Ni}^c,\ \underline{\sigma}_{Nj}^{\dagger}-\underline{\sigma}_{Nj}^c) = \frac{1}{2}\ t\Delta\,(\underline{\sigma}_{Ni}^{\dagger}-\underline{\sigma}_{Ni}^c)^T\ \underline{A}\ (\underline{\sigma}_{Nj}^{\dagger}-\underline{\sigma}_{Nj}^c) \qquad (4.2)$$

where the subscript N implies the N'th element. The strain energy term is stored in the array element DCONT(I,J).

4.2.8 Correction to matrix $\underline{D}_S$

Some elements of the matrix $\underline{D}_S$ (in the program, the array DS) must be replaced due to the fact that no integration of the loading function was carried out around the contour of the hole (see section 2.7). The array is corrected at this point in the program.

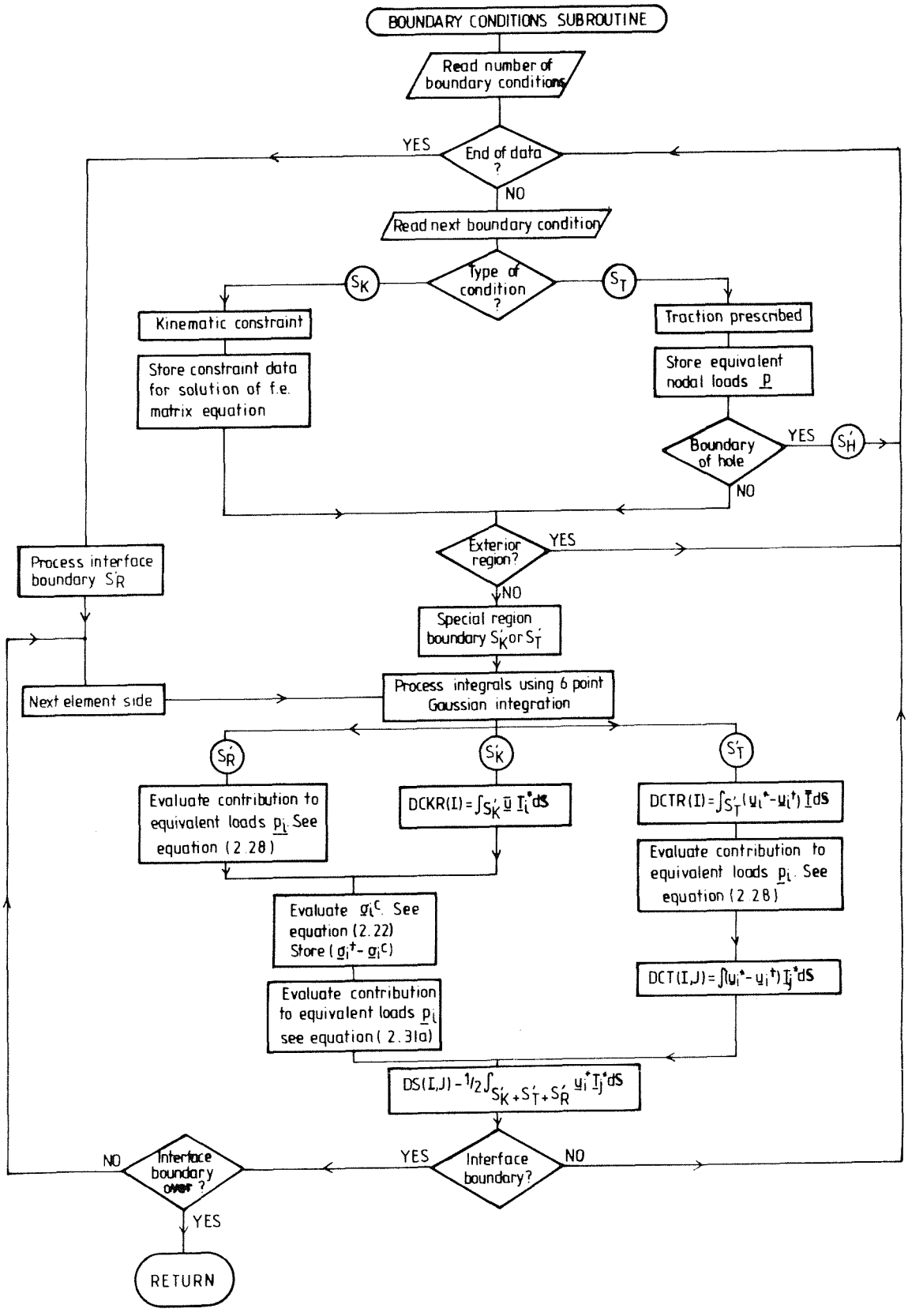

Figure 4.3 Boundary Conditions subroutine

4.2.9 Solution of the equations

The simultaneous equations (2.33) and (2.34), subject to the specified kinematic constraints, (2.35), are now solved using standard finite element subroutines which were developed at R.A.E. [4.3] and have remained unchanged.

4.2.10 Trial function coefficients

The trial function coefficients α_i (i = 1 to k) are determined in the subroutine "ALPHAS" (see appendix B for listing), following the method formulated in section 2.7. Firstly the matrices $\underline{D}'$ and $\underline{F}'$ of equation (2.44) are formed from the arrays, DCT, DS, DCONT, the vectors, DCTR, DCKR, and the loads and displacements, $\underline{p}$, $\underline{p}_i$, $\underline{q}$, $\underline{q}_i$. The stiffness matrix $\underline{K}$ is also required. The final set of equations (2.45) is formed using the relations (2.46) and (2.47) to form the matrices $\underline{D}$ and $\underline{F}$, which correspond to the arrays D and DRHS respectively in the subroutine "ALPHAS".

4.2.11 Displacement and stresses

The displacements and stresses are determined from equations (2.2) and (2.6) as explained in section 2.8. The output required is printed and in addition the coefficients, α_i , and the stresses, $\underline{\sigma}^F - \sum_{i=0}^{k} \alpha_i (\underline{\sigma}_i^\dagger - \underline{\sigma}_i^c)$, for each element are stored on the direct access file. The data on this file may then be used to determine the stress at any point for graphical display or further computation, using the trial functions and loading function subroutines.

4.3 Using the program

This brief section is included in the report to acquaint the readers with the method of using the program on the ICL 2970 computer. Actual users are referred to appendices C and D for further details.

The input data files may be set up as specified in appendix C or by using the automatic mesh generator (see appendix D) which requires fewer parameters for a simple mesh. The "macro" or command "NOTCH" prepares the input and output channels and runs the program with the specified data. If required the graphical output of the stresses on

the boundaries of elements may be obtained, either at a graphics terminal or a hard-copy plotter. When the program has finished running the direct access file will contain all the initial data and the results for the stresses. Further graphs of the stresses may therefore be obtained using the macro "VUSTRESS" or the data may be modified for another run using the macro "MESH".

A convenient way to define the loading on the hole is via the macro "LOADLOAD". If the loading is of the form of those detailed in section 5.4.1 only the magnitude and type of load need be specified and the correct Fourier coefficients will be input to the direct access file.

In conclusion the input and output facilities of the package have been designed to enable the user to run the program quickly and easily, with the minimum of data preparation, and to obtain graphs of the stresses if they are required which facilitate the interpretation of the results.

CHAPTER 5

FINITE ELEMENT RESULTS

5.1 Introduction

Initially the aim in running the new program was to determine the accuracy of the finite element superposition method (FESM) for traction-free holes and the effect on the accuracy of such factors as hole size, mesh refinement and special region size. The configuration chosen for this study was a rectangular plate in uniaxial tension with a central circular or elliptical hole, since alternative estimates of stress for comparison are available in this case. The stress concentration factors obtained were compared with those given by Howland [5.1] and Isida [5.2, 5.3] for similar holes in long strips. This work is described in section 5.2.

In order to compare the accuracy of the stresses at a hole with two other finite element methods, a square plate in tension with a central circular hole was analysed in section 5.3.1. The stress concentration factors are compared with estimates by Allman [5.4] who produced results for this configuration using higher order finite elements. An accurate value for the stress concentration factor for this case was obtained by Hengst [5.5], using an alternating method, and this value was compared with the finite element solutions. New results for the stress concentration near elliptical holes in square plates were also obtained. These stress concentrations for various sizes and aspect ratios of elliptical holes in square plates are presented in section 5.3.2.

The results of sections 5.2 and 5.3 demonstrate the use of FESM for traction-free holes. The method however, as formulated in chapter 2, was specifically developed for the important case of configurations in which tractions exist on the hole, and for these problems FESM has several distinct advantages over other methods of analysis. Firstly, as with traction-free holes, the trial functions can model the boundary of the hole so that only relatively few finite elements are required to represent the geometry of the configuration. Secondly the Fourier representation of load distribution on the hole means that the loading is modelled accurately and, since the stress concentrations required generally occur at or near the application of the load on the hole, this near exact

representation of loading can be expected to give significantly better results than by representing the load in a piece-wise linear form or as nodal forces. The accuracy of the Fourier representation depends on the number of terms included and this can be varied to suit the application. There are relatively few solutions available in the literature for configurations with loaded holes [5.6-5.12] and the available photoelastic results [5.13] are of limited accuracy and applicable only to the particular geometry and loading for which they were prepared. Thus this is an important area of application for the FESM program.

The aim of the work reported in section 5.4 is to confirm the accuracy of the method for configurations with loaded holes by comparison with solutions from other methods. These results are then extended by producing new results for rectangular lugs. In order to carry out the analysis it is necessary to simulate the distributions of the tractions on a loaded hole near a pin. Several such distributions are discussed and their Fourier representations given (section 5.4.1). The hoop stress (i.e. σ_θ at r = a) arising at the hole in an infinite sheet with these loadings is calculated from the loading functions and for some cases compared with the values given by Bickley [5.14]. The stress concentrations for a pressurized hole in an annulus or large plate (section 5.4.2) and those for a symmetrical rectangular lug (section 5.4.3) are compared with known solutions to assess the accuracy of FESM for loaded holes. Finally the new results for stress concentration factors in loaded rectangular lugs are presented (section 5.4.4).

5.2 Rectangular plate with central traction-free hole

The configuration analysed in this section is shown in figure 5.1. A rectangular plate of length 2ℓ and width $2w$, with a central elliptical or circular hole, semi-major axis length a and semi-minor axis length b, is stressed in uni-axial tension by a uniform stress σ_o on its ends. The major axis of the hole is parallel to the shorter sides of the rectangle; the hole boundary is traction-free. When a = b the hole is taken to be a circle of radius a. The ratio of length to width of the rectangle, ℓ/w, is 2.0 for all configurations analysed in this section. This was considered to be the minimum ratio for which good agreement with infinite strips could be expected for hole sizes up to a/w = 0.5.

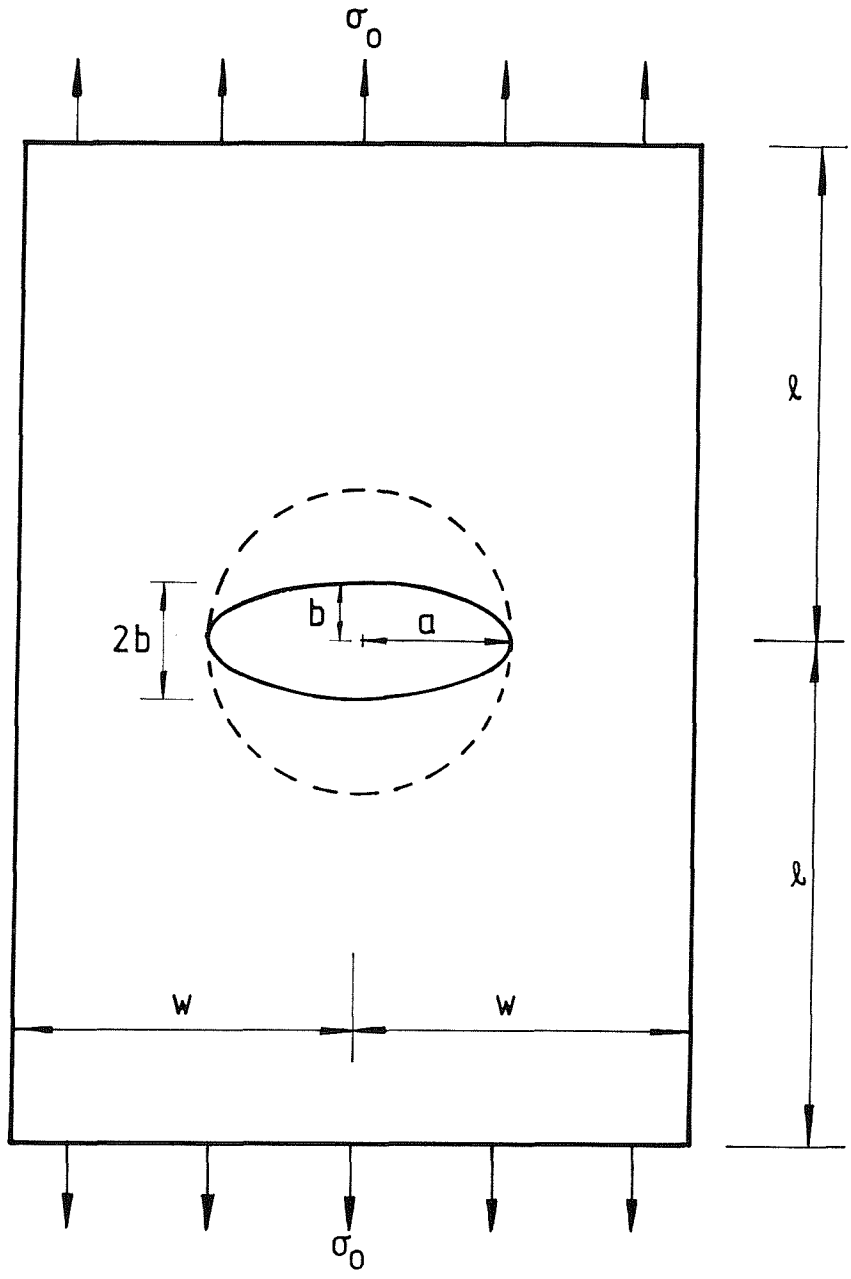

Figure 5.1 Rectangular plate with a central elliptical (or circular) hole.

The maximum stress on the minimum section of the plate calculated by the present method is denoted σ_{max}. A corresponding value of stress determined in previous studies, denoted σ_{ref}, is used to determine a percentage difference term, ε_{ref}, defined as

$$\varepsilon_{ref} = \frac{\sigma_{max} - \sigma_{ref}}{\sigma_{ref}} \times 100\% \qquad (5.1)$$

which is used for comparison of results. The reference values σ_{ref} used throughout section 5.2 were taken from Isida's results for the stress concentration in an infinite strip in tension with a circular or elliptical

hole [5.2, 5.3], which agree with Howland's results for circular holes [5.1] to within 0.7%.

In order for comparison to be made between the FESM results for circular and elliptical holes the trial functions used in sections 5.2.1 to 5.2.3 are those given by equations (3.8) where i = 1 and 2, with the special regions covering the complete mesh in all cases. Identical results are obtained for circular holes by using the trial functions of equations (3.19) to (3.22) with i = 1 and 4.

5.2.1 Effect of mesh refinement

The effect of mesh refinement on the accuracy of solution was shown by analysing the configuration with a circular hole of size a/w = 0.5. Because of symmetry only a quarter of the plate need be divided into elements, and this is done in four regular meshes of varying size which are shown in Appendix E, figures E1 to E4. The mesh size is quantified by the parameter N_o, given by:

$$N_o = a/\delta_o \tag{5.2}$$

where δ_o is a linear dimension of a typical element near to the edge of the hole.

The values of stress concentration calculated firstly by FESM and secondly by the basic constant strain finite element method are shown in Table 5.1. Both solutions are obtained from the program, the basic solution arising from equation (2.33) of the formulation. Comparing the two solutions shows how much improvement is given by the trial functions. The percentage difference between the calculated stress concentration factor, σ_{max}/σ_o, and the value $K_t = 4.348$, given by Isida [5.3] is plotted in figure 5.2 against the mesh size parameter N_o.

Mesh Size Parameter N_o	FESM		Constant Strain Elements	
	$\frac{\sigma_{max}}{\sigma_o}$	ϵ_{ref} c.f. Ref [5.3]	$\frac{\sigma_{max}}{\sigma_o}$	ϵ_{ref} c.f. Ref [5.3]
1	3.923	- 9.8%	2.123	- 51%
2	4.059	- 6.6%	3.145	- 28%
5	4.231	- 2.7%	4.004	- 7.9%
10	4.329	- 0.4%	4.361	+ 0.3%

Table 5.1 The stress concentration factor for rectangular plate in tension (a/w = 0.5) for different meshes.

Figure 5.2 clearly shows the advantage of FESM over constant strain elements for relatively coarse meshes. Both solutions improve in accuracy as the mesh is refined but for the finest mesh, N_o = 10, no advantage is apparent for the superposition method, both methods giving a K_t within 0.5% of that given by Isida. However it was for coarse and medium meshes, which require relatively little data preparation and post-processing, that the superposition method was formulated. Considering that the accuracy will be improved if the additional trial functions are used or if the hole is elliptical or smaller in size, the 3% error obtained with a mesh size of N_o = 5 is satisfactory.

5.2.2 Effect of hole size

A number of rectangular plates with different sizes of circular hole, between a/w = 0.1 and 0.5, were analysed using the FESM program. The same two trial functions were used as in the previous section, derived from equations (3.8) with i = 1 and 2. Typical meshes used for this analysis are shown in Appendix E, figures E5 and E6. The average mesh size parameter N_o for these meshes is approximately 2.

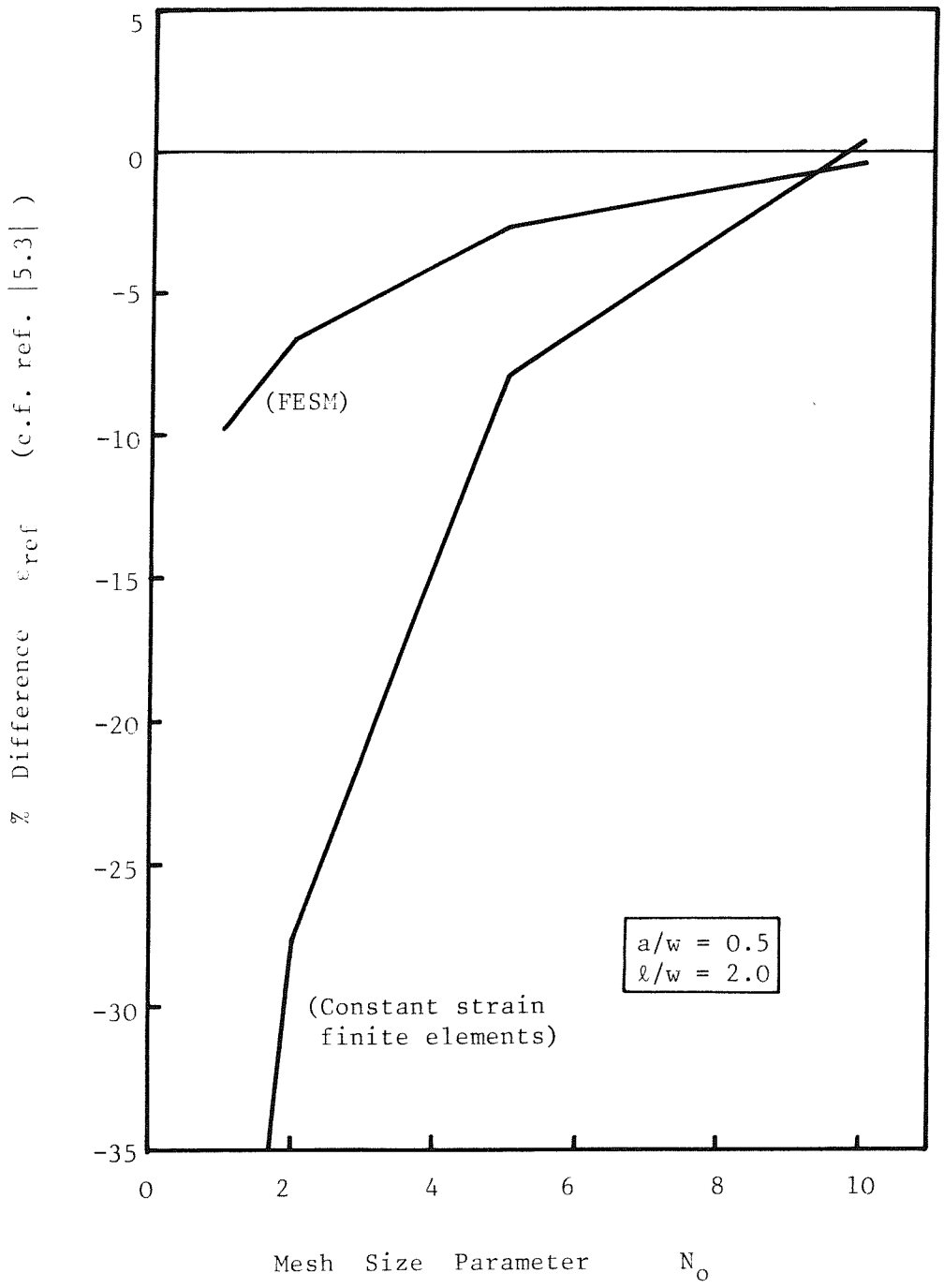

Figure 5.2 Effect of mesh refinement on the accuracy of the stress concentration factor.

Table 5.2 shows the values of stress concentration factor calculated for four sizes of hole using FESM and constant strain finite elements. They are compared with the results given by reference [5.3] and the percentage difference between them is plotted in figure 5.3. Again these results show the superiority of the FESM solutions. Errors in the constant strain finite element solutions of between 20% and 30% are improved by the use of the superimposed trial functions to less than 8% - considerably better for small holes. The accuracy of FESM improves as the hole size is reduced, thus for holes smaller than a third of the plate width the results differ by less than 3% from those of Isida.

	Stress Concentration Factor $\frac{\sigma_{max}}{\sigma_o}$		
Hole Size a/w	FESM	Constant Strain Elements	Ref. [5.3]
0.1	3.033	2.476	3.036
0.15	3.076	2.106	3.084
0.3	3.322	2.527	3.374
0.5	4.018	3.034	4.348

Table 5.2 The stress concentration factor for rectangular plate in tension with various sizes of circular hole.

The reason for the greater accuracy with smaller holes is that the trial functions used in these cases, derived from solutions to an infinite region, model the configuration more closely. The influence of the straight boundaries of the plate on the stress near the hole is less significant with smaller holes and thus there is less correction required from the constant strain finite element field.

5.2.3 Effect of the hole aspect ratio

Stress concentration factors were obtained for the configuration in figure 5.1 ($\ell/w = 2.0$) for elliptical holes with aspect ratios, a/b, in the range 1.0 to 100. Two sizes of hole were analysed, $a/w = 0.25$ and 0.50. The mesh size parameter, N_o was between 1 and 2 for the meshes used, typical examples of which are shown in appendix E, figures E7 to

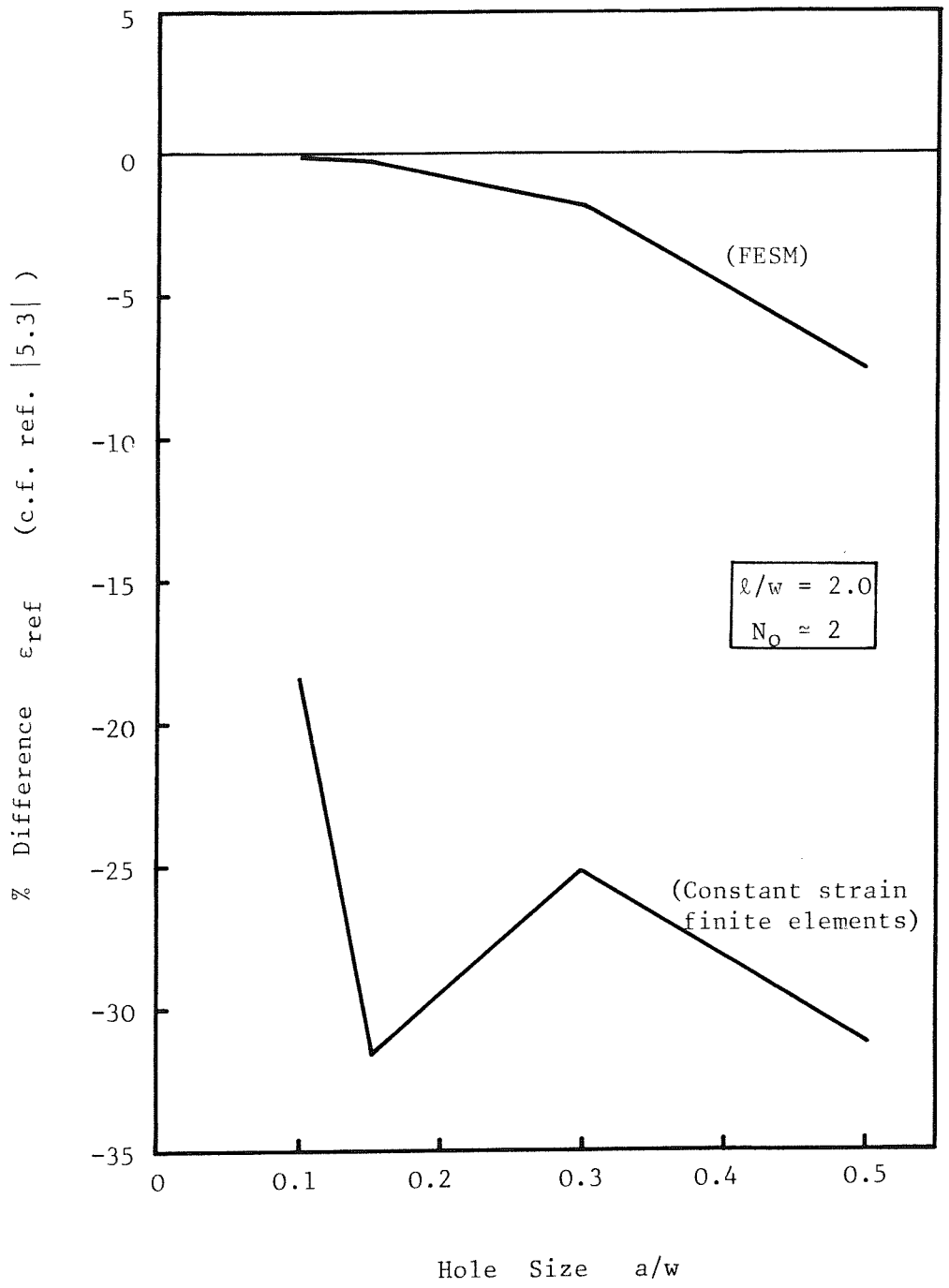

Figure 5.3 Effect of hole size on the accuracy of the stress concentration factor.

E10. The same two trial functions of equation (3.8) were used with the special region covering the complete mesh.

The values of stress concentration factors from the FESM and constant strain finite element solutions are shown in tables 5.3 and 5.4 together with Isida's results with which they are compared. The constant strain finite element solutions become progressively less accurate for sharper elliptical holes, as the meshes used are very coarse, and only a few of these results are entered in the tables. The percentage difference between the FESM and Isida's results are plotted in Figure 5.4.

	Stress Concentration Factor σ_{max}/σ_o		
Hole Aspect Ratio a/b	FESM	Constant Strain Elements	Ref. [5.3]
1.00	3.199	2.15	3.248
1.43	4.082	1.76	4.118
2.00	5.261	-	5.288
3.33	8.018	-	8.044
10.00	21.837	-	21.885
100.00	208.526	-	208.927

Table 5.3 The stress concentration factor for rectangular plate in tension with elliptical hole of varying aspect ratio (a/w = 0.25)

	Stress Concentration Factor σ_{max}/σ_o		
Hole Aspect Ratio a/b	FESM	Constant Strain Elements	Ref. [5.3]
1.00	3.895	4.28	4.348
1.43	4.886	3.12	4.225
2.00	6.215	2.60	6.480
3.33	9.314	-	9.545
10.00	24.892	-	25.265
100.00	235.838	-	238.748

Table 5.4 The stress concentration factor for rectangular plate in tension with elliptical hole of varying aspect ratio (a/w = 0.5).

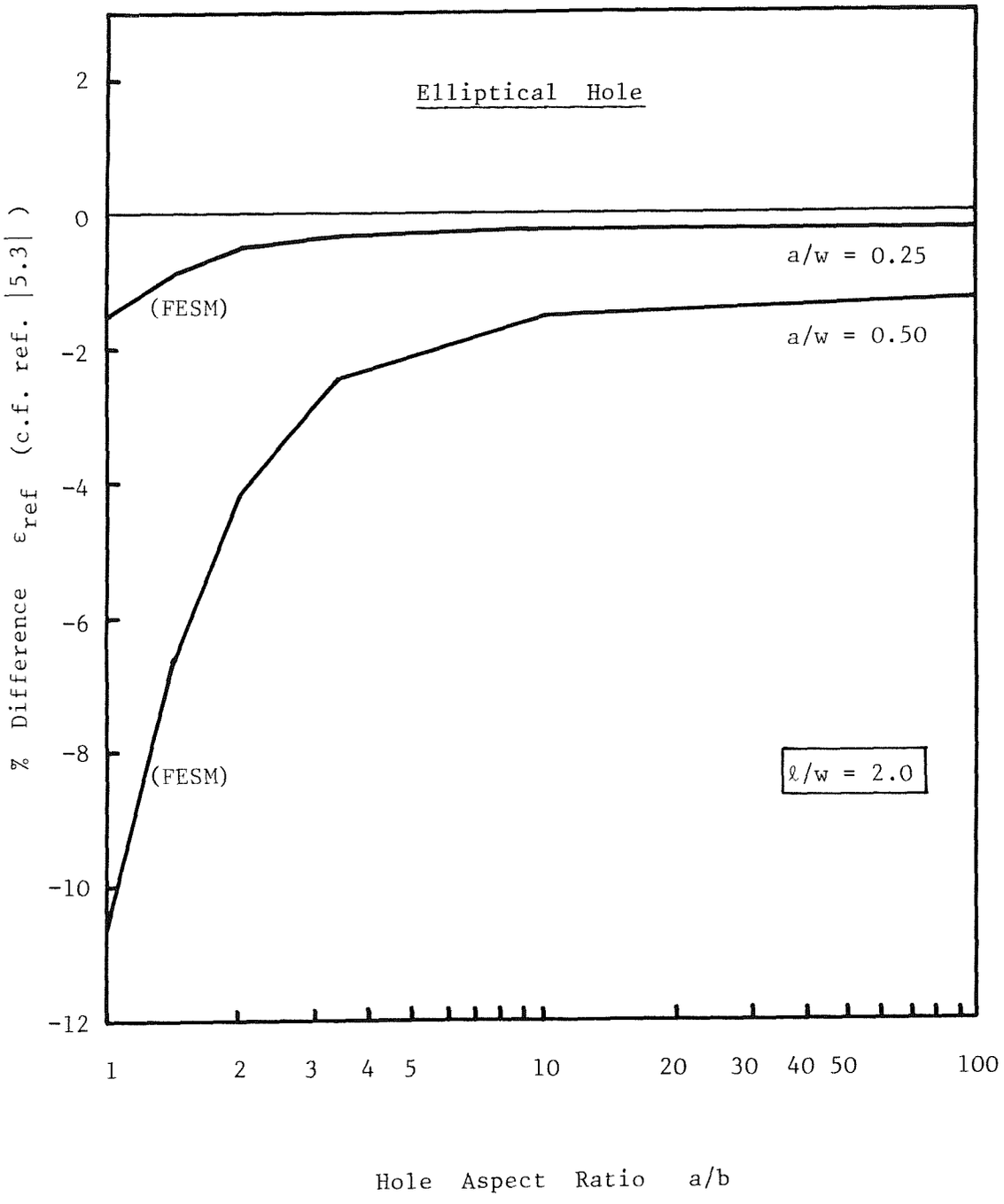

Figure 5.4 Effect of hole aspect ratio on the accuracy of the stress concentration factor.

It will be seen from figure 5.4 that, in contrast to constant strain element results, the accuracy of the FESM solutions increases for sharper elliptical holes. This effect occurs for both hole sizes. Even for these coarse meshes, agreement with Isida to within about 3% is achieved for elliptical holes with a/b > 3 extending up to half the plate width (a/w = 0.5). For the smaller hole size (a/w = 0.25) this accuracy is maintained over the entire range of aspect ratio down to a/b = 1 and for most of the range it is within 1%.

The reason for the increased accuracy with elliptical rather than circular holes may be related to the magnitude of the stress gradient at the edge of the hole. Since with a sharp elliptical hole there is a high stress gradient, the stress reduces rapidly towards the remotely applied stress level and the straight boundaries of the plate affect the solution near the hole less than for holes with larger radii of curvature. Since the trial functions do not model the straight boundaries the less these affect the solution the more accurate FESM will be. FESM is most effective therefore for small holes with small radii of curvature at the tip, or, more generally, where the trial functions chosen closely match the exact solution in the region of the stress concentration.

5.2.4 Effect of special region size and additional trial functions

The two trial functions of equation (3.8) used in the previous sections are sufficient to give accurate results for elliptical holes with quite coarse finite element meshes. In order to achieve similar accuracy for large circular holes (a/w = 0.5), without refining the meshes excessively, the effect of using the additional trial functions given by equation (3.19) to (3.22) with i = 1 to 8 was investigated. Since the configuration analysed has two axes of symmetry only five of these trial functions are appropriate: those with i = 1, 3, 4, 7 and 8. In addition the size of the special region over which the trial functions are superimposed, which in previous examples has covered the entire finite element mesh, was varied restricting it to a smaller area around the hole.

Two new finite element meshes were used for this investigation, denoted A and B, and these are shown in appendix E, figures E11 and E12,

the mesh size parameter N_o being 2 and 3 respectively for the two meshes. The values of K_t estimated from constant strain finite elements alone using meshes A and B differed from the reference value [5.3] by approximately 30% and 15% respectively. The maximum compressive stress, denoted σ_{com}, was included in the comparisons for this study the reference values being given in table 5.5.

Reference	Maximum Stress σ_{max}/σ_o	Maximum Compressive Stress: σ_{com}/σ_o
Isida [5.3]	4.35	-
Howland [5.1]	4.32	- 1.58

Table 5.5 Reference values of stress at the edge of a circular hole in an infinite strip in tension (a/w = 0.5).

The results for σ_{max}/σ_o and σ_{com}/σ_o obtained by FESM are given in table 5.6 for mesh A and table 5.7 for mesh B. The special regions used in each case are shown on the inset figures in the tables. The ratio of the area of the special region to the area taken up by the hole is given by R_A, thus

$$R_A = \frac{\text{Area of special region}}{\text{Area of hole}} \tag{5.3}$$

In this case, since only a quarter of the plate is divided into elements, the denominator in equation (5.3) is a quarter of the total area of the hole.

Three sets of trial functions are used, with each special region, derived from equations (3.19) and (3.22), in order to show the effect of additional functions. These are:

Set i) 2 trial functions (i = 1 and 4)

Set ii) 3 trial functions (i = 1, 3 and 4)

Set iii) 5 trial functions (i = 1, 3, 4, 7 and 8)

SPECIAL REGION	No. of Trial Fns.	$\frac{\sigma_{max}}{\sigma_o}$	$\frac{\sigma_{com}}{\sigma_o}$	ε_{ref} See ref [5.3]	SPECIAL REGION	No. of Trial Fns.	$\frac{\sigma_{max}}{\sigma_o}$	$\frac{\sigma_{com}}{\sigma_o}$	ε_{ref} See ref [5.3]
A0 R_A=9.2	2	4.043	-1.755	-7.1%	A5 R_A=3.6	2	3.895	-1.588	-10.5%
	3	4.043	-1.762	-7.1%		3	3.899	-1.595	-10.4%
	5	4.062	-1.748	-6.6%		5	4.153	-1.397	-4.5%
A1 R_A=6.6	2	4.022	-1.727	-7.5%	A6 R_A=2.9	2	3.907	-1.591	-10.2%
	3	4.020	-1.734	-7.6%		3	3.955	-1.599	-9.1%
	5	4.093	-1.683	-5.9%		5	4.192	-1.435	-3.6%
A2 R_A=5.3	2	3.977	-1.681	-8.6%	A7 R_A=2.6	2	3.869	-1.572	-11.1%
	3	3.975	-1.691	-8.6%		3	3.871	-1.573	-11.0%
	5	4.328	-1.460	-0.5%		5	4.063	-1.406	-6.6%
A3 R_A=5.3	2	3.985	-1.667	-8.4%	A8 R_A=1.8	2	3.844	-1.531	-11.6%
	3	3.986	-1.671	-8.4%		3	3.846	-1.529	-11.6%
	5	4.098	-1.583	-5.8%		5	4.135	-1.339	-4.9%
A4 R_A=4.0	2	3.916	-1.597	-10.0%	A9 R_A=1.5	2	3.925	-	-9.8%
	3	3.986	-1.671	-8.4%		3	3.957	-	-9.0%
	5	4.177	-1.406	-4.0%		5	4.247	-	-4.3%

Table 5.6 The stress concentration factors for different special regions. Mesh A.

SPECIAL REGION	No. of Trial Fns.	$\frac{\sigma_{max}}{\sigma_o}$	$\frac{\sigma_{com}}{\sigma_o}$	ϵ_{ref} See ref [5.3]	SPECIAL REGION	No. of Trial Fns.	$\frac{\sigma_{max}}{\sigma_o}$	$\frac{\sigma_{com}}{\sigma_o}$	ϵ_{ref} See ref [5.3]
B0 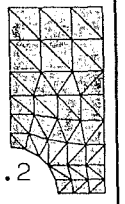 R_A=9.2	2	4.149	-1.752	-4.6%	B5 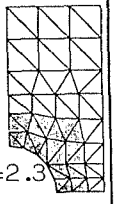 R_A=2.3	2	4.057	-1.658	-6.7%
	3	4.147	-1.757	-4.7%		3	4.052	-1.660	-6.9%
	5	4.158	-1.750	-4.4%		5	4.205	-1.521	-3.3%
B1 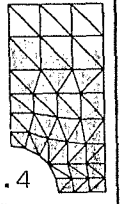 R_A=7.4	2	4.144	-1.745	-4.7%	B6 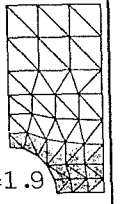 R_A=1.9	2	4.058	-1.559	-6.7%
	3	4.143	-1.748	-4.8%		3	4.059	-1.551	-6.7%
	5	4.177	-1.721	-4.0%		5	4.197	-1.443	-3.5%
B2 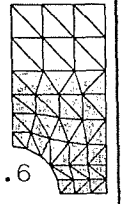 R_A=5.6	2	4.129	-1.722	-5.1%	B7 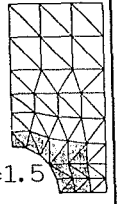 R_A=1.5	2	4.043	-1.551	-7.1%
	3	4.127	-1.726	-5.1%		3	4.039	-1.539	-7.1%
	5	4.212	-1.660	-3.2%		5	4.185	-1.412	-3.8%
B3 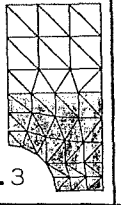 R_A=4.3	2	4.117	-1.710	-5.3%	B8 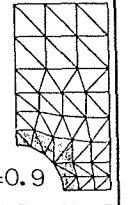 R_A=0.9	2	3.996	-1.538	-8.1%
	3	4.115	-1.716	-5.4%		3	4.005	-1.526	-7.9%
	5	4.236	-1.622	-2.6%		5	4.250	-1.402	-2.3%
B4 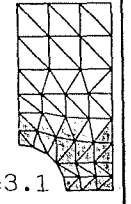 R_A=3.1	2	4.077	-1.665	-6.3%	B9 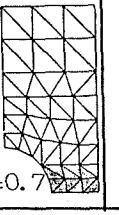 R_A=0.7	2	3.963	-	-8.9%
	3	4.074	-1.668	-6.4%		3	3.970	-	-8.7%
	5	4.206	-1.554	-3.3%		5	4.344	-	-0.1%

Table 5.7 The stress concentration factors for different special regions. Mesh B.

The two trial functions of set (i) give identical results to the two functions from equation (3.8) and correspond to exact solutions for an infinite region with a circular hole under certain remote loading conditions. With the other three functions used in sets (ii) and (iii) the stresses do not die away at infinity and therefore they correspond to exact solutions for plates of finite size. This important fact means that the additional trial functions may introduce some modelling of the finite boundaries of the configuration which was not present in the original two trial functions.

Figures 5.5 and 5.6 show the percentage difference in maximum stress, ε_{ref}, (compared to the results of reference [5.3]) plotted against the special region size R_A for the meshes A and B respectively. The accuracy of the method depends on the shape of the special region as well as its size, which in part accounts for the scatter in the results. Nevertheless a clear trend can be seen in both cases which is indicated by the lines drawn through the points. When only the 2 trial functions of set (i) are used, the most reliable results are given when the special region covers the entire region of the problem, smaller special regions with both meshes giving less accurate results. Adding the third trial function - set (ii) - does not significantly improve the accuracy when the special region extends over the whole plate. This is because the large values of stress given by this function (equation (3.21), i = 3) remote from the hole do not correspond closely to the stresses in the rectangular plate and consequently a small value for its coefficient α_3 is found. For smaller special regions the results for the 3 trial functions are slightly better than for the 2 trial functions with the same special region, however these results are still less accurate than for the 2 functions with a complete special region.

When the 5 trial functions are used in set (iii) the accuracy of the results is improved by up to 3% in each case but it is also found that for special regions sizes from about $R_A = 2$ to $R_A = 6$ an improvement in accuracy is made compared to larger special regions. The value of the maximum compressive stress is also found to be closest to the reference value (see table 5.5) for these special regions. The reason for the improved accuracy with limited special region sizes again relates to the fact that the extra three trial functions in set (iii) (equations

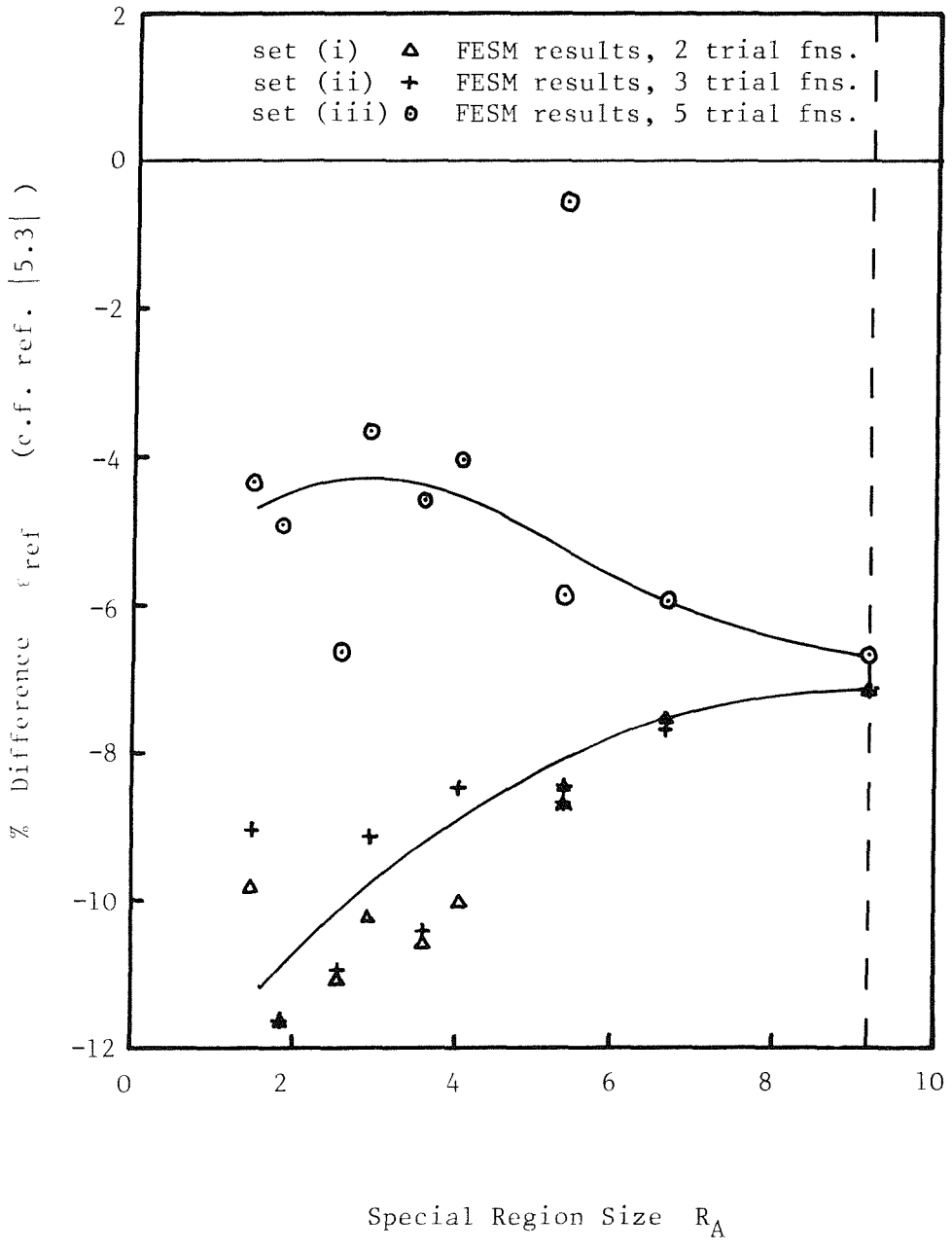

Figure 5.5 Effect of special region size on accuracy for Mesh A

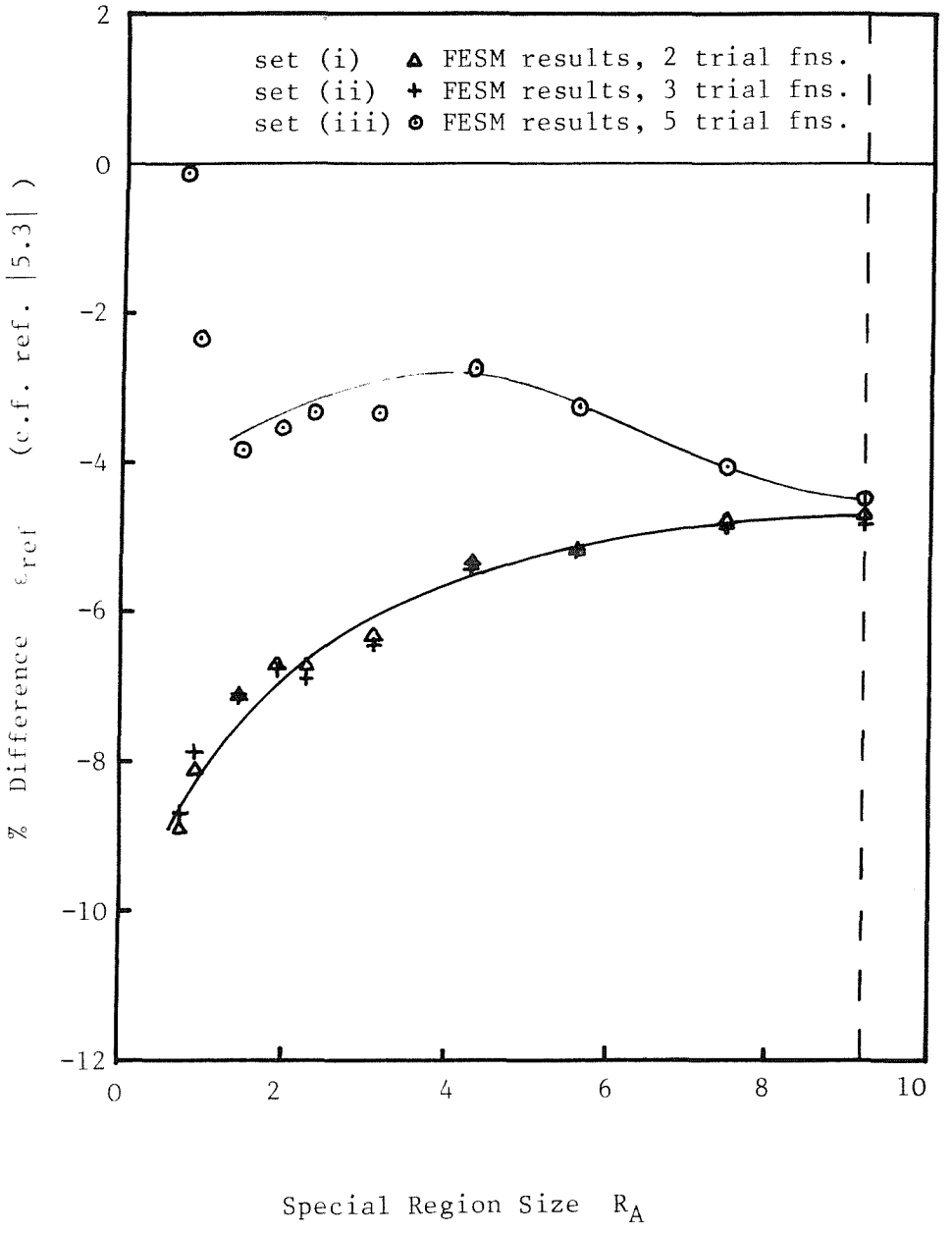

Figure 5.6 Effect of special region size on accuracy for Mesh B.

(3.21)-(3.22) with i = 3, 7 and 8) are not applicable to an infinite region and are therefore more effective with smaller special regions. Very small special regions, for example the smallest regions in tables 5.6 and 5.7, may apparently give quite accurate stress concentration factors, However it is not recommended to use special regions which are so small that significant stress gradients arising from the hole are having to be modelled by the constant strain finite elements of the exterior region. This may lead to inconsistent results and unpredictable errors. The optimum special region size in this case seems to be around $R_A = 4$, and with 5 trial functions this gives an improvement in accuracy of about 2%-3% compared with the results from the 2 trial functions used previously with a complete special region.

5.2.5 Effect of local mesh refinement

Another simple method for improving the accuracy of results is to refine the mesh in the region of the stress concentration. Such a procedure is commonly used in standard finite element solutions, and with FESM it has been found that adding even two or three small elements near the point of interest may improve the accuracy of solution significantly while hardly affecting solution time or data preparation.

Several elements were added to the meshes A and B to give the locally refined meshes A(i), A(ii), B(i) and B(ii) which are shown in appendix E, figures E13-16. These meshes were used to given the results shown in table 5.8 for the rectangular plate in tension with a circular hole (a/w = 0.5). The 5 trial functions (equations (3.19)-(3.22) i =1, 3, 4, 7 and 8) were used in each case and two special regions were used with each mesh: firstly a special region covering the entire mesh (corresponding to the cases A0 and B0 in tables 5.6 and 5.7) and secondly a limited special region (corresponding to the cases A4 and B3 in tables 5.5 and 5.6). The maximum stress concentration is again compared with Isida's results [5.3] and the difference term ε_{ref} is shown in the table 5.8.

These results show that the local refinement of the mesh near to the point of interest does improve the accuracy of the stress concentration factor. The improvement from restricting the special region however, which was observed in section 5.2.4, is not as marked with the

refined meshes. The estimates for K_t from constant strain finite elements alone are also improved by the mesh refinement but unfortunately not consistently. Indeed for the mesh B(ii) the basic finite element solution is much less accurate than for the mesh B which does not have the additional elements.

To summarize the results from sections 5.2.4 and 5.2.5 therefore it may be concluded that the accuracy of solutions is improved by the inclusion of 5 rather than 2 trial functions, particularly if either the special region is of limited size or extra elements are included near to the point of stress concentration.

Mesh	Special Region*	$\frac{\sigma_{max}}{\sigma_o}$	$\frac{\sigma_{com}}{\sigma_o}$	ε_{ref} c.f. Ref.[5.3]
A	A0	4.062	-1.748	-6.6%
	A4	4.177	-1.406	-4.0%
A(i)	A0	4.188	-1.745	-3.7%
	A4	4.198	-1.405	-3.5%
A(ii)	A0	4.247	-1.744	-2.4%
	A4	4.207	-1.405	-3.3%
B	B0	4.158	-1.750	-4.4%
	B4	4.206	-1.554	-2.6%
B(i)	B0	4.272	-1.747	-1.8%
	B4	4.292	-1.621	-1.3%
B(ii)	B0	4.366	-1.747	+0.4%
	B4	4.342	-1.621	-0.2%

(* For shape of special region see tables 5.6 and 5.7).

Table 5.8 Stress concentration factors for plate with circular hole (a/w = 0.5) using different finite element meshes.

5.3 Square plate with central traction-free hole

FESM is used to analyse a square plate in tension with a central circular hole of size a/w = 0.5 (section 5.3.1) and with a central elliptical hole of varying size and aspect ratio (section 5.3.2). In the first case the aim is to compare the results of the new method with those from other finite element methods, more sophisticated than constant strain finite elements. Allman [5.4] gives results from two such methods for the above configuration and Hengst's results [5.5], from an alternating method, give an accurate estimate of stress with which all the finite element results may be compared.

Stress concentration factors for an elliptical hole in a square plate, in common with many configurations with plates of finite size, do not appear in the literature thus such data must be approximated from infinite solutions or obtained from detailed finite element or boundary element analysis. The aim in this case therefore was to obtain new results showing the effect of the finite plate size.

5.3.1 Circular hole

The configuration solved by the FESM program is shown in figure 5.7. The size of the circular hole is a/w = 0.5 and the constant stress on two sides of the square plate is σ_o, the other two sides being traction-free. Hengst's results for this configuration [5.5] are given in table 5.9 showing the maximum tensile stress, σ_{max}/σ_o, and the maximum compressive stress, σ_{com}/σ_o, which occur at the boundary of the hole. The values for a/w = 0.5 are compared with the finite element results of this section.

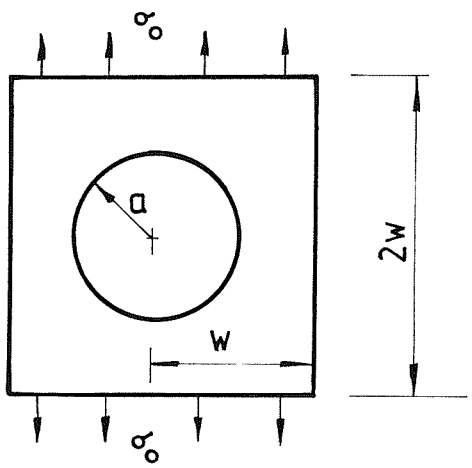

Figure 5.7 Square plate with circular hole.

a/w	Max. Tensile Stress σ_{max}/σ_o	Max. Compressive Stress σ_{com}/σ_o
0.5	6.328	- 3.912
0.375	4.494	- 2.258
0.25	3.580	- 1.472
0.125	3.135	- 1.107

Table 5.9 Stress concentration factors given by reference [5.5] for square plate in tension with circular hole.

Table 5.10 gives the values of stress at the edge of the hole obtained by the FESM program using two finite element meshes, mesh C and mesh D, which are shown on the table and in appendix E, figures E17 and E18. The mesh size parameter for mesh C is approximately $N_o = 4$. The only difference between the two meshes is that in mesh D the nodes near to the points of maximum tensile and maximum compressive stress are moved closer together to give two smaller elements at the corners of the mesh near the hole. Since the rest of the mesh is unchanged it appears somewhat distorted, However this was done to see if improved results would be obtained by this local mesh refinement which does not affect the solution time at all. The same sets of trial functions (from equation (3.19)-(3.22), i = 1, 3, 4, 7 and 8) were used as in section 5.2.4, with 2, 3 or 5 functions being used with each mesh. The special region covered the entire mesh since this corresponds to the optimum special region size ($R_A = 4$) for the rectangular plate used in section 5.2.4.

The percentage difference between the FESM solution and Hengst's results [5.5], shown in table 5.10, indicates close agreement between them. It is interesting to note that mesh D does give better estimates of stress due to the local mesh refinement and that using 3 or 5 trial functions improves the solutions considerably compared to those obtained using only 2 trial functions.

The results from the finite element methods used by Allman [5.4] for the same configuration and using the same mesh (mesh C) are given in table 5.11. The first method was based on a compatible finite element

MESH	No. of trial fns.	$\frac{\sigma_{max}}{\sigma_o}$	% Diff. ε_{ref} cf. [5.5]	$\frac{\sigma_{com}}{\sigma_o}$	% Diff. σ_{com} cf. [5.5]	Unconstr. d.o.f.*
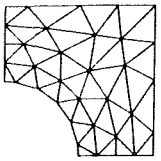 C	2	6.007	-5.1%	-3.538	9.6%	64
	3	6.191	-2.2%	-3.720	4.9%	65
	5	6.179	-2.4%	-3.732	4.6%	67
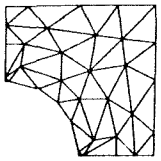 D	2	6.079	-3.9%	-3.662	6.4%	64
	3	6.226	-1.6%	-3.809	2.6%	65
	5	6.231	-1.5%	-3.804	2.8%	67

(* d.o.f. = degrees of freedom)

Table 5.10 Stress concentration factors for square plate with circular hole (a/w = 0.5) by FESM.

model using 6-noded triangular elements with a quadratic displacement field. The second method, developed to avoid the discontinuities of stress that occur across inter-element boundaries in compatible finite element methods, was based on an equilibrium finite element model. The triangular elements were divided into three subregions of equal area with a linear distribution of stress over each subregion and conditions of equilibrium being satisfied between subregions and between elements.

Type of finite element method (Ref. [5.4])	$\frac{\sigma_{max}}{\sigma_o}$	% Diff. ε_{ref} cf. [5.5]	$\frac{\sigma_{com}}{\sigma_o}$	% Diff. σ_{com} cf. [5.5]	Unconstr. d.o.f.*
Compatible F.E. method (Quadratic displacement field)	6.55	3.5%	-4.03	-3.0%	220
Equilibrium F.E. method (Linear stress field)	6.06	-4.2%	-3.52	10.0%	116

(* d.o.f. = degrees of freedom)

Table 5.11 Stress concentration factors for square plate with circular hole (a/w = 0.5) by other finite element methods.

A comparison between the FESM results in table 5.10 and those from the other finite element methods in table 5.11 shows that better accuracy is obtained for the same mesh using FESM provided that at least 3 trial functions are used. The marked advantage of the FESM solution however is shown by the very much smaller number of degrees of freedom (i.e. the number of unknowns in the final set of equations). It gives an indication that the FESM program would require less storage and less solution time than the other methods and possibly less data preparation and post-processing.

5.3.2 Elliptical hole

Stress concentration factors for a square plate in uniaxial tension with a central elliptical hole were obtained using the FESM program for various sizes of hole a/w and various aspect ratios of the hole a/b. The two trial functions for an elliptical hole given by equations (3.8) with i = 1 and 2, were used with several different finite element meshes. For the circular holes analysed (a/b = 1.0) the five trial functions of equations (3.19)-(3.22), i = 1, 3, 4, 7 and 8, were used. Three examples of the meshes are shown in appendix E, figures E19 to E21. The special regions covered the total area of the mesh.

A parameter Q is defined as the ratio between the stress concentration factor in the square plate, K_t, and the stress concentration factor for a similar hole in an infinite plate under similar loading, which is denoted K_∞. Thus

$$Q = K_t/K_\infty \tag{5.4}$$

K_∞ may be determined analytically [5.15], for example from equations (3.8), and it is given by the formula:

$$K_\infty = 1 + \frac{2a}{b} \tag{5.5}$$

The parameter Q is given together with the stress concentration factor in table 5.12 for three sizes of elliptical hole, a/w = 0.25, 0.375 and 0.5, and for various aspect ratios. The ratio Q is also given for the limit as $a/b \to \infty$ which is obtained from the stress intensity factor of a crack of length 2a in a square plate. The values shown in table 5.12

		a/w = 0.25		a/w = 0.375		a/w = 0.5	
a/b	TFs*	K_t	Q	K_t	Q	K_t	Q
1.0	2	3.530	1.177	4.284	1.428	6.079	2.026
1.0	5	3.566	1.189	4.433	1.487	6.231	2.077
2.0	2	5.621	1.124	6.442	1.288	7.833	1.567
5.0	2	12.08	1.098	13.39	1.218	15.51	1.410
10.0	2	22.90	1.090	25.17	1.199	28.78	1.370
100.0	2	217.9	1.084	237.8	1.183	269.3	1.340
Crack [5.16]	-	-	1.08	-	1.18	-	1.33

(* No. of trial functions).

Table 5.12 Stress concentration factors for square plate in tension with elliptical hole.

were determined by Isida [5.16] and show good agreement with the FESM results for a narrow elliptical hole with an aspect ratio a/b = 100. The stress concentration factors for circular holes (a/b = 1.0) agree well with the results of Hengst [5.5] (cf. table 5.6), the maximum discrepancy when 5 trial functions are used being 1.5% for the largest hole size, a/w = 0.5. It is difficult to give a reliable estimate of accuracy for the elliptical hole results but by comparison with the results for rectangular plates, errors of less than 3% would be expected in all cases and most of the results should be within 1.5% of the true value.

The ratio of the stress concentration factors for the square plate and infinite plate, Q, has been plotted in figure 5.8 against the hole aspect ratio a/b and, in figure 5.9, against the hole size a/w. Figure 5.8 shows that the variation of Q with aspect ratio is similar for the three sizes of hole, Q reducing as the ratio a/b increases. The insensitivity of the K_t to plate width for larger values of a/b is due to the fact that the higher stresses that occur at the edge of the hole die away rapidly further from the hole, and consequently there is less interaction with the boundary of the finite plate than in the case of circular or near circular holes. The variation of Q with the size of hole, plotted in figure 5.9 shows that Q increases with increasing hole

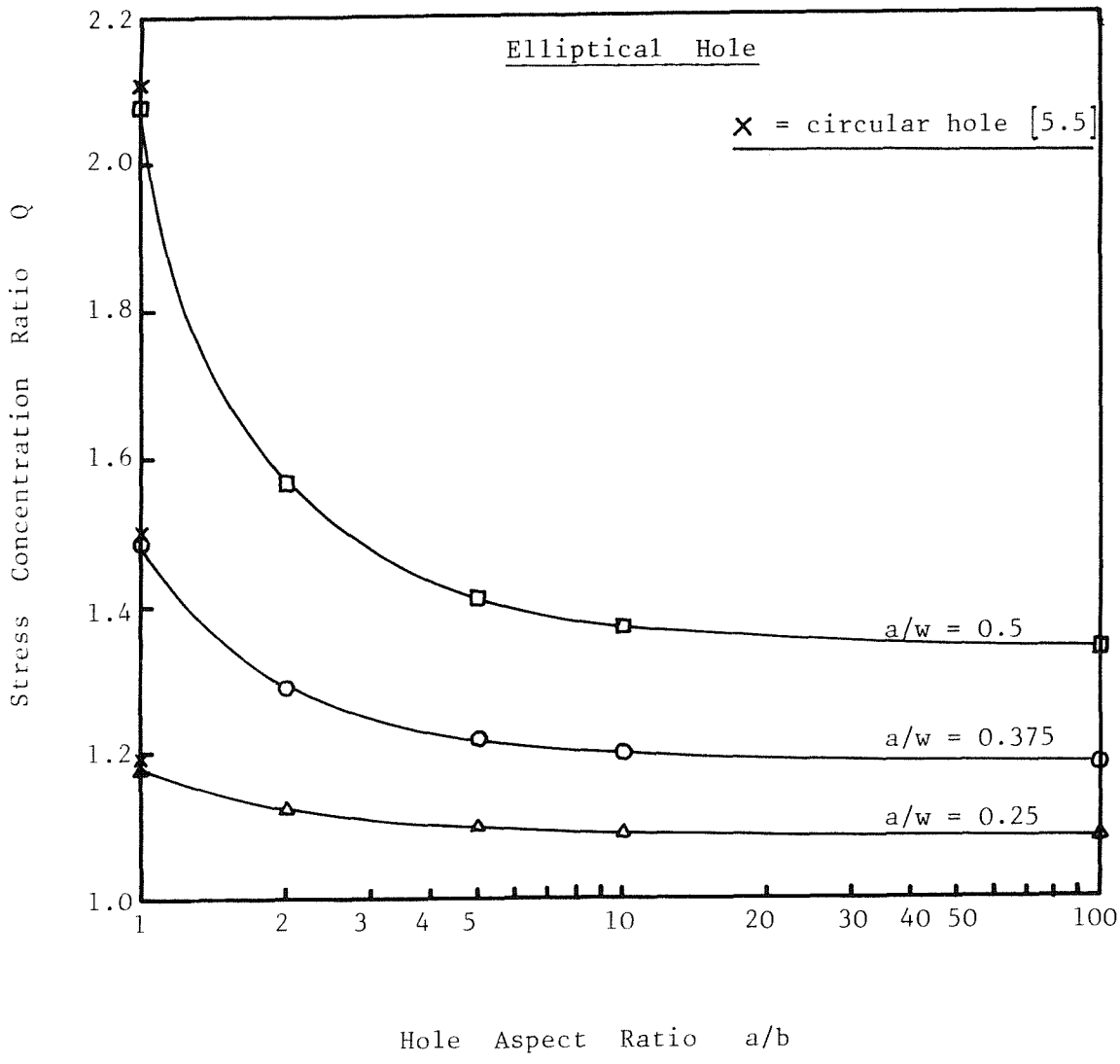

Figure 5.8 Stress concentration results for square plate with elliptical holes of varying aspect ratio

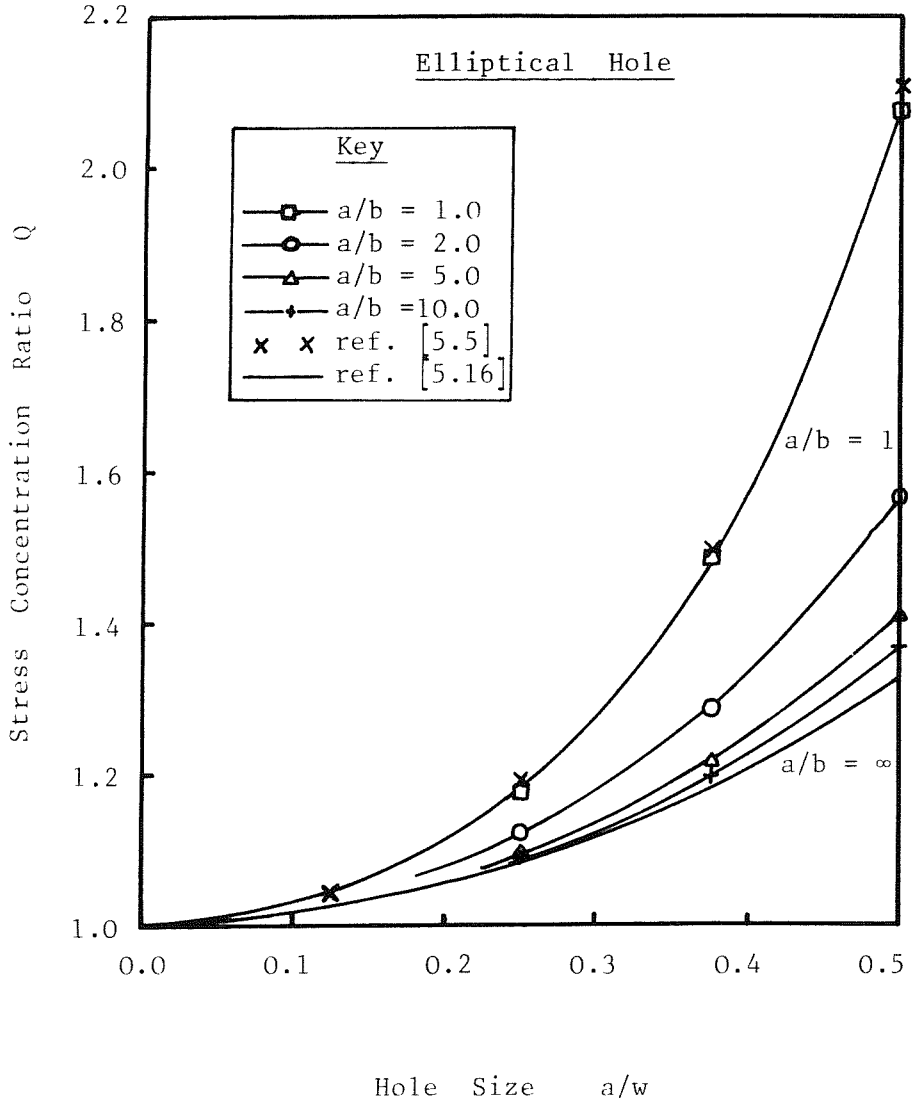

Figure 5.9 Stress concentration results for square plate with elliptical holes of varying size

size. This also is to be expected from considering the influence of the plate boundary on the stress at the hole, as the distance between the hole and plate boundary is reduced for larger a/w ratios. The results for cracks, determined by Isida, are shown on figure 5.9 as they give the limit for elliptical holes as the aspect ratio a/b tends to infinity. As was seen from table 5.8 these results lie very close to the FESM results for elliptical holes with a/b = 100.

5.4 Configurations with loaded circular holes

Having confirmed that the finite element superposition method yields accurate results (typically within 3%) for stress concentration factors in configurations with traction-free holes, and having used the method for the determination of unknown stress concentrations factors in such cases, the application of the method is extended to configurations with loaded holes using a loading function. The loading function was introduced in the formulation of the method in section 2.4 and derived in terms of arbitrary Fourier coefficients A_n and D_n in section 3.4. Thus the boundary conditions on the hole are given by:

$$\left.\begin{aligned} \sigma_r\ (r = a) &= \sum_{n=0}^{m_1} A_n \cos n\theta \\ \tau_{r\theta}\ (r = a) &= \sum_{n=1}^{m_2} D_n \sin n\theta \end{aligned}\right\} \qquad (5.6)$$

where r and θ are polar coordinates relative to the trial function axes (origin at the centre of the hole) and m_1 and m_2 are the limits of the Fourier approximations.

The trial function axes may be rotated by an angle γ relative to the global axes, which define the finite element geometry. In the lugs discussed in sections 5.4.3 and 5.4.4 , $\gamma = \pi/2$. Before the method can be used to analyse simple lug joints for example, the coefficients A_n and D_n must be determined for typical loadings on the hole. This is done in section 5.4.1 and for each loading considered the stresses that would occur around the hole in an infinite sheet are given.

In order to determine the accuracy of the method for loaded holes the values of stress obtained by FESM for an internally pressurized

annulus and a large plate with a pressurized hole are compared with the exact solutions for these geometries in section 5.4.2. Stress concentration factors are also obtained for a rectangular plate with a central circular hole loaded with uniform tension on one end and different "pin-load" distributions on the hole (section 5.4.3). These results are compared with those of Knight [5.6], Theocaris [5.7], Cartwright [5.8], Newman [5.10] and Whitehead [5.9].

Finally some new results are obtained in section 5.4.4 for loaded rectangular lugs showing the effect of varying the amount of material above the hole for different load distributions. These results supplement those given by Whitehead [5.9] for lugs with rounded ends.

5.4.1 Various loadings on a circular hole

The exact distribution of load transferred by a rivet or bolt to a lug is in general unknown and will depend on many factors including the geometry of the lug, the clearance between the bolt and the hole, the magnitude of the force and the joint lubrication. Several simple approximate loadings have been used by other workers to represent the radial pressure at the hole ($r = a$) and these include:

a) Pressure proportional to $[\cos\theta + 1]$ $\quad (-\pi < \theta \leq \pi)$

b) Pressure proportional to $\cos\theta$ $\quad (-\pi/2 \leq \theta \leq \pi/2)$

c) Pressure proportional to $\cos^2\theta$ $\quad (-\pi/2 \leq \theta \leq \pi/2)$

d) Constant pressure over an arc $\quad (-\beta \leq \theta \leq \beta)$

where the radial pressure is zero over the remainder of the hole, if not specified, and where 2β is the magnitude of the arc in loading (d).

These load distributions, together with some shear loadings considered later in this section, are used in the present work to represent the load on the hole due to a pin or bolt. Other feasible distributions might have been used and indeed some work has been done on more accurate estimates of the load on a pin joint [5.17-5.20] which could have been represented as Fourier series in a similar way. However these load distributions have the advantages of simplicity and the fact that, having been used by other workers, comparisons may be made with other methods.

If loadings d) and c) are applied to both halves of the hole two other load distributions arise which are very simply represented in Fourier form:

e) Constant pressure over the hole $(-\pi < \theta \leq \pi)$

f) Pressure proportional to $\cos^2\theta$ $(-\pi < \theta \leq \pi)$

However these loadings are in equilibrium without other loads on the lug, i.e. there is no resultant load on the hole, and thus in order to use them to obtain the stress concentrations at the mid-section of pin-loaded symmetrical lugs, a superposition principle must be used as explained below. If it is required to find the stress at the point A in figure 5.10 (ii) for example, the configuration in figure 5.10(i) may be analysed instead using the equilibriated loading on the hole, since from symmetry it is clear that the stress at A in figure 5.10(i) is twice that in either 5.10(ii) or 5.10(iii). It should be noted however that only points on the mid-section of a symmetrical component may be dealt with in this way since at other points the stresses in figures 5.10(ii) and 5.10(iii) are not equal. The two load distributions e) and f) have been used in this way for the analysis of symmetrical lugs by FESM and the results compared with those from loadings c) and d) which require more Fourier coefficients to be represented closely (see section 5.4.3).

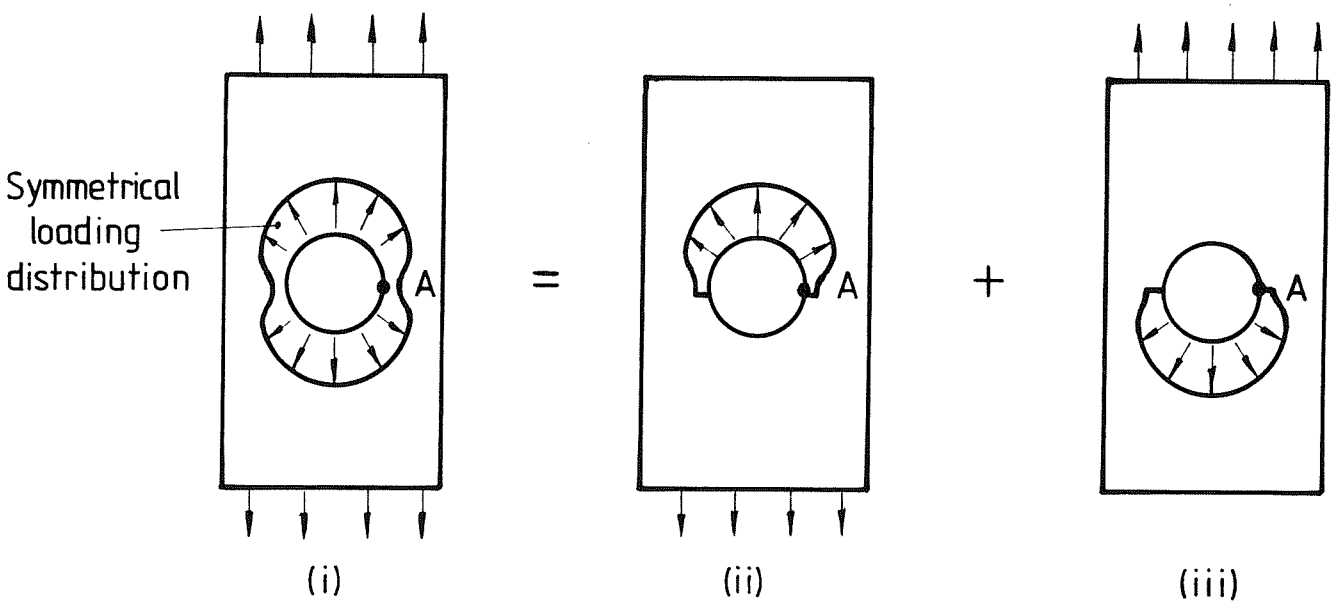

Figure 5.10 Use of a superposition principle to derive the stress concentration factor for the loaded lug (ii) from the configuration (i).

In table 5.13 the following information is given for each of the loadings a) to f).

i) The applied tractions are specified in terms of P which is the resultant force per unit thickness on the hole. In the cases of loadings e) and f) P is the resultant over half the hole ($-\pi/2 \leq \theta \leq \pi/2$) only.

ii) The Fourier coefficients, A_n (n = 0 to m,), are specified. This enables the loading function stresses and displacements to be determined explicitly from equation (3.26).

iii) The figure number for each case shows the Fourier representation of the stresses σ_r and σ_θ at the hole (r = a), in an *infinite* plate, loaded with the particular loading distribution.

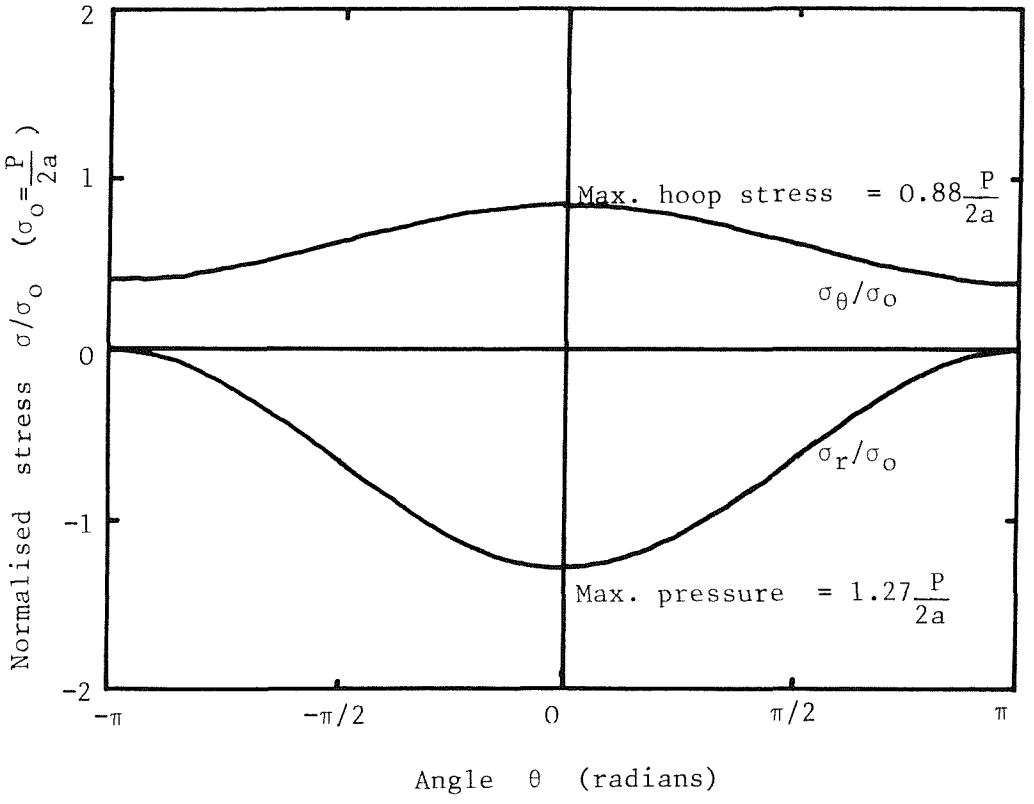

Figure 5.11 Stresses around boundary of hole in infinite sheet
Loading a) Pressure $\propto [\cos\theta + 1]$ $(-\pi < \theta \leq \pi)$.

	Tractions (at r = a)	Fourier coeffs.	Figure
a) $[\cos\theta+1]$ Loading $-\pi<\theta\leq\pi/2$	$\sigma_r = -\frac{P}{\pi a}[\cos\theta+1]$ $\tau_{r\theta} = 0$	$A_o = -\frac{P}{\pi a}$, $A_1 = -\frac{P}{\pi a}$ Other coefficients $= 0$	Fig 5.11
b) $\cos\theta$ Loading $-\pi/2\leq\theta\leq\pi/2$	$\sigma_r = -\frac{2P}{\pi a}\cos\theta$ $(-\pi/2 \leq\theta\leq\pi/2)$ $= 0$ $(\pi/2<\lvert\theta\rvert\leq\pi)$ $\tau_{r\theta} = 0$	$A_o = -\frac{2P}{\pi^2 a}$, $A_1 = -\frac{P}{\pi a}$ $A_n = (-1)^{n/2}[\frac{4P}{\pi^2 a(n^2-1)}]$ where $2\leq n\leq m_1$ & even other coeff. $= 0$	Fig 5.12
c) $\cos^2\theta$ Loading $-\pi/2\leq\theta\leq\pi/2$	$\sigma_r = -\frac{3P}{4a}\cos^2\theta$ $(-\pi/2\leq\theta\leq\pi/2)$ $= 0$ $(\pi/2<\lvert\theta\rvert\leq\pi)$ $\tau_{r\theta} = 0$	$A_o = A_2 = -\frac{3P}{16a}$ $A_n = (-1)^{\frac{n-1}{2}}[\frac{3P}{\pi an(n^2-4)}]$ where $1\leq n\leq m_1$ and odd other coeff. $= 0$	Fig 5.13
d) Constant pressure over an arc $-\beta\leq\theta\leq\beta$	$\sigma_r = -\frac{P}{2a\sin\beta}$ $(-\beta\leq\theta\leq\beta)$ $= 0$ $(\beta\leq\lvert\theta\rvert\leq\pi)$ $\tau_{r\theta} = 0$	$A_o = -\frac{P\beta}{2\pi a\sin\beta}$ $A_n = -\frac{P}{\pi an}\frac{\sin n\beta}{\sin\beta}$ where $1\leq n\leq m_1$	$\beta = \pi/2$ Fig 5.14 $\beta = \pi/6$ Fig 5.15
e) Constant pressure $-\pi<\theta\leq\pi$	$\sigma_r = -\frac{P}{2a}$ $\tau_{r\theta} = 0$	$A_o = -\frac{P}{2a}$ Other coefficients $= 0$	Fig 5.16
f) $\cos^2\theta$ Loading $-\pi<\theta\leq\pi$	$\sigma_r = -\frac{3P}{4a}\cos^2\theta$ $\tau_{r\theta} = 0$	$A_o = -\frac{3P}{8a}$, $A_2 = -\frac{3P}{8a}$ Other coefficients $= 0$	Fig 5.17

Table 5.13 Tractions and Fourier coefficients for various distributions of radial load.

Figure 5.11 shows the distribution of the stresses σ_r and σ_θ (normalized with respect to $\sigma_o = P/2a$) around the hole boundary for loading a). Only two Fourier coefficients are required to represent this loading exactly which may be considered to model approximately the tractions on a hole due to a sideways force on an interference fit pin. It is a special case in that radial pressure at $\theta = \pi$ is zero.

Figure 5.12 shows the stresses around the hole boundary for the more usual representation of a pin load, loading b), where the radial pressure is proportional to cos θ. In common with loadings c) and d) an infinite Fourier series is truncated to a finite number of terms (in this case 30 terms) and consequently the load represented is not exactly a cosine distribution. The exact solution is given by Bickley [5.14] and the difference in the maximum hoop stress (σ_θ at r = a) for $m_1 = 29$ was found to be less than 2%. When used for the analysis of lugs this error is a smaller fraction of the total stress, its effect occurring in the region of the discontinuity in the stress gradient at $\theta = \pi/2$.

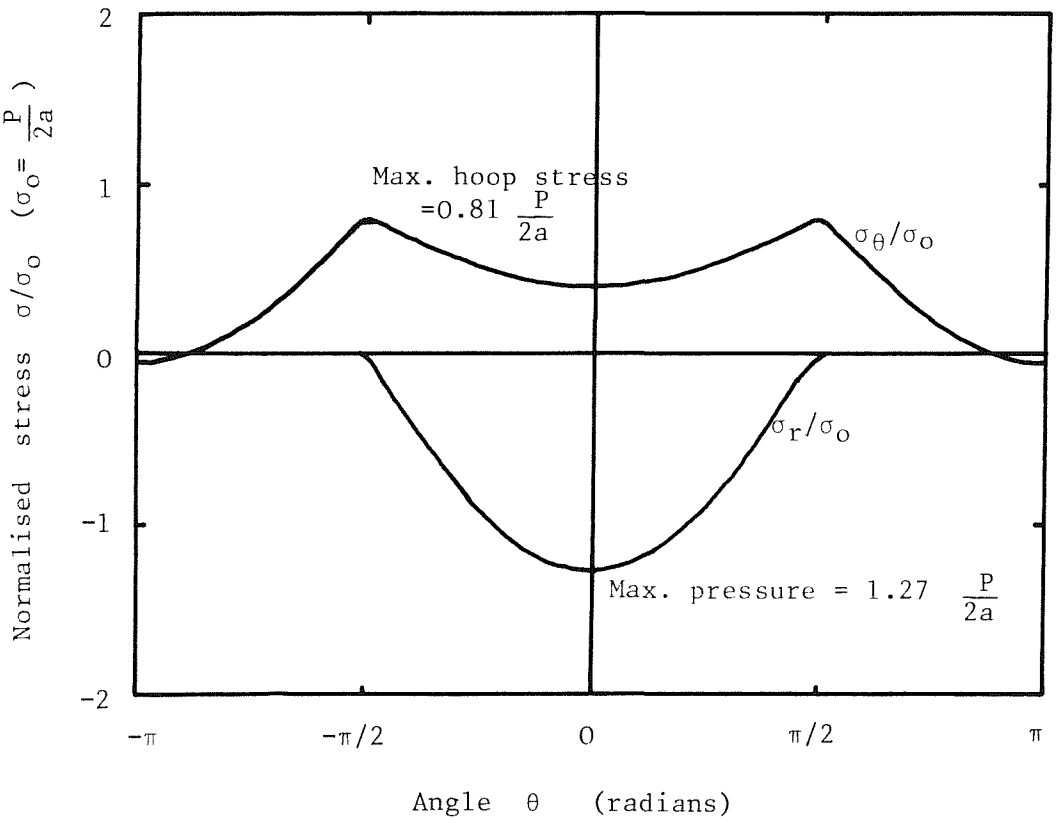

Figure 5.12 Stress around boundary of hole in infinite sheet
Loading b) Pressure $\propto \cos\theta$ $(-\pi/2 \leq \theta \leq \pi/2)$.

As an alternative to this loading the $\cos^2\theta$ loading (c) has some advantages (see figure 5.13). There is no discontinuity in the stress gradient at $\theta = \pi/2$ and consequently the Fourier approximation converges more rapidly and is more accurate for the same number of terms. More of the load is concentrated near to $\theta = 0$ and thus the loading (c) may be considered to model the tractions due to a pin with clearance between the pin and hole. The maximum hoop stress in an infinite sheet with a hole loaded in this way is higher than for loading b) and occurs at an angle θ less than $\pi/2$. The maximum radial pressure is also higher.

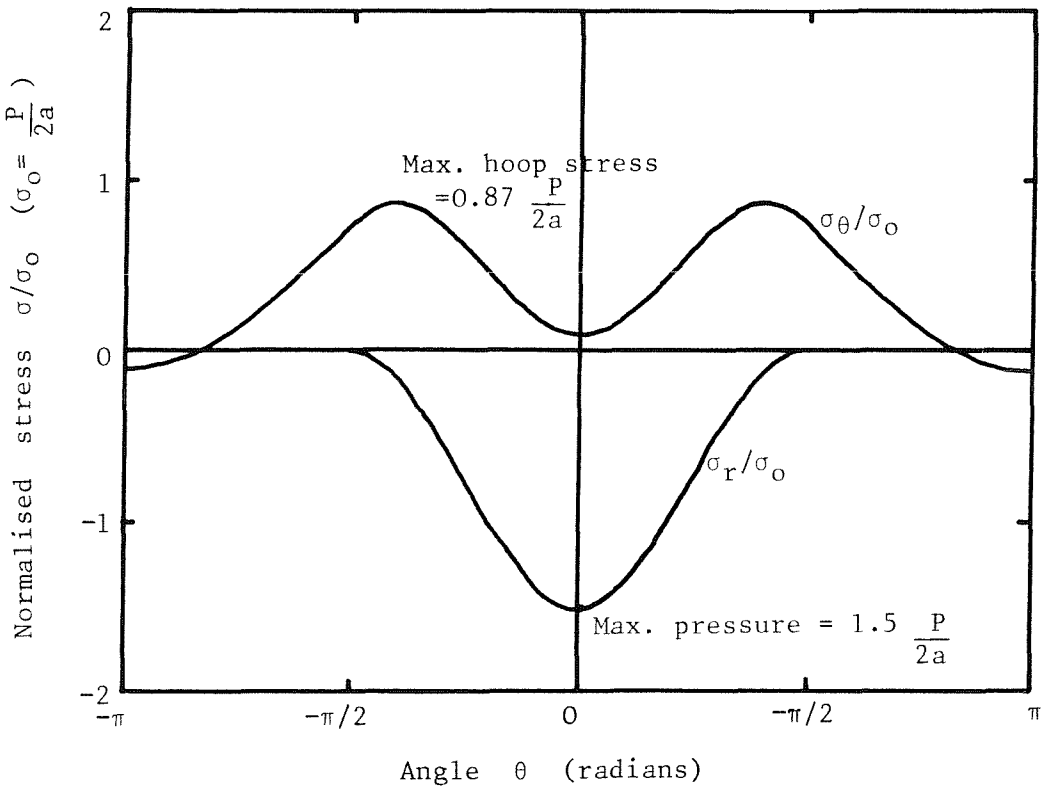

Figure 5.13 Stresses around boundary of hole in infinite sheet
Loading c) Pressure $\propto \cos^2\theta\ (-\pi/2 \leq \theta \leq \pi/2)$.

The Fourier representation of the constant loading over an arc subtending an angle 2β, loading (d), is the slowest to converge (see figures 5.14 ($\beta = \pi/2$) and 5.15 ($\beta = \pi/6$)). This is due to the step change in the magnitude of the radial pressure, which in actual practice is not a feasible distribution of load. For finite element analysis the oscillations in the Fourier representation make exact determination of the stresses more uncertain, However good agreement was found between results from this loading and from loading (e) for symmetrical lugs, which suggests that the inaccuracies in the representation may not be

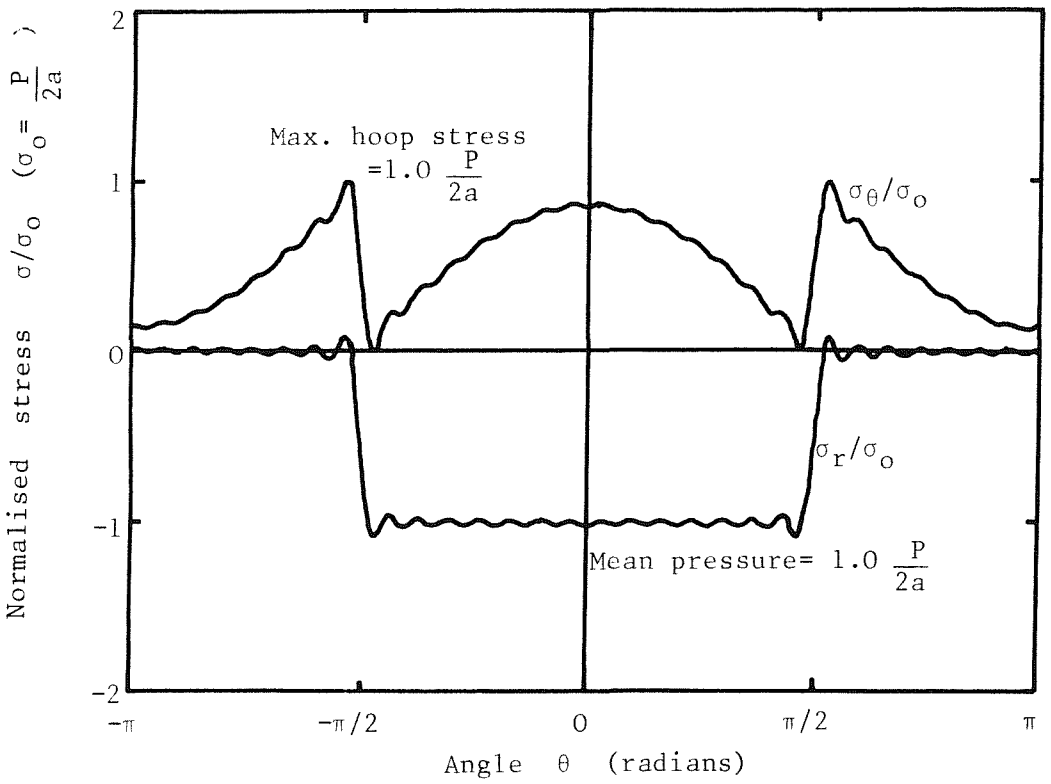

Figure 5.14 Stresses around boundary of hole in infinite sheet Loading d) Constant pressure over ½ of the boundary ($-\pi/2 \leq \theta \leq \pi/2$).

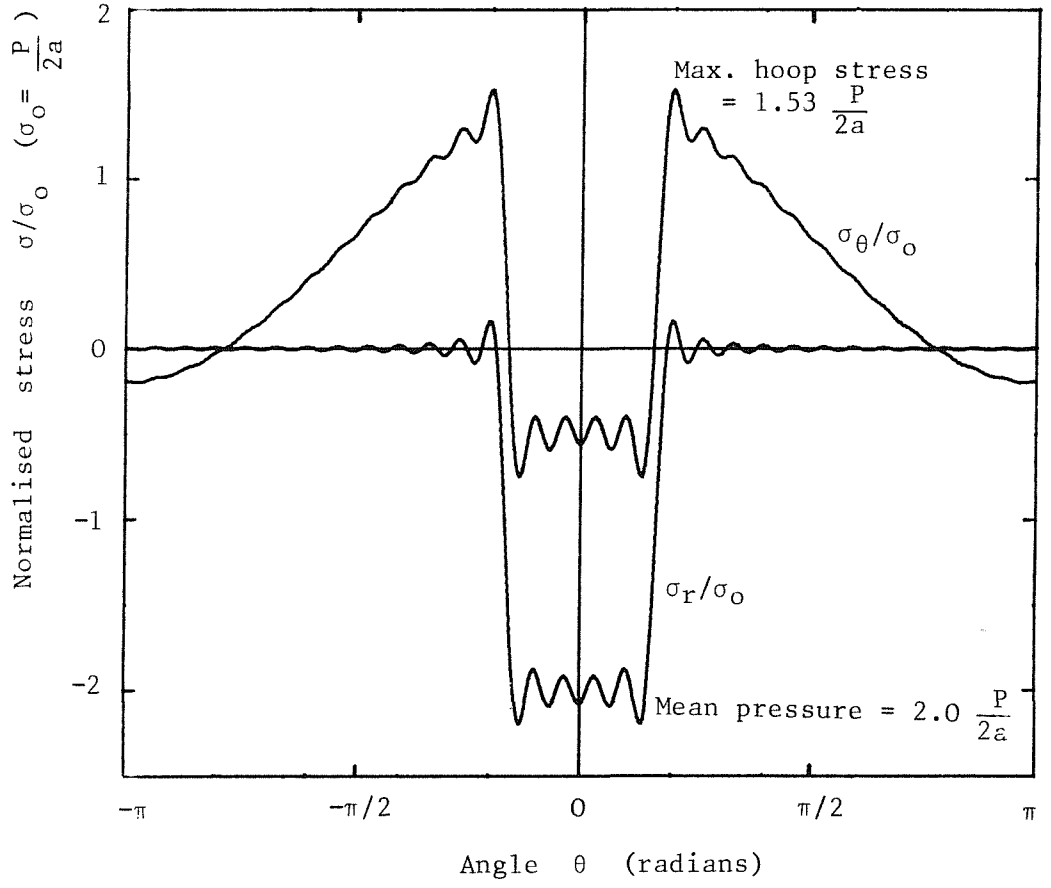

Figure 5.15 Stresses around boundary of hole in infinite sheet Loading d) Constant pressure over 1/6 of the boundary ($-\pi/6 \leq \theta \leq \pi/6$).

important. Bickley [5.14] gives the exact solution for the two cases, $\beta = \pi/2$ and $\beta = \pi/6$, and satisfactory agreement is found. Comparing figures 5.14 and 5.15 it may be seen that reducing the size of the arc of contact increases the maximum radial pressure and the maximum hoop stress for a constant resultant force.

Loadings e) and f) are simply represented using 1 and 2 Fourier coefficients respectively. Figure 5.16 shows that constant pressure over the complete hole causes a constant hoop stress of equal magnitude in an infinite sheet. Loading e) may be used to analyse a symmetrical lug with constant pressure over half the hole (using superposition), or to represent a pressurized hole, or added to other distributions to simulate an interference fit pin (e.g. loading a)). Loading f) is shown in figure 5.17 and also has no resultant load on the hole. It is used for the analysis of symmetrical lugs and gives an estimate for the same stress concentration factor as that obtained from loading c).

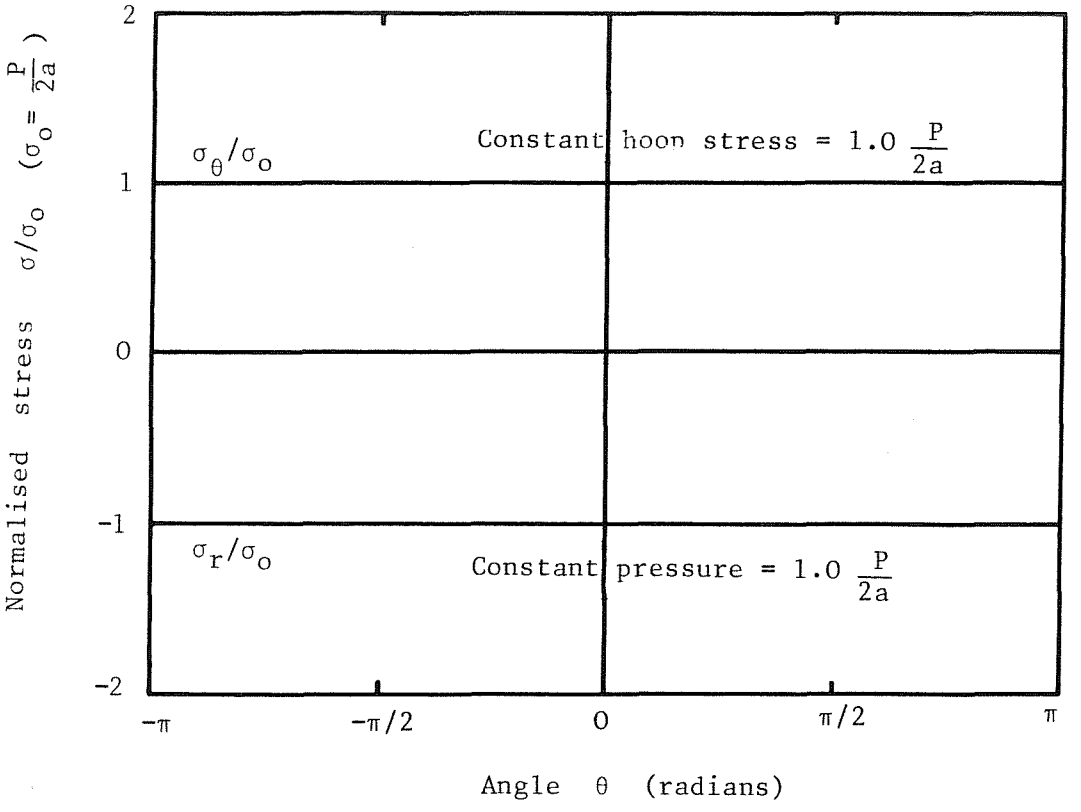

Figure 5.16 Stresses around boundary of hole in infinite sheet
Loading e) Constant pressure ($-\pi < \theta \leq \pi$).

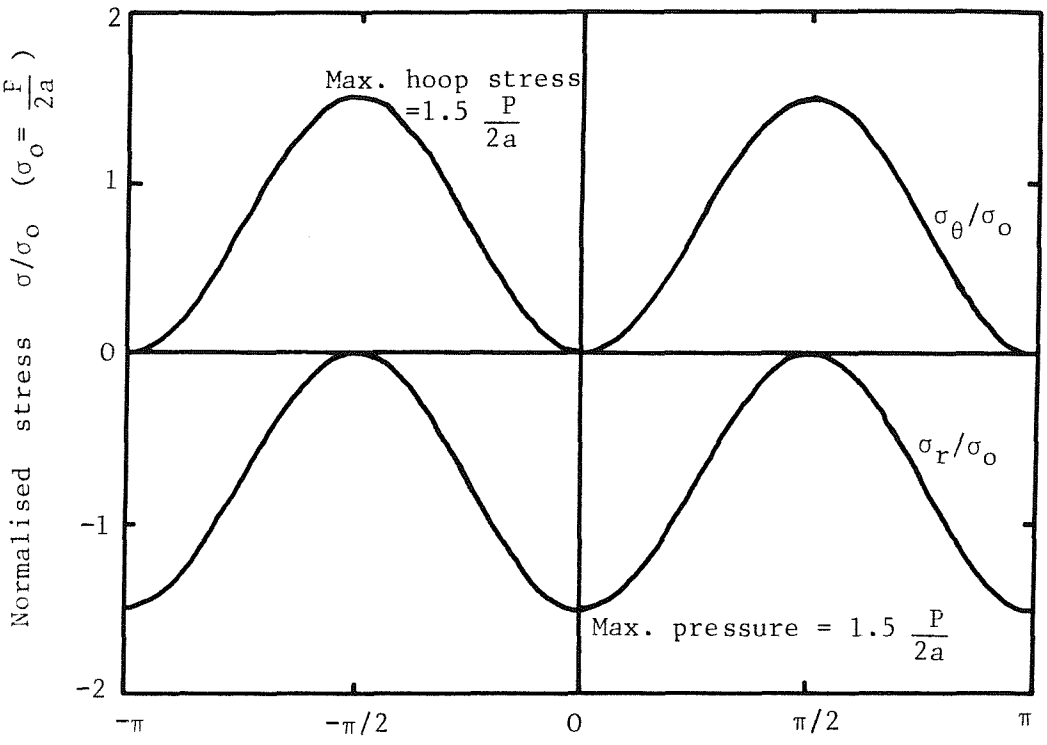

Figure 5.17 Stresses around boundary of hole in infinite sheet. Loading f) Pressure $\propto \cos^2\theta$ $(-\pi < \theta \leq \pi)$

Friction at a bolt or rivet will result in shear tractions thus possible distributions for the shear are now considered. The effect of these is added to the radial pressure such that the resultant force on the hole remains constant. Three possible distributions were used

g) Shear proportional to $\sin\theta$ $(-\pi/2 \leq \theta \leq \pi/2)$

h) Shear proportional to $\sin 2\theta$ $(-\pi/2 \leq \theta \leq \pi/2)$

j) Shear proportional to $\sin^3\theta \cos\theta$ $(-\pi/2 \leq \theta \leq \pi/2)$

The expressions for the tractions and the Fourier coefficients are given in table 5.14. P_s is the resultant force (per unit thickness) on the hole due to the shear tractions and the limit of the Fourier series is m_2.

	Tractions (at r = a)	Fourier Coefficients
g) Sin θ Shear	$\sigma_r = 0$ $\tau_{r\theta} = \frac{2P_s}{\pi a} \sin\theta \; (-\pi/2 \leq \theta \leq \pi/2)$ $= 0 \quad (\pi/2 < \lvert\theta\rvert \leq \pi)$	$D_1 = \frac{P_s}{\pi a}$ $D_n = (-1)^{\frac{n+2}{2}} \frac{4nP_s}{\pi^2 a(n^2-1)}$ for $2 \leq n \leq m_2$ and <u>even</u> Other coefficients = 0
h) Sin 2θ Shear	$\sigma_r = 0$ $\tau_{r\theta} = \frac{3P_s}{4a} \sin 2\theta \; (-\pi/2 \leq \theta \leq \pi/2)$ $= 0 \quad (\pi/2 < \lvert\theta\rvert \leq \pi)$	$D_2 = \frac{3P_s}{8a}$ $D_n = (-1)^{\frac{n+1}{2}} \frac{3P}{\pi a(n^2-4)}$ for $1 < n < m_2$ and <u>odd</u> Other coefficients = 0
j) $\sin^3\theta \cos\theta$ Shear	$\sigma_r = 0$ $\tau_{r\theta} = \frac{15\sqrt{3}\,P_s}{32a} \sin^3\theta \cos\theta \; (-\pi/2 \leq \theta \leq \pi/2)$ $= 0 \quad (\pi/2 < \lvert\theta\rvert \leq \pi)$	$D_2 = \frac{5P_s}{16a}$ $D_4 = -\frac{5P_s}{32a}$ $D_n = (-1)^{\frac{n+1}{2}} \frac{5P_s(n^2-10)}{\pi a(n^2-4)(n^2-16)}$ for $1 \leq n \leq m_2$ and <u>odd</u> Other coefficients = 0

Table 5.14 Tractions and Fourier coefficients for various distributions of shear.

A combination of the shear distribution (g) and the radial pressure distribution (b) was proposed by Knight [5.6] who suggested that the tractions on the loaded half of a hole which is pulled in the direction $\theta = 0$ by a bolt or rivet would be similar to the tractions on a circular contour around a point force in an infinite medium, the other half of the hole being traction free. These tractions are given by:

$$\sigma_r \; (r = a) = \left[\frac{P}{2\pi a} \; \frac{(3-2\nu)}{2(1-\nu)} \right] \cos\theta$$

$$\tau_{r\theta} \; (r = a) = -\left[\frac{P}{2\pi a} \; \frac{(1-2\nu)}{2(1-\nu)} \right] \sin\theta \qquad (5.7)$$

Equation (5.7) gives the ratio of the shear resultant to the radial pressure resultant as:

$$\frac{(1-2\nu)}{(3-2\nu)} \tag{5.8}$$

If ν is taken as 0.25 the ratio of shear to radial pressure resultants is 0.2 which is the value used for the combination of shear and radial loadings in the present work.

The distribution of stresses around the hole in an infinite sheet for this loading (i), which is a combination of loadings b) and g), is shown in figure 5.18. The limits of the Fourier series m_1 and m_2 were chosen to be 29 and 24 respectively. The maximum radial pressure, $\sigma_r(\max)$, shear stress, $\tau_{r\theta}(\max)$, and hoop stress, $\sigma_\theta(\max)$, are found to be:

$$\left.\begin{aligned} \sigma_r(\max) &= -1.06\ \frac{P}{2a} \quad \text{at } \theta = 0 \\ \tau_{r\theta}(\max) &= 0.21\ \frac{P}{2a} \quad \text{at } \theta \simeq \pi/2 \\ \sigma_\theta(\max) &= 1.13\ \frac{P}{2a} \quad \text{at } \theta = \pi/2 \end{aligned}\right\}$$

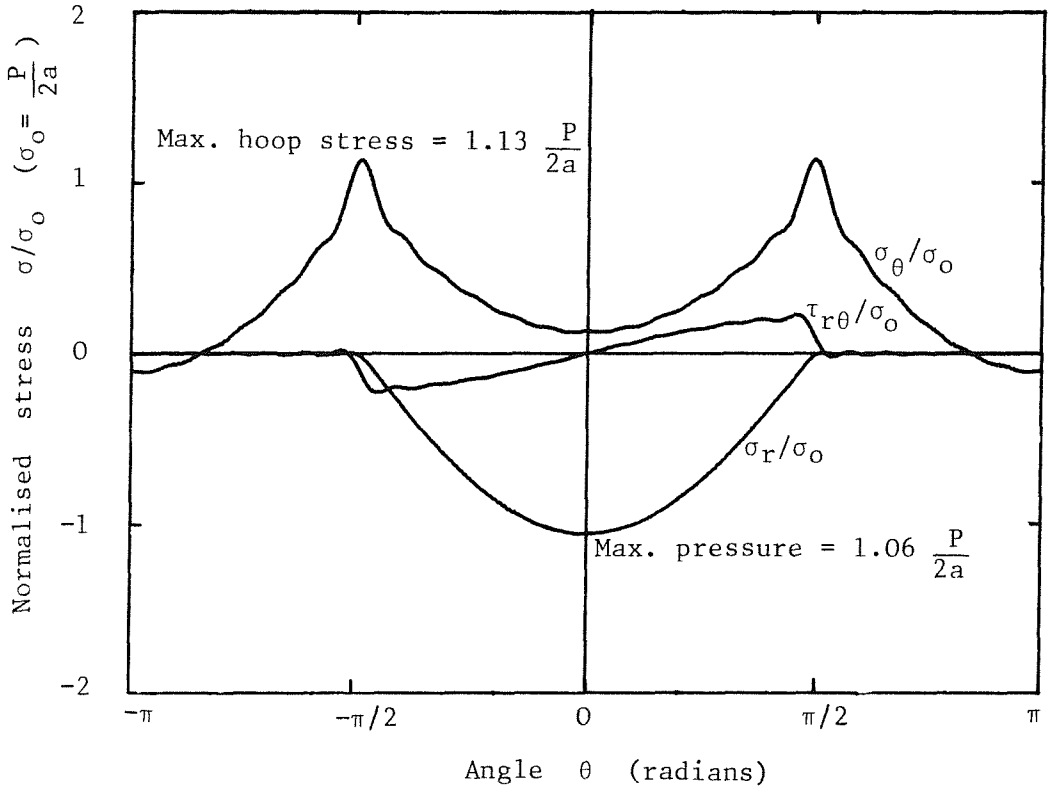

Figure 5.18 Stresses around boundary of hole in infinite sheet.
(i) Loading b) + g) cos θ normal pressure & sin θ shear.

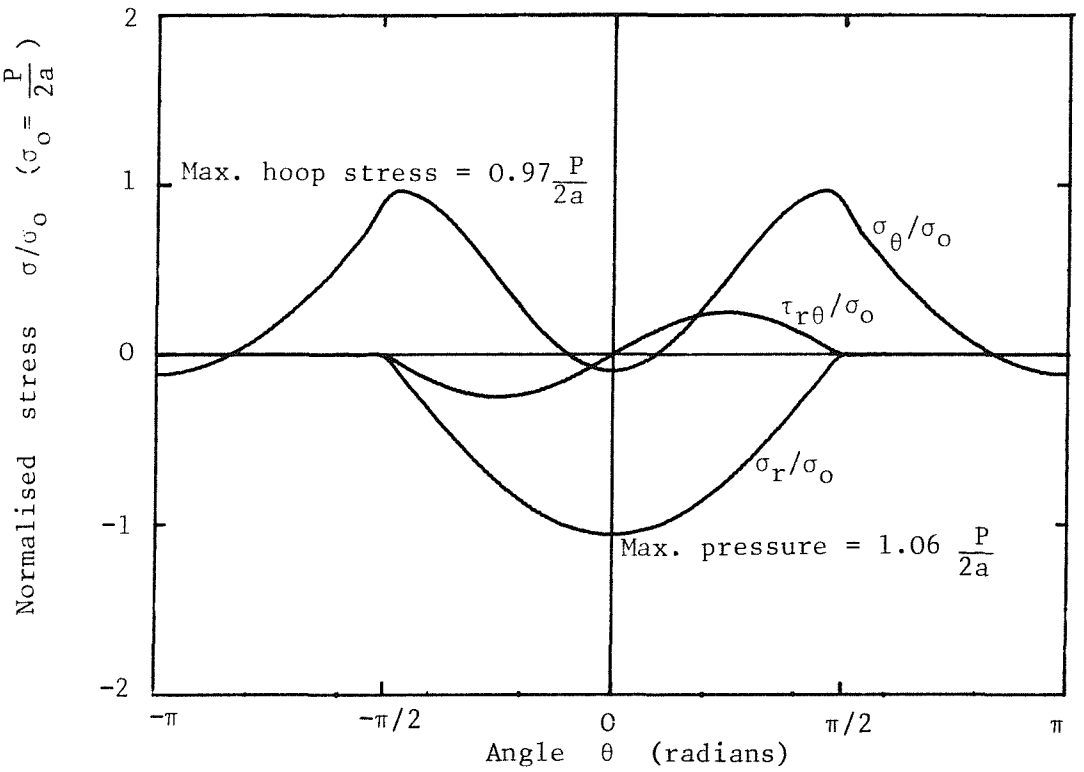

Figure 5.19 Stresses around boundary of hole in infinite sheet
(ii) Loading b) + h) $\cos\theta$ normal pressure and $\sin\theta$ shear.

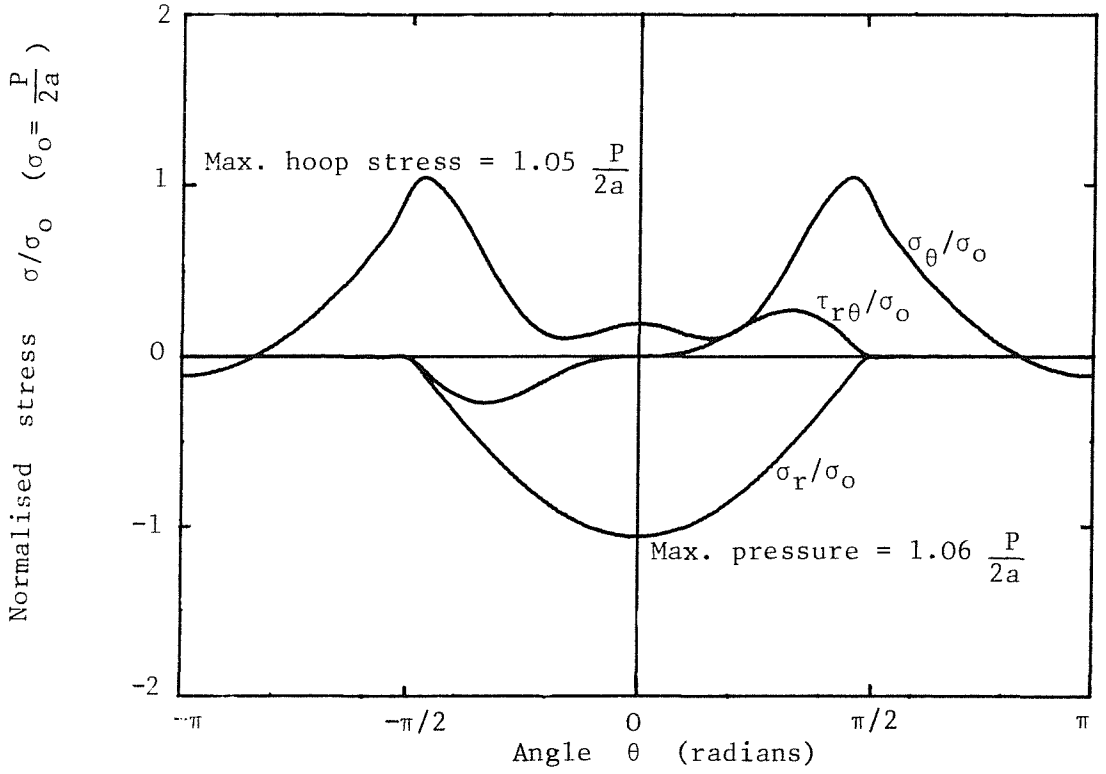

Figure 5.20 Stresses around boundary of hole in infinite sheet
(iii) Loading b) + j) $\cos\theta$ normal pressure and $\sin^3\theta\cos\theta$ shear.

The difficulty with this loading combination is the discontinuity in the shear at $|\theta| = \pi/2$. Not only does this cause some inaccuracy in the Fourier representation, but in fact the shear distribution is physically impossible, having the maximum friction occurring where the normal pressure is zero.

A simple alternative is to use the shear distribution h) which is zero at both $\theta = 0$ and $\pi/2$. Used in combination with radial distribution b) the loading is denoted (ii). For an infinite sheet the maximum hoop stress is found to be approximately 15% lower than loading (i). The stresses from the loading (ii) are plotted in figure 5.19 and the maximum values are given below:

$$\left.\begin{aligned} \sigma_r(\max) &= -1.06\ \frac{P}{2a} && \text{at } \theta = 0 \\ \tau_{r\theta}(\max) &= 0.25\ \frac{P}{2a} && \text{at } \theta = \pi/4 \\ \sigma_\theta(\max) &= 0.97\ \frac{P}{2a} && \text{at } \theta \simeq \pi/2 \end{aligned}\right\}$$

The shear loading j), suggested by Bickley [5.14] is another possibility. The shear is zero at $\theta = 0$ and $\pi/2$ but the maximum value is closer to $\pi/2$ than for the shear loading h). This results in a higher maximum hoop stress in most cases. Figure 5.20 shows the stresses round the hole in an infinite sheet for the loading (iii), a combination of j) + b). The maximum values of stress are:

$$\left.\begin{aligned} \sigma_r(\max) &= -1.06\ \frac{P}{2a} && \text{at } \theta = 0 \\ \tau_{r\theta}(\max) &= 0.27\ \frac{P}{2a} && \text{at } \theta = \pi/3 \\ \sigma_\theta(\max) &= 1.05\ \frac{P}{2a} && \text{at } \theta \simeq \pi/2 \end{aligned}\right\}$$

The shear loadings g), h) and j) may of course be combined with any of the radial pressure distributions a) to d). Figures 5.21 to 5.23 show the stresses resulting from combining them with the loading c) - loadings (iv) to (vi) - and the slightly higher maximum hoop stresses that result.

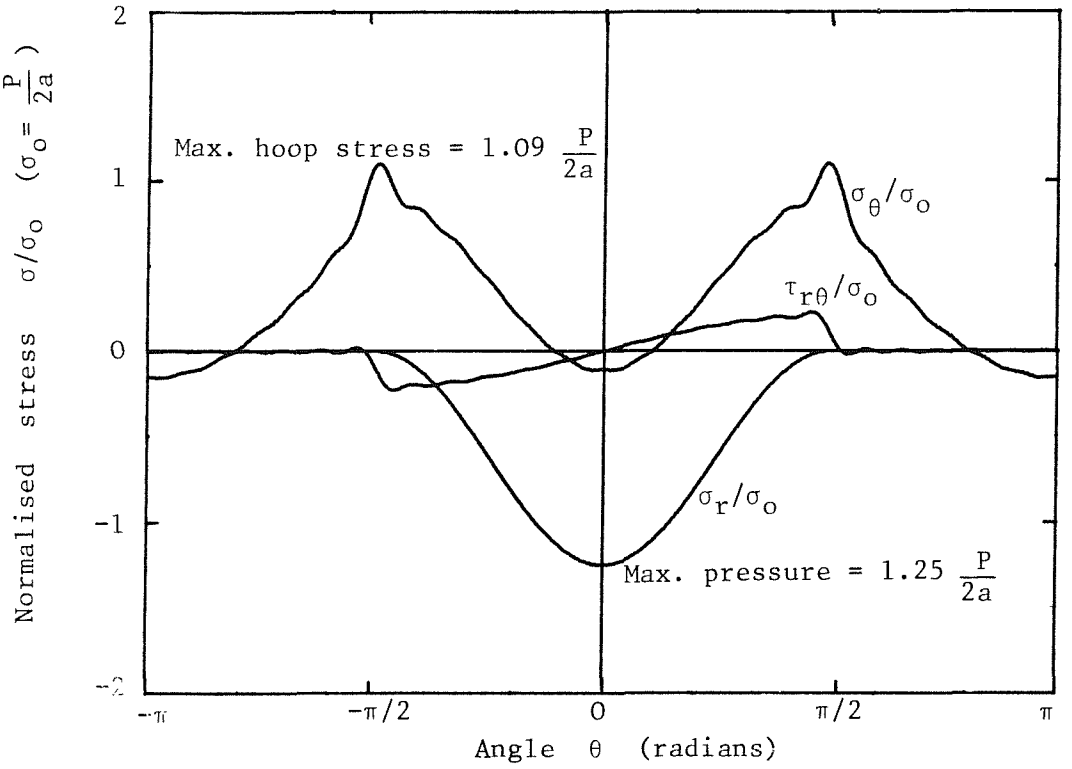

Figure 5.21 Stresses around boundary of hole in infinite sheet
(iv) Loading c) + g) $\cos^2\theta$ normal pressure and $\sin\theta$ shear.

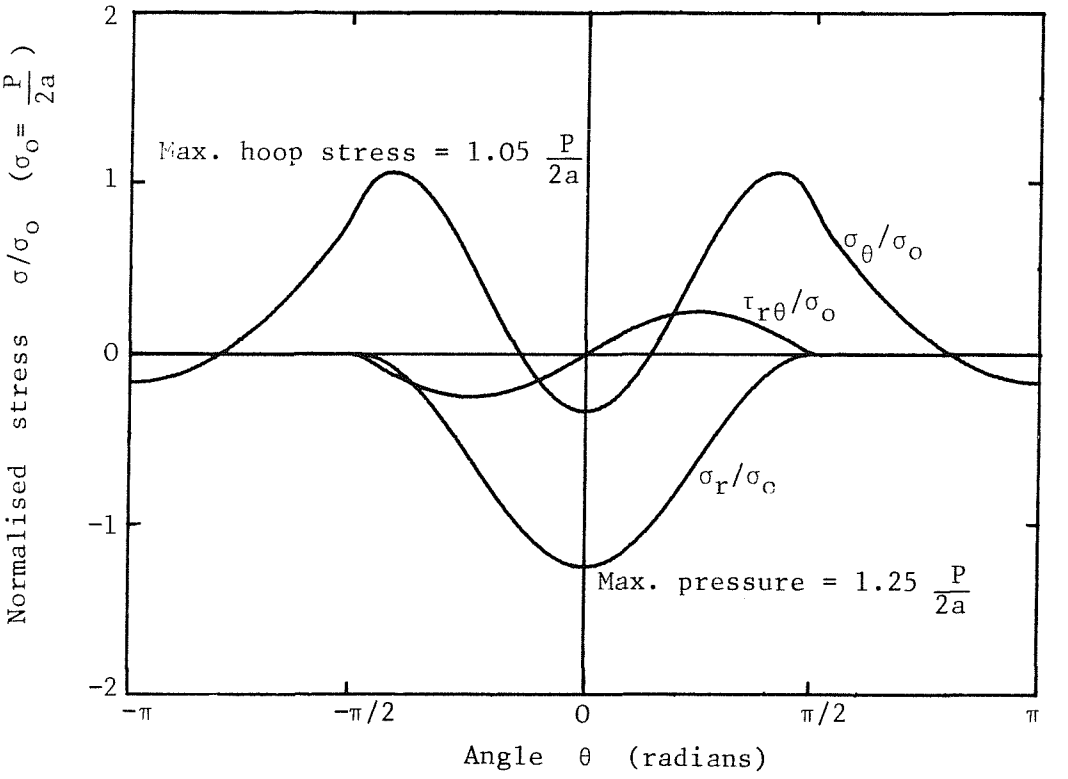

Figure 5.22 Stresses around boundary of hole in infinite sheet
(v) Loading c) + h) $\cos^2\theta$ normal pressure and $\sin 2\theta$ shear.

In conclusion, several Fourier representations for the loading on a hole due to a pin or bolt have been derived and examined in this section. The tractions and Fourier coefficients have been given in each case and the stresses determined from equation (3.26) (the loading function) for the loading applied to a hole in an infinite sheet. These loadings and combinations of loadings will now be applied to several configurations using FESM.

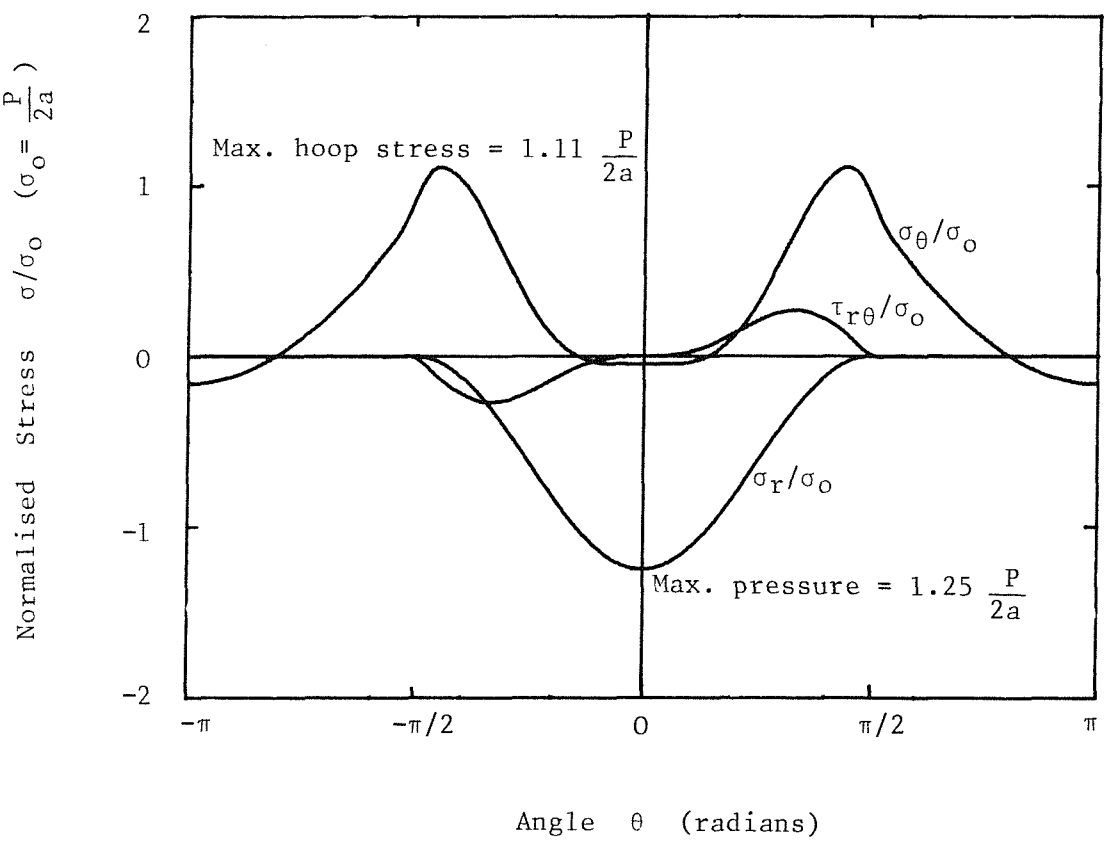

Figure 5.23 Stresses around boundary of hole in infinite sheet. (vi) Loading c) + j) $\cos^2\theta$ normal pressure and $\sin^3\theta \cos\theta$ shear.

5.4.2 Pressurized hole in an annulus or large plate

The hoop stress, for an annulus with a constant internal pressure equal to p_o (see figure 5.24) is known analytically to be:

$$\sigma_{(r = a)} = \frac{1 + (a/w)^2}{1 - (a/w)^2} \; p_o \qquad (5.9)$$

where w in this case denotes the external radius of the annulus. This formula will also be approximately correct for a square plate with a circular hole where w denotes half the plate width, provided that the hole is small relative to w.

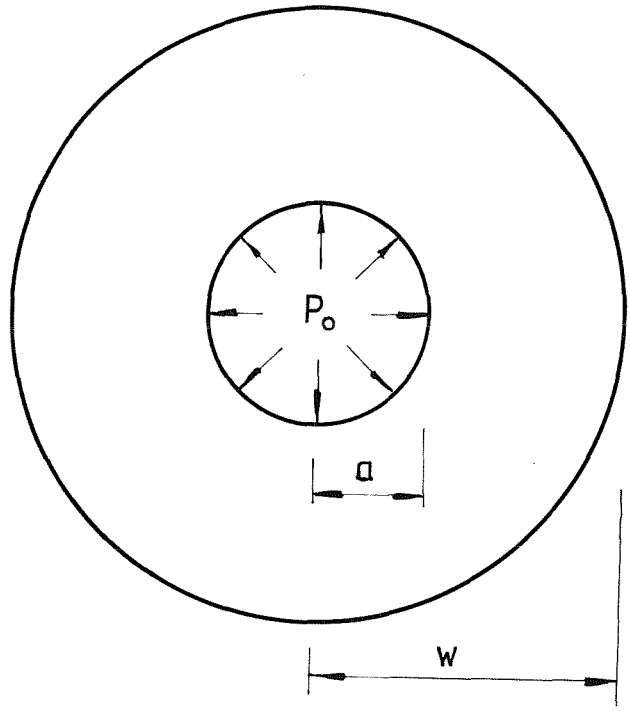

Figure 5.24 Pressurized annulus.

An annulus with hole size a/w = 0.5, loaded with a constant internal pressure [loading (e)] and a square plate with a central hole of size a/w = 0.1 with the same loading were analysed using the FESM program. Five trial functions and the loading function were used in each case with the finite element meshes shown in appendix E, figures E22 and E23. The special region covered the entire mesh in both cases. The values for the maximum hoop stress obtained are given in table 5.15 together with the analytic solution from equation (5.9).

	MAXIMUM HOOP STRESS σ_θ/p_o	
	FESM Solution	Equation (5.9)
ANNULUS a/w = 0.5	1.677	1.667
SQUARE PLATE a/w = 0.1	1.018	1.020

Table 5.15 Results for pressurized hole.

The results in both cases are accurate to within 1%. While this accuracy confirms the validity of the new method for loaded holes it should be expected since the exact solution of equation (5.9) may be obtained from a combination of the loading function and trial function 1. In fact an almost identical estimate for K_t is obtained for the annulus, when only this one trial function is used rather than all five functions. The errors arise in both cases from finite element representation of the outer boundary and, in the second case, from the fact that equation (5.9) is strictly valid for an annulus not a square plate.

5.4.3 Symmetrical rectangular lug

The pin-loaded rectangular lug shown in figure 5.25, with two geometrical axes of symmetry, was analysed using the FESM program. The size of the hole is given by a/w = 0.5, and the stress on one end of the lug by $\sigma_o = P/2w$, where P is the resultant load on the hole per unit thickness. The distance from the hole centre to the stress-free end of the lug, ℓ_1, is equal to the distance from the hole centre to the other end and $\ell_1/w = 2.0$. The angle θ is measured from the axis shown vertical in figure 5.25.

The loading on the hole was represented using the various distributions of radial and tangential tractions discussed in section 5.4.1.

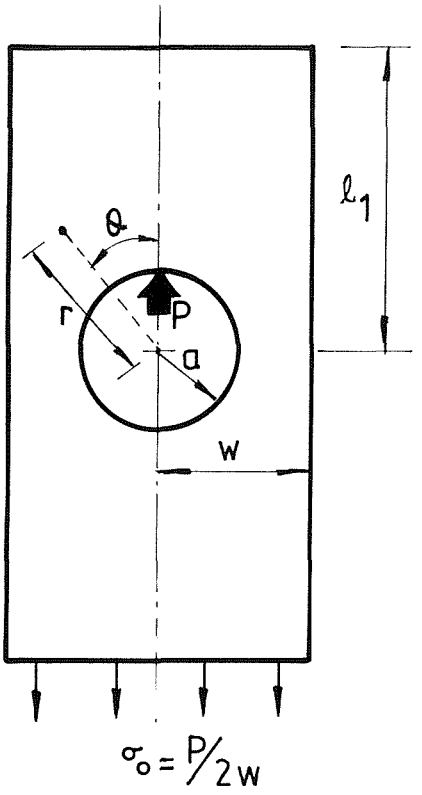

Figure 5.25: Symmetrical lug (pin-loaded)

Half of the lug was modelled with the finite element mesh shown in appendix E, figure E.24, which has a similar element size to meshes which were satisfactory for traction free holes. Since the loading causes asymmetry about the horizontal axis through the hole centre, overall there is only one axis of symmetry in the configuration. The special region used, also shown in the figure E.24, is of similar size to the special regions found to be most effective for configurations with traction-free holes in section 5.2.4. All of the 8 trial functions of equations (3.19) to (3.22), i = 1 to 8, were used in this study in addition to the loading function of equation (3.26) with the Fourier coefficients as specified in section 5.4.1 for each loading.

The results for the stress concentration factors, K_t, which occur with the different load distributions are shown in table 5.16. The maximum stress occurs in each case at the edges of the hole on the line

Loading on hole	$K_t = \frac{\sigma_{max}}{\sigma_o}$	Value of K_t for comparison	% Difference ε_{ref}
a) to f) radial tractions only			
a) $[\cos\theta+1]$ loading	3.551	-	-
b) $\cos\theta$ loading $(-\pi/2 \leq \theta \leq \pi/2)$	4.500	[5.10] 4.621	-2.6%
c) $\cos^2\theta$ loading $(-\pi/2 \leq \theta \leq \pi/2)$	4.639	c.f. case b)	+3.1%
d) Pressure over arc $(-\pi/2 \leq \theta \leq \pi/2)$	3.245	c.f. case e)	0%
e) Constant pressure (by superposition)	3.245	c.f. case d)	0%
f) $\cos^2\theta$ loading (by superposition)	4.638	c.f. case c)	-0%
i)- vi) radial & tangential tractions			
i) (b&g) $\cos\theta/\sin\theta$ shear	5.264	[5.6] 5.03	+4.7%
		[5.7] 5.06	+4.0%
		[5.8] 5.21	+1.0%
		[5.9] 5.13	+2.6%
ii) (b&h) $\cos\theta/\sin2\theta$ shear	4.889	c.f. case i)	-7.1%
iii) (b&j) $\cos\theta/\sin^2\theta\cos\theta$ shear	4.983	c.f. case i)	-5.3%
iv) (e&g) $\cos^2\theta/\sin\theta$ shear	5.379	c.f. case i)	+2.2%
v) (e&h) $\cos^2\theta/\sin2\theta$ shear	5.004	c.f. case ii)	+2.4%
		c.f. case iv)	-7.0%
vi) (e&j) $\cos^2\theta/\sin^3\theta\cos\theta$ shear	5.098	c.f. case iii)	+2.3%
		c.f. case iv)	-5.2%
Details of lug: $a/w = 0.5$, $\ell_1/w = 2$, $\ell_2 = \ell_1$, $\nu = 0.3$			

Table 5.16 Stress concentrations for symmetrical lug with different distributions of load.

of minimum section. The values are compared with those obtained by other workers for certain loadings (references in square brackets)and also with FESM results for other loadings, the percentage difference between the values, ε_{ref}, being shown in the table 5.16.

The first noticeable feature of these results is the large difference that the distribution of the load may make to the stress concentration factor. From the lowest of these values (d) to the highest (iv) is a change of over 60% and this emphasises the importance of accurate representation of the tractions on the hole. The accuracy of the results by comparison with results from other methods is good, less than 5% difference in all cases.

The loadings a) to f) give only radial tractions on the hole and therefore model the loading due to a frictionless pin. For loading b) the radial tractions are proportional to cos θ over half the hole ($-\pi/2 \leq \theta \leq \pi/2$) and this loading was used by Newman [5.10] to analyse the configuration with radial cracks growing at the hole. A comparison is made with these results in the limit as the crack length tends to zero and agreement is found to be within 3%. The $\cos^2\theta$ loading, (c), which models a bolt with greater clearance between the bolt and the hole, results in a higher stress concentration whereas loading a), which models an interference fit pin gives a lower maximum stress. Lower than any of these is the stress concentration due to a constant pressure over half the hole, loading (d), which is some 30% below that for loading b). These results show that if there is no friction the stress concentration will be lower for a close fitting pin. Unfortunately this may not be so if friction is included since when the load is partially transmitted by the shear tractions, which is more likely for a close fitting pin, the stress concentration is increased.

The results from loadings e) and f) are equivalent to those from loadings d) and c) respectively but were obtained using the superposition principle explained in section 5.4.1. Only one quarter of the plate need be analysed in these cases since the configuration for which a solution is sought has two axes of symmetry rather than the one axis of symmetry in the equivalent problem. The close agreement between the results is shown in table 5.16.

Loadings i) to vi) in table 5.16 have both radial and tangential tractions on the hole. Loading i) has been used by several other workers in analysing this configuration and the FESM result agrees to within 5% with all these values. The configuration analysed by Knight [5.6] and Theocaris [5.7] using an alternating method, was an infinite strip ($\ell_1/w = \infty$) rather than the finite plate, for which a slightly higher stress concentration factor might be expected. Cartwright [5.8] and Whitehead [5.9] both used a finite element method for their analysis and represented the tractions on the hole by point forces at the nodes. The length of the plate used was the same as in the present case ($\ell_1/w = 2.0$) and the agreement with these methods is within 3%.

The effect of introducing shear loading on the hole is to increase the stress concentration factor, in this case by up to 17%. Comparing the three different distributions of shear, g), h) and j), it may be seen that g) (shear tractions proportional to sin θ) results in the highest maximum stress, with cases h) and j) resulting in stress concentration factors approximately 7% and 5% lower respectively. When the loading c) is used for the radial pressure in cases iv) to vi),(i.e. tractions proportional to $\cos^2\theta$), the stress concentration factor is approximately 2% higher than when the loading b) is used (tractions proportional to $\cos\theta$). Thus the case with loading iv) has the highest stress concentration factor with a value of $K_t = 5.38$.

These results show that the FESM program is effective in giving accurate stress concentration factors for configurations with loaded holes. Furthermore the importance of knowing the form of the loading on the hole and closely representing it in the model is shown by the wide variation in stress concentration factors for different loadings that may occur. When no friction is assumed on the hole the analysis shows that the stress concentration factors are lower for distributions of load which model a tightly fitting pin (e.g. loading a)) than for a loose fitting pin. However in practice the effect of friction must be considered particularly when there are smaller clearances between the hole and pin. When this is done, by including shear tractions in the analysis, the stress concentration factors are significantly increased.

5.4.4 Rectangular lugs

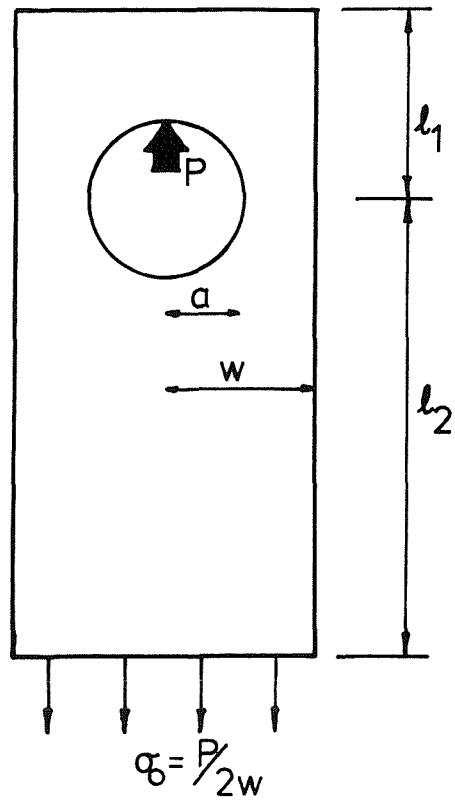

Fig. 5.26 Rectangular lug (pin-loaded)

A number of rectangular pin-loaded lugs, were analysed where the amount of material above the hole, expressed by ℓ_1/w (see figure 5.26), was varied. The hole size was held constant for all the lugs studied at a/w = 0.5 and the stress on one end of the lug is again given by $\sigma_o = P/2w$ where P is the resultant load on the hole per unit thickness. Three different distributions of load on the hole were investigated which were considered to be the most appropriate for the pin loaded joint: loading b) where the radial tractions are proportional to cos θ with zero shear loading; loading c) where the radial tractions are proportional to $\cos^2\theta$ with zero shear loading; and loading i) where the radial tractions are proportional to cos θ and the tangential tractions to sin θ. The angle θ is measured from the vertical axis and the lower portion of the hole ($\pi/2 < \theta < 3\pi/2$) is not loaded. The proportion of resultant

load carried by the tangential tractions over the radial tractions in the loading i) was, as previously, 0.2. For most of the lugs the distance from the hole centre to the external load was given by $\ell_2/w = 2.5$, slightly longer than for the lug used in section 5.4.3. However three lugs with two geometrical axes of symmetry ($\ell_2 = \ell_1$) were also analysed using loading f), which is the $\cos^2\theta$ distribution ($-\pi<\theta\leq\pi$), by applying the superposition principle explained in section 5.4.1. Typical finite element meshes for the lugs analysed in this section are shown in appendix E, figures E.25-E.28, which also show the special regions used with each mesh. The 8 trial functions of equations (3.19) to (3.22), i = 1 to 8, were used with the loading function, equation (3.26).

The values obtained for the stress concentration factors at the edge of the hole on the line of minimum section are given in table 5.17 for the different distributions of load and different values of ℓ_1/w. These values are plotted in figures 5.27 and 5.28 which show the variation in the stress concentration factor on the line of minimum section with the amount of material over the hole (ℓ_1/w) for the different loadings and geometries.

	STRESS CONCENTRATION FACTORS, K_t			
ℓ_1/w	$\cos\theta$ loading (b) $\ell_2/w = 2.5$	$\cos^2\theta$ loading (c) $\ell_2/w = 2.5$	$\cos\theta/\sin\theta$ loading (i) $\ell_2/w = 2.5$	$\cos^2\theta$ loading (f) ($\ell_2 = \ell_1$)
0.75	7.428	8.303	7.899	10.575
0.80		7.817		
0.85	6.557	7.374	7.231	
0.90		6.983		
0.95		6.613		
1.00	5.704	6.282	6.453	7.685
1.25		5.164		
1.50	4.604	4.769	5.369	
1.75		4.611		
2.00	4.426	4.553	5.179	4.638
$a/w = 0.5$, $\nu = 0.3$				

Table 5.17 Stress concentration factors for rectangular pin-loaded lugs.

In figure 5.27 the K_t for the rectangular lugs with $\ell_2/w = 2.5$ is compared with that for the symmetrical lugs ($\ell_1 = \ell_2$), as ℓ_1/w is varied. The lugs are both loaded by normal tractions proportional to $\cos^2\theta$ over the top half of the hole. For long lugs, $\ell_1/w = 2.0$, the geometry in both cases is very similar and the stress concentration factors differ by less than 2%. As ℓ_1 is shortened the stress concentration increases, the rise being particularly rapid as ℓ_1/w falls below 1.0. In this region the symmetrical lug has a K_t significantly higher than the other lug due to the proximity of both the upper and lower edges of the lug.

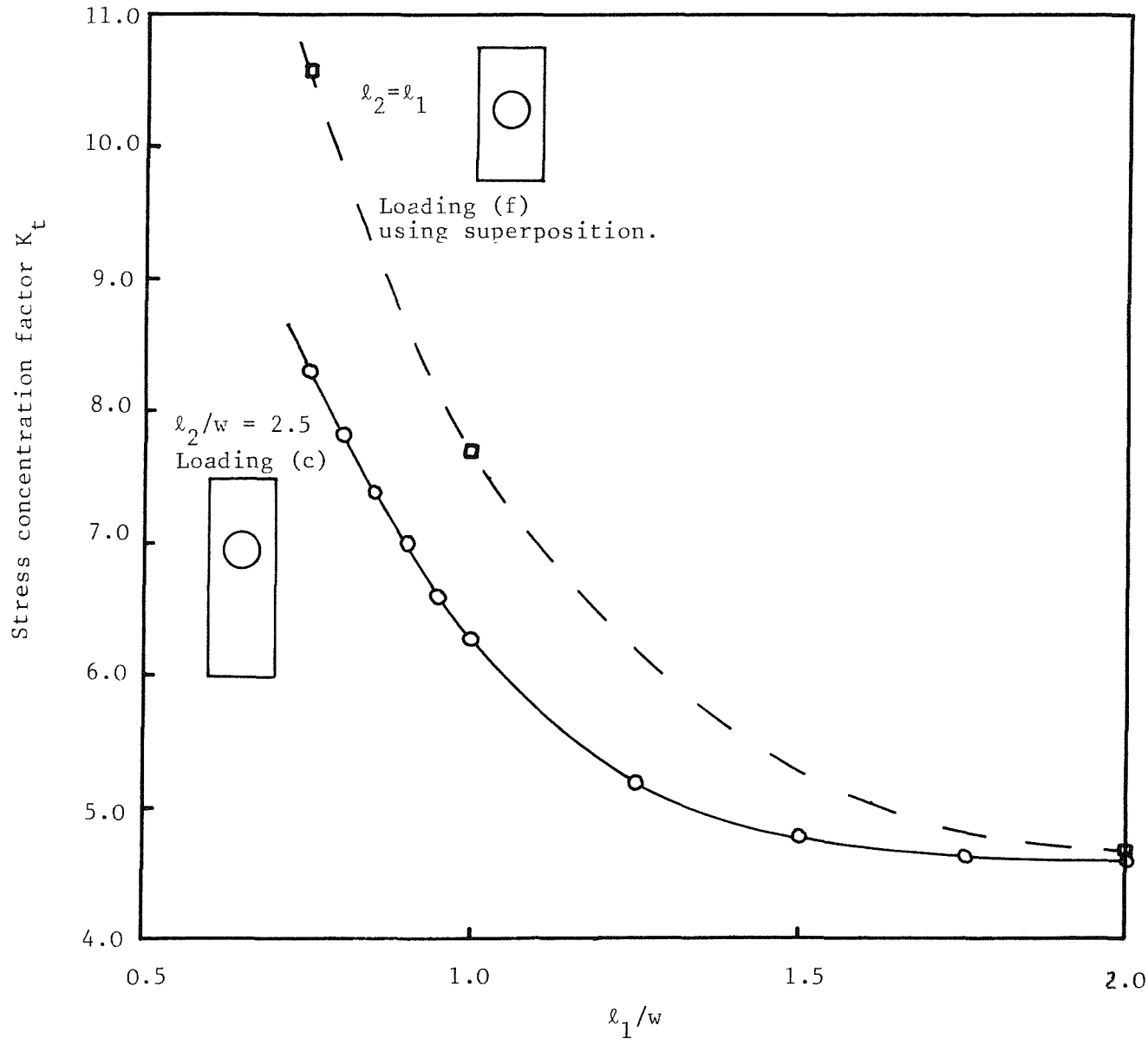

Fig. 5.27 Stress concentration factors for symmetrical/assymmetrical loaded lugs.

Figure 5.28 shows the stress concentration factors for lugs with $\ell_2/w = 2.5$, having different distributions of tractions on the hole boundary. The results for the $\cos^2\theta$ distribution c) are again shown in the figure together with results from the loading cases b) and i). It is found that loading b), the $\cos\theta$ distribution without shear tractions gives the lowest stress concentrations for all values of ℓ_1/w.

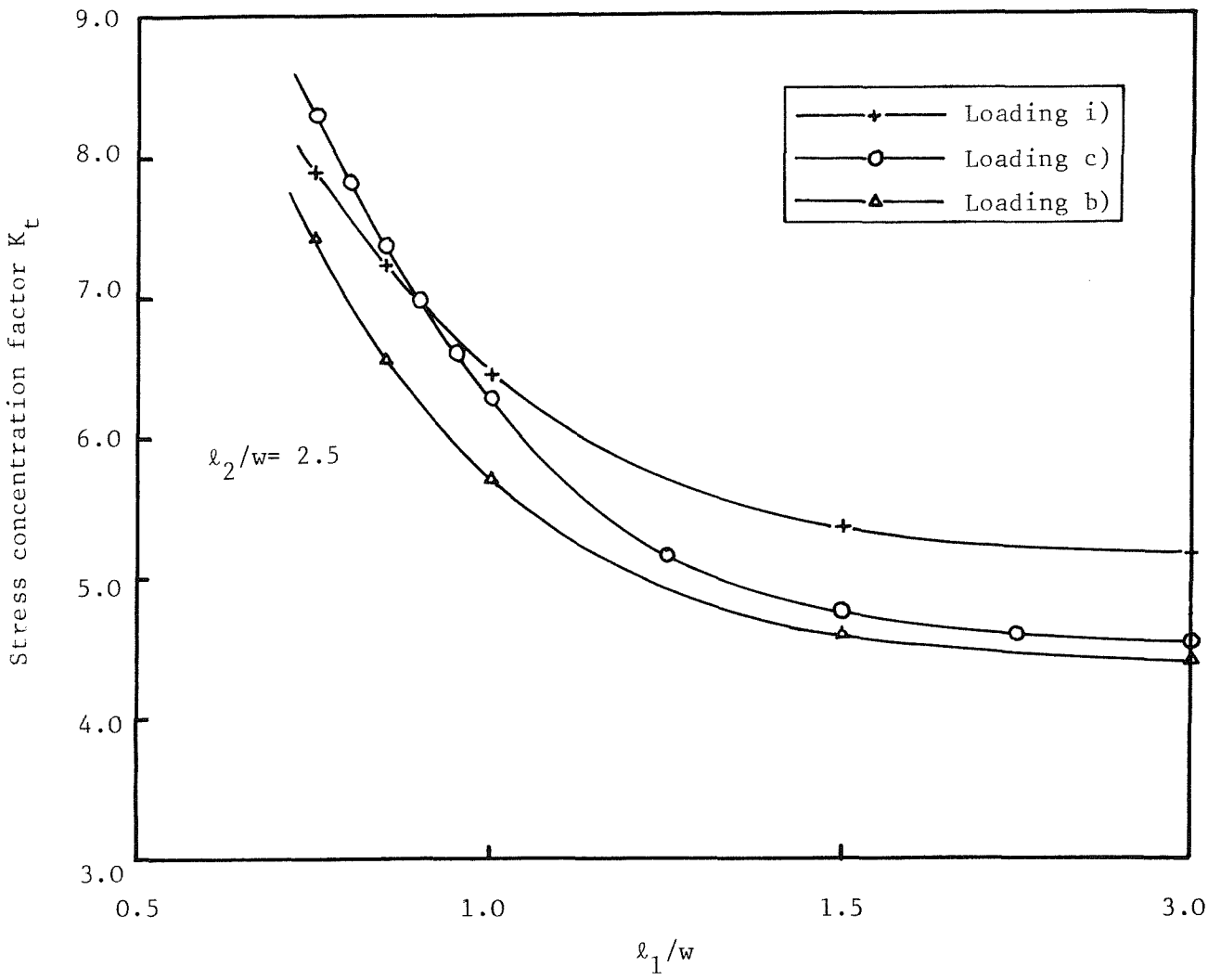

Fig. 5.28 Stress concentration factors for loaded lugs.

For long lugs ($\ell_1/w = 2.0$) loading c), the $\cos^2\theta$ distribution, and loading i) the cos θ radial and sin θ tangential distribution, give stress concentration factors 3% and 17% higher respectively. However, with only a small amount of material above the lug the values for the loadings c) and i) cross over and for $\ell_1/w = 0.75$, the stress concentration factors of loadings c) and i) are 12% and 6% higher respectively than loading b). This could mean that a slack-fitting pin with little or no friction would be of advantage with the long lug whereas a tighter fitting pin, which therefore had friction, would be of advantage with the shorter lug. However greater knowledge of the actual distribution of loads would be required before any firm conclusions of this kind could be made.

Whitehead [5.9] has analysed a number of lugs with rounded ends as shown in figure 5.29. A set of three stress concentration factors for different values of ℓ_1/w, a hole size of $a/w = 0.5$ and a cosine load distribution, are shown in table 5.18. The results were taken from figure 30 in reference [5.9] and have been plotted in figure 5.30 together with the FESM results for a rectangular lug. The figure 5.30 shows that the stress concentration factors for these lugs are very similar, with the maximum difference between the two cases being approximately 7%. Since this is close to the combined error that might be expected from the finite element analyses and also since ℓ_2/w is not specified exactly for the rounded lug in reference [5.9] more detailed conclusions would not be justified. It is sufficient to note that the stress concentration factors are of similar magnitude and slightly higher for the rounded lug. This is to be expected as adding material to the corners of the rounded lug is likely to lower the stress.

ℓ_1/w	Stress concentration factor K_t
0.8	6.97
1.0	6.12
1.2	5.33

Table 5.18 Stress concentration factors for a lug with rounded end from reference [5.9].

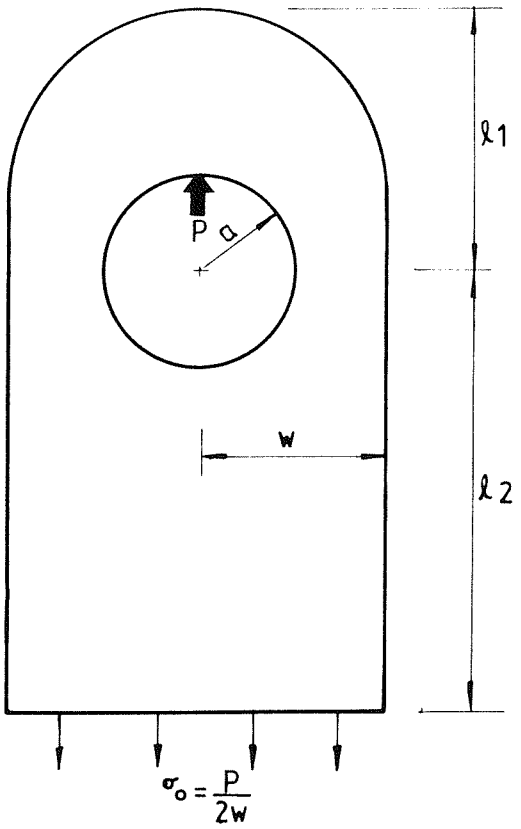

Figure 5.29 Lug with rounded end.

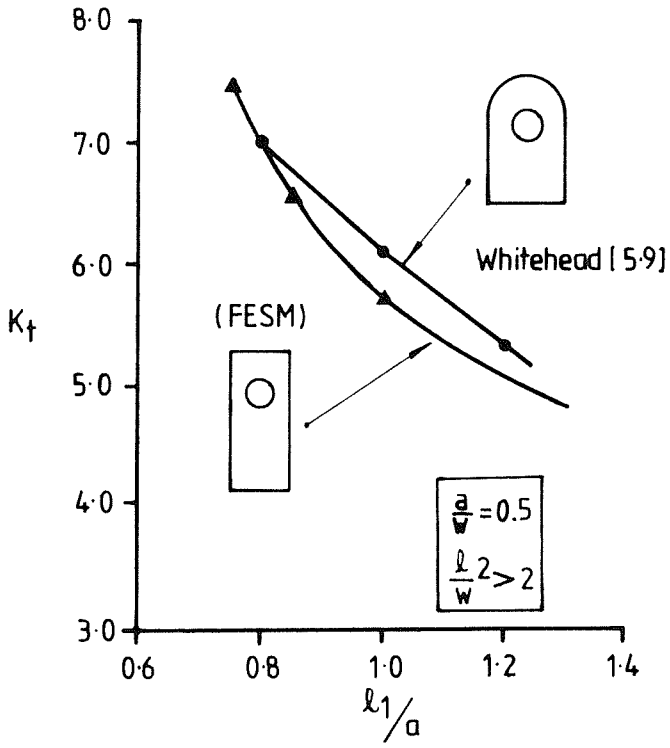

Figure 5.30 Comparison of stress concentration factors for rectangular lugs (FESM) with rounded lugs

To conclude this section it may be noted that the stress concentration factor in loaded lugs varies considerably according to the distribution of load on the hole. The effect of changing the load distribution also depends on the particular geometry of the lug, however in general higher stresses occur near the hole when more of the resultant force is carried by the shear tractions and/or when the radial tractions are concentrated more towards the point $\theta = 0$.

PART II

THE MODIFIED BOUNDARY ELEMENT METHOD

CHAPTER 6

BOUNDARY ELEMENT FORMULATION

6.1 Introduction

As an alternative to the finite element method the boundary element method (BEM) has been growing in importance in recent years. Complicated geometries may be tackled with this method and, unlike finite elements which require the whole region of the problem to be discretised into elements, only the boundary of the configuration need be discretised unless body forces or non-linearities exist which cannot be reduced to boundary conditions. This effectively reduces the dimensionality of the problem by one and so greatly reduces the amount of data required and the number of degrees of freedom for most configurations. On the other hand slightly more numerical analysis is necessary to form the matrix of simultaneous equations associated with these freedoms and the matrix is full rather than banded as in finite element methods. Nevertheless the effectiveness of the boundary element method and its superiority over finite elements for some classes of problem in continuum analysis has been clearly shown [6.1-6.3].

The approach adopted in boundary element methods is to transform the governing differential equations into equivalent sets of integral equations involving values on the boundaries of the region only. This approach involves the use of a "fundamental solution" as the kernel function of the integral equations. A fundamental solution is an exact elasticity solution for a region containing a point force. Usually the function is the solution for a point force in an infinite volume, due to Kelvin [6.4], or its equivalent in two-dimensions. However fundamental solutions for regions which contain a traction-free hole or other boundaries coinciding with part of the boundary of the region under analysis could also be used and it is this modification to the standard BEM which has been developed here for configurations with circular holes.

A difficulty encountered using standard BEM for stress concentration problems is that of determining the stress at or near to a boundary with similar accuracy to internal points, since only values of displacements and tractions are calculated directly, and the method used to calculate the stress at internal points breaks down at the boundary due to the singularity in the kernel functions. An approach used in some commercially

available boundary element programs [6.5] and elsewhere [6.6] is to estimate the tangential strain at the point on the boundary from the displacements. Using Hooke's law to obtain the tangential component of stress, together with the known tractions, the full stress tensor may be estimated. However this method involves the differentiation of approximate values of displacement and inevitably accuracy is lost, thus attempts to deal explicitly with the singularity by using more complex integration techniques have been made [6.7]. The method of the present work however, in using a kernel function for which boundary conditions on a circular hole are exactly satisfied, overcomes the problem of determining the stress on this boundary since boundary elements are not required to model the hole, and thus points on the hole may be treated in the same way as internal points. Furthermore the number of boundaries to be modelled and thus the number of degrees of freedom is reduced and the boundary conditions on the hole are precisely represented. Stresses and displacements at points on or near the hole may be determined with similar accuracy to internal points remote from boundaries.

The approach is similar to that used by Nisitani and Murakami [6.8] for their "body force method", also by Cruse [6.9, 6.10] in the case of cracks, and Telles and Brebbia [6.11] in the case of a long straight boundary for the boundary element method. The method could also be extended to configurations with elliptical holes, since the required fundamental solution is known [6.12] or to other geometries. Indeed the BEM program could be structured such that it contains a library of different fundamental solutions (e.g. circular hole or disc, elliptical hole, long straight boundary) so that a wide range of problems can be solved more easily and accurately by including the most important boundary conditions in the fundamental solution.

An important area of application for the finite element superposition method discussed in part I of this thesis, is to loaded holes. As yet the modified BEM has been applied only to configurations with traction-free circular holes. However by using a superposition principle, problems involving loading on the hole can be reduced to ones with no loading on the hole boundary and with modified tractions on other boundaries. This would avoid the necessity for boundary elements on the

hole boundary to model the loading and would retain the advantages of the modified method. The loading function of chapter 3 could be used to supply the required exact elasticity solution for the loaded hole in an infinite region.

In chapters 6 and 7, the modification to the standard BEM formulation is considered and initial results presented. The work has comprised a smaller fraction of the total than the finite element work and is consequently less complete, but the new analysis for the method has been completed and incorporated into a boundary element program. The results show both the potential for the method and the areas where improvement should be made. In this chapter the formulation of the direct boundary element method [6.2, 6.13] is presented, together with the modifications required to implement the new kernel function. The computer program was developed from a simple BEM program produced by Brebbia [6.2].

6.2 Notation

In the following analysis cartesian tensor notation is used throughout since this enables the equations to be written more briefly and follows the presentation commonly used. This means that the notation of part II is quite separate from the notation of part I. In particular it should be noted that the subscripts in part II define the coordinate directions.

In tensor notation the equations of equilibrium for a point x (coordinates x_1, x_2 and x_3) in an elastic three dimensional medium may be expressed as:

$$\sigma_{ij,j} + b_i = 0 \qquad \begin{matrix} i = 1,2,3 \\ j = 1,2,3 \end{matrix} \tag{6.1}$$

where σ_{ij} is the stress field, b_i is the body force per unit volume and the suffix $_{,j}$ means partial differentiation with respect to the coordinate component x_j. The repeated suffix in this notation implies summation.

Equation (6.1) is also valid in two dimensions with the range of the suffices reduced: $i,j = 1,2$.

The stress, σ_{ij}, and strain, ε_{ij}, in an elastic isotropic material are related by Hooke's law which in three dimensions may be expressed as:

$$\sigma_{ij} = \lambda \delta_{ij} \varepsilon_{kk} + 2G \varepsilon_{ij} \quad (i,j,k = 1,2,3) \tag{6.2}$$

where G, the shear modulus, and λ are Lamé's constants and related to Young's modulus E, and Poisson's ratio ν as follows:

$$\lambda = \frac{E\nu}{(1+\nu)(1-2\nu)} \tag{6.3}$$

$$G = \frac{E}{2(1+\nu)} \quad . \tag{6.4}$$

δ_{ij} is the Kronecker delta which has the properties that:

$$\begin{aligned} \delta_{ij} &= 0 \quad \text{when } i \neq j \\ \delta_{ij} &= 1 \quad \text{when } i = j \end{aligned} \tag{6.5}$$

The strain may be expressed in terms of the displacements u_i as:

$$\varepsilon_{ij} = \frac{1}{2}(u_{i,j} + u_{j,i}) \tag{6.6}$$

Substituting this expression in equation (6.2) gives the stress-displacement relationship as:

$$\sigma_{ij} = \lambda \delta_{ij} u_{k,k} + G(u_{i,j} + u_{j,i}) \quad (i,j,k = 1,2,3) \tag{6.7}$$

This equation is also valid for two dimensional plane strain problems since then $u_3 = 0$ and thus $u_{3,3} = 0$. For plane stress problem equation (6.7) may be used only if the Lamé constant λ is replaced by λ' where:

$$\lambda' = \frac{E\,\nu}{1-\nu^2} \tag{6.8}$$

6.3 Basis of the boundary element method

The boundary element method determines the unknown stress field σ_{ij} and displacement field u_i in a region in terms of their values at the boundary of the region. To do this the fundamental or kernel function is used. In the present work the stresses, displacements, body forces, etc. resulting from this exact elasticity solution are represented by the superscript *, i.e σ^*_{ij}, u^*_i, b^*_i, etc. The properties of the fundamental solution will be considered in more detail later, however it is required that the function is a known elasticity solution for a point force in a given region which includes the region of the problem.

The reciprocal work theorem [6.14] states that if two distinct elastic equilibrium states exist in a region V bounded by the surface S, then the work done by the boundary tractions and body forces of the first system (T_i, in this case) on the displacements of the second (u^*_i, in this case) is equal to the work done by the tractions and body forces of the second system (T^*_i and b^*_i) on the displacements of the first (u_i). The theorem may be proved using the divergence theorem and for this case may be stated as:

$$\int_S u_i \sigma^*_{ij} \ell_j \, dS + \int_V u_i b^*_i \, dV = \int_S u^*_i \sigma_{ij} \ell_j \, dS + \int_V u^*_i b_i \, dV \qquad (6.9)$$

where ℓ_j is the cosine of the angle between the boundary normal and the j coordinate direction, and the tractions on the boundary, T_i, are defined as:

$$T_i = \sigma_{ij} \ell_j \qquad (6.10)$$

Thus equation (6.9) may be written as:

$$\int_V \{u_i b^*_i - u^*_i b_i\} \, dV = \int_S \{u^*_i T_i - u_i T^*_i\} \, dS \qquad (6.11)$$

The displacements and tractions of the fundamental solution are functions of two points, x and ξ, and are defined as $u^*_{k\ell}(x, \xi)$ and $T^*_{k\ell}(x,\xi)$ respectively, representing the displacements and tractions at the point ξ in the ℓ direction, due to a unit point force acting at the point x in the k direction. The corresponding body force $b^*_{k\ell}(x,\xi)$ is given by:

$$b^*_{k\ell}(x,\xi) = \delta_{k\ell} \, \delta(x-\xi) \qquad (6.12)$$

where $\delta_{k\ell}$ is the Kronecker delta and $\delta(x-\xi)$ is the Dirac delta function which has the following properties:

$$\delta(x-\xi) = 0 \qquad \text{if } x \neq \xi$$

$$\text{and} \qquad \delta(x-\xi) = \infty \qquad \text{if } x = \xi \tag{6.13}$$

$$\text{such that} \qquad \int_V \delta(x-\xi)\, dV(\xi) = 1 \quad \text{when } x \in V$$

$$\text{and} \qquad \int_V \delta(x-\xi)\, dV(\xi) = 0 \quad \text{when } x \notin V \tag{6.14}$$

where $\int_V \{\ \} dV(\xi)$ denotes integration over V with respect to the variable ξ. Thus for any function of ξ, f:

$$\int_V f(\xi)\, \delta(x-\xi)\, dV(\xi) = f(x) \quad \text{if } x \in V \tag{6.15}$$

Substituting equation (6.12) for b_i^* in equation (6.11) and specifying ξ as the variable of integration gives, for the unit force acting in the k direction:

$$\int_V \{u_\ell(\xi)\delta_{k\ell}\delta(x-\xi) - u_{k\ell}^*(x,\xi)\, b_\ell(x)\}\, dV(\xi) =$$

$$\int_S \{u_{k\ell}^*(x,\xi)\, T_\ell(\xi) - u_\ell(\xi)\, T_{k\ell}^*(x,\xi)\}\, dS(\xi) \tag{6.16}$$

From the properties of the Dirac delta function [equations (6.13) to (6.15)] equation (6.16) may be re-written as:

$$c_{k\ell}\, u_\ell(x) + \int_S u_\ell(\xi)\, T_{k\ell}^*(x,\xi)\, dS(\xi) =$$

$$\int_S u_{k\ell}^*(x,\xi)\, T_\ell(\xi)\, dS(\xi) + \int_V u_{k\ell}^*(x,\xi)\, b_\ell(\xi)\, dV(\xi) \tag{6.17}$$

where $c_{k\ell} = \delta_{k\ell}$ when x is inside S and would be zero if x were outside S. If the point x is on the boundary S the singular point is included in the contour integrals which must now be interpreted in a Cauchy principal value sense. For a smooth boundary the coefficients $c_{k\ell}$ are then found to be $\frac{1}{2}\,\delta_{k\ell}$ [6.2] and they may also be evaluated for non-smooth boundaries. In practice it is generally unnecessary to evaluate $c_{k\ell}$ explicitly as the terms to which $c_{k\ell}$ contributes can be obtained from consideration of rigid body motions (see page 112).

Equation (6.17), for an internal point x, is referred to as Somigliana's identity [6.4, 6.15] and it is the basis of direct boundary element formulations in elasticity. Using this expression the displacement at a point x, u(x), can be determined from the displacements and tractions on the boundary only and a volume integral of known functions. The volume integral may be dealt with numerically by dividing the region into elements or, for certain types of body forces (e.g. gravity, rotational inertia, steady-state thermal loads), the volume integral may be reduced to a surface integral by further application of the divergence theorem [6.16, 6.17] . However for many classes of problem body forces may be ignored and in this case equation (6.17) for an interior point reduces to:

$$u_k(x) + \int_S u_\ell(\xi)\, T^*_{k\ell}(x,\xi)\, dS(\xi) = \int_S u^*_{k\ell}(x,\xi)\, T_\ell(\xi)\, dS(\xi) \qquad (6.18)$$

For a general point x the equation is:

$$c_{k\ell} u_\ell(x) + \int_S u_\ell(\xi)\, T^*_{k\ell}(x,\xi)\, dS(\xi) = \int_S u^*_{k\ell}(x,\xi)\, T_\ell(\xi)\, dS(\xi) \qquad (6.19)$$

where $c_{k\ell} = \delta_{k\ell}$ for an interior point and depends on the form of the boundary when x lies on the boundary.

6.4 Discretization of the equations

In order to approximate the unknown functions u_ℓ and T_ℓ the boundary S is divided into a number of elements containing one or more nodes. A shape function is chosen which describes the assumed form of u_ℓ and T_ℓ over the boundary element in terms of the nodal values in a similar manner to the shape function for finite elements. The simplest case, that of constant tractions and displacements over the element with a single node at the centroid of each element, is used in the present work. Applying this to equation (6.19) and letting the point x be at each node in turn, gives the following for a configuration with N boundary elements.

For element m (m = 1 to N)

$$c^m_{k\ell} u_\ell(x^m) + \sum_{n=1}^{N} u_\ell(x^n) \int_{S_n} T^*_{k\ell}(x^m,\xi)dS(\xi) = \sum_{n=1}^{N} T_\ell(x^n) \int_{S_n} u^*_{k\ell}(x^m,\xi)dS(\xi) \qquad (6.20)$$

where x^m and x^n refer to the coordinates of nodes m and n respectively, S_n is the n'th boundary element and $c^m_{k\ell}$ is the value of $c_{k\ell}$ for the m'th element. The equations (6.20) may be written:

$$h_{k\ell mn}\, u_\ell(x^n) = g_{k\ell mn}\, T_\ell(x^n) \qquad k,\ell = 1 \text{ to } K \quad m,n = 1 \text{ to } N \tag{6.21}$$

where K is 2 or 3, the number of dimensions of the problem, and:

$$h_{k\ell mn} = \int_{S_n} T^*_{k\ell}(x^m,\xi)\, dS(\xi) \qquad m \neq n \tag{6.22}$$

$$h_{k\ell mn} = c^m_{k\ell} + \int_{S_m} T^*_{k\ell}(x^m,\xi)\, dS(\xi) \qquad m = n \tag{6.23}$$

$$g_{k\ell mn} = \int_{S_n} u^*_{k\ell}(x^m,\xi)\, dS(\xi) \tag{6.24}$$

These integrals may be evaluated numerically on the computer using Gauss quadrature, except that particular care must be taken when m = n. In this case the path of integration includes the singular point and for $h_{k\ell mn}$ and additional term, $c^m_{k\ell}$, is included. In fact the evaluation of $c^m_{k\ell}$ and the integral to which it is added may be avoided by considering a rigid body displacement in the ℓ direction. No boundary tractions must result from such a displacement and thus it follows from (6.21) that:

$$\sum_{n=1}^{N} h_{k\ell mn} = 0 \tag{6.25}$$

Hence the term for m = n may be obtained from the other coefficients.

The term $g_{k\ell mn}$ when m = n must be evaluated however, and since a logarithmic singularity occurs in the kernel of the integral, $u^*_K(x^m,\xi)$, a logarithmically weighted integration formula [6.13, 6.18] may be used. Alternatively the integration may be carried out analytically [6.2] as is usually done for the case when the kernel is the solution for a point force in an infinite region (the Kelvin solution). The more complicated kernels, such as the one used in the present work for configurations with a circular hole, may be written as the sum of the Kelvin solution, $u^K_{k\ell}(x^m,\xi)$, and a complementary part, $u^c_{k\ell}(x^m,\xi)$. This opens a third possible way to evaluate the integral of equation (6.24) when

$m = n$ which is the method used in the present work. Equation (6.24) may be written:

$$g_{k\ell mn} = \int_{S_n} u_{k\ell}^{K}(x^m,\xi)\, dS(\xi) + \int_{S_n} u_{k\ell}^{c}(x^m,\xi)\, dS(\xi) \qquad (6.26)$$

Thus when $m = n$ the non-singular part, resulting from $u_{k\ell}^{c}(x^n,\xi)$, is evaluated numerically using the same procedure as for $m \neq n$ and then added to the singular part from $u_{k\ell}^{K}(x^n,\xi)$ which is evaluated analytically as in reference [6.2].

6.5 Solution of the equations

The simultaneous equations (6.21) may be assembled in matrix form as:

$$\underline{H}\,\underline{u} = \underline{G}\,\underline{T} \qquad (6.27)$$

where $\underline{u}$ and $\underline{T}$ are vectors containing the components at the nodes of displacement and traction respectively. $\underline{H}$ and $\underline{G}$ are square matrices of order 2N for two-dimensional analysis or 3N for three dimensions.

In a well posed problem either the displacements, the tractions or sufficient components of both will be specified on each element of the boundary. The matrix equation (6.27) may be rearranged therefore so that all the unknown components are contained in a vector $\underline{X}$ and the known components multiplied by their coefficients are contained in a vector $\underline{F}$. Thus:

$$\underline{A}\,\underline{X} = \underline{F} \qquad (6.28)$$

where $\underline{A}$ is a matrix containing the appropriate coefficients from $\underline{H}$ and $\underline{G}$. Having solved the simultaneous equations (6.28) the displacements $\underline{u}$ and tractions $\underline{T}$ will be known for the complete boundary and may be used to calculate the displacements and stresses at interior points.

6.6 Interior points

The displacement at an interior point, denoted x^P, follows from equation (6.18) and may be given by:

$$u_k(x^P) = g_{k\ell pn}\, T_\ell(x^n) - h_{k\ell pn}\, u_\ell(x^n) \qquad (6.29)$$

The stress at the point x^P may be obtained using equation (6.7), remembering that this is valid for three-dimensions or plane strain but must be modified for plane stress. Substituting for $u_k(x^P)$ from equation (6.18) into equation (6.7) gives

$$\sigma_{ij}(x^P) = \int_S \{\lambda\delta_{ij} \frac{\partial}{\partial x_k}[u^*_{k\ell}(x^P,\xi)] + G(\frac{\partial}{\partial x_j}[u^*_{i\ell}(x^P,\xi)] + \frac{\partial}{\partial x_i}[u^*_{j\ell}(x^P,\xi)])\}$$

$$T_\ell(\xi)dS(\xi)$$

$$- \int_S \{\lambda\delta_{ij} \frac{\partial}{\partial x_k}[T^*_{k\ell}(x^P,\xi)] + G(\frac{\partial}{\partial x_j}[T^*_{i\ell}(x^P,\xi)] + \frac{\partial}{\partial x_i}[T^*_{j\ell}(x^P,\xi)])\} u_\ell(\xi)dS(\xi) \tag{6.30}$$

This equation may be summarized as:

$$\sigma_{ij}(x^P) = \int_S D_{\ell ij}(x^P,\xi)\, T_\ell(\xi)\, dS(\xi) - \int_S S_{\ell ij}(x^P,\xi)\, u_\ell(\xi)\, dS(\xi) \tag{6.31}$$

where

$$D_{\ell ij}(x^P,\xi) = \lambda\delta_{ij}\, u^*_{k\ell,k}(x^P,\xi) + G[u^*_{i\ell,j}(x^P,\xi) + u^*_{j\ell,i}(x^P,\xi)] \tag{6.32}$$

and

$$S_{\ell ij}(x^P,\xi) = \lambda\delta_{ij}\, T^*_{k\ell,k}(x^P,\xi) + G[T^*_{i\ell,j}(x^P,\xi) + T^*_{j\ell,i}(x^P,\xi)] \tag{6.33}$$

The discretized form of equation (6.31) for constant elements is:

$$\sigma_{ij}(x^P) = \sum_{n=1}^{N} \{T_\ell(x^n) \int_{S_n} D_{\ell ij}(x^P,\xi)\, dS(\xi) - u_\ell(x^n) \int_{S_n} S_{\ell ij}(x^P,\xi) dS(\xi)\} \tag{6.34}$$

The coefficients $D_{\ell ij},(x^P,\xi)$ and $S_{\ell ij}(x^P,\xi)$ are obtained from the kernel functions differentiated with respect to x_k (coordinates of the point at which the force is applied). The integration is then carried out numerically using Gaussian quadrature.

This completes the general formulation of the boundary element method which is valid for two or three dimensions provided the correct fundamental solution is used. In the present work the two dimensional fundamental solution satisfies the boundary conditions on a traction-free circular hole exactly. The effect of this is considered in the next section.

6.7 Modified kernel function

Generally in the boundary element method the kernel function corresponds to Kelvin's solution for a point force in an infinite region or its equivalent in two dimensions. However the formulation is valid for fundamental solutions for a point force in any region which includes the region of the problem. Consider now the case where the kernel corresponds to the solution for a point force in a region with a traction - free boundary S*. The boundary of the problem S may coincide with all or part of S* (see figure 6.1). The part of the boundary of the problem

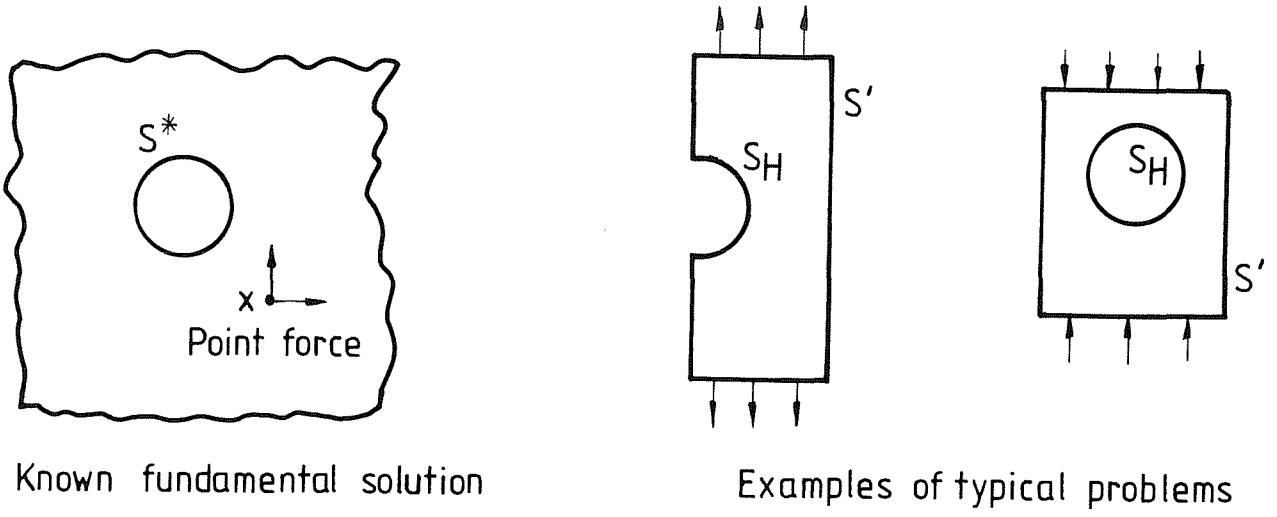

Figure 6.1 Boundaries with the modified kernel function

to be solved which coincides with S* is denoted S_H and the remainder of the boundary S'. The tractions $T^*_{k\ell}(x,\xi)$ are zero on S* unless the singular point x coincides with this part of the boundary. Even in this case analytic integration along the boundary will show that:

$$\int_{S_H} u_\ell(\xi) T^*_{k\ell}(x,\xi) dS(\xi) = 0 \quad \text{when } x \in S_H \tag{6.35}$$

The integral on the left-hand side of equation (6.19) therefore need only be carried out numerically for the boundary S'.

If all or part of S_H is loaded in the configuration being analysed, the integral on the right-hand side of equation (6.19) will have a contribution on the boundary S_H and either that part of the boundary must be divided into elements or a superposition principle must be used as was mentioned in section 6.1. If S_H is traction-free the integrals of equation (6.19) may be evaluated on the boundary S' only and therefore no elements will be required on the boundary S_H. Points on S_H where stresses or displacements are required may then be treated as internal points.

The modified fundamental solution must provide values for the following:

$$u^*_{k\ell}(x,\xi), \quad u^c_{k\ell}(x,\xi), \quad u^*_{k\ell,j}(x,\xi)$$

$$T^*_{k\ell}(x,\xi) \quad \text{and} \quad T^*_{k\ell,j}(x,\xi) \tag{6.36}$$

For the Kelvin solution in two dimensions the tractions and displacements may be readily obtained in terms of the spatial components (x,ξ). However for more complicated kernels in two dimensions which include other boundaries, explicit expressions are more difficult to obtain. These solutions are generally expressed in terms of complex potential functions $\phi_k(z,z_o)$ and $\psi_k(z,z_o)$ where k refers to the direction of the unit point force at z_o, and z is a general position in the region. In terms of x and ξ, z and z_o may be expressed as:

$$z = \xi_1 + i\xi_2$$

$$\text{and} \qquad z_o = x_1 + ix_2 \tag{6.37}$$

Differentiation with respect to z is denoted by ' (hence ϕ'_k, ϕ''_k, etc) and differentiation with respect to x_j by the subscript $,j$, (hence $\phi_{k,j}$, etc). The displacement components $u^*_{k\ell}$ and $u^*_{k\ell,j}$ are then given by

$$u^*_{k1} + i\, u^*_{k2} = \frac{1}{2G} \left(\kappa \phi_k - z\, \bar{\phi}'_k - \bar{\psi}_k\right) \tag{6.38}$$

and

$$u^*_{k1,j} + i\, u^*_{k2,j} = \frac{1}{2G} \left(\kappa \phi_{k,j} - z\bar{\phi}'_{k,j} - \bar{\psi}_{k,j}\right) \tag{6.39}$$

where $\kappa = (3 - 4\nu)$ for plane strain

or $\frac{3-\nu}{1+\nu}$ for plane stress (6.40)

Bar denotes the complex conjugate of a function.

The tractions depend on the direction cosines of ℓ_j of the normal to the boundary. Defining the complex number L as:

$$L = \ell_1 + i\ell_2 \tag{6.41}$$

the tractions are given by:

$$T^*_{k1} + iT^*_{k2} = (\phi'_k + \bar{\phi}'_k)\, L - (z\bar{\phi}''_k + \bar{\psi}'_k)\, \bar{L} \tag{6.42}$$

and the terms $T^*_{k\ell,j}$ are given by:

$$T^*_{k1,j} + iT^*_{k2,j} = (\phi'_{k,j} + \bar{\phi}'_{k,j})\, L - (z\bar{\phi}''_{k,j} + \bar{\psi}'_{k,j})\, \bar{L} \tag{6.43}$$

The required components are therefore given by equations (6.38), (6.39), (6.42) and (6.43) in terms of the complex potentials ϕ_k and ψ_k and their derivatives. These are given, together with the expression for $u^c_{k\ell}$, in Appendix F for a point force near a circular hole, which is the kernel function used to obtain the results of the next chapter. The expressions for the complex potentials were obtained by Murakami and Nisitani [6.19].

6.8 Implementation

The modified boundary element method was implemented on an ICL 2970 computer. The existing simple boundary element program [6.2] employing a constant shape function over each element, was modified in the following manner:

* A new subroutine was written corresponding to the modified kernel function for a region with a circular hole given in Appendix F. The subroutine yields the values of the parameters specified in equation (6.36) using 'complex' arithmetic facilities.

* A subroutine was also written to replace references to the standard Kelvin kernel function so that having chosen which subroutine to use for either the standard or modified method, the remainder of the program would remain unchanged. The modifications also allow other kernel functions to be implemented simply.

* Reference to the kernel function is made at several points in the program which therefore required modification. These are: a) the evaluation of coefficients $h_{k\ell mn}$ and $g_{k\ell mn}$ $(m \neq n)$ using equations (6.22) and (6.24). b) the evaluation of $g_{k\ell mn}$ $(m = n)$ using equation (6.26). c) the evaluation of $D_{\ell ij}(x^P,\xi)$ and $S_{\ell ij}(x^P,\xi)$ using equation (6.32) and (6.33).

* Options for additional Gauss points (4 points are used for the results quoted in Chapter 7), plane stress rather than plane strain [see equation (6.8)], automatic grid generation and other facilities were also added to the software.

Initial tests with the modified program showed that a considerable increase in run time resulted when the modified kernel function was used instead of the standard kernel function (up to a factor of 10 for the same number of elements). This is due to the additional computation required in evaluating the displacements, tractions, etc. [equation (6.36)] from several general 'complex' expressions rather than one explicit algebraic expression. (The increase in run time occurs even if the standard kernel function is evaluated from the general complex expressions). To improve the efficiency of the program to a comparable speed to the original would require these explicit expressions to be obtained. However as the program stands its run time is acceptable and it has the advantage that new kernel functions may be implemented relatively easily given the knowledge of ϕ_k and ψ_k.

The method for preparing the data and using the modified BEM program on the ICL 2970 computer is explained in appendix G.

CHAPTER 7

BOUNDARY ELEMENT RESULTS

7.1 Configurations analysed

The modified BEM program has been used to analyse two simple configurations in order to assess the accuracy and effectiveness of the method. The configurations are shown in figures 7.1 and 7.2:

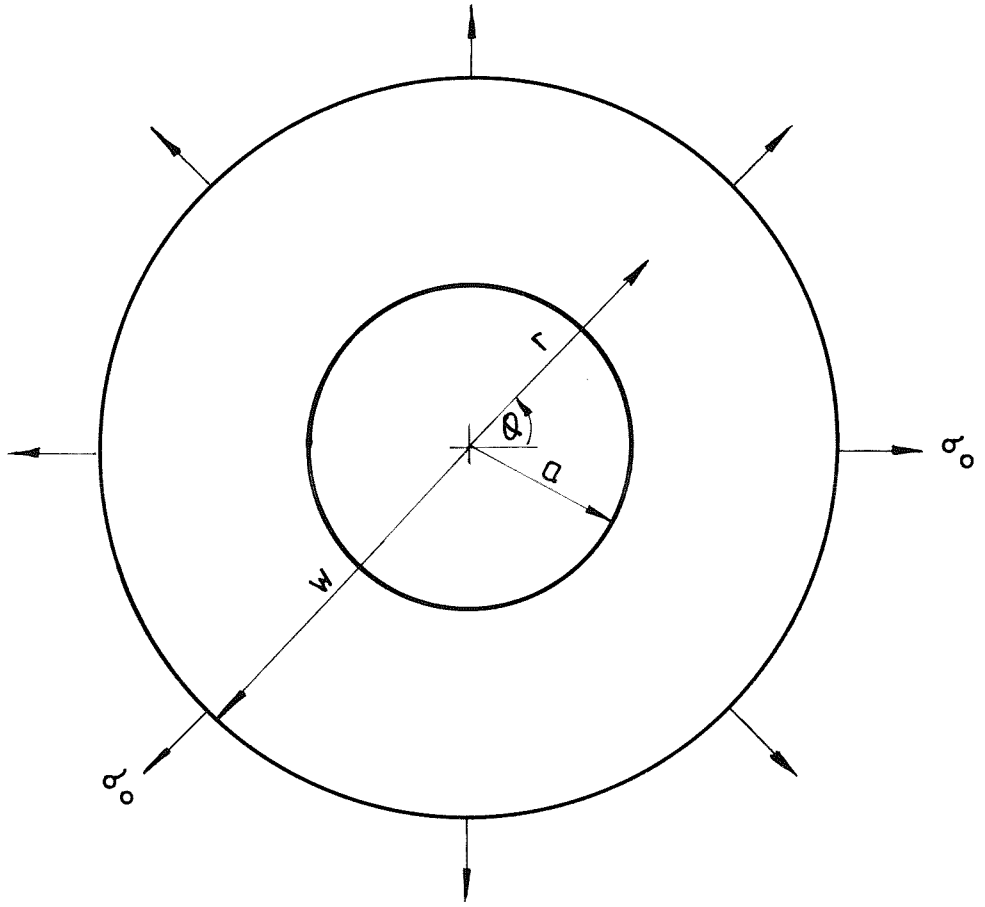

Figure 7.1 Externally loaded annulus.

an externally loaded annulus with a traction free hole and a square plate in biaxial tension with a central traction free hole. The radius of the hole is denoted a, half the width of the disc or plate is denoted w and the distanceof a general point from the centre of the hole is denoted r. The radial and tangential stresses are given by σ_r and σ_θ respectively and the external normal stress on the outer boundary in both cases is σ_o. The stresses in the annulus are known analytically [7.1] and for the square plate were determined by Hengst [7.2], thus comparisons may be made with these results to show the accuracy of the method.

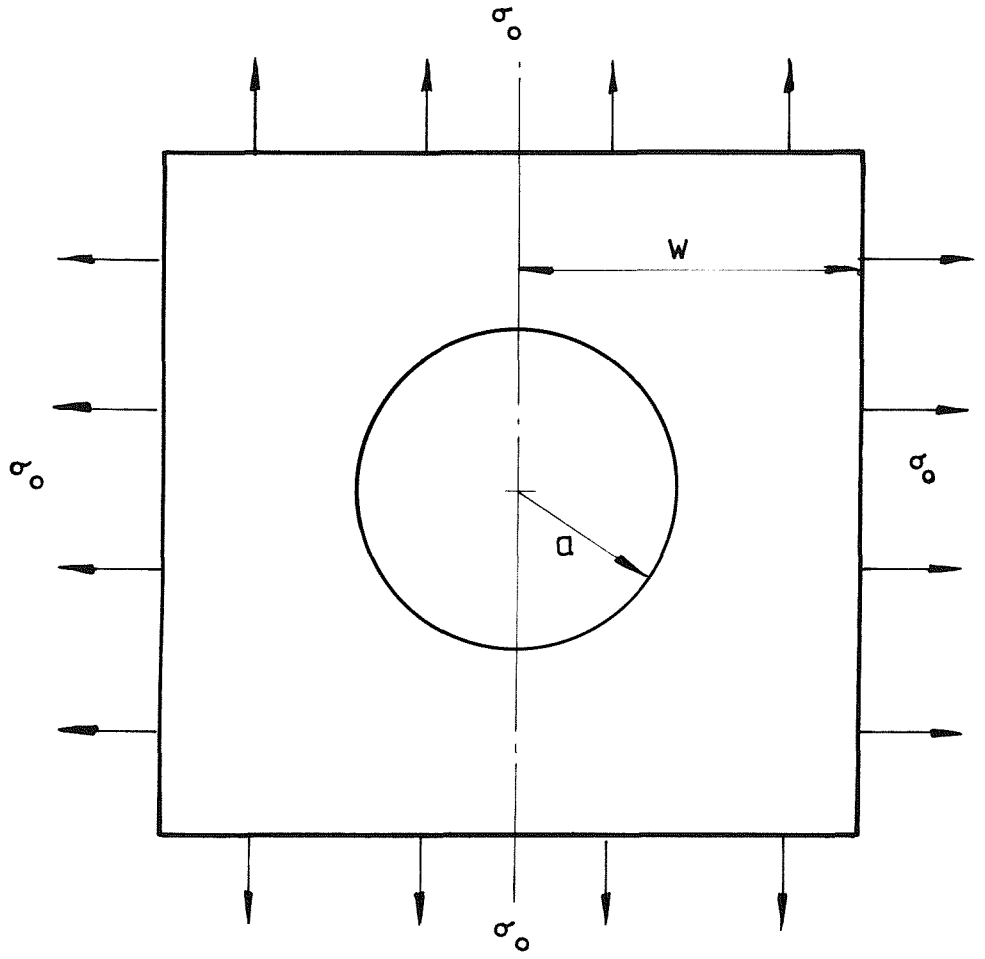

Figure 7.2 Square plate with central circular hole in biaxial tension.

7.2 Comparison between the modified and standard kernel functions

An annulus with a medium sized hole, a/w = 0.3, was analysed using the BEM program with the modified kernel function for configurations with circular holes. The outer boundary of the annulus was modelled using 8, 12 or 24 boundary elements. The values obtained for the radial and tangential stresses across the section of the annulus were compared with:

i) the known analytic solution given by the formulae:

$$\sigma_r = \frac{(1 - a^2/r^2)}{(1 - a^2/w^2)} \sigma_o \qquad (7.1)$$

$$\sigma_\theta = \frac{(1 + a^2/r^2)}{(1 - a^2/w^2)} \sigma_o \qquad (7.2)$$

ii) the stress calculated using the BEM program with the standard Kelvin kernel function, using a total of 16 or 24 boundary elements to model both the outer and inner boundaries of the annulus.

Figure 7.3 shows these results for the normalised tangential stress, σ_θ/σ_o, across the section of the annulus. The maximum stress occurs at the edge of the hole thus the stress concentration factor, K_t, is σ_θ/σ_o at r = a.

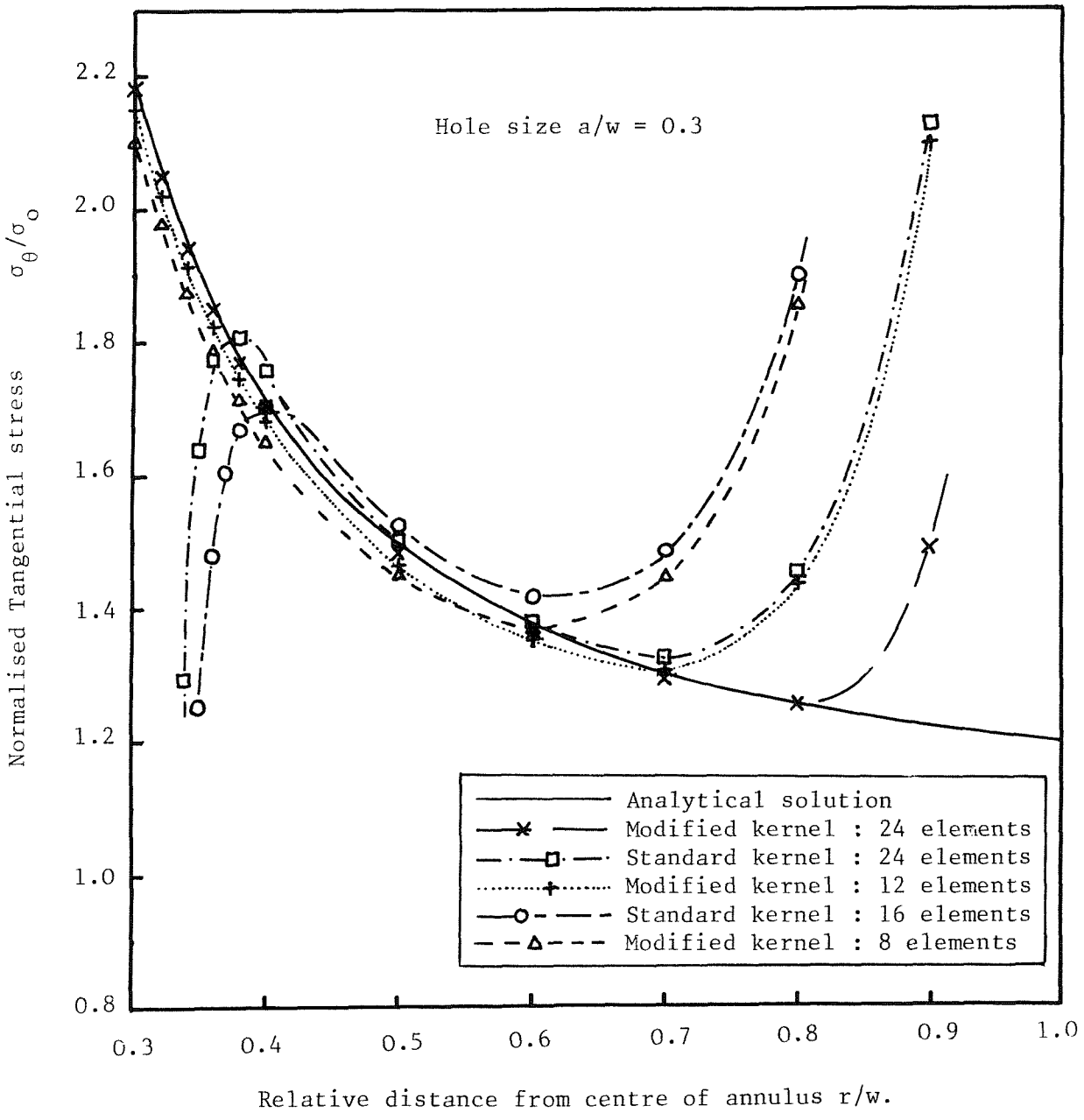

Figure 7.3 Comparison of results for σ_θ in externally loaded annulus.

Near the outer boundary (r/w = 1) all the BEM results become inaccurate due to the proximity of the outer boundary. This is because the numerical integration techniques are inaccurate close to the singularity in the kernel function. The fall off in accuracy occurs with these results at a distance from the outer boundary equivalent to between 1 and 2 times the lengths of the elements on this boundary. Thus the results for 16 elements with the standard kernel function are similar to those for 8 elements with the modified kernel function in this region since both have the same number of elements on the outer boundary. Similarly 24 elements with the standard kernel and 12 elements with the modified kernel have approximately equal errors approaching the outer boundary. However the real advantage of the modified kernel functions is seen as the inner boundary is approached. Using the standard kernel function with elements round the hole a similar deterioration in the accuracy of the boundary element solution occurs as with the outer boundary. Thus no value for the stress concentration factor may be obtained with this method except by extrapolating the interior values to the boundary in some way. With the modified kernel functions no elements are required round the hole and therefore there is no deterioration of the results right up to the hole boundary. Accurate values of the stress concentration factor may therefore be obtained without the need for extrapolation. The errors are approximately 4.5%, 2% and 1% with 8, 12 and 24 elements respectively.

The same pattern emerges when looking at the radial stress in the annulus (Figure 7.4). The radial stress dies away to zero as the hole is approached and the BEM results with the modified kernel function closely follows the analytic solution over this region. The values of radial stress obtained from the method with the standard kernel function are considerably less accurate over the entire range but in particular close to the hole.

These results show the effectiveness of the modified kernel function in obtaining accurate values of stress, and in particular the stress concentration factor, near the edge of a circular hole. Further results have been obtained to show the variation in accuracy obtained using the modified kernel for different sizes of hole.

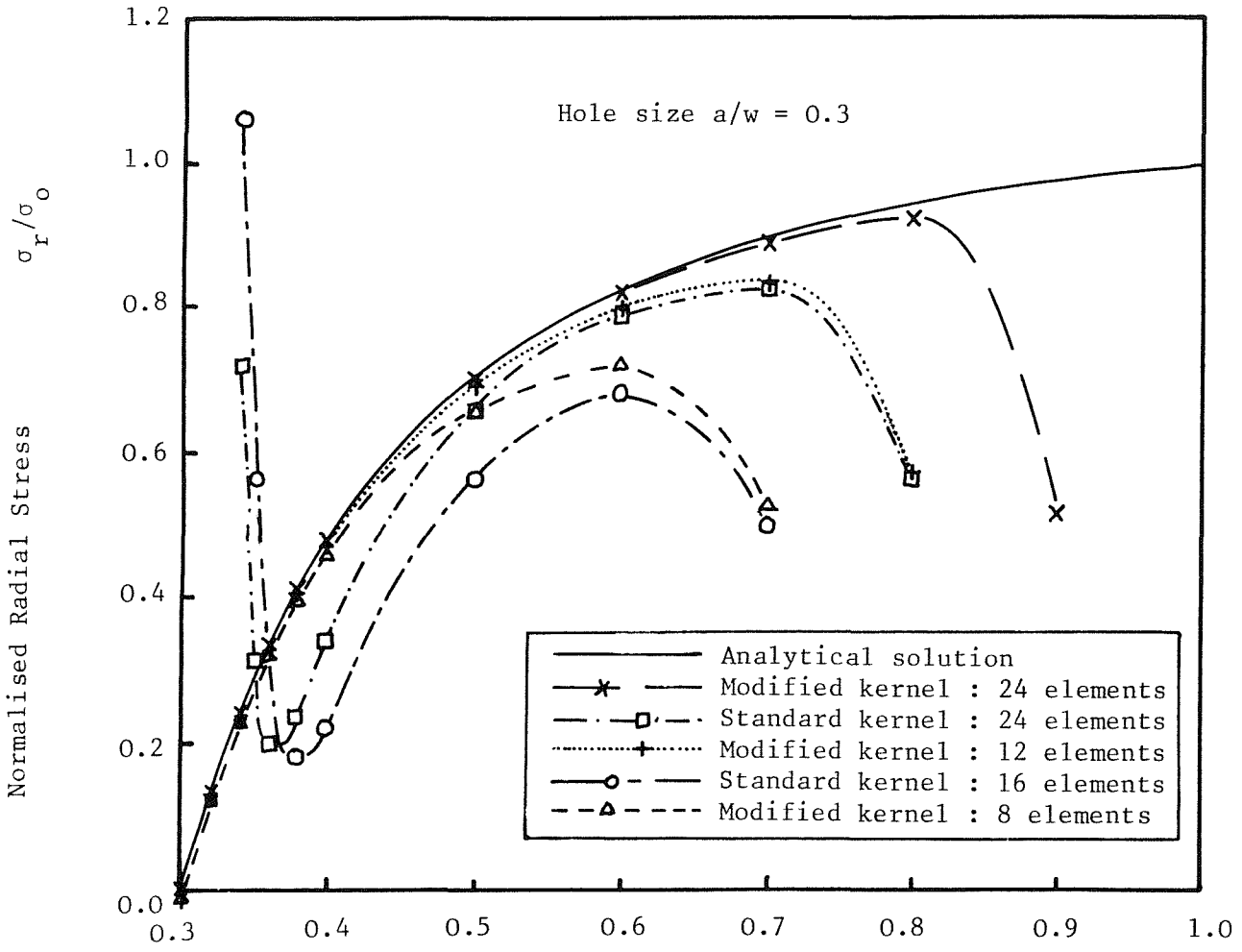

Figure 7.4 Comparison of results for σ_r in externally loaded annulus.

7.3 Annuli with various sizes of hole

The maximum stress in annuli with holes varying in size from a/w = 0.5 to zero (no hole) was calculated using the modified kernel function with 8, 12, 24 and 48 elements on the outer boundary of the annulus. The values obtained were compared with the known values from equation (7.2) with r = a and the percentage error, given by ε_{ref}, was plotted against the hole size, a/w, in figure 7.5 where ε_{ref} is defined by equation (5.1).

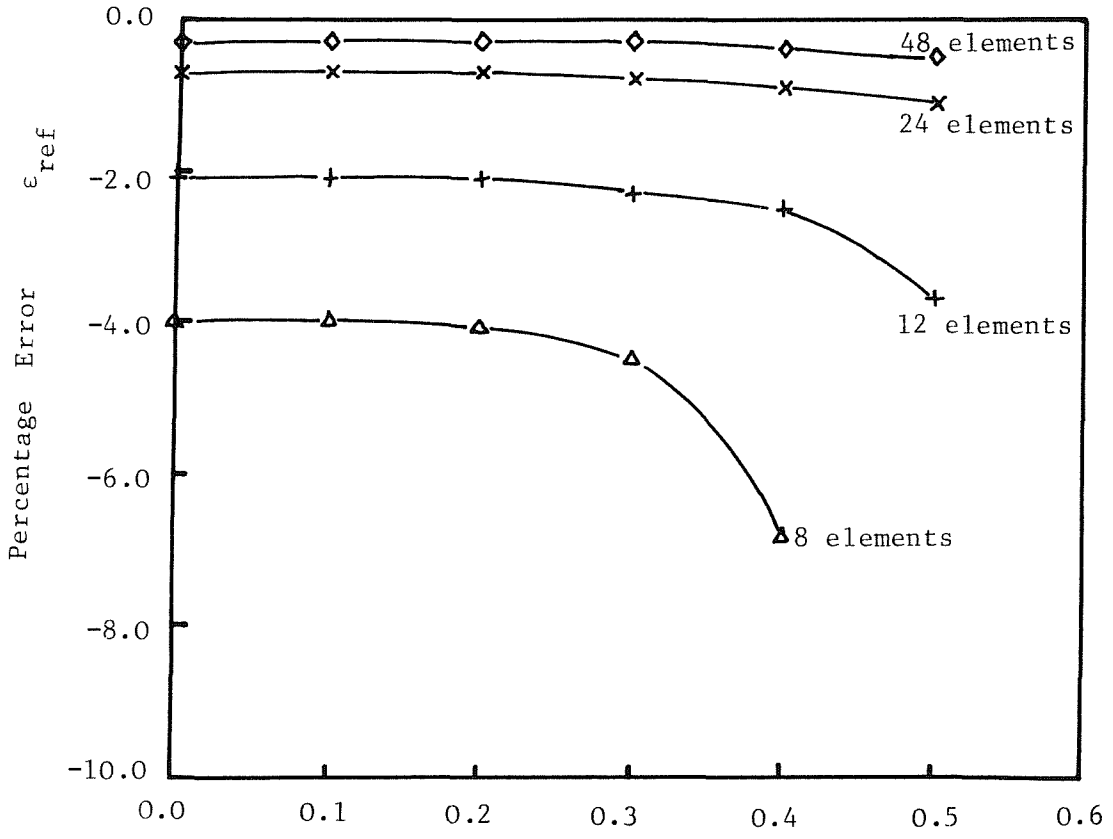

Figure 7.5 Accuracy of the modified BEM solution for annuli with various sizes of hole.

The values of stress concentration given by the modified boundary element method were all below the theoretical value and, as expected, the error decreases as the number of elements is increased. With no hole, a/w = 0, the modified kernel functions are equivalent to the standard Kelvin functions and the configuration is simply a disc in constant biaxial tension. The error in the BEM solution in this case is approximately 4%, 2%, 1% and 0.3% with 8, 12, 24 and 48 elements respectively. No improvement on this level of accuracy could be expected when the hole is introduced in to the configuration and the kernel function. However it is interesting that the same accuracy is maintained up to hole sizes of about a/w = 0.3. For larger holes the error increases quite rapidly when only 8 elements are used on the outer boundary and less

severely the more elements are used. This effect is related to the size of the elements on the outer boundary in a similar way to the deterioration of accuracy close to the boundary observed in Figure 7.3. The inaccuracy is caused, at least in part, by the approximate numerical integration in the proximity of a singularity in the kernel function.

To summarize, the accuracy of the BEM solution with the new kernel functions improves as more (or smaller) elements are used round the boundary. For a given number of boundary elements the accuracy is better for smaller holes, but if the hole is below a certain size (e.g. a/w = 0.3 for 8 elements) the accuracy is approximately the same as would be achieved using the standard kernel function on the configuration without the hole.

7.4 Square plates with various sizes of hole

The other configuration analysed was a square plate with circular hole in biaxial tension. In this case the numbers of elements on the outer boundary were 4, 12, 20, 28 and 44 which, having an odd number of nodes on each side, enabled the rigid body motion to be constrained while preserving two axes of symmetry. A graph of the percentage error ε_{ref} was again plotted against the hole size a/w and this is shown in figure 7.6. The smaller scale on the vertical axis compared to figure 7.5 should be noted.

The general features of these results resemble those for annuli, i.e. greater accuracy for smaller holes and for a larger number of smaller elements on the outer boundary. However the deterioration in the accuracy as the hole size increases is very much more marked in the case of the square plate. The BEM results for no hole (a/w = 0) are in fact more accurate than in the case of the annulus and for a hole size of a/w = 0.1 the errors in the two cases are approximately equal. For larger holes however the errors are considerably greater in the square plate case and the rate of the decline in accuracy is also greater. Nevertheless errors of less than 10% are achieved using 12 elements for hole sizes up to a/w = 0.3, and using 44 elements 10% accuracy is maintained up to a/w = 0.5.

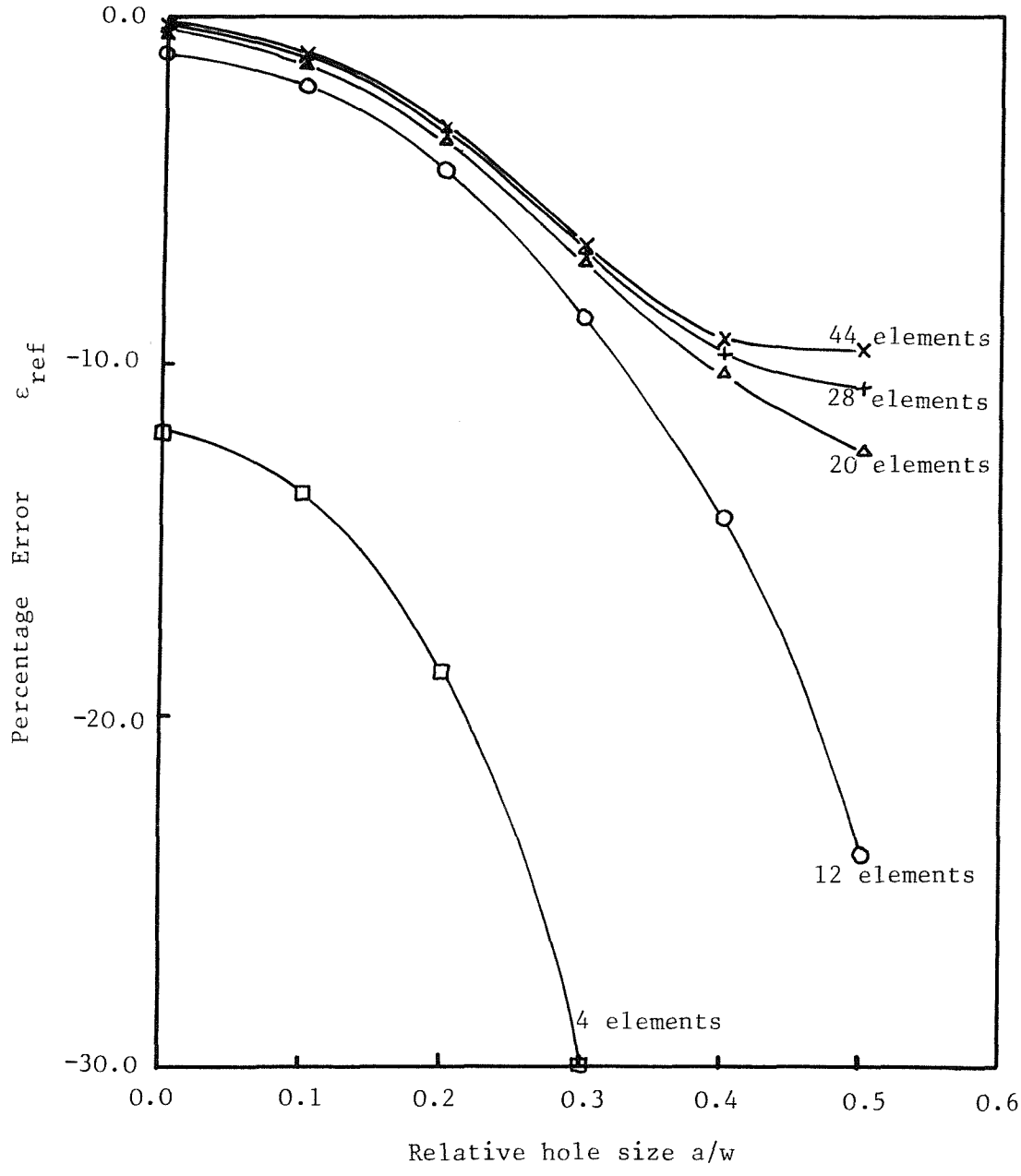

Figure 7.6 Accuracy of the modified BEM solution for square plates with various sizes of hole.

A possible reason for the appreciable decline in the accuracy of results for square plates compared with annuli may be understood by considering the modelling of the displacements, $u_i(\xi)$, by the boundary elements (see section 6.4 of the formulation). A constant shape function for tractions and displacements was assumed over each boundary element - this being the simplest form of the boundary element method. Constant displacement over elements can only model *exactly* a zero strain/zero stress condition, and whereas linear elements would yield the exact solution (save rounding errors) for a constant stress state such as the

square plate with no hole in biaxial tension, the constant elements give only an approximation to this case. In spite of this drawback quite accurate values for stress may be obtained using constant elements in the BEM, particularly if the displacements are approximately constant over each element. They are approximately constant over the elements in the square plate only while the hole is very small, but in the case of the annulus the presence of the hole affects the magnitude of the displacements but not the fact that they are constant in the radial direction and thus approximately constant over the elements. These results therefore, clearly show the need to extend the method to at least linear elements before attempting more complex geometries and loadings and consequently no further results are presented in this thesis.

CHAPTER 8

GENERAL CONCLUSIONS

8.1 The finite element superposition method

The finite element superposition method (FESM) described in Part I was formulated and applied to the analysis of stress concentrations in configurations with traction-free or loaded holes. Important modifications were made to the superposition method which had previously been used to determine stress *intensity* factors in configurations with cracks, including introducing the loading function which accurately represents the tractions on a hole. It was found to be possible to modify the form of the functional in the formulation such that no explicit integration was required on the hole boundary, which meant that the increase in the computation required to analyse loaded configurations was kept to a minimum. The analytical trial functions and loading function used for determining the stress near holes were derived from the known solutions for elliptical or circular holes in stressed sheets. Two trial functions for elliptical holes and up to eight trial functions plus the loading function for circular holes were implemented in the computer program and results were obtained for configurations with both traction-free and loaded holes. Initial results for traction-free holes confirmed the validity of the method and showed the effect on accuracy of various parameters. The conclusions from this work may be summarized as follows.

1. FESM improves the accuracy of basic constant strain finite elements while adding very few degrees of freedom (equal to the number of trial functions) to the system of equations. Comparison with more sophisticated finite element methods (i.e. with linear stress fields within elements) shows that FESM is able to achieve similar or improved accuracy with very many fewer degrees of freedom.

2. Refining the finite element mesh improves the accuracy of the method, but solution time and the quantity of data is increased. Furthermore the improvement of FESM over conventional finite elements is less marked for fine meshes. A compromise between accuracy and efficiency must be sought and in practice, a ratio of the hole radius to a typical element dimension of about 2 to 3 was found to be suitable for the applications discussed.

3. The accuracy of the method is greater for small ratios of the hole size to plate width; narrow elliptical holes also show greater accuracy. In general the FESM solutions are more accurate where the trial functions chosen closely match the exact solutions in the region of stress concentration, as occurs, with the particular trial functions used in this study, for small or sharp holes.

4. Additional trial functions, provided that they are applicable to the particular geometry, will in general improve the accuracy of solution. A total of 8 trial functions for circular holes were implemented in the computer program, 5 of which were applicable to configurations with two axes of symmetry. Quite accurate results were generally achieved with just 2 trial functions (equations (3.19) and (3.22), i = 1 and 4) but using the full set of trial functions was found to improve the accuracy by up to 3%, particularly if either the special region was of limited size or extra elements were included just near to the point of stress concentration. The optimum area for the special region was found to be approximately 4 times the area of the hole when 5 trial functions were used.

5. The accuracy of the stress concentration factors, for circular holes of less than half the plate width in diameter, could be expected to be within approximately 3% of the true value when using 5 trial functions.

New results for the stress concentration factors at traction-free elliptical holes in square plates were obtained using the method. The stress concentration increases rapidly as the aspect ratio a/b rises, as also occurs for an elliptical hole in the infinite sheet. Comparing the square plate results with those for the infinite sheet, K_t is higher in all cases for the square plate, but the proportional difference is less for small holes and higher aspect ratios. Thus the effect of the finite size of plate was shown to be more significant for large holes of circular or near-circular shape.

In applying FESM to configurations with loaded holes, suitable representations for the radial and tangential tractions round a pin-loaded hole were discussed. Several configurations were analysed in order to compare the K_t obtained with, firstly analytical values and

secondly, values obtained by other numerical methods. The close agreement between the FESM and analytical results was to be expected since the trial functions and loading function themselves contained the analytical solution. However close agreement (5% or better) was also obtained with the results from more complex configurations which were compared with the estimates of K_t from other numerical methods.

New values of stress concentration factor were produced for configurations with loaded holes to show the effect of different distributions of load on the hole and to give values of K_t for rectangular lugs of varying dimensions. The stress concentration varied significantly with the different loadings applied (an increase of 60% being noted for one configuration between constant pressure over half the hole and a $\cos^2\theta$ distribution of load with friction). For configurations without friction the load distributions modelling close-fitting pins gave the lower stress concentrations. However when friction was introduced the stress concentration was markedly increased - by up to 17% when the proportion of the resultant load carried by the shear tractions was 0.2.

The stress concentration factors for rectangular lugs with loaded circular holes of diameter half the plate width, were determined using FESM. The K_t for the lugs increased as the distance between the hole and the top of the lug was reduced, especially when this distance became less than the hole diameter. A comparison between these results and independent estimates for the K_t in rounded lugs, showed a close correlation, with the K_t for rounded lugs being higher by approximately 7%.

The finite element superposition method has been shown to be effective in the analysis of stress concentrations near loaded or unloaded holes. Compared to other finite element methods it is efficient in terms of the number of degrees of freedom in the problem, and hence requires only limited data preparation, computer storage and post-processing. The accuracy of the method for the applications discussed was shown to be adequate for engineering purposes, in most cases being accurate to within 3%. Its limitations are that it is applicable only to two-dimensional configurations, and ones for which suitable trial functions exist. Thus, for example, changes in section near to the hole would be very difficult to model with simple trial functions. The

most likely potential for further development of the method is to incorporate FESM as a substructure within larger finite element schemes (see reference [8.1] for example). This is discussed briefly in the future work section 8.4.

8.2 The modified boundary element method

The simple boundary element program, using a constant shape function for the displacements and tractions on the elements, was modified by using a new fundamental solution for a region containing a circular hole. This change to the method was shown to have the effect that for configurations with traction-free holes the boundary conditions on the hole could be satisfied exactly and no discretisation of this part of the boundary was required. Since the fundamental solution was more complicated and required the use of complex algebra, additional computation was introduced, but this was offset by the fact that stress concentration factors at the hole could be calculated directly and with similar accuracy to other internal points, and by the fact that fewer elements were required to model the configuration. Furthermore the increase in run time would be substantially reduced if explicit expressions for the modified kernel function were obtained and this is recommended as a priority for future work.

The program was tested by solving for the stresses in an externally pressurized annulus and a square plate with a central circular hole in biaxial tension. The following conclusions were reached from the results of the computation.

1. For an externally pressurized annulus accurate values of stress concentration (less than 5% error) were obtained from the modified method using only a few elements on the outer boundary (8 elements with a hole size of $a/w = 0.3$). For larger numbers of elements on the outer boundary or for smaller holes the accuracy of the method improved.

2. The standard boundary element method was much less effective for the analysis of this configuration since both the inner and outer boundaries of the annulus had to be modelled, and since when using constant elements the stress can only be calculated accurately some distance away from boundary elements (typically the length of the element), no direct estimate of K_t could be obtained.

3. For a square plate with a circular hole in biaxial tension the modified BEM estimate for K_t was less accurate than for the annulus and the accuracy decreased for larger holes more rapidly than for the case of the annulus. With a hole size of a/w = 0.3 an error of approximately 10% occurred with 12 elements modelling the outer boundary.

4. The larger errors occurring in the square plate case suggested that the constant shape function over the boundary elements was insufficient for this configuration. The superiority of the modified kernel functions however has been shown and it is suggested for future work that the modified kernels are incorporated in a boundary element formulation with higher order elements.

In spite of the fact that the boundary element work has not yet produced a program for general application in the determination of stress near holes, the present work has demonstrated the potential of the method when using modified fundamental solutions. The next stage in the development of this work will be the incorporation of explicit expressions for the modified kernel function in a BEM program with either a linear or quadratic shape function over the elements.

8.3 Comparison of the methods

The two methods described in this thesis, the finite element superposition method and the modified boundary element method, were developed for analysing the stress concentrations near holes or other cut-outs in two dimensional configurations. Both methods are extensions to established numerical techniques, modifications to which have been made by incorporating known analytical solutions to problems in elasticity which are related to the actual problems to be solved. Thus FESM uses as trial functions solutions for an infinite plate with a circular hole, to solve configurations of finite size containing such a hole. For modified BEM the relevant fundamental solution for this problem, the solution for a point force near the circular hole in an infinite region, is incorporated as the kernel function. The methods are therefore related and ultimately have similar limitations in that they may be used only for configurations for which suitable analytical solutions, for the trial functions or kernel function, can be found or are already known. In practice this may not be a severe limitation since commonly occurring causes of stress concentration are holes for which analytical solutions exist.

A feature of both methods is that they require less modelling (i.e. fewer elements) in the region of the stress concentration. This is an important asset, particularly as the trend in computing continues toward fast but small machines which may not have the large core storage required by traditional finite element programs, but which could adequately deal with the relatively modest requirements of these formulations of the methods.

The two methods are presently at different stages of development; FESM being ready for application to the real configurations for which concentration factors are required, but the modified BEM still needs further work in developing the method.

8.4 Future work

The FESM computer program has been shown to be effective for configurations with loaded or traction-free holes, particularly for determining the stress near to a hole with a specified loading. Future work on this program therefore should initially be concerned with its application to important engineering components such as lugs of varying dimensions. Optimum geometries of lugs could be determined for particular loadings. Additional trial functions may be found to be advantageous for some configurations and the program could easily be modified to accommodate more than the 8 functions at present available.

The distribution of tractions on the hole boundary will be of particular importance in studies such as that of lug geometries, and it may become necessary to make the loading an unknown in the problem and incorporate modelling of the pin into the finite element scheme. Providing contact between the hole and pin was maintained a loading function for the pin could be incorporated into the method, being the solution to a circular disc with arbitrary tractions on the boundary. The Fourier coefficients for the loading functions of the hole and disc would be unknowns in the system of equations to be determined from the variational principle.

The immediate priority for the BEM work is to incorporate the modified kernels for circular holes into a BEM program with a linear or quadratic variation of displacements and tractions over the elements rather than constant shape function used at present. Not only would this enable a wider range of configurations to be analysed accurately but it would also allow the validity of the method to be checked more readily.

Another area of immediate interest would be in the production of explicit algebraic expressions for the modified kernel functions. This would reduce considerably the amount of computation required to form the simultaneous equations, but due to the complexity of the functions concerned (see appendix F) would involve a significant amount of analysis.

When analysing configurations with one or two axes of symmetry it is convenient to deal with only one half or quarter of the complete region. This may be done by specifying kinematic boundary conditions on the axes of symmetry, as was done for the finite element method, or by symmetrical assembly of the boundary element matrices which avoids the need for elements on the axes of symmetry. This assembly of the matrices was proposed by Telles [8.2] and could usefully be incorporated as an option for symmetrical configurations in the present method.

One area of potential application for both FESM and the modified BEM is as small sub-structures in much larger analyses. Thus large structures or components containing several holes, cracks, stiffeners etc. could be sub-divided into a region to be analysed with conventional finite elements and sub-regions round stress concentrations which would require more accurate analysis from the new methods. Compatibility between these regions could be readily specified if shape functions of the same order were used (e.g. constant strain elements).

Types of stress concentrations other than the ones so far considered might be solved with FESM or modified BEM. New trial functions would be required for FESM for such configurations as loaded elliptical holes or rows or arrays of holes. For BEM the fundamental solutions for an ellipse, a crack, a long straight boundary or a disc could be incorporated into the existing program. The boundary element work

could be extended to three dimensional analysis if the fundamental solution for a point force near an ellipsoidal cavity were derived. This would enable 3-D configurations containing cylindrical or spherical holes, for example, to be solved.

REFERENCES

1.1 R.E. Peterson. "Stress Concentration Factors". John Wiley and Sons, Inc. (1974).

1.2 D.P. Rooke & D.J. Cartwright. "Compendium of stress intensity factors". HMSO, London (1976).

1.3 H. Tada, P. Paris and G. Irwin. "The stress analysis of cracks handbook". Hellertown, Pa., Del Research Corp. (1973).

1.4 G.C. Sih. "Handbook of stress intensity factors". Bethlehem Pa., Lehigh University (1973).

1.5 D.P. Rooke, F.L. Baratta and D.J. Cartwright. "Simple methods of determining stress intensity factors". Practical Applications of Fracture Mechanics, (H. Liebowitz, Ed.) AGARDograph No. 257, 10.1-10.31, (1980).

1.6 D.J. Cartwright. "Stress intensity factor determination". Developments in Fracture Mechanics, 1, (G.G. Chell, Ed.), Applied Science Publishers Ltd., (1980).

1.7 D.J. Cartwright and D.P. Rooke. "Approximate stress intensity compounded from known solutions". Engng. Fract. Mech., 6, 563-571, (1974), (RAE TR75063).

1.8 D.P. Rooke and D.J. Cartwright. "The compounding method applied to the cracks in stiffened sheets". Engng. Fract. Mech. 8, 567-573, (1976), (RAE TR75072).

1.9 Engineering Sciences Data Unit. "The compounding method of estimating stress intensity factors for cracks in complex configurations using solutions from simple configurations". ESDU, Fatigue Sub-series, 4, 78036. (1978).

1.10 D.P. Rooke. "Stress intensity factors for cracked holes in the presence of other boundaries". Fract. Mech. in Engng. Pract. (P. Stanley, Ed.) Applied Science Publishers Ltd., 143-163, (1976), (RAE TR76087, TR77073).

1.11 R.V. Southwell. "Relaxation methods in theoretical physics". Oxford University Press, London. (1946).

1.12 O.C. Zienkiewicz. "The Finite Element Method". 3rd Edition, McGraw Hill Ltd. (1977).

1.13 D.H. Norrie and G. de Vries. "The Finite Element Method". Academic Press. (1973).

1.14 M.J. Turner, R.W. Clough, H.C. Martin and L.J. Topp. "Stiffness and deflection analysis of complex structures". J.Aero. Sci., 23, 805-23, (1956).

1.15 B.A. Finlayson. "The method of weighted residuals and variational principles". Academic Press. (1972).

1.16 K. Washizu. "Variational methods in elasticity and plasticity" 2nd Ed., Pergamon Press. (1975).

1.17 C.A. Brebbia. "The Boundary Element Method for Engineers". 2nd Ed., Pentech Press. (1980).

1.18 P.K. Banerjee and R. Butterfield. "Boundary Element Methods in Engineering Science". McGraw Hill Ltd. (1981).

1.19 G. Lamé. "Lecons sur la théorie ... de l'élasticité". Gauthiers-Viliars, Paris (1852).

1.20 G. Kirsch. "Die Theorie d. Elastizitat u.d. Bedurinisse d. Festigkeitslehre", VDJ 42, 29, S799 (1898).

1.21 C. Wilson, Phil. Mag., 32, 481 (1891).

1.22 H. Neuber and H.G. Hahn, "Stress concentration in scientific research and engineering". Appl. Mech. Rev., 19, 187-199 (1966).

1.23 P.P. Teodorescu. "One hundred years of investigations in the plane problem of the theory of elasticity". Appl. Mech. Rev. 17, 175-186 (1964).

1.24 G.C. Sih. (Ed.) "Stress Analysis of Notch Problems". Mechanics of Fracture, 5, Sijhoff and Noordhoff. (1978).

1.25 Engineering Science Data Unit "Stress Concentrations". ESDU, Fatigue Sub-series, Vol. 3.1.

1.26 G.N. Savin. "Stress Concentration around Holes". Pergamon Press. (1961). (In Russian (1951)).

1.27 G.N. Savin. "Stress Distribution around Holes". NASA TT F-607. (1970). (In Russian (1968)).

1.28 W. Griffel. "Stress concentration factors for plates with holes" and "More concentration factors for stresses around holes". Product Engineering, 34, 98-113 (1963).

1.29 R.B. Heywood. "Designing by Photoelasticity". London, Chapman & Hall (1952).

1.30 R.B. Heywood. "Designing against Fatigue". London, Chapman & Hall (1962).

1.31 H. Neuber. "Kerbspannungslehre". Springer, Berlin, 2nd Ed. (1958). Translation: "Theory of Notch Stresses", US-AEC-tr-4547 (1961).

1.32 C.L.M.H. Navier. Memoires de l'Académie des Sciences, 7, Paris (1827).

1.33 A. Cauchy. Bulletin de la Société Philomathique, Paris (1823).

1.34 G.B. Airy. "On the strains in the interior of beams". Rep. Brit. Assoc. Adv. Sci. p.82 (1862). Phil. Trans. Roy. Soc., London, 153, 49 (1863).

1.35 C.E. Inglis. "Stresses in a plate due to the pressure of cracks and sharp corners". Transactions of the Inst. of Naval Architects, 55, 219-230 (1913).

1.36 W.G. Bickley. "Distribution of stress round a circular hole in a plate". Phil. Trans. Roy. Soc. A, 227, 383-415 (1928).

1.37 G.V. Kolosov. "On the application of complex function theory to a plane problem of the mathematical theory of elasticity". Dorpat (Yuriev) University. (1909).

1.38 N.I. Muskhelishivili. "New general method of solution of basic contour problems of plane elasticity theory". DAN SSSR 3 (1934).

1.39 N.I. Muskhelishvili. "Some basic problems of the mathematical theory of elasticity". Noordhoff. (1953).

1.40 N.I. Muskhelishvili. "Singular Integral Equations". Moscow-Leningrad (1946), Noordhoff (1953).

1.41 A.C. Stevenson. "Some boundary problems in two-dimensional elasticity". Phil. Mag. (VII), 34, 766-793 (1943).

1.42 A.C. Stevenson. "Complex potentials in two-dimensional elasticity". Proc. Roy. Soc. London, A, 184, 129-179, 218-229 (1945).

1.43 A.E. Green. "Stress systems in aeolotropic plates". Proc. Roy. Soc. London A, 180, 173-208 (1942).

1.44 L.M. Milne-Thomson. "Consistency equations for the stresses in isotropic elastic and plastic materials". J. Lond. Math. Soc., 17, 115-128 (1942).

1.45 J.M. Bloom. "The effect of a riveted stringer on the stress in a sheet with a circular cutout". Trans. ASME, J.Appl.Mech., 33, 198-199 (1966).

1.46 Y. Murakami. "Application of the body force method to the calculation of stress intensity factors for a crack in the arbitrarily shaped plate". Eng. Fract. Mech. 10, 497-513 (1978).

1.47 A.E. Green. "General bi-harmonic analysis for a plate containing circular holes". Proc. Roy. Soc., London, A. 176, 121-139 (1940).

1.48 R.C.J. Howland. "On the stresses in the neighbourhood of a circular hole in a strip under tension". Phil. Trans. Roy. Soc. London, A. 229, 49-86 (1930).

1.49 R.C.J. Howland and A.C. Stevenson. "Biharmonic analysis in a perforated strip". Phil.Trans.Roy.Soc.London A., 232, 155-222 (1933).

1.50 R.C.J. Howland. "Stresses in a plate containing an infinite row of holes". Proc.Roy.Soc. A, 148, 471-491, (1935).

1.51 R.C.J. Howland and R.C. Knight. "Stress functions for a plate containing groups of circular holes". Phil.Trans.Roy. Soc. London A, 238, 357-392 (1939).

1.52 V.H. Hengst. "Beitrag zur Beurteilung des Spannungszustandes einer gelochten Scheibe". (Stress in a square plate with circular hole). Ztschr. f. angew.Math. und Mech. 18, 44-48 (1938).

1.53 R.C.J. Howland. "Stress systems in an infinite strip". Proc. Roy. Soc. London A, 124, 89-119 (1929).

1.54 R.C. Knight. "The action of a rivet in a plate of finite breadth". Phil.Mag. 19, 517-540 (1935).

1.55 P.S. Theocaris. "The stress distribution in a strip loaded in tension by means of a central pin". Trans. ASME, J.Appl. Mech. 78, 85-90 (1956).

1.56 C-B. Ling. "Stresses in a perforated strip". Trans. ASME, J.Appl. Mech. 24, 365-375 (1957).

1.57 C-B. Ling. "The stresses in a plate containing two circular holes". J.Appl.Phys. 19, 77-82 (1948).

1.58 C-B. Ling. "The stresses in a plate containing an overlapping circular hole". Trans. ASME, J.Appl. Mech., 19, 405-411 (1948).

1.59 M. Isida. "On the bending of an infinite strip with an eccentric circular hole". Proc. 2nd Jap.Nat. Cong. Appl. Mech. 57-60 (1952).

1.60 M. Isida. "On the tension of the strip with semi-circular notches". Trans. JSME 19, 5-10 (1953).

1.61 M. Isida. "On the tension of an infinite strip with an eccentric circular hole". Trans. JSME, 19, 100-106 (1953).

1.62 M. Isida. "On the tension of a strip with a central elliptical hole". Trans. JSME 21, 501-517 (1955).

1.63 M. Isida and S. Tagami. "On the tension of an infinite strip containing a hole of arbitrary profile". Proc. 9th Jap.Nat. Cong. Appl.Mech. 51-54 (1959).

1.64 M. Isida. "On the tension of an infinite strip containing a square hole with rounded corners". Bull.JSME., 3, 254-259 (1960).

1.65 M. Isida. "On some plane problems of an infinite plate containing an infinite row of circular holes". Bull. JSME 3, 259-265 (1960).

1.66 T. Shibuya and I. Nakahara. "An approximate analysis of stress concentration around a conical hole in a plate". Bull. JSME., 17, 655-660 (1974).

1.67 M.Z. Narodeskiy. "Tension of a square plate weakened by round hole in centre". Inzh. Sb. 14, AN SSSR Press, Moscow (1953).

1.68 N.F. Guryev. "The distribution of tension stresses in an isotropic finite rectangular plate weakened by a circular opening". Scientific Annals of the Poltava Pedagogical Inst. 8, (1955).

1.69 V.M. Rakivnenko and V.I. Makhorikov. "Stress concentration around round hole in square plate". DAN URSR, 4, 464-468 (1961).

1.70 G.N. Savin. "Distribution of stresses in a plane field containing a hole of any type". Trudy Dnepropet. Inzh-Konstr. Inst., Comm. 10 (1936).

1.71 P.A. Sokolov. "Distribution of stresses in a plane field weakened by a hole of any type". Bull.Scient.-Tech.Comm., Upr. Voyenno-Morsk, sil.rab.-krest.kras.arm. 4, 39-71 (1930).

1.72 Y.P. Anikin. "Stress concentration in plate with rectangular notch". Trudy Dal'nevostochn.Politekhn. In-ta., 45, 63-81 (1956).

1.73 S.R. Heller, J.S. Brock and R. Bart. "The stresses around a rectangular opening with rounded corners in a uniformly loaded plate". Proc. 3rd U.S. Nat. Cong. Appl. Mech., ASME 357-368 (1958).

1.74 H.B. Phillips, F.Asce and I.E. Allen. "Stresses around rectangular openings in a plate". J.Engin.Mech.Div., Proc. ASCE (1960).

1.75 G.N. Savin. "Influence of an inserted elastic ring on the stress state around a circular hole". Dokl.otd.tekh.nauk.Akad.Nauk. Ukr. SSR 4 (1947).

1.76 M.P. Sheremeter. "Influence of a uniformly stressed plane field of an elastic ring which is welded into a curvilinear hole". Ukr. Mat.Zh. 3, Kiev (1949).

1.77 W.H. Wittrick. "Stress around reinforced elliptical holes with applications to pressure cabin windows". Aero.Quart., 10, 373-400 (1959).

1.78 R.A.W. Haddon. "Stresses in an infinite plate with two unequal circular holes". Quart. J. Mech. and Appl. Math., 20, 277-291 (1967).

1.79 W. Olszak. "The compression of an infinite plate having circular holes". Warsaw (1934). Also: Ingenieur Archiv., 6, 402-418 (1935).

1.80 K.I. Schulz. "Over den Spannungstoestand in doorborde Platen" Diss.Techn.Hoschschule, Delft (1941). See also: "Survey of papers on elasticity published in Holland 1940-1946" (C.B. Biezeno) Adv. Appl. Mech., 1, 121-129 (1948).

1.81 F.I. Baratta and D.M. Neal. "Stress concentration factors in U-shaped and semi-elliptical edge notches". J.Strain Anal., 5, 121-127 (1970).

1.82 V.Y. Rubenchik. "Stress concentration close to grooves". Vestnik Mashinostroeniya, 55, 26-28 (1975).

1.83 C-B. Ling. "Stress analysis of edge notches". Ibid [1.24]. 135-172 (1978).

1.84 A.P. Parker. "Mechanics of fracture and fatigue in some common structural configurations". Ph.D. Thesis, Southampton University (1979).

1.85 C.J. Hooke. "Numerical solution of plane elastostatic problems by point matching". J.Strain Anal., 3, 109-114 (1968).

1.86 C.J. Hooke. "Numerical solution of axisymmetric stress problems by point matching". J.Strain Anal. 5, 25-37 (1970).

1.87 O.L. Bowie and D.M. Neal. "A modified mapping-collocation technique for accurate calculation of stress intensity factors". Int. J. Fract. Mech. 6, 199-206 (1970).

1.88 O.L. Bowie and C.E. Freese, "Central crack in plane orthotropic rectangular sheet". Int.J.Fract.Mech., 8, 49-57 (1972).

1.89 O.L. Bowie, C.E. Freese and D.M. Neal. "Solution of plane problems of elasticity utilizing partitioning concepts". Trans. ASME., J.Appl.Mech. 40, 767-772 (1973).

1.90 O.L. Bowie and C.E. Freese. "Analysis of notches using conformal mapping". Ibid [1.24].69-134 (1978).

1.91 C.E. Freese. "Collocation and finite elements - a combined method" AMMRC-TR73-28, Army Materials and Mechanics Research Center, Watertown, Mass. (1973).

1.92 D.J. Cartwright and D.P. Rooke. "Evaluation of stress intensity factors". J.Strain. Anal., 10, 217-224 (1975).

1.93 M.J. Follows and D.J. Cartwright. "Stress intensity factors for fretting fatigue". (in preparation).

1.94 J. Robinson. "Integrated theory of finite element methods". John Wiley & Sons Ltd. (1973).

1.95 R.H. Gallagher. "A review of finite element techniques in fracture mechanics". Proc. 1st Int. Conf. on Num. Meth. in Fract.Mech., (A.R. Luxmore and D.R.J. Owen, Ed.), Swansea, 1-25 (1978) .

1.96 A.J. Faukes, D.R.J. Owen and A.R. Luxmore. "An assessment of crack tip singularity models for use with isoparametric elements". Eng.Fract.Mech. 11, 143-159 (1979).

1.97 T.H.H. Pian. "Formulations of finite element methods for solid continua". Recent Advances in Matrix Methods of Structural Analysis and Design (R.H. Gallagher et al, Ed.) Univ. of Alabama Press, 49-83 (1971).

1.98 T.H.H. Pian and P. Tong. "Basis of finite element methods for solid continua". Int.J.Num.Meth.Eng., 1, 3-28 (1969).

1.99 E. Byskov. "The calculation of stress intensity factors using the finite element method with cracked elements". Int. J. Fract. Mech., 6, 157-167 (1970).

1.100 D.M. Tracey. "Finite elements for determination of crack tip stress intensity factors". Eng. Fract. Mech. 3, 255-265 (1971).

1.101 P. Tong and S.J. Lasry. "A super-element for crack analysis". Int.J. Fract. 9, 234-236 (1973).

1.102 P. Tong, T.H.H. Pian and S.J. Lasry. "A hybrid element approach to crack problems in plane elasticity". Int.J.Num.Meth.Eng., 7, 297-309 (1973).

1.103 A.K. Rao, I.S. Raju, A.V.K. Murty. "A powerful hybrid method in finite element analysis". Int.J.Num.Meth.Eng., 3, 389-403. (1971).

1.104 L.S.D. Morley. "A finite element application of the modified Rayleigh Ritz method". Int.J.Num.Meth.Eng., 2, 85-98 (1970).

1.105 L.S.D. Morley. "Finite element solution of boundary value problems with non-removable singularities". Phil.Trans.Roy. Soc. London, A, 275, 463-488 (1973).

1.106 Y. Yamamoto. "Finite element approaches with the aid of analytical solutions". Recent Advances in Matrix Methods of Structural Analysis and Design. (R.H. Gallagher et al., Ed.), Univ. of Alabama Press, 85-103 (1971).

1.107 Y. Yamamoto and H. Tokuda. "Determination of stress intensity factors in cracked plates by the finite element method". Int. J.Num.Meth.Eng. 6, 427-439, (1973).

1.108 G. Yagawa, T. Nishioka, Y. Ando and N. Ogura. "Finite element calculation of stress intensity factors using superposition" 2nd ASME Pressure Vessel and Piping Conf., San Francisco (1975).

1.109 P. Bartholomew. "Solution of elastic crack problems by superposition of finite elements and singular fields". Computer Methods in Appl.Mech. and Eng., 13, 59-78 (1978) (RAE TR 76165).

1.110 P. Bartholomew. "The implementation and practical verification of a superposition method for the solution of elastic crack problems". Proc. 1st Int.Conf. on Num.Meth. in Fract.Mech., (A.R. Luxmore and D.R.J. Owen, Ed.) Swansea, 336-349 (1978) (RAE Tech.Memo.Str.940).

1.111 E. Schnack and M. Wolf. "Application of displacement and hybrid stress methods to plane notch and crack problems". Int.J.Num. Meth.Eng. 12, 963-975 (1978).

1.112 M.A. Jaswon. "Integral equation methods in potential theory". Proc. Roy.Soc. London A, 275, 23-32 (1963).

1.113 G.T. Symm. "Integral equation methods in potential theory". Proc.Roy.Soc. London, A, 275, 33-46 (1963).

1.114 T.A. Cruse. "Numerical solutions in three-dimensional elastostatics". Q.Appl.Math., 25, 83-92 (1967).

1.115 F.J. Rizzo. "An integral equation approach to boundary value problems of classical elastostatics". Q.Appl.Math. 25, 93-95 (1967).

1.116 S.T. Wang and G.E. Blandford. "Comparison of boundary integral equation and finite element methods". J. Struct.Div., Proc. ASCE, 102, 1941-1947 (1976).

1.117 C.A. Brebbia. "Weighted residual classification of approximate methods". Appl.Math.Modelling 2, 160 (1978).

1.118 J.C. Lachat. "A further development of the boundary integral technique for elastostatics". Ph.D. Thesis, Southampton University (1975).

1.119 J.C. Lachat and J.O. Watson. "Effective numerical treatment of boundary integral equations: a formulation for three dimensional elastostatics". Int.J.Num.Meth.Eng., 10, 991-1005 (1976).

1.120 T.A. Cruse and R.B. Wilson. "Advanced applications of boundary integral equation methods". Nuclear Eng. Des. 46, 223-234 (1978).

1.121 C.A. Brebbia and O.V. Chang. "Boundary elements applied to seepage problems in zoned anisotropic soils". Adv.Eng.Software 1, 95-105 (1979).

1.122 M.A. Jaswon and G.T. Symm. "Integral equation methods in potential theory and elastostatics". Academic Press (1977).

1.123 E.R.A. Oliviera. "Plane stress analysis by a general integral method". J.ASCE, Engng. Mech. Div., 79-85 (1968).

1.124 J.O. Watson. "Analysis of thick shells with holes by using integral equation method". Ph.D. Thesis, University of Southampton (1973).

1.125 P.K. Banerjee and R. Butterfield. "Boundary element methods in geomechanics", Finite Elements in Geo-mechanics, (G. Gudehus, Ed.), Chapter 16, Wiley, London (1976).

1.126 H. Nisitani. "The two dimensional stress problem solved using an electric digital computer". Bull. JSME, 11, 14-23 (1968).

1.127 H. Nisitani and Y. Murakami. "Stress intensity factors of an elliptical crack or a semi-elliptical crack subject to tension". Int.J.Fract. 10, 353-368 (1974).

1.128 H. Nisitani. "A method for calculating stress concentrations and its applications". Strength and Structure of Solid Materials (H. Miyamoto et al, Ed.) Noordhoff, 55-69. (1976).

1.129 H. Nisitani. "Solutions of notch problems by body force method" Ibid [19] 1-68, (1978).

1.130 M.D. Snyder and T.A. Cruse. "Boundary integral equation analysis of cracked anisotropic plates". Int.J.Fract.Mech., 11, 315-328 (1975).

1.131 H. Nisitani and Y. Murakami. "Stress intensity factors of an elliptical crack or a semi-elliptical crack subject to tension". Int.J. Fracture 10, 353-368 (1974).

1.132 Y. Murakami. "Application of the body force method to the calculation of stress intensity factors for a crack in the arbitrarily shaped plate". Engng. Fract. Mech., 10, 497-513. (1978).

1.133 J.C.F. Telles and C.A. Brebbia. "Boundary Element solution for half plane problems". Int.J. Solids and Structures. 17, 1149-1158. (1981).

1.134 J.C.F. Telles. "On the application of the boundary element method to inelastic problems". Ph.D. thesis, University of Southampton (1982).

CHAPTER 2

2.1 L.S.D. Morley. Ibid [1.105] (1973).

2.2 P. Bartholomew. Ibid [1.109] (1978).

2.3 P. Bartholomew. Ibid [1.110] (1978).

2.4 O.C. Zienkiewicz. Ibid [1.12] (1977).

2.5 T.H.H. Pian and P. Tong. Ibid [1.98] (1969).

2.6 L.S.D. Morley. "Bending of a square plate with central square hole". RAE TR69031. (1969).

2.7 R.S. Martin and J.H. Wilkinson. "Symmetric decomposition of positive definite band matrices". Numerische Mathematik, 7, 355-361. (1965).

2.8 B.C. Merrifield. "Fortran subroutines for finite element analysis". RAE TR71156. (1971).

CHAPTER 3

3.1 I.S. Sokolnikoff. "Mathematical Theory of Elasticity. McGraw-Hill, 2nd Edition (1956).

3.2 S. Timoshenko and J.N. Goodier. "Theory of Elasticity". McGraw-Hill, 2nd Edition (1951).

CHAPTER 4

4.1 P. Bartholomew. Ibid [1.109] (1978).

4.2 P. Bartholomew. Ibid [1.110] (1978).

4.3 B.C. Merrifield. Ibid [2.8] (1971).

CHAPTER 5

5.1 R.C.J. Howland. Ibid [1.48] (1930).

5.2 M. Isida. Ibid [1.62] (1955).

5.3 M. Isida. Private communication (1979).

5.4 D.J. Allman. "On compatible and equilibrium models with linear stress for stretching of elastic plates". in Energy Methods in Finite Element Analysis. (R. Glowinski, E.Y. Rodin, O.C. Zienkiewicz, Eds.) John Wiley. (1979).

5.5 V.H. Hengst. Ibid [1.52] (1938).

5.6 R.C. Knight. Ibid [1.54] (1935).

5.7 P.S. Theocaris. Ibid [1.55] (1956).

5.8 D.J. Cartwright. "Stress intensity factors and residual static strength in certain cracked structural elements". Ph.D. Thesis, University of Southampton (1971).

5.9 R.S. Whitehead. "Analytical determination of stress intensity factors for attachment lugs". British Aerospace Report No. SON(P) 199, Warton. (1978).

5.10 J.C. Newman. Private communication (1979).

5.11 W. Geier. "Strength behaviour of fatigue cracked lugs". RAE Library translation 2057. Dissertation Technical University Munich. (1980).

5.12 R.D. Gregory. "Stress concentration around a loaded bolt in an axially loaded bar". Proc. Camb. Phil. Soc., 64, 1215-1236, (1967).

5.13 R.B. Heywood. Ibid [1.30] (1962).

5.14 W.G. Bickley. Ibid [1.36] (1928).

5.15 S. Timoshenko and J.N. Goodier. Ibid [3.2] (1951).

5.16 M. Isida. "Effect of width and length on stress intensity factors of internally cracked plates under various boundary conditions". Int. J. Fract. Mech., 7, 301-310. (1971).

5.17 J.E. Moon. "Crack growth in pin loaded lugs", Proc. 17th Conf. of I.C.A.F. Noordwijkerhout, The Netherlands, (1981).

5.18 O. Gencoz, U.G. Goranson and R.R. Merrill. "Application of finite element analysis techniques for predicting crack propagation in lugs". Int.J. Fatigue, 121-129, (1980).

5.19 H.T. Jessop, C. Snell, G.S. Holister. "Photoelastic investigation on plates with single interference fit pits with load applied a) to pin only and, b) to pin and plate simultaneously". Aero. Quart., 9, 147-163. (1958).

5.20 D.J. White and L.R. Enderby. "Finite element stress analysis of a non-linear problem: A connecting rod eye loaded by means of a pin". J. Strain Anal., 5, 41-48 (1970).

CHAPTER 6

6.1 S.T. Wang and G.E. Blandford. Ibid [1.116] (1976).

6.2 C.A. Brebbia. Ibid [1.117] (1980).

6.3 J.C. Lachat. Ibid [1.118] (1975).

6.4 A.E.H. Love. "A Treatise on the Mathematical Theory of Elasticity". Dover, New York, (1944).

6.5 B.E.S.Y. "Boundary Element Analysis System". User Manual, Computational Mechanics Consultants. (1983).

6.6 E.M. Remzi. "Boundary integral equation stress analysis of incompressible and nearly incompressible materials". Ph.D. Thesis, Department of Mechanical Engineering, Imperial College of Science & Technology, London (1981).

6.7 T.A. Cruse. "Boundary Integral equation methods in solid mechanics". Report SM 7317. Carnegie Institute of Technology. (1973).

6.8 H. Nisitani and Y. Murakami. Ibid [1.131] (1974).

6.9 T.A. Cruse. Ibid [1.130] (1975).

6.10 M.D. Snyder and T.A. Cruse. "Crack tip stress intensity factors in finite anisotropic plates". Tech. Report. AFML-TR-73-209. (1973).

6.11 J.C.F. Telles and C.A. Brebbia. Ibid [1.133] (1981).

6.12 Y. Murakami. Ibid [1.132] (1978).

6.13 P.K. Banerjee and R. Butterfield. Ibid [1.125] (1976).

6.14 I.S. Sokolnikoff. Ibid [3.1] (1956).

6.15 C. Somigliana. "Sopra l'equilibrio di un corpo elastico isotropo". Il Nuovo Ciemento, 17-19. (1886).

6.16 T.A. Cruse. "Boundary integral equation method for three-dimensional elastic fracture mechanics analysis". AFOSR-TR-75-0813. (1975).

6.17 T.A. Cruse, D.W. Snow and R.B. Wilson. "Numerical solutions in axisymmetric elasticity". Computers and Structures, 445. (1977).

6.18 A.H. Stroud and D. Secrest. "Gaussian quadrature formulas". Prentice-Hall, Englewood Cliffs, N.J. (1966).

6.19 Y. Murakami and H. Nisitani. "A method for calculating stress intensity factors in an arbitrarily shaped finite plate with a crack". Proc. int. conf. on Fracture Mechanics and Technology (G.C. Sih and C.L. Chow, Eds.), Hong Kong, Noordhoff. 1171-1185. (1977).

CHAPTER 7

7.1 S. Timoshenko and J.N. Goodier. Ibid [3.2] (1951).

7.2 V.H. Hengst. Ibid [1.52] (1938).

CHAPTER 8

8.1 P. Bartholomew. Ibid [1.110] (1978).

8.2 J.C.F. Telles. Ibid [1.134] (1982).

APPENDIX A

Derivation of the Variational Principle

The principle of minimum complementary energy states that the complementary energy is a minimum when the system considered is equilibrium. A functional [2.5] based on this principle may therefore be expressed:

$$\Pi = -U(\underline{\sigma}^I) + \int_{S_K} (\underline{T}^I)^T \bar{\underline{u}}\, dS \qquad (A.1)$$

where Π = the complementary energy functional

$\underline{\sigma}^I$ = the stress field over the region considered

$U(\underline{\sigma}^I)$ = the strain energy

S_K = boundaries having kinematic constraints

$\underline{T}^I$ = the tractions on the boundary arising from σ^I

$\bar{\underline{u}}$ = the prescribed displacements on S_K .

$(\ )^T$ = denotes the transpose of a vector or matrix.

When the complementary energy is a minimum, the variation of the functional is zero, thus:

$$\delta \Pi = 0 \qquad (A.2)$$

To use this variational principle in a finite element scheme the equilibrium of the stress field $\underline{\sigma}^I$ is required across element boundaries. This may be introduced using Lagrange multipliers rather than as a constraint on the choice of possible functions for $\underline{\sigma}^I$. Thus at any point on a boundary between two elements, element 'a' and element 'b' say, the equilibrium conditions may be expressed as follows:

$$\underline{T}_a^I + \underline{T}_b^I = 0 \qquad (A.3)$$

where $\underline{T}_a^I$ and $\underline{T}_b^I$ are the tractions due to the stress field $\underline{\sigma}^I$ in elements 'a' and 'b' respectively along the inter-element boundary, S_{ab}. Introducing the Lagrange multiplier, $\underline{\lambda}$, this constraint may be expressed as:

$$\delta \{ \int_{S_{ab}} (\underline{\lambda})^T (\underline{T}_a^I + \underline{T}_b^I)\, dS \} = 0 \qquad (A.4)$$

where $\delta\{\ \}$ denotes the variation of the expression and S_{ab} is the boundary between elements 'a' and 'b'. The term within the curly brackets in equation (A.4), summed over all elements, may therefore be added to the functional, equation (A.1). The new functional, Π_c, may then be written:

$$\Pi_c = \sum_N \{- U_N(\underline{\sigma}^I) + \int_{S_{E_N}} (\underline{\lambda})^T \underline{T}^I \, dS + \int_{S_{K_N}} (\underline{T}^I)^T \underline{\bar{u}} \, dS \} \qquad (A.5)$$

where the summation is carried out over all the elements, the subscript N refers to the N'th element and in particular S_{E_N} denotes the *inter-element* boundaries of the N'th element. The complete element boundary, denoted S_N, is made up of inter element boundaries S_{E_N}, and/or kinematic boundaries S_{K_N} and/or traction boundaries S_{T_N}. Thus:

$$S_N = S_{E_N} + S_{K_N} + S_{T_N} \qquad (A.6)$$

The Lagrange multiplier $\underline{\lambda}$ in equation (A.5) may be identified by taking the variation of Π_c with respect to $\underline{\sigma}^I$ and $\underline{\lambda}$. This yields the following:

$$\delta\Pi_c = \sum_N \{-\int_{S_N} (\tilde{\underline{u}})^T \delta\underline{T}^I \, dS + \int_{S_{E_N}} (\delta\underline{\lambda})^T \underline{T}^I \, dS + \int_{S_{E_N}} (\underline{\lambda})^T \delta\underline{T} \, dS + \int_{S_{K_N}} (\delta\underline{T}^I)^T \underline{\bar{u}} \, dS \} \qquad (A.7)$$

$$= 0$$

where $\tilde{\underline{u}}$ are the displacements defined on the element boundary and are equal to $\underline{\bar{u}}$ on S_K. Since $\delta\underline{T}^I$ must be zero on the traction boundaries, equation (A.7) may be written:

$$\sum_N \{ \int_{S_{E_N}} (\underline{\lambda}-\tilde{\underline{u}})^T \delta\underline{T}^I \, dS + \int_{S_{E_N}} (\delta\underline{\lambda})^T \underline{T}^I \, dS \} = 0 \qquad (A.8)$$

from which it is clear that $\underline{\lambda}$ is equal to the displacement field $\tilde{\underline{u}}$. Substituting for $\underline{\lambda}$ in equation (A.5) gives:

$$\Pi_c = \sum_N \{- U_N (\underline{\sigma}^I) + \int_{S_{E_N}} (\underline{\tilde{u}})^T \underline{T}^I \, dS + \int_{S_{K_N}} (\underline{\bar{u}})^T \underline{T}^I \, dS \} \qquad (A.9)$$

or more conveniently:

$$\Pi_c = \sum_N \{- U_N (\underline{\sigma}^I) + \int_{S_N} (\underline{\tilde{u}})^T \underline{T}^I \, dS - \int_{S_{T_N}} (\underline{\tilde{u}})^T \underline{\bar{T}} \, dS \} \qquad (A.10)$$

where $\underline{\bar{T}}$ denotes the prescribed tractions on the traction boundary S_{T_N}.

APPENDIX B

Listings of selected finite element program segments

This appendix contains listings of the following program segments from the FESM program

Segment Name	Function	Page No.
NOTCH	Program master segment	159
AREAS	Calculates element areas	163
TRLFNS1	Trial functions for circular hole	163
TRLFNS2	Trial functions for elliptical hole	165
LOADFN	Loading function	166
BCONDS	Applies boundary conditions	167
ALPHAS	Calculates the coefficients α_i	172

Table B.1 Program segments listed in this appendix.

The program segments shown in table B.2 are also used by the FESM program but are not listed in this thesis since they are not primarily concerned with the theoretical changes to the method which have been discussed in chapters 2 to 4.

Segment Name	Function
ADJUST	Adjusts the direct access file data if too many nodes defined.
BCDATA	Inputs boundary condition data.
COMP	Compares two character strings.
DETAILS	Prints details of options selected.
ELEMDATA	Inputs element data
ELEMPRINT	Prints element data
KASSEM	Assembles element stiffness matrix in global matrix.
KCNSTR	Solves constrained banded matrix equation.
KMAT	Forms global stiffness matrix.
KSOLVE	Solves simultaneous equations. Called by KCNSTR.
KVECT	Post-multiplies banded matrix by vector.
MINAX	Determines minimum and maximum value in array.
MINV	Inverts matrix.
NODEDATA	Inputs node data.
PARAMS	Calculates and checks various parameters.
PRINT	Prints displacements and stresses.
SIGSTAR	Evaluates stresses.
SPRBND	Assembles list of nodes on special region boundary.
SPRINT	Calculates strain energy term for elements in special region.
SPRLDS	Evaluates $\underline{\sigma}_i^{\dagger}$ and corresponding nodal loads for elements in special region.
SRDATA	Inputs data for special region.
TRANSAX	Converts stresses and displacements to new coordinate axes.
TRAX	Rotates coordinate axes.
TRLFNSO	Trial functions for cracked configurations.

Table B.2. Other program segments used by FESM program.

```
CODE FOR NOTCH
      PROGRAM NOTCH
C
C                  $$$$$$$$$$$$$$$$$$$$$$$$$$$$$$$$$$$$
C
C                  $   $   $$$$   $$$$$$   $$$$  $   $$
C                  $$  $  $$  $     $$    $$  $    $  $$
C                  $$$ $  $$  $     $$    $$  $    $  $$
C                  $$ $$  $$  $     $$    $$  $    $$$$$$
C                  $$  $   $$$$     $$     $$$$  $   $$
C
C                  $$$$$$$$$$$$$$$$$$$$$$$$$$$$$$$$$$$$
C
C              ================================================
C                   THE FINITE ELEMENT SUPERPOSITION METHOD
C              ================================================
C
C              A FINITE ELEMENT PROGRAM FOR THE DETERMINATION OF
C
C              STRESS CONCENTRATION AND STRESS INTENSITY FACTORS
C
C              USING A METHOD DEVELOPED AT RAE BY  P BARTHOLOMEW
C
C                           MODIFIED  AND  EXTENDED
C
C                 AT SOUTHAMPTON UNIVERSITY BY A R CARMICHAEL
C                 ===========================================
C
C    THE METHOD EMPLOYS A SUPERPOSITION OF CONSTANT STRAIN TRIANGULAR
C    ELEMENTS AND  TRIAL  FUNCTIONS WITH A SPECIAL REGION. BAR  (FLA)
C    ELEMENTS ARE  ALSO AVAILABLE FOR USE OUTSIDE THE SPECIAL REGION.
C    LOADING  ON  HOLE  APPLIED  USING  FOURIER  SERIES OF TRACTIONS.
C
C    DIMENSIONS
C    ----------
C               IDIM.GE.NUMBER OF EQUATIONS = NEQ
C               INAM.GE.NUMBER OF NODES     = NNODE
C               IDE .GE.NUMBER OF ELEMENTS  = NEL
C
C    MINIMUM DIMENSIONS
C    ------------------
C               STIF(NEQ,ISEMI) RHS(NEQ,5) BC(NEQ,5) RHS1(NEQ)
C               CT(NEQ,2) DT(NEQ,5) CONROW(NEQ)
C               X(NNODE) Y(NNODE) IDENT(NNODE) NBA(NNODE)
C               LSTBA(NNODE,3) LSTBL(NNODE,3)
C               ELNO(NEL,3) LSTSRN(NEL) T(NEL)
C
C    IDIM MUST BE FIRST DIMENSION OF  STIF, RHS, BC, DT, CT
C    INAM MUST BE FIRST DIMENSION OF  LSTBA, LSTBL
C    IDE  MUST BE FIRST DIMENSION OF  ELNO
C
C    IN SUBROUTINE KONSTR CHECK THAT THE DIMENSION OF SPARE IS GE.IDIM
C    IN SUBROUTINE KVECT  CHECK THAT THE DIMENSION OF SPARE IS GE.IDIM
C
C***      ***      ***      ***      ***      ***      ***      ***
C
C  IPR =-1   MINIMUM OUTPUT.              (CHANNEL 7)
C      = 0   HEADING & MINIMUM OUTPUT.    (CHANNEL 7)
C      = 1   STRESSES OUTPUT.             (CHANNEL 7)
C      = 2   DISPLACEMENTS OUTPUT.        (CHANNEL 7)
C      = 4   DATA OUTPUT.                 (CHANNEL 7)
C      = 8
C      = 16
C      = 32  ADDITIONAL OUTPUT.           (CHANNEL 7)
C      = 64  EXTRA DE-BUG OUTPUT.         (CHANNEL 7)
C
C  ADD NUMBERS 1-64 TOGETHER FOR COMBINATION OF OPTIONS.
C  [ ERROR AND WARNING MESSAGES ALSO OUTPUT ON CHANNEL 6 ]
C
      INTEGER ISYM(10)
      INTEGER CONROW(450),LSTSRN(400),IDENT(250),ELNO(400,3)
      INTEGER NBA(250),LSTBA(250,3),LSTBL(250,3)
      INTEGER ITITLEM(20),ITITLEC(20),OPTIONS(16)
C
      LOGICAL CONVERT,OK,MDAF,CDAF
C
      REAL STIF(450,80),RHS(450,10),RHS1(450),BC(450,10),CT(450,2)
      REAL DT(450,10),SIGMA(27,400),T(400),AREA(400),X(250),Y(250)
      REAL NU,DCT(9,9),DCTR(9),DS(9,9),DCKR(9),DCONT(9,9),ALPHA(9)
      REAL*4 AN(30)/30*0./,DN(30)/30*0./
C
      CHARACTER*4 IDATA(20)
      CHARACTER*1 DATE(18)
C
      COMMON STIF,RHS,RHS1,BC,CT,DT,SIGMA,T,AREA,X,Y
      COMMON /BNOTCH/ISYM
      COMMON /TRL/CONVERT,SSS(9,6),AN,DN,SICO(58)
      COMMON /SIZE/ID,MTF,MRHS,MTF3,MA
      COMMON /TRX/XC,YC
C***      ***      ***      ***      ***      ***      ***      ***
C
C  INITIALIZE PARAMETERS
      CALL ICL9HEMASK(64,IRESP)
      OK=.TRUE.
      MDAF=.FALSE.
      CDAF=.FALSE.
      CONVERT=.FALSE.
      IDIM=450
      IDE=400
      INAM=250
      MRHS=10
      MTF=8
      MTF3=27
      MA=81
      NRHS=MRHS
      IM=20
      IC=20
      NU=0.3
      E=1.0
      DO 20 I=1,IDE
20    LSTSRN(I)=0
```

```
C=========================================
C  READ AND CHECK DATA FOR ELEMENTS AND NODES
C=========================================
C  FIND BEGINNING OF MESH DATA
40     READ(5,620,END=60)IDATA
       N=2
       CALL COMP(N,IDATA(2),3,'IN',1)
       IF(N.EQ.2)GOTO 100
       OK=.FALSE.
       GOTO 40
C
C  READ MESH DATA FROM D.A.F.
60     IF(.NOT.OK)GOTO 80
       MDAF=.TRUE.
       READ(9,REC=1)NEL,NNODE,NBC
       READ(9,REC=2)XCRACK,YCRACK
       READ(9,REC=3)A,B,THETA
       READ(9,REC=17)(ITITLEM(I),I=1,4)
       IM=4
       GOTO 100
80     WRITE(6,1340)
       WRITE(7,1340)
       STOP '*FAIL*'
100    CALL ICL9LGGDATE(DATE(1))
       CALL ICL9LGGTIME(DATE(9))
C
C  READ "CONTROL" DATA
       READ(4,640,END=140)(OPTIONS(I),I=1,6)
       READ(4,620)ITITLEC
       READ(4,640)ITF,ISYM
       ISYM(MRHS)=ITF
       IF(ISYM(MRHS-1).NE.1)GOTO 110
       READ(4,*)AN
       READ(4,*)(DN(I),I=2,25)
110    DO 120 IR=7,11
       WRITE(9,REC=IR)(AN(I),I=IR*6-41,IR*6-36)
120    CONTINUE
       DO 130 IR=12,15
       WRITE(9,REC=IR)(DN(I),I=IR*6-70,IR*6-65)
130    CONTINUE
       WRITE(9,REC=16)(OPTIONS(I),I=1,6)
       WRITE(9,REC=19)(ISYM(I),I=1,6)
       WRITE(9,REC=20)(ISYM(I),I=7,MRHS)
       WRITE(9,REC=21)E,NU
       GOTO 180
C
C  READ CONTROL DATA FROM D.A.F.
140    CDAF=.TRUE.
       READ(9,REC=16)(OPTIONS(I),I=1,6)
       READ(9,REC=18)(ITITLEC(I),I=1,4)
       READ(9,REC=19)(ISYM(I),I=1,6)
       READ(9,REC=20)(ISYM(I),I=7,MRHS)
       ITF=ISYM(MRHS)
       IF(ISYM(MRHS-1).NE.1)GOTO 170
       DO 150 IR=7,11
       READ(9,REC=IR)(AN(I),I=IR*6-41,IR*6-36)
150    CONTINUE
       DO 160 IR=12,15
       READ(9,REC=IR)(DN(I),I=IR*6-70,IR*6-65)
160    CONTINUE
170    READ(9,REC=21)E,NU
       IC=4
C
C  READ "MESH" DATA
180    IF(MDAF)GOTO 200
       READ(5,620)ITITLEM
       READ(5,660)XCRACK,YCRACK,A,THETA,B
       READ(5,640)NEL
       WRITE(9,REC=2)XCRACK,YCRACK
       WRITE(9,REC=3)A,B,THETA
200    WRITE(9,REC=17)(ITITLEM(I),I=1,4),(DATE(II),II=9,16)
       WRITE(9,REC=18)(ITITLEC(I),I=1,4),(DATE(II),II=1,8)
       IPR=OPTIONS(1)
       IMD=OPTIONS(2)
       IF((B.LT.1.E-20).AND.(ITF.NE.0))B=A
       IF(IPR.LT.0)GOTO 220
       WRITE(7,680)
       WRITE(7,700)
220    WRITE(7,720)(ITITLEM(I),I=1,IM)
       IF(MDAF)WRITE(7,1220)
       WRITE(7,720)(ITITLEC(I),I=1,IC)
       IF(CDAF)WRITE(7,1240)
       WRITE(7,1200)(DATE(II),II=1,16)
       IF(IPR.LT.0)GOTO 240
       WRITE(7,740)XCRACK,YCRACK,A,B,THETA,E,NU
       WRITE(7,760)ITF
       CALL DETAILS(ISYM,IPR,IMD,AN,DN)
240    THETA=3.1415926536*THETA/180.0
       DO 260 I=1,MTF
       IF(ISYM(I).GE.1)ID=I
260    CONTINUE
C
C  READ ELEMENT DATA
       CALL ELEMDATA(ELNO,T,LSTSRN,IDE,NEL,NELSP,MDAF)
C
C  DETERMINE PARAMETERS FROM ELEMENT DATA
       MNODE=NNODE
       CALL PARAMS(NEL,ELNO,IDE,3,IDENT,INAM,2,0,NEQ,NAM,NNODE,ISEMI)
C
C  CHECK WHETHER DIMENSIONING IS O.K.
       IF(NEQ.GT.IDIM)WRITE(7,1260)IDIM
       IF(NEL.GT.IDE)WRITE(7,1280)IDE
       IF(NNODE.GT.INAM)WRITE(7,1300)INAM
       IF(ISEMI.GT.80)WRITE(7,1320)
       IF(NEQ.GT.IDIM)WRITE(6,1260)IDIM
       IF(NEL.GT.IDE)WRITE(6,1280)IDE
       IF(NNODE.GT.INAM)WRITE(6,1300)INAM
       IF(ISEMI.GT.80)WRITE(6,1320)
       IF(.NOT.MDAF.OR.MNODE.EQ.NNODE)GOTO 280
       WRITE(7,1360)NNODE,MNODE
       WRITE(6,1360)NNODE,MNODE
       WRITE(9,REC=1)NEL,NNODE,NBC
```

```
      CALL ADJUST(NEL,NNODE,MNODE,NBC,9)
C
C  PRINT DATA IF REQUIRED
280   IF(IPR.LT.0)GOTO 300
      WRITE(7,780)NAM,NEQ,NEL,NNODE
      WRITE(7,800)ISEMI
      IF(IPR-IPR/8*8.LT.4)GOTO 300
      WRITE(7,820)
      CALL ELEMPRINT(ELNO,T,NEL,IDE)
      WRITE(7,840)
300   CONTINUE
      SA=SIN(THETA)
      CA=COS(THETA)
C
C  READ NODE AND COORDINATE DATA
      CALL NODEDATA(X,Y,NAM,INAM,NEL,NNODE,MDAF)
C
C  TRANSFORM AXES (XCRACK,YCRACK,THETA)
      CALL TRAX(XCRACK,YCRACK,SA,CA)
      DO 320 I=1,NNODE
      J=IDENT(I)
      IF(J.EQ.0)GOTO 320
      CALL TRAX(X(I),Y(I),SA,CA)
      IF(IPR-IPR/8*8.GE.4)WRITE(7,860)I,XC,YC,I,X(I),Y(I)
320   CONTINUE
C=============================
C  CALCULATE AREAS OF ELEMENTS
C=============================
      CALL AREAS(AREA,X,Y,ELNO,INAM,IDE,NEL,A,B,XCRACK,YCRACK,IPR)
      IAJSEM=IDIM*ISEMI
C========================
C  STIFFNESS MATRIX FORMED
C========================
      CALL KMAT(STIF,IDIM,IAJSEM,NEL,ELNO,IDE,X,Y,INAM,E,T,NU,IDENT,
     2 AREA)
C
C  READ SPECIAL REGION DATA IF REQUIRED
      IF(.NOT.CDAF)CALL SRDATA(LSTSRN,NELSP,ELNO,T,IDE)
C
C  DEFINE BOUNDARY OF SPECIAL REGION
      CALL SPRBND(LSTSRN,ELNO,LSTBA,LSTBL,NBA,NNODE,NEL,IDE,INAM)
C=============================================================
C  EVALUATE DAGGER FIELD STRESSES AND EQUIV. NODAL LOADS IN SP.R.
C=============================================================
      CALL SPRLDS(RHS,ELNO,X,Y,IDIM,IDE,A,B,E,T,NU,INAM,XCRACK,YCRACK,
     2 LSTSRN,NELSP,SIGMA,NEL,IDENT,ITF,AREA)
C=============================================================
C  APPLY BOUNDARY CONDITIONS AND EVALUATE BOUNDARY INTEGRALS
C=============================================================
      IF(IPR-IPR/8*8.GE.4)WRITE(7,880)
      CALL BCONDS(X,Y,RHS,E,NU,IDIM,XCRACK,YCRACK,T,LSTSRN,A,B,CT,DT,
     2 CONROW,INAM,ELNO,IDE,DCT,DCTR,DCKR,DS,SIGMA,NELSP,LSTBA,
     3 LSTBL,NBA,NNODE,NEL,IPR,IDENT,ITF,AREA,MDAF)
C
C  COPY RHS INTO BC
      DO 340 J=1,MRHS
      DO 340 I=1,IDIM
      BC(I,J)=RHS(I,J)
340   CONTINUE
C=============================================
C  FORM "DCONT" MATRIX  (SP. R. STRAIN ENERGY TERM)
C=============================================
      CALL SPRINT(SIGMA,NELSP,DCONT,T,E,NU,IDE,NEL,LSTSRN,AREA)
C
C  PRINT ADDITIONAL OUTPUT IF REQD.
      IF(IPR-IPR/64*64.LT.32)GOTO 460
      WRITE(7,900)
      DO 360 I=1,ID
      WRITE(7,920)(DCT(I,J),J=1,ID)
      WRITE(7,940)DCTR(I)
360   CONTINUE
      WRITE(7,980)
      DO 400 I=1,ID
      WRITE(7,1020)(DS(I,J),J=1,ID)
      WRITE(7,940)DCKR(I)
400   CONTINUE
      WRITE(7,1040)
      DO 420 I=1,ID
      WRITE(7,1020)(DCONT(I,J),J=1,ID)
420   CONTINUE
      WRITE(7,1060)
      DO 440 I=1,NEQ
      WRITE(7,920)(RHS(I,J),J=1,10)
440   CONTINUE
460   IF(IPR-IPR/128*128.LT.64)GOTO 520
      WRITE(7,1080)
      DO 480 I=1,NEQ
      WRITE(7,1100)(STIF(I,J),J=1,ISEMI)
480   CONTINUE
      WRITE(7,1120)(IDENT(I),I=1,NNODE)
      WRITE(7,1140)((CT(I,J),J=1,2),I=1,NEQ)
      WRITE(7,1160)
      DO 500 I=1,NEQ
      WRITE(7,920)(DT(I,J),J=1,10)
500   CONTINUE
      WRITE(7,1180)(CONROW(I),I=1,NEQ)
C================================
C  SOLVE CONSTRAINED BANDED MATRIX
C================================
520   CALL KCNSTR(STIF,RHS,CT,DT,IDIM,ISEMI,CONROW,IDENT,NEQ,NNODE,
     2 NRHS)
C
C  PRINT NEW "RHS" IF REQD.
      IF(IPR-IPR/64*64.LT.32)GOTO 560
      WRITE(7,1060)
      DO 540 I=1,NEQ
      WRITE(7,920)(RHS(I,J),J=1,10)
540   CONTINUE
C==========================
C  STIFFNESS MATRIX RE-FORMED
C==========================
560   CALL KMAT(STIF,IDIM,IAJSEM,NEL,ELNO,IDE,X,Y,INAM,E,T,NU,IDENT,
```

```
     2 AREA)
C=================================
C  CORRECT NON-SYMMETRIC TERMS IN DS
C=================================
      IF(ISYM(9).NE.1)GOTO 600
      IF(IPR-IPR/64*64.GE.32)WRITE(7,1000)
      DO 580 I=1,ID
      DS(I,9)=DS(9,I)
      IF(IPR-IPR/64*64.GE.32)WRITE(7,1020)(DS(I,J),J=1,ID)
580   CONTINUE
C=================
C  CALCULATE ALPHAS
C=================
600   CALL ALPHAS(STIF,IDIM,ISEMI,BC,RHS,RHS1,NEQ,DCT,DCTR,DCKR,DS,
     2 DCONT,ALPHA,ISYM,IPR)
C==============================
C  PRINT DISPLACEMENTS & STRESSES
C==============================
      CALL PRINT(RHS,IDIM,NRHS,NEL,ELNO,IDE,IDENT,X,Y,INAM,E,NU,LSTSRN,
     2 NELSP,SIGMA,ALPHA,XCRACK,YCRACK,A,B,NNODE,IPR,ITF,AREA)
C
      STOP
C
CFORMATS=========================================================================
620   FORMAT(20A4)
640   FORMAT(16I5)
660   FORMAT(5F10.0)
680   FORMAT(1X,36('$'),16X,
     2 'A FINITE ELEMENT PROGRAM FOR THE DETERMINATION OF'//
     3 ' $    $    $$$$   $$$$$$   $$$$  $   $$',16X,
     4 'STRESS CONCENTRATION AND STRESS INTENSITY FACTORS'/
     5 ' $$  $  $$   $    $$    $$     $   $$'/
     6 ' $$$ $  $$   $    $$    $$     $   $$',8X,'****',4X,
     7 'USING A METHOD DEVELOPED AT RAE BY  P BARTHOLOMEW    ****'/
     8 ' $$ $$  $$   $    $$    $$     $$$$$$'/
     9 ' $$  $   $$$$     $$     $$$$  $   $$',16X,4X,
     1 '          MODIFIED  AND  EXTENDED'//1X,36('$')19X,
     2 'AT SOUTHAMPTON UNIVERSITY BY A R CARMICHAEL')
700   FORMAT(/1X,28HPLANE STRESS,ISOTROPIC,PLATE/
     2 54H LINEAR VARIATION OF U,V DISPLACEMENTS IN EACH ELEMENT)
720   FORMAT(/1X,20A4)
740   FORMAT(/1X,'COORDINATES OF CENTRE OF HOLE ARE XCRACK =',F10.6,3X,
     2 'YCRACK=',F10.6/' HOLE: SEMIMAJOR AXIS LENGTH IS  A =',F10.6,
     3 '  SEMIMINOR AXIS LENGTH IS  B =',F10.6/
     4 ' ANGLE BETWEEN "X" AXIS OF HOLE (OR LOADING) AND OX COORDINATE',
     5 ' AXIS IS',F11.7,9H  DEGREES,//' E =',E12.5,10X,'NU =',F9.5)
760   FORMAT(//' AUGMENTING TRIAL FUNCTIONS:    SUBROUTINE TRLENS',I1/
     2 ' --------------------------')
780   FORMAT(/1X,7HNAM   =,I5/8H NEQ   =,I5/8H NEL   =,I5/8H NNODE =,
     2 I5)
800   FORMAT(/1X,14HSEMIBANDWIDTH=,I5)
820   FORMAT(/1X,'        ELEMENTS',/)
840   FORMAT(/1X,20HORIGINAL COORDINATES,70X,
     2 23HTRANSFORMED COORDINATES/6H  NODE,6X,1HX,8X,1HY,65X,6H  NODE,
     3 6X,1HX,8X,1HY)
860   FORMAT(1H ,I5,2F10.6,60X,I5,2E12.4)
880   FORMAT(/' BOUNDARY CONDITIONS'/,' -------- ----------'//
     2 ' DESCRIPTION'/)
900   FORMAT(//,4X,'DCT',114X,'DCTR',/)
920   FORMAT(10(1X,E12.5))
940   FORMAT(1H+,116X,E12.5)
980   FORMAT(//,4X,'DS',114X,'DCKR',/)
1000  FORMAT(//,4X,'CORRECTED DS',/)
1020  FORMAT(9(1X,E12.5))
1040  FORMAT(/1X,4X,'DCONT')
1060  FORMAT(/1X,'    RHS',/)
1080  FORMAT('1STIF'/)
1100  FORMAT((12(E10.3,1X)))
1120  FORMAT(//' IDENT'//(20I5))
1140  FORMAT(//' CT'//(5(2(E10.3,1X),3X)))
1160  FORMAT(//' DT'/)
1180  FORMAT(//' CONROW'//(20I5))
1200  FORMAT(/' DATE:  ',4A1,'/',2A1,'/',2A1/' TIME:  ',2A1,':',2A1,
     2 ':',4A1)
1220  FORMAT(' MESH DATA READ FROM DIRECT ACCESS FILE.')
1240  FORMAT(' CONTROL DATA READ FROM DIRECT ACCESS FILE.')
1260  FORMAT(//' ****  ERROR  ****    NEQ EXCEEDS ',I4/)
1280  FORMAT(//' ****  ERROR  ****    NEL EXCEEDS ',I4/)
1300  FORMAT(//' ****  ERROR  ****    NNODE EXCEEDS ',I4/)
1320  FORMAT(//' ****  ERROR  ****    SEMI BANDWIDTH EXCEEDS  80')
1340  FORMAT(//' ****  ERROR  ****    INITIAL DATA CARD MISSING.')
1360  FORMAT(//' ***  WARNING  ***    D.A.F. DATA ERROR.'/' NNODE =',
     2 I4,'  NOT',I4,'  -  D.A.F. ADJUSTED :',' JOB CONTINUING.')
      END
```

```
      SUBROUTINE AREAS(AREA,XX,YY,ELNO,INAM,IDE,NEL,A,B,XC,YC,IPR)
C
C  SUBROUTINE TO CALCULATE THE AREAS OF THE ELEMENTS.
C  IF MID-POINT OF ELEMENT SIDE IS INSIDE HOLE ASSUME CURVED SIDE.
C
      REAL AREA(NEL),XX(INAM),YY(INAM),X(3),Y(3)
      INTEGER ELNO(IDE,3)
      LOGICAL LPR,NEWAREA
      LPR=.TRUE.
      NEWAREA=.TRUE.
      IF(IPR-IPR/8*8.LT.4) LPR=.FALSE.
      DO 4 IL=1,NEL
      DO 1  I=1,3
      N=ELNO(IL,I)
      X(I)=XX(N)
      Y(I)=YY(N)
    1 CONTINUE
      AREA(IL)=0.5*((X(2)-X(1))*(Y(3)-Y(1))-(X(1)-X(3))*(Y(1)-Y(2)))
      IF(A*B.LT.1.E-10.OR..NOT.NEWAREA) GO TO 4
      DO 2 IS=1,3
      I2=IS+1-IS/3*3
      XM=0.5*(X(IS)+X(I2))-XC
      YM=0.5*(Y(IS)+Y(I2))-YC
      IF(XM*XM/(A*A)+YM*YM/(B*B).LT.1.) GO TO 3
    2 CONTINUE
      GO TO 4
    3 AT=0.5*((X(I2)-XC)*(Y(IS)-YC)-(XC-X(IS))*(YC-Y(I2)))
      SEG=0.5*A*B*ABS(ACOS((X(I2)-XC)/A)-ACOS((X(IS)-XC)/A))-AT
      AREA(IL)=AREA(IL)-SEG
      IF(IPR-IPR/8*8.LT.4)GOTO 4
      IF (LPR) WRITE(7,800)
      WRITE(7,801) IL,AREA(IL),SEG
      LPR=.FALSE.
      IF(AREA(IL).LE.0.) I=I/0
    4 CONTINUE
      RETURN
  800 FORMAT(//' AREA CHANGED OF FOLLOWING ELEMENTS ON HOLE BOUNDARY:'/
     *         ' ELEMENT    NEW AREA       DIFFERENCE')
  801 FORMAT(I6,2(4X,E12.5))
      END
```

```
      SUBROUTINE TRLFNS1(A,B1,X1,Y1,S1,C1,E,NU,U,V,SX,SY,TXY,UN,US,
     2    SN,TNS,ID)
C
C  TRIAL FUNCTIONS FOR LOADED CIRCULAR HOLE BASED ON GENERAL SOLUTION
C  UP TO TERMS IN M*THETA.
C
      REAL NU
      REAL U(ID),V(ID),SX(ID),SY(ID),TXY(ID),UN(ID),US(ID),SN(ID),
     2     TNS(ID),UR(9),UT(9),SR(9),ST(9),TRT(9),SSS(9),AN(15),
     3     DN(15),SI(29),CO(29)
      LOGICAL CONVERT
C
      COMMON /BNOTCH/ ISYM(10)
      COMMON /TRL/ CONVERT,SSS,TRT,ST,SR,UT,UR,AN,DN,SI,CO
C
      M=4
      ML=29
      X=X1
      Y=Y1
      S=S1
      C=C1
      DO 3 I=1,ID
      U(I)=0.
      V(I)=0.
      SX(I)=0.
      SY(I)=0.
      TXY(I)=0.
      UN(I)=0.
      US(I)=0.
      SN(I)=0.
      TNS(I)=0.
      UR(I)=0.
      UT(I)=0.
      SR(I)=0.
      ST(I)=0.
      TRT(I)=0.
    3 CONTINUE
C
      R=SQRT(X*X+Y*Y)
      IF(R.GE.A*1.0001) GO TO 5
      X=A*X/R
      R=A
      IF(X1*X1.GT.1.E-8) GO TO 4
      X=0.
      Y=SIGN(A,Y1)
      GO TO 5
    4 Y=X*Y1/X1
    5 AR=A/R
      AR2=AR*AR
      SI(1)=Y/R
      CO(1)=X/R
      DO 8 I=2,ML
      SI(I)=SI(I-1)*CO(1)+CO(I-1)*SI(1)
      CO(I)=CO(I-1)*CO(1)-SI(I-1)*SI(1)
    8 CONTINUE
C
```

```
C  LOAD FUNCTION
C
      IF (ISYM(9).NE.1) GOTO 10
      CALL LOADFN(A,R,E,NU)
C
C  OTHER FUNCTIONS
C
C   FUNCTION (1)
10    IF(ISYM(1).NE.1)GOTO20
      SR(1)=(1.-AR2)/2.
      ST(1)=(1.+AR2)/2.
      UR(1)=A*((1.-NU)/AR+(1.+NU)*AR)/2./E
C
C   FUNCTION (2)
20    IF(ISYM(2).NE.1) GOTO 30
      SR(2)=(R/A-AR2*AR)*CO(1)/4.
      ST(2)=(3./AR+AR2*AR)*CO(1)/4.
      TRT(2)=(R/A-AR2*AR)*SI(1)/4.
      UR(2)=A*((1.-3.*NU)/AR2+(1.+NU)*AR2+2.*(3.+NU))*CO(1)/8./E
      UT(2)=A*((5.+NU)/AR2+(1.+NU)*AR2-2.*(3.+NU))*SI(1)/8./E
C
30    DO 100 N=2,M
      EN=FLOAT(N)
      ARN=AR**N
      EL=0.
      IF(N-N/2*2.NE.0) EL=FLOAT((-1)**((N+1)/2))
C
C   FUNCTION (2N-1)
      I=2*N-1
      IF(ID.LT.I) GOTO 200
      IF(ISYM(I).NE.1) GOTO 50
      SR(I)=((EN-1.)*AR2/ARN-ARN*AR2-(EN-2.)/ARN)*CO(N)/4.
      ST(I)=-((EN-1.)*AR2/ARN-ARN*AR2-(EN+2.)/ARN)*CO(N)/4.
      TRT(I)=-((EN-1.)*AR2/ARN+ARN*AR2-EN/ARN)*SI(N)/4.
      UR(I)=A*(((1.+NU)*((EN+1.)*AR/ARN+ARN*AR)-(EN-2.+NU*(EN+2.))/ARN/
     2         AR)*CO(N)-4.*EL*CO(1))/4./E/(EN+1.)
      UT(I)=-A*(((1.+NU)*((EN+1.)*AR/ARN-ARN*AR)-(EN+4.+EN*NU)/ARN/AR)
     2         *SI(N)-4.*EL*SI(1))/4./E/(EN+1.)
C
C   FUNCTION (2N)
50    I=2*N
      IF(ID.LT.I) GOTO 200
      IF(ISYM(I).NE.1) GOTO 100
      SR(I)=-(AR2/ARN+ARN*AR2*(EN+1.)-ARN*(EN+2.))*CO(N)/4.
      ST(I)=(AR2/ARN+ARN*AR2*(EN+1.)-ARN*(EN-2.))*CO(N)/4.
      TRT(I)=(AR2/ARN-ARN*AR2*(EN+1.)+ARN*EN)*SI(N)/4.
      UR(I)=-A*(((1.+NU)*(AR/ARN-ARN*AR*(EN-1.))+(EN+2.+NU*(EN-2.))*ARN/
     2         AR)*CO(N)+4.*EL*CO(1))/4./E/(EN-1.)
      UT(I)=A*(((1.+NU)*(AR/ARN+ARN*AR*(EN-1.))-(EN-4.+EN*NU)*ARN/AR)
     2         *SI(N)+4.*EL*SI(1))/4./E/(EN-1.)
C
100   CONTINUE
200   CONTINUE
C
C  TRANSFORM AXES
C
      CALL TRANSAX(SI(1),CO(1),UR,UT,SR,ST,TRT,U,V,SX,SY,TXY,ID)
      SG=-S*CO(1)+C*SI(1)
      CG=C*CO(1)+S*SI(1)
      CALL TRANSAX(SG,CG,UR,UT,SR,ST,TRT,UN,US,SN,SSS,TNS,ID)
      RETURN
      END
```

```
      SUBROUTINE TRLFNS2(A,B,X1,Y1,S1,C1,E,NU,U,V,SX,SY,TXY,UN,US,SN,
     * TNS,ID)
      REAL NU,MU,KAP,M,
     *    U(ID),V(ID),SX(ID),SY(ID),TXY(ID),UN(ID),US(ID),SN(ID),TNS(ID),
     *    UR(9),UT(9),SR(9),ST(9),TRT(9),SSS(9)
      COMPLEX Z,DZE,D2ZE,CS,PHI,DPHI,D2PHI,PSI,DPSI,ZE,EX
      LOGICAL CONVERT
      COMMON /TRL/ CONVERT,SSS,TRT,ST,SR,UT,UR
      IF (B.LT.0.1E-20) B=A
      X=X1
      Y=Y1
      S=S1
      C=C1
      DO 3 I=1,ID
      U(I)=0.0
      V(I)=0.0
      SX(I)=0.0
      SY(I)=0.0
      TXY(I)=0.0
      UN(I)=0.0
      US(I)=0.0
      SN(I)=0.0
      TNS(I)=0.0
3     CONTINUE
      IF((X*X/(A*A)+Y*Y/(B*B)).LT.0.5) GO TO 1000
      IF((X*X/(A*A)+Y*Y/(B*B)).GE.1.001) GO TO 4
      X=A*B*X/SQRT(B*B*X*X+A*A*Y*Y)
      IF(X1.GT.1.E-20) GO TO 5
      Y=SIGN(B,Y1)
      GO TO 6
5     Y=X*Y1/X1
6     IF(.NOT.CONVERT) GOTO 4
C  CHANGE SINE AND COSINE
      IF(X*X.LT.0.00000001) GO TO 7
      T=A*SQRT(A*A-X*X)/B/X
      S=SIGN(T/SQRT(T*T+1.),X)
      C=SIGN(1./SQRT(T*T+1.),X)
      GO TO 4
7     S=SIGN(1.,Y)
      C=0.0
C
4     Z=CMPLX(X,Y)
      M=(A-B)/(A+B)
      R=(A+B)/2
      ALF=1.5707963
      TH=ATAN2(Y,X)
      KAP=(3-NU)/(1+NU)
      MU=E/(2*(1+NU))
C
C
      IF(M.GT.0.0001) GO TO 1
      ZE=R/Z
      DZE=-R/(Z*Z)
      D2ZE=2*R/(Z*Z*Z)
      GO TO 2
1     CS=-CSQRT(Z-2*R*SQRT(M))*CSQRT(Z+2*R*SQRT(M))
      ZE=(Z*CS)/(2*R*M)
      DZE=(1+Z/CS)/(2*R*M)
      D2ZE=(1-Z*Z/(Z*Z-4*R*R*M))/(2*R*M*CS)
C
C
2     IDD=ID
      IF(ID.GT.2) IDD=2
      DO 10 I=1,IDD
      PHI=(R*ZE/4)*(2*CEXP((0.0,1.0)*2*ALF)-M+1/(ZE*ZE))
      DPHI=(R/2)*(CEXP((0.0,1.0)*2*ALF)-M/2-1/(2*ZE*ZE))
      D2PHI=(R/2)/ZE**3
C     WRITE(6,
C     WRITE(6,600) X,Y,A,B,M,R,ALF,TH,Z,ZE,DZE,D2ZE,CS,PHI,DPHI,D2PHI
      D2PHI=D2PHI*DZE*DZE+DPHI*D2ZE
      DPHI=DPHI*DZE
      EX=ZE*(1+M*M-CEXP((0.0,1.0)*2*ALF)*(ZE*ZE+M))/(1-M*ZE*ZE)
      PSI=(-R/2)*(CEXP((0.0,-1.0)*2*ALF)/ZE+EX)
      DPSI=(R/2)*(CEXP((0.0,-1.0)*2*ALF)/(ZE*ZE)-EX*(2*M*ZE)
     *     /(1-M*ZE*ZE)-(1+M*M-CEXP((0.0,1.0)*2*ALF)*
     *     (3*ZE*ZE+M))/(1-M*ZE*ZE))
C     WRITE(6,601) DPHI,D2PHI,EX,PSI,DPSI
      DPSI=DPSI*DZE
C     WRITE(6,602) DPSI
      UR(I)=(1/(2*MU))*REAL(CEXP((0.0,1.0)*(-TH))*(KAP*PHI-Z*CONJG(DPHI)
     *    -CONJG(PSI)))
      UT(I)=(1/(2*MU))*AIMAG(CEXP((0.0,1.0)*(-TH))*(KAP*PHI-Z*CONJG
     *    (DPHI)
     *    -CONJG(PSI)))
      ST(I)=2*REAL(DPHI)+REAL((CONJG(Z)*D2PHI+DPSI)*CEXP((0.0,1.0)*2
     *    *TH))
      SR(I)=2*REAL(DPHI)-REAL((CONJG( Z)*D2PHI+DPSI)*CEXP((0.0,1.0)*2
     *    *TH))
      TRT(I)=AIMAG((CONJG(Z)*D2PHI+DPSI)*CEXP((0.0,1.0)*2*TH))
      ALF=ALF-1.5707963
10    CONTINUE
      CO=COS(TH)
      SI=SIN(TH)
      CALL TRANSAX(SI,CO,UR,UT,SR,ST,TRT,U,V,SX,SY,TXY,IDD)
      SG= -S*CO + C*SI
      CG=C*CO +S*SI
      CALL TRANSAX(SG,CG,UR,UT,SR,ST,TRT,UN,US,SN,SSS,TNS,IDD)
C     WRITE(16,1603)A,B,X,Y,S,C,E,NU,(U(I),V(I),SX(I),SY(I),TXY(I),
C    *                UN(I),US(I),SN(I),TNS(I),I=1,4)
C1000 WRITE(6,*) X1,Y1,U,V,SX,SY,TXY
 1000 RETURN
C 600 FORMAT(//' X =',E14.5,5X,'Y =',E14.5,5X,'A =',E14.5,5X,'B =',E14.5
C    *         /' M =',E14.5,5X,'R =',E14.5,5X,'ALF =',E14.5,5X,'TH =',
C    *    E14.5/' Z = (',2E14.5,')     ZE = (',2E14.5,')     DZE = (',
C    *          2E14.5,')'/
C    *          ' D2ZE = (',2E14.5,')     CS = (',2E14.5,
C    *          ')     PHI = (',2E14.5,')'/
C    *          'DPHI = (',2E14.5,')     D2PHI = (',2E14.5,')')
C 601 FORMAT(  ' DPHI = (',2E14.5,')     D2PHI = (',2E14.5,')'/
C    *          ' EX = (',2E14.5,')     PSI = (',2E14.5,')'/
C    *          ' DPSI = (',2E14.5,')')
C 602 FORMAT(  ' DPSI = (',2E14.5,')')
```


B

```
C1603 FORMAT(/' A:',F5.2,'  B:',F5.2,'  X:',E10.3,'  Y:',E10.3,'  S:',
C     *         E10.3,'  C:',E10.3,'  E:',E10.3,'  NU:',E10.3/
C     *         (' DIS: ',2(E12.5,3X),'STR: ',2(E12.5,3X),'T: ',E12.5/
C     *         6X,2(E12.5,3X),5X,F12.5,21X,E12.5))
      END
```



```
      SUBROUTINE LOADFN(A,R,E,NU)
C  CALCULATES STRESSES AND DISPLACEMENTS DUE TO LOAD TRIAL FUNCTION.
C
      REAL NU,KN
      REAL*4 AN,DN
      LOGICAL CONVERT
      COMMON /TRL/ CONVERT,SSS(9),TRT(9),ST(9),SR(9),UT(9),UR(9),
     1  AN(30),DN(30),SI(29),CO(29)
C
      AR=A/R
      AR2=AR*AR
      AR4=AR2*AR2
      F1=AN(1)*AR2
      F2=AR*(AN(2)-DN(2))/4.
      F3=AR*AR2*(AN(2)*(1.-NU)+DN(2)*(3.+NU))/4.
      F4=F2*(3.-NU)*ALOG(R/A)
      F5=(AN(3)-DN(3))/2.
      F6=(AN(3)+DN(3))*AR4/2.
C
      SR(9)=F1+(F2*(3.+NU)+F3)*CO(1)
      ST(9)=-F1-(F2*(1.-NU)+F3)*CO(1)
      TRT(9)=(-F2*(1.-NU)+F3)*SI(1)
      UR(9)=(-F1+(F4-(AN(2)*(3.+NU)+DN(2)*(1.-NU))*AR/8.-F3/2.)*CO(1)
     1  )*(1.+NU)
      UT(9)=-((F4-AR*((AN(2)*(1.-NU)+DN(2)*(3.+NU))*(1.-AR2))/8.)*SI(1)
     1  )*(1.+NU)
C
      DO 10 N=2,29
      IF(ABS(AN(N+1))+ABS(DN(N+1)).LT.0.000001) GOTO 10
      EN=FLOAT(N)
      F5=(EN*AN(N+1)-(EN+2.)*DN(N+1))*AR**(N+2)/2.
      F6=(AN(N+1)-DN(N+1))*AR**N/2.
      SR(9)=SR(9)-(F5-(EN+2.)*F6)*CO(N)
      ST(9)=ST(9)+(F5-(EN-2.)*F6)*CO(N)
      TRT(9)=TRT(9)-(F5-EN*F6)*SI(N)
      UR(9)=UR(9)+(F5*(1.+NU)/(EN+1.)-F6*(EN+2.+(EN-2)*NU)/(EN-1.))*
     1  CO(N)
      UT(9)=UT(9)+(F5*(1.+NU)/(EN+1.)-F6*(EN-4.+EN*NU)/(EN-1.))*SI(N)
C
      IF(N-N/2*2.LE.0)GOTO 10
      KN=FLOAT((-1)**((N+1)/2))*AR*(AN(N+1)*(EN+2.-EN*NU)-DN(N+1)*
     1  (2.*EN+1.+NU))/(EN*EN-1.)
      UR(9)=UR(9)-KN*CO(1)
      UT(9)=UT(9)+KN*SI(1)
10    CONTINUE
C
      UR(9)=UR(9)*R/E
      UT(9)=UT(9)*R/E
C
      RETURN
      END
```

```
      SUBROUTINE BCONDS(X,Y,RHS,E,NU,IDIM,XCRACK,YCRACK,T,LSTSRN,A,B,
     2  CT,DT,CONROW,INAM,ELNO,IDE,DCT,DCTR,DCKR,DS,SIGMA,NELSP,
     3  LSTBA,LSTBL,NBA,NNODE,NEL,IPR,IDENT,ISYM,AREA,MDAF)
C
C  SUBROUTINE TO ENFORCE BOUNDARY CONDITIONS AND TO EVALUATE ALL
C  BOUNDARY INTEGRALS
C
C  INTF     INTERFACE BETWEEN SPECIAL ORDINARY REGION        TYPE 0
C  TRCT     SN AND TNS PRESCRIBED                            TYPE 1
C  ASYM     SN,USJ1 AND USJ2 PRESCRIBED                      TYPE 2
C  SYMM     TNS,UNJ1 AND UNJ2 PRESCRIBED                     TYPE 3
C  CLMP     USJ1,USJ2,UNJ1 AND UNJ2 PRESCRIBED               TYPE 4
C  UDSP     U PRESCRIBED AT SINGLE NODE                      TYPE 5
C  VDSP     V PRESCRIBED AT SINGLE NODE                      TYPE 6
C  X-LD     X LOAD PRESCRIBED AT SINGLE NODE                 TYPE 7
C  Y-LD     Y LOAD PRESCRIBED AT SINGLE NODE                 TYPE 8
C  HOLE     TRACTIONS ON HOLE BOUNDARY                       TYPE 9
C
      INTEGER LSTBA(INAM,3),LSTBL(INAM,3),NBA(INAM)
      INTEGER LSTSRN(IDE),FLAG,BCTYPE,CONROW(IDIM),ELNO(IDE,3)
      INTEGER IDENT(INAM)
C
      LOGICAL LPR,INTEGR,CONVERT,MDAF
C
      REAL X(INAM),Y(INAM),RHS(IDIM,MRHS),CT(IDIM,2),DT(IDIM,MRHS)
      REAL NU,DCT(MTF,MTF),DCTR(MTF),DCKR(MTF),DS(MTF,MTF)
      REAL AU(9),AV(9),ASX(9),ASY(9),ATXY(9),AUN(9),AUS(9),ASN(9)
      REAL AUNJ1(9),AUNJ2(9),AUNJ3(9),AUSJ1(9),AUSJ2(9),AUSJ3(9)
      REAL UNCMP(9),USCMP(9),SNCMP(9),TNSCMP(9),L1,L2,ATNS(9)
      REAL SXCMP(9),SYCMP(9),TXYCMP(9),SND(9),TNSD(9)
      REAL SIGMA(MTF3,NELSP),T(IDE),AREA(IDE)
C
      CHARACTER*4 IDATA(20),ICODE(10)
C
      COMMON /SIZE/ID,MTF,MRHS,MTF3
      COMMON /TRL/CONVERT
C
      DATA ICODE/'INTF','TRCT','ASYM','SYMM','CLMP','UDSP','VDSP',
     2 'X-LD','Y-LD','HOLE'/
C
      CONVERT=.FALSE.
      INTEGR=.FALSE.
C
C  FLAG=1 FOR EXTERNAL REGION
C  FLAG=0 FOR BOUNDARY OF SPECIAL REGIONS
C
C  INIZIALISE ARRAYS
      DO 20 I=1,IDIM
      CT(I,1)=0.0
      CT(I,2)=0.0
20    CONROW(I)=0
      DO 40 J=1,MRHS
      DO 40 I=1,IDIM
      DT(I,J)=0.0
40    CONTINUE
      DO 60 I=1,ID
      DCTR(I)=0.0
      DCKR(I)=0.0
      DO 60 J=1,ID
      DCT(I,J)=0.0
      DS(I,J)=0.0
60    CONTINUE
C***
C***     READ IN NUMBER & TYPES OF BOUNDARY CONDITIONS
C***
      KTR=0
      IF(MDAF)GOTO 80
      READ(5,1440)NBCTYPE
      WRITE(9,REC=1)NEL,NNODE,NBCTYPE
      GOTO 100
80    READ(9,REC=1)I,J,NBCTYPE
100   KTR=KTR+1
      LPR=.TRUE.
      IF(BCTYPE.NE.0)LASTBC=BCTYPE
      CALL BCDATA(MDAF,KTR,NBCTYPE,NEL,NNODE,BCTYPE,IBC,J1,J2,SN,TNS,
     2 USJ1,USJ2,UNJ1,UNJ2,XX)
C     END OF DATA?
      IF(KTR.LT.0)GOTO 1320
      FLAG=0
      IF(BCTYPE.GT.0)FLAG=1
      IF(BCTYPE.EQ.LASTBC.OR.IPR-IPR/8*8.LT.4)LPR=.FALSE.
C     SINGLE NODE B.C. CONDITION?
      IF(BCTYPE.GE.5)GOTO 500
      SIDE=SQRT((X(J1)-X(J2))**2+(Y(J1)-Y(J2))**2)
C     SINE AND COSINE (BETA)
      S=(X(J1)-X(J2))/SIDE
      C=(Y(J2)-Y(J1))/SIDE
C
C     NA = NUMBER OF S.R. BOUNDARY ARCS LEAVING NODE
      NA=NBA(J1)
      IF(NA.EQ.0)GOTO 140
      DO 120 IA=1,NA
      JT=LSTBA(J1,IA)
      IF(JT.EQ.J2)GOTO 160
120   CONTINUE
C
C  EXTERNAL BOUNDARY
140   IF(FLAG.EQ.1)GOTO 360
      WRITE(6,1720)J1,J2
      WRITE(7,1720)J1,J2
      IF(BCTYPE.EQ.0)GOTO 100
      FLAG=1
      GOTO 360
C
C  SPECIAL REGION BOUNDARY
160   IF(BCTYPE.EQ.0)GOTO 100
      FLAG=0
C     MARK BOUNDARY AS NOT INTERFACE
      LNUM=LSTBL(J1,IA)
      LSTBL(J1,IA)=-LNUM
C
C  EVALUATE TRIAL FNS ON BOUNDARY
```

```
180   TH=T(LNUM)
      ISRN=LSTSRN(LNUM)
      JL1=ELNO(LNUM,1)
      JL2=ELNO(LNUM,2)
      JL3=ELNO(LNUM,3)
      DO 200 I=1,3
      IF(J1.EQ.JL1.AND.J2.EQ.JL2)GOTO 220
      JL4=JL1
      JL1=JL2
      JL2=JL3
      JL3=JL4
200   CONTINUE
C     NODES NOT IN SAME ELEMENT
      WRITE(6,1780)J1,J2
      WRITE(7,1780)J1,J2
      STOP
220   J3=JL3
      I3=IDENT(J3)
      L1=S*(X(J3)-X(J2))+C*(Y(J2)-Y(J3))
      L2=S*(X(J1)-X(J3))+C*(Y(J3)-Y(J1))
      PERP=C*(X(J2)-X(J3))+S*(Y(J2)-Y(J3))
      DO 240 I=1,10
      UNCMP(I)=0.0
      USCMP(I)=0.0
      SNCMP(I)=0.0
      TNSCMP(I)=0.0
      SXCMP(I)=0.0
      SYCMP(I)=0.0
      TXYCMP(I)=0.0
240   CONTINUE
C
      GOTO(260,280,300,320)ISYM
      CALL TRLFNS0(A,B,(X(J1)-XCRACK),(Y(J1)-YCRACK),S,C,E,NU,AU,AV,
     2 ASX,ASY,ATXY,AUNJ1,AUSJ1,ASN,ATNS,ID)
      CALL TRLFNS0(A,B,(X(J2)-XCRACK),(Y(J2)-YCRACK),S,C,E,NU,AU,AV,
     2 ASX,ASY,ATXY,AUNJ2,AUSJ2,ASN,ATNS,ID)
      GOTO 340
260   CALL TRLFNS1(A,B,(X(J1)-XCRACK),(Y(J1)-YCRACK),S,C,E,NU,AU,AV,
     2 ASX,ASY,ATXY,AUNJ1,AUSJ1,ASN,ATNS,ID)
      CALL TRLFNS1(A,B,(X(J2)-XCRACK),(Y(J2)-YCRACK),S,C,E,NU,AU,AV,
     2 ASX,ASY,ATXY,AUNJ2,AUSJ2,ASN,ATNS,ID)
      GOTO 340
280   CALL TRLFNS2(A,B,(X(J1)-XCRACK),(Y(J1)-YCRACK),S,C,E,NU,AU,AV,
     2 ASX,ASY,ATXY,AUNJ1,AUSJ1,ASN,ATNS,ID)
      CALL TRLFNS2(A,B,(X(J2)-XCRACK),(Y(J2)-YCRACK),S,C,E,NU,AU,AV,
     2 ASX,ASY,ATXY,AUNJ2,AUSJ2,ASN,ATNS,ID)
      GOTO 340
300   CALL TRLFNS3(A,B,(X(J1)-XCRACK),(Y(J1)-YCRACK),S,C,E,NU,AU,AV,
     2 ASX,ASY,ATXY,AUNJ1,AUSJ1,ASN,ATNS,ID)
      CALL TRLFNS3(A,B,(X(J2)-XCRACK),(Y(J2)-YCRACK),S,C,E,NU,AU,AV,
     2 ASX,ASY,ATXY,AUNJ2,AUSJ2,ASN,ATNS,ID)
      GOTO 340
320   CALL TRLFNS4(A,B,(X(J1)-XCRACK),(Y(J1)-YCRACK),S,C,E,NU,AU,AV,
     2 ASX,ASY,ATXY,AUNJ1,AUSJ1,ASN,ATNS,ID)
      CALL TRLFNS4(A,B,(X(J2)-XCRACK),(Y(J2)-YCRACK),S,C,E,NU,AU,AV,
     2 ASX,ASY,ATXY,AUNJ2,AUSJ2,ASN,ATNS,ID)
C
340   IF(BCTYPE.EQ.0)GOTO 580
360   GOTO(380,440,460,480),BCTYPE
C
C  BOUNDARY CONDITION TYPE 1 & 9                                    (TRCT)
C                                                                  (HOLE)
380   IF(LPR)WRITE(7,1480)
      IF(IPR-IPR/8*8.GE.4)WRITE(7,1460)J1,J2,SN,TNS
C
C     SKIP INTEGRATION ON HOLE BOUNDARY?
      IF(INTEGR.OR.FLAG.EQ.1)GOTO 420
      IF(A*B.LT.1.E-10)GOTO 400
      CR=(XCRACK-(X(J1)+X(J2))/2)**2/(A*A)+(YCRACK-(Y(J1)+Y(J2))/2)**2/
     2 (B*B)
      IF(CR.GT.0.999999)GOTO 400
      IF(IPR-IPR/2*2.GE.1)WRITE(7,1700)
      GOTO 100
C
400   IF(IBC.EQ.10)WRITE(6,1760)
      IF(IBC.EQ.10)WRITE(7,1760)
420   I1=IDENT(J1)
      I2=IDENT(J2)
C     NODAL LOADS DUE TO TRACTIONS
      RHS(I1,1)=RHS(I1,1)+0.5*SIDE*(SN*C-TNS*S)
      RHS(I1+1,1)=RHS(I1+1,1)+0.5*SIDE*(SN*S+TNS*C)
      RHS(I2,1)=RHS(I2,1)+0.5*SIDE*(SN*C-TNS*S)
      RHS(I2+1,1)=RHS(I2+1,1)+0.5*SIDE*(SN*S+TNS*C)
      GOTO 580
C
C  BOUNDARY CONDITION TYPE 2                                        (ASYM)
C
440   IF(LPR)WRITE(7,1500)
      IF(IPR-IPR/8*8.GE.4)WRITE(7,1460)J1,J2,SN,USJ1,USJ2
      I1=IDENT(J1)
      I2=IDENT(J2)
C     NODAL LOADS DUE TO TRACTIONS
      RHS(I1,1)=RHS(I1,1)+0.5*SIDE*SN*C
      RHS(I1+1,1)=RHS(I1+1,1)+0.5*SIDE*SN*S
      RHS(I2,1)=RHS(I2,1)+0.5*SIDE*SN*C
      RHS(I2+1,1)=RHS(I2+1,1)+0.5*SIDE*SN*S
C     DISPLACEMENT CONSTRAINTS
      IF(CONROW(I1).EQ.2)I1=I1+1
      CONROW(I1)=2
      BT(I1,1)=USJ1
      CT(I1,1)=-S
      CT(I1,2)=C
      IF(CONROW(I2).EQ.2)I2=I2+1
      CONROW(I2)=2
      BT(I2,1)=USJ2
      CT(I2,1)=-S
      CT(I2,2)=C
      GOTO 580
C
C  BOUNDARY CONDITION TYPE 3                                        (SYMM)
C
460   IF(LPR)WRITE(7,1520)
```

```
      IF(IPR-IPR/8*8.GE.4)WRITE(7,1460)J1,J2,TNS,UNJ1,UNJ2
      I1=IDENT(J1)
      I2=IDENT(J2)
C     NODAL LOADS DUE TO TRACTIONS
      RHS(I1,1)=RHS(I1,1)-0.5*SIDE*TNS*S
      RHS(I1+1,1)=RHS(I1+1,1)+0.5*SIDE*TNS*C
      RHS(I2,1)=RHS(I2,1)-0.5*SIDE*TNS*S
      RHS(I2+1,1)=RHS(I2+1,1)+0.5*SIDE*TNS*C
C     DISPLACEMENT CONSTRAINTS
      IF(CONROW(I1).EQ.2)I1=I1+1
      CONROW(I1)=2
      DT(I1,1)=UNJ1
      CT(I1,1)=C
      CT(I1,2)=S
      IF(CONROW(I2).EQ.2)I2=I2+1
      CONROW(I2)=2
      DT(I2,1)=UNJ2
      CT(I2,1)=C
      CT(I2,2)=S
      GOTO 580
C
C  BOUNDARY CONDITION TYPE 4                                    (CLMP)
C
480   IF(LPR)WRITE(7,1540)
      IF(IPR-IPR/8*8.GE.4)WRITE(7,1460)J1,J2,USJ1,USJ2,UNJ1,UNJ2
      I1=IDENT(J1)
C     DISPLACEMENT CONSTRAINTS
      CONROW(I1)=2
      DT(I1,1)=USJ1
      CT(I1,1)=-S
      CT(I1,2)=C
      CONROW(I1+1)=2
      DT(I1+1,1)=UNJ1
      CT(I1+1,1)=C
      CT(I1+1,2)=S
      I2=IDENT(J2)
      CONROW(I2)=2
      DT(I2,1)=USJ2
      CT(I2,1)=-S
      CT(I2,2)=C
      CONROW(I2+1)=2
      DT(I2+1,1)=UNJ2
      CT(I2+1,1)=C
      CT(I2+1,2)=S
      GOTO 580
C
500   IF(BCTYPE.GE.7)GOTO 540
C
C  BOUNDARY CONDITIONS TYPE 5 OR 6                        (UDSP OR VDSP)
C
C     DISPLACEMENT CONSTRAINT
      I1=IDENT(J1)
      IF(CONROW(I1).EQ.2)I1=I1+1
      CONROW(I1)=2
      IF(BCTYPE.NE.5)GOTO 520
C
C  BOUNDARY CONDITION TYPE 5                                    (UDSP)
C
      IF(LPR)WRITE(7,1560)
      IF(IPR-IPR/8*8.GE.4)WRITE(7,1640)J1,UNJ1
      DT(I1,1)=U
      CT(I1,1)=1.0
      CT(I1,2)=0.0
      GOTO 100
C
C  BOUNDARY CONDITION TYPE 6                                    (VDSP)
C
520   V=UNJ1
      IF(LPR)WRITE(7,1580)
      IF(IPR-IPR/8*8.GE.4)WRITE(7,1640)J1,V
      DT(I1,1)=V
      CT(I1,1)=0.0
      CT(I1,2)=1.0
      GOTO 100
C
C  BOUNDARY CONDITION TYPE 7 OR 8                    (X-LD OR Y-LD)
C
540   I1=IDENT(J1)
      IF(BCTYPE.EQ.8)GOTO 560
C
C  BOUNDARY CONDITION TYPE 7                                    (X-LD)
C
      IF(LPR)WRITE(7,1600)
      IF(IPR-IPR/8*8.GE.4)WRITE(7,1640)J1,XX
C     NODAL LOAD
      RHS(I1,1)=RHS(I1,1)+XX
      GOTO 100
C
C  BOUNDARY CONDITION TYPE 8                                    (Y-LD)
C
560   YY=XX
      IF(LPR)WRITE(7,1620)
      IF(IPR-IPR/8*8.GE.4)WRITE(7,1640)J1,YY
      I1=I1+1
C     NODAL LOAD
      RHS(I1,1)=RHS(I1,1)+YY
      GOTO 100
C
580   IF(FLAG.EQ.1)GOTO 100
C
C-------------------------------------------------------------------------
C******************
C  S.R. INTEGRALS
C******************
      I1=IDENT(J1)
      I2=IDENT(J2)
C***
C***     SIX POINT GAUSSIAN QUADRATURE
C***
      AA=-0.932469514203
      H=0.171324492379*TH*SIDE*0.5
      ASSIGN 600 TO LABEL
```

```
      GOTO 700
600   AA=-AA
      ASSIGN 620 TO LABEL
      GOTO 700
620   AA=-0.66120938646
      H=0.360761573048*TH*SIDE*0.5
      ASSIGN 640 TO LABEL
      GOTO 700
640   AA=-AA
      ASSIGN 660 TO LABEL
      GOTO 700
660   AA=-0.238619186083
      H=0.467913934573*TH*SIDE*0.5
      ASSIGN 680 TO LABEL
      GOTO 700
680   AA=-AA
      ASSIGN 1100 TO LABEL
700   ZL1=(1.0-AA)*0.5
      ZL2=(1.0+AA)*0.5
      XL=(X(J1)*ZL1+X(J2)*ZL2)-XCRACK
      YL=(Y(J1)*ZL1+Y(J2)*ZL2)-YCRACK
C
      GOTO(720,740,760,780)ISYM
      CALL TRLFNS0(A,B,XL,YL,S,C,E,NU,AU,AV,ASX,ASY,ATXY,AUN,AUS,ASN,
     2 ATNS,ID)
      GOTO 800
720   CALL TRLFNS1(A,B,XL,YL,S,C,E,NU,AU,AV,ASX,ASY,ATXY,AUN,AUS,ASN,
     2 ATNS,ID)
      GOTO 800
740   CALL TRLFNS2(A,B,XL,YL,S,C,E,NU,AU,AV,ASX,ASY,ATXY,AUN,AUS,ASN,
     2 ATNS,ID)
      GOTO 800
760   CALL TRLFNS3(A,B,XL,YL,S,C,E,NU,AU,AV,ASX,ASY,ATXY,AUN,AUS,ASN,
     2 ATNS,ID)
      GOTO 800
780   CALL TRLFNS4(A,B,XL,YL,S,C,E,NU,AU,AV,ASX,ASY,ATXY,AUN,AUS,ASN,
     2 ATNS,ID)
C
800   DO 1040 N=1,ID
      IF(BCTYPE.EQ.0)GOTO 1060
      GOTO(820,820,860,860),BCTYPE
C
C  CALCULATE NORMAL COMPONENTS FOR BCTYPES 1 & 2
C
820   RHS(I1,N+1)=RHS(I1,N+1)+ZL1*ASN(N)*H*C
      RHS(I1+1,N+1)=RHS(I1+1,N+1)+ZL1*ASN(N)*H*S
      RHS(I2,N+1)=RHS(I2,N+1)+ZL2*ASN(N)*H*C
      RHS(I2+1,N+1)=RHS(I2+1,N+1)+ZL2*ASN(N)*H*S
      DO 840 M=1,ID
      DS(M,N)=DS(M,N)-ASN(N)*H*AUN(M)
840   DCT(M,N)=DCT(M,N)+ASN(N)*H*(AUN(M)-(AUNJ1(M)*ZL1+AUNJ2(M)*ZL2))
     2 *2.
      DCTR(N)=DCTR(N)+SN*H*(-AUN(N)+AUNJ1(N)*ZL1+AUNJ2(N)*ZL2)
860   GOTO(880,920,880,920),BCTYPE
C
C  CALCULATE TANGENTIAL COMPONENTS FOR BCTYPES 1 & 3
C
880   RHS(I1,N+1)=RHS(I1,N+1)-ZL1*ATNS(N)*H*S
      RHS(I1+1,N+1)=RHS(I1+1,N+1)+ZL1*ATNS(N)*H*C
      RHS(I2,N+1)=RHS(I2,N+1)-ZL2*ATNS(N)*H*S
      RHS(I2+1,N+1)=RHS(I2+1,N+1)+ZL2*ATNS(N)*H*C
      DO 900 M=1,ID
      DS(M,N)=DS(M,N)-ATNS(N)*H*AUS(M)
900   DCT(M,N)=DCT(M,N)+ATNS(N)*H*(AUS(M)-(AUSJ1(M)*ZL1+AUSJ2(M)*ZL2))
     2 *2
      DCTR(N)=DCTR(N)+TNS*H*(-AUS(N)+AUSJ1(N)*ZL1+AUSJ2(N)*ZL2)
920   GOTO(980,980,940,940),BCTYPE
C
C  CALCULATE NORMAL COMPONENTS FOR BCTYPES 3 & 4
C
940   UNCMP(N)=UNCMP(N)+H*(AUN(N)-AUNJ1(N)*ZL1-AUNJ2(N)*ZL2)
      DO 960 M=1,ID
960   DS(M,N)=DS(M,N)-ASN(N)*H*AUN(M)
      DCKR(N)=DCKR(N)+ASN(N)*H*(UNJ1*ZL1+UNJ2*ZL2)
980   GOTO(1040,1000,1040,1000),BCTYPE
C
C  CALCULATE TANGENTIAL COMPONENTS FOR BCTYPES 2 & 4
C
1000  USCMP(N)=USCMP(N)+H*(AUS(N)-AUSJ1(N)*ZL1-AUSJ2(N)*ZL2)
      DO 1020 M=1,ID
1020  DS(M,N)=DS(M,N)-ATNS(N)*H*AUS(M)
      DCKR(N)=DCKR(N)+ATNS(N)*H*(USJ1*ZL1+USJ2*ZL2)
      GOTO 1040
C
C  INTERFACE BOUNDARY
C
1060  RHS(I1,N+1)=RHS(I1,N+1)+H*ZL1*(ASN(N)*C-ATNS(N)*S)
      RHS(I1+1,N+1)=RHS(I1+1,N+1)+H*ZL1*(ASN(N)*S+ATNS(N)*C)
      RHS(I2,N+1)=RHS(I2,N+1)+H*ZL2*(ASN(N)*C-ATNS(N)*S)
      RHS(I2+1,N+1)=RHS(I2+1,N+1)+H*ZL2*(ASN(N)*S+ATNS(N)*C)
      UNCMP(N)=UNCMP(N)+H*(AUN(N)-AUNJ1(N)*ZL1-AUNJ2(N)*ZL2)
      USCMP(N)=USCMP(N)+H*(AUS(N)-AUSJ1(N)*ZL1-AUSJ2(N)*ZL2)
      DO 1080 M=1,ID
      DS(M,N)=DS(M,N)-ASN(N)*H*AUN(M)
      DS(M,N)=DS(M,N)-ATNS(N)*H*AUS(M)
1080  CONTINUE
C
1040  CONTINUE
      GOTOLABEL,(600,620,640,660,680,1100)
C***
C***  PROCESS QUADRATURES ON BOUNDARIES  K AND R
C***
1100  IF(BCTYPE.EQ.0)GOTO 1240
      GOTO(100,1120,1180,1240),BCTYPE
C
C  BCTYPE  2
C
1120  DO 1140 I=1,ID
      TNSCMP(I)=-E*USCMP(I)/(2.0*TH*AREA(LNUM)*(1.+NU))
      RHS(I1,I+1)=RHS(I1,I+1)+TNSCMP(I)*0.5*TH*(-L1*S-PERP*C)
      RHS(I1+1,I+1)=RHS(I1+1,I+1)+TNSCMP(I)*0.5*TH*(L1*C-PERP*S)
      RHS(I2,I+1)=RHS(I2,I+1)+TNSCMP(I)*0.5*TH*(-L2*S+PERP*C)
```

```
      RHS(I2+1,I+1)=RHS(I2+1,I+1)+TNSCMP(I)*0.5*TH*(L2*C+PERP*S)
      RHS(I3,I+1)=RHS(I3,I+1)+TNSCMP(I)*0.5*TH*(SIDE*S)
      RHS(I3+1,I+1)=RHS(I3+1,I+1)+TNSCMP(I)*0.5*TH*(-SIDE*C)
1140  CONTINUE
      DO 1160 I=1,ID
      SXCMP(I)=2.*C*S*TNSCMP(I)
      SYCMP(I)=-(2.)*C*S*TNSCMP(I)
      TXYCMP(I)=-(C*C-S*S)*TNSCMP(I)
      SIGMA(I*3-2,ISRN)=SIGMA(I*3-2,ISRN)+SXCMP(I)
      SIGMA(I*3-1,ISRN)=SIGMA(I*3-1,ISRN)+SYCMP(I)
      SIGMA(I*3,ISRN)=SIGMA(I*3,ISRN)+TXYCMP(I)
1160  CONTINUE
      GOTO 1300
C
C  BCTYPE  3
C
1180  DO 1200 I=1,ID
      SNCMP(I)=-E*UNCMP(I)/(TH*AREA(LNUM)*(1.-NU*NU))
      RHS(I1,I+1)=RHS(I1,I+1)+SNCMP(I)*0.5*TH*(L1*C+PERP*NU*S)
      RHS(I1+1,I+1)=RHS(I1+1,I+1)+SNCMP(I)*0.5*TH*(L1*S-PERP*NU*C)
      RHS(I2,I+1)=RHS(I2,I+1)+SNCMP(I)*0.5*TH*(L2*C-PERP*NU*S)
      RHS(I2+1,I+1)=RHS(I2+1,I+1)+SNCMP(I)*0.5*TH*(L2*S+PERP*NU*C)
      RHS(I3,I+1)=RHS(I3,I+1)+SNCMP(I)*0.5*TH*(-SIDE*C)
      RHS(I3+1,I+1)=RHS(I3+1,I+1)+SNCMP(I)*0.5*TH*(-SIDE*S)
1200  CONTINUE
      DO 1220 I=1,ID
      SXCMP(I)=-(C*C+NU*S*S)*SNCMP(I)
      SYCMP(I)=-(NU*C*C+S*S)*SNCMP(I)
      TXYCMP(I)=-(C*S*(1.-NU))*SNCMP(I)
      SIGMA(I*3-2,ISRN)=SIGMA(I*3-2,ISRN)+SXCMP(I)
      SIGMA(I*3-1,ISRN)=SIGMA(I*3-1,ISRN)+SYCMP(I)
      SIGMA(I*3,ISRN)=SIGMA(I*3,ISRN)+TXYCMP(I)
1220  CONTINUE
      GOTO 1300
C
C  BCTYPE  4  OR  INTERFACE
C
1240  DO 1260 I=1,ID
      SNCMP(I)=-E*UNCMP(I)/(TH*AREA(LNUM)*(1.-NU*NU))
      TNSCMP(I)=-E*LSCMP(I)/(2.*TH*AREA(LNUM)*(1.+NU))
      RHS(I1,I+1)=RHS(I1,I+1)+TNSCMP(I)*.5*TH*(-L1*S-PERP*C)+SNCMP(I)
     2 *0.5*TH*(L1*C+PERP*NU*S)
      RHS(I1+1,I+1)=RHS(I1+1,I+1)+TNSCMP(I)*0.5*TH*(L1*C-PERP*S)
     2 +SNCMP(I)*0.5*TH*(L1*S-PERP*NU*C)
      RHS(I2,I+1)=RHS(I2,I+1)+TNSCMP(I)*.5*TH*(-L2*S+PERP*C)+SNCMP(I)
     2 *0.5*TH*(L2*C-PERP*NU*S)
      RHS(I2+1,I+1)=RHS(I2+1,I+1)+TNSCMP(I)*0.5*TH*(L2*C+PERP*S)
     2 +SNCMP(I)*0.5*TH*(L2*S+PERP*NU*C)
      RHS(I3,I+1)=RHS(I3,I+1)+TNSCMP(I)*0.5*TH*(SIDE*S)+SNCMP(I)
     2 *0.5*TH*(-SIDE*C)
      RHS(I3+1,I+1)=RHS(I3+1,I+1)+TNSCMP(I)*0.5*TH*(-SIDE*C)+SNCMP(I)
     2 *0.5*TH*(-SIDE*S)
1260  CONTINUE
      DO 1280 I=1,ID
      SXCMP(I)=-(C*C+NU*S*S)*SNCMP(I)+2.*C*S*TNSCMP(I)
      SYCMP(I)=-(NU*C*C+S*S)*SNCMP(I)-2.*C*S*TNSCMP(I)
      TXYCMP(I)=-(C*C-S*S)*TNSCMP(I)-C*S*(1.-NU)*SNCMP(I)
      SIGMA(I*3-2,ISRN)=SIGMA(I*3-2,ISRN)+SXCMP(I)
      SIGMA(I*3-1,ISRN)=SIGMA(I*3-1,ISRN)+SYCMP(I)
      SIGMA(I*3,ISRN)=SIGMA(I*3,ISRN)+TXYCMP(I)
1280  CONTINUE
1300  CONTINUE
C
      IF(BCTYPE.EQ.0)GOTO 1420
      GOTO 100
C
C-----------------------------------------------------------------------
C
C  ALL B. CONDS COMPLETED - CHECK KTR THEN DO SP. REGION INTERFACE.
1320  KTR=-KTR-1
      IF(KTR.NE.NBCTYPE)WRITE(6,1740)KTR,NBCTYPE
      IF(KTR.NE.NBCTYPE)WRITE(7,1740)KTR,NBCTYPE
      IF(KTR.NE.NBCTYPE)WRITE(9,REC=1)NEL,NNODE,KTR
C***
C***    OUTLINE SPECIAL REGION AND
C***    APPLY CONDITIONS AT INTERFACE
C***
      LOOP=0
      FLAG=0
      BCTYPE=0
1340  LOOP=LOOP+1
      DO 1360 J1=1,NNODE
      NA=NBA(J1)
      IF(NA.NE.0)GOTO 1380
1360  CONTINUE
      RETURN
C
1380  IF(IPR-IPR/8*8.GE.4)WRITE(7,1660)LOOP
1400  J2=LSTBA(J1,NA)
      NBA(J1)=NA-1
      IF(IPR-IPR/8*8.GE.4)WRITE(7,1680)J1,J2
      LNUM=LSTEL(J1,NA)
      IF(LNUM.LE.0)GOTO 1420
      SIDE=SQRT((X(J1)-X(J2))**2+(Y(J1)-Y(J2))**2)
      S=(X(J1)-X(J2))/SIDE
      C=(Y(J2)-Y(J1))/SIDE
      GOTO 180
C
1420  J1=J2
      NA=NBA(J1)
      IF(NA.EQ.0)GOTO 1340
      GOTO 1400
C
C-----------------------------------------------------------------------
1440  FORMAT(I5)
1460  FORMAT(18X,I4,'  -',I4,4(F10.4))
1480  FORMAT(/1X,' TRACTION  ',10X,'SIDE',8X,'SN  ',6X,'TNS ')
1500  FORMAT(/1X,'(ASYMMETRY)',10X,'SIDE',8X,'SN  ',6X,'USJ1',6X,
     2 'USJ2')
1520  FORMAT(/1X,'(SYMMETRY) ',10X,'SIDE',8X,'TNS ',6X,'UNJ1',6X,
     2 'UNJ2')
1540  FORMAT(/1X,' KINEMATIC ',10X,'SIDE',8X,'USJ1',6X,'USJ2',6X,
```

```
     2 'UNJ1',6X,'UNJ2')
1560  FORMAT(/1X,' U-DISP FIXED ',7X,'NODE',8X,'MAGNITUDE')
1580  FORMAT(/1X,' V-DISP FIXED ',7X,'NODE',8X,'MAGNITUDE')
1600  FORMAT(/1X,' PT LOAD X-DIR',7X,'NODE',8X,'MAGNITUDE')
1620  FORMAT(/1X,' PT LOAD Y-DIR',7X,'NODE',8X,'MAGNITUDE')
1640  FORMAT(22X,I4,4X,F8.2)
1660  FORMAT(/' SPECIAL REGION BOUNDARY'/' LOOP',I2/)
1680  FORMAT(1X,I4,'  -',I4)
1700  FORMAT(1H+,52X,'ELLIPTICAL/CIRCULAR HOLE BOUNDARY')
1720  FORMAT(' *** WARNING ***'/' ARC',I4,'  -',I4,'   DOES NOT'/
     2 ' LIE ON PERIMETER OF SP. REGION'/)
1740  FORMAT(' *** WARNING ***'/I4,' B.CONDS.DEFINED'/I4,
     2 ' B.CONDS.EXPECTED'/)
1760  FORMAT(' *** WARNING ***     BOUNDARY NOT ON HOLE PERIMETER')
1780  FORMAT(1H ,2I6,'**** ERROR IN DATA.  PROGRAM TERMINATING')
      END
```



```
      SUBROUTINE ALPHAS(KSTIF,IDIM,ISEMI,BC,RHS,RHS1,NEQ,DCT,DCTR,
     2 DCKR,DS,DCONT,ALPHA,ISYM,IPR)
C
C     SUBROUTINE TO CALCULATE COEFFICIENTS  ALPHA  OF AUGMENTING TRIAL
C     FUNCTIONS (STRESS FIELDS) GIVEN BOUNDARY INTEGRALS AND
C     FINITE ELEMENT SOLUTIONS.
C
      INTEGER LW(9),MW(9)
      INTEGER ISYM(MRHS)
      REAL KSTIF(IDIM,ISEMI),BC(IDIM,MRHS),RHS(IDIM,MRHS),RHS1(IDIM)
      REAL DCT(MTF,MTF),DCTR(MTF),DCKR(MTF),D(9,9),DRHS(9)
      REAL DS(MTF,MTF),DCONT(MTF,MTF),ALPHA(MTF)
      COMMON /SIZE/ID,MTF,MRHS
C
      SUM=0.0
      IAJSEM=ISEMI*IDIM
C
C  FORM VECTOR "DRHS"
      DO 20 M=1,NEQ
20    RHS1(M)=RHS(M,1)
      CALL KVECT(KSTIF,IAJSEM,IDIM,RHS1,NEQ)
      DO 60 J=1,ID
      DIJ=-DCTR(J)-DCKR(J)
      DO 40 M=1,NEQ
40    DIJ=DIJ+(-BC(M,1)+RHS1(M))*RHS(M,J+1)-BC(M,J+1)*RHS(M,1)
      DRHS(J)=DIJ
60    CONTINUE
C
      DIJ=0
      DO 80 M=1,NEQ
      DIJ=DIJ+(2*BC(M,1)-RHS1(M))*RHS(M,1)
80    CONTINUE
      PI=DIJ
C
C  FORM MATRIX "D"
      DO 140 I=1,ID
      DO 100 M=1,NEQ
100   RHS1(M)=RHS(M,I+1)
      CALL KVECT(KSTIF,IAJSEM,IDIM,RHS1,NEQ)
      DO 140 J=1,ID
      DIJ=DCT(J,I)+DS(J,I)+DCONT(J,I)
      DO 120 M=1,NEQ
120   DIJ=DIJ+(-BC(M,I+1)+RHS1(M))*RHS(M,J+1)-BC(M,J+1)*RHS(M,I+1)
      D(I,J)=DIJ
140   CONTINUE
C
C  CANCEL UNUSED ROWS & COLUMNS OF "D"
      DO 180 I=1,ID
      IF(ISYM(I).EQ.1)GOTO 180
      DO 160 J=1,ID
      D(I,J)=0.0
160   D(J,I)=0.0
      D(I,I)=1.0
      DRHS(I)=0.0
180   CONTINUE
C
```

```
C  FORM NEW SYMMETRIC MATRIX "D"
      DO 200 I=1,ID
      DO 200 J=1,ID
      D(I,J)=(D(I,J)+D(J,I))*0.5
      D(J,I)=D(I,J)
200   CONTINUE
      WRITE(7,480)
      IF(IPR.LT.1)GOTO 240
      WRITE(7,500)
      DO 220 I=1,ID
      WRITE(7,520)(D(I,J),J=1,ID)
      WRITE(7,540)DRHS(I)
220   CONTINUE
C
C  LOADED HOLE CASE [ALPHA(9)=1.0]
240   IF(ISYM(9).NE.1)GOTO 300
      DO 260 I=1,8
      IF(ISYM(I).EQ.1)ID=I
260   CONTINUE
      ALPHA(9)=1.0
      IF(IPR.GE.1)WRITE(7,500)
      DO 280 I=1,ID
      DRHS(I)=DRHS(I)-D(I,9)*ALPHA(9)
      IF(IPR.LT.1)GOTO 280
      WRITE(7,520)(D(I,J),J=1,ID)
      WRITE(7,540)DRHS(I)
280   CONTINUE
C
C  INVERT MATRIX "D"
C  -----------------
300   CALL MINV(D,ID,DET,LW,MW)
      WRITE(7,560)DET
      IF(IPR-IPR/64*64.LT.32)GOTO 340
      DO 320 I=1,ID
      WRITE(7,580)(D(I,J),J=1,ID)
320   CONTINUE
C
C  DETERMINE VALUE OF ALPHAS & FUNCTIONALS (PI &PI0)
340   PI0=PI*0.5
      DO 360 I=1,ID
      ALPHA(I)=0.0
      DO 360 J=1,ID
360   ALPHA(I)=ALPHA(I)+D(I,J)*DRHS(J)
      DO 380 J=1,ID
      PI=PI+DRHS(J)*ALPHA(J)
      SUM=SUM+ALPHA(J)
380   CONTINUE
      PI=PI*0.5
      WRITE(7,600)PI0,PI
C
C  EVALUATE STRESS INTENSITY FACTORS (CRACKS ONLY)
      IF(ISYM(MRHS).GT.0)GOTO 400
      P=2.506626
      A1=ALPHA(1)+ALPHA(2)
      A2=ALPHA(1)-ALPHA(2)
      A3=ALPHA(3)+ALPHA(4)
      A4=ALPHA(3)-ALPHA(4)
      A1=A1*P
      A2=A2*P
      A3=A3*P
      A4=A4*P
C  PRINT ALPHAS
      WRITE(7,620)ALPHA(1),A1,ALPHA(2),A2,ALPHA(3),A3,ALPHA(4),A4
      RETURN
400   WRITE(7,640)(I,ALPHA(I),I=1,ID)
C
C  RE-ADJUST ID (LOADED HOLE CASE)
      IF(ISYM(9).NE.1)GOTO 460
420   ID=ID+1
      IF(ID.EQ.9)GOTO 440
      ALPHA(ID)=0.0
      GOTO 420
440   WRITE(7,640)ID,ALPHA(ID)
460   WRITE(7,660)SUM
      RETURN
C
480   FORMAT(///,30X,'R E S U L T S'/30X,'-------------')
500   FORMAT(//' DMAT',116X,'DRHS',/)
520   FORMAT(1X,9(E12.5,1X))
540   FORMAT(1H+,119X,E12.5)
560   FORMAT(1H0,'DETERMINANT OF MATRIX = ',E10.3,/)
580   FORMAT(' INVERSE OF MATRIX'//1X,9(E12.5,2X))
600   FORMAT(/' PI0 =  ',E15.8,10X,'PI = ',E15.8)
620   FORMAT(/' ALPHA1=',F10.6,20X,'OPENING STRESS FACTOR AT X=+A IS',
     2 F10.6/' ALPHA2=',F10.6,20X,'OPENING STRESS FACTOR AT X=-A IS',
     3 F10.6/' ALPHA3=',F10.6,20X,'  SHEAR STRESS FACTOR AT X=+A IS',
     4 F10.6/' ALPHA4=',F10.6,20X,'  SHEAR STRESS FACTOR AT X=-A IS',
     5 F10.6)
640   FORMAT(/(' ALPHA',I1,'=',F10.6))
660   FORMAT(/' SUM OF ALPHAS =',F10.6)
      END
```

APPENDIX C

Preparation of data for the finite element program

Three files are involved in the input of data to the FESM program: a direct access file, the mesh data file and the control data file. The latter two files are optional and if either or both of these files are "empty" the relevant data is taken from the direct access file. Data taken from the mesh or control data files is stored in the direct access file.

C.1 Mesh data file

The mesh data file (if required) may be input sequentially on cards or from the filestore. It must contain the following records:

1. Initial card with the legend "MESH$^{\nabla\nabla}$IN" in the first 8 characters. Any data before this record is ignored.

2. Title. (Format A16) This title is printed in the heading on output.

3. Coordinates and dimensions of hole. (Format 5 F10.0) The five parameters required are:
   - i) "x" coordinate of centre of hole or crack.
   - ii) "y" coordinate of centre of hole or crack.
   - iii) a, radius or semi-major axis length of hole/crack.
   - iv) γ, angle between trial function axis and corresponding global coordinate axis.
   - v) b, semi-minor axis of hole. (Default for this parameter is zero if the crack trial functions are specified, or a if the hole trial functions are specified).

4. Number of elements. (Format I5)

5. Element data This section must contain a record for each element and may contain the following element descriptors which define the type of elements after that record:

"FLA" - Flange elements (permitted only outside the special region).

"TRM" - Triangular membrane elements.

"TRMSP" - As TRM but within the special region.

The element data records are as follows:

FLA (Format 3I5, F10.0). The parameters required are:

i) element number

ii) and iii) end nodes

iv) cross-sectional area.

TRM (Format 4I5, F10.0). The parameters required are:

i) element number

ii) iii) and iv) nodes, numbered counter-clockwise round the element.

v) thickness of element.

TRMSP as TRM but the thickness of all elements in the special region must be constant.

This section must be terminated with the following record : ////.

6. Number of nodes. (Format I5)

7. Nodal coordinate data. This section must contain one record for each node.
(Format I5, 2F10.0). The parameters required are:

i) node number

ii) "x" coordinate of node

iii) "y" coordinate of node

This section must be terminated with the following record : ////.

8. Number of boundary conditions. (Format I5)

9. Boundary condition data. This section must contain one record for each boundary condition specified.

The boundary condition types and their parameters are as follows:

Traction: TRCT n_1 n_2 t_n t_s
(Format A4, 2I5, 2F10.0)

Asymmetry: ASYM n_1 n_2 t_n u_{s1} u_{s2}
(Format A4, 2I5, 3F10.0)

Symmetry: SYMM n_1 n_2 t_s u_{n1} u_{n2}
(Format A4, 2I5, 3F10.0)

Clamped: CLMP n_1 n_2 u_{s1} u_{s2} u_{n1} u_{n2}
(Format A4, 2I5, 4F10.0)

u-displacement: UDSP n_1 u_1
(Format A4, I5, F10.0)

v-displacement: VDSP n_1 v_1
(Format A4, I5, F10.0)

X-load: X-LD n_1 p_X
(Format A4, I5, F10.0)

Y-load: Y-LD n_1 p_Y
(Format A4, I5, F10.0)

where: n_1 = 1st node number
n_2 = 2nd node number in counter-clockwise order
u_{n1} = prescribed normal displacement at n_1
u_{n2} = ----"--------"----------"------" n_2
u_{s1} = ----"-- tangential -----"------" n_1
u_{s2} = ----"-------'└----------"------" n_2
t_n = ----"----- normal traction on n_1 - n_2
t_s = ----"----- tangential traction on n_1 - n_2
u_1 = ----"----- displacement in "X" direction at n_1
v_1 = ----"----- displacement in "Y" direction at n_1
p_X = ----"----- load in "X" direction at n_1
p_Y = ----"----- load in "Y" direction at n_1

This section must be terminated with the following record:
////.

C.2 Control data file

The control data file (if required) may be input on cards or from the filestore. It must contain the following records:

1. Options integer (Format I5). This integer is used to specify the amount of output required as follows:

   = -1 Minimum output.
   = 0 Heading and minimum output.
   = 1 Stresses output.
   = 2 Displacements output.
   = 4 Initial data output.
   = 32 Additional output.
   = 64 Extra "de-bug" output.

   The numbers 1-64 may be added together for a combination of options.

2. Control title (Format A16). This is printed in the heading on output.

3. Trial function parameters (Format 10I5). These parameters specify which trial function subroutine is to be used and which functions from the subroutine are to be selected. The parameters are:

   i) to specify the subroutine:
      = 0 TRLFNSØ subroutine for cracks.
      = 1 TRLFNS1 subroutine for loaded or traction-free circular holes.
      = 2 TRLFNS2 subroutine for traction-free circular or elliptical holes.

   (ii) - ix) to specify if the particular trial function 1 to 8 is to be used.
      = 0 function not used.
      = 1 function included.

   x) to specify if the loading function (for use only with subroutine TRLFNS1) is to be used:
      = 0 loading function not used.
      = 1 loading function included.

4. Fourier coefficients for hole loading (Free Format).
This section is included only if the loading function is used. The coefficients A_n (n = 0 to 29) and D_n (n = 1 to 24) must be input sequentially in free format.

5. Special region data. This section is optional but if it is included it supersedes the special region data which may be contained in the mesh data file or direct access file. The first record of this section should contain the number of elements in the special region (Format I5) followed by the characters "$^{\nabla}$SP" (Format A3). The element numbers are then input, one per record (Format I5).
The section must be terminated with the following record :
////.

C.3 The direct access file

The direct access file must have a record size of 24 bytes and a total size of between 6 and 28 kilobytes depending on the number of elements in the mesh. Generally the data is put into the file by running the program having prepared mesh and control data files, or by using the automatic mesh generator (see appendix D). However, when a number of cases are to be run with identical or similar meshes it is most convenient to make the minor changes to the direct access file using the macro "MESH" (see appendix D) and dispense with the other input files.

The information stored in the direct access file is shown in table C.1. This data is written on the direct access file by the machine, not the user.

Record Number	Details
1	NEL NNODE NBC
2	XC YC
3	A B Y
4	α_1 α_2 α_3
5	α_4 α_5 α_6
6	α_7 α_8 α_0
7 to 11	A_n (n = 0 to 29) six items per record.
12 to 15	D_n (n = 1 to 24) six items per record.
16	OPTIONS
17	Mesh title (16 characters) TIME (8 characters)
18	Control title (16 characters) DATE (8 charact)
19	ISYM (1-6)
20	ISYM (7-9), ITF
21	E, NU
22 to 30	(not used)
31 to (30 + NEL)	Element data: N1, N2, N3, T, SPREG
(31+NEL)to (30+NEL +NNODE)	Node data: X, Y
(31+NEL+NNODE) to (30+2*NEL+NNODE)	Stress data: SXA, SYA, TXYA
(31+2*NEL+NNODE) to (30+2*NEL+NNODE+NBC)	Boundary data: ITYPE, J1, J2, Z1, Z2, Z3, Z4

Table C.1 Information stored in the direct access file.

The variables referred to in table C.1 are defined in the table C.2 overleaf.

Variable	Meaning	Type
NEL	Number of elements	INTEGER
NNODE	Number of nodes	INTEGER
NBC	Number of boundary conditions	INTEGER
XC	"X" coordinate of hole centre	REAL
YC	"Y" coordinate of hole centre	REAL
A	semi-major axis length of hole, a	REAL
B	semi-minor axis length of hole, b	REAL
γ	Angle between major axis of hole and "X" coordinate axis	REAL
α_i	Trial function coefficient	REAL
A_n	Fourier coefficient of normal loading	REAL * 4
D_n	Fourier coefficient of tangential "	REAL * 4
OPTIONS	Options integer	INTEGER
ISYM(1-8)	Specifies if trial function is used (1 or 0)	INTEGER
ISYM(9)	Specifies if loading function is used (1 or 0)	INTEGER
ITF	Specifies which trial function sub-routine is used (0, 1 or 2)	INTEGER
E	Young's modulus	REAL
NU	Poisson's ratio	REAL
N1, N2, N3	Node numbers of element	INTEGER
T	Thickness of element	REAL
SPREG	Specifies if element is within special region (true or false)	LOGICAL
X, Y	"X" and "Y" coordinates of node	REAL
SXA	Stress components of	REAL
SYA	$\underline{\sigma}^F - \sum_{i=0}^{k} (\underline{\sigma}_i^\dagger - \underline{\sigma}_i^c)$ for element	REAL
TXYA		REAL
ITYPE	Type of boundary condition	INTEGER
J1, J2	Node numbers	INTEGER*2
Z1-Z4	Boundary condition parameters	REAL*4

Table C.2 Variables in the direct access file.

APPENDIX D

Running the finite element program

This appendix is included primarily for the benefit of those who may wish to use the FESM program on the ICL 2970 computer at Southampton University. Table D.1 shows the "macros" which may be used for running the program and for preparing and interpreting the data. Macros are commands which may be input to the computer to control a particular process, and general instructions for using and modifying macros are found in the system reference manuals. The appendix sets out instructions for using these macros for the purposes shown in table D.1.

Section	Macro Name	Purpose
D.1	NOTCH:	To run the finite element program.
D.2	MESH:	To generate or modify finite element mesh or other input data.
D.3	DRAWMESHES:	To produce plot of finite element mesh.
D.4	LOADLOAD:	To input Fourier coefficients to direct access file for standard loadings.
D.5	HOLE:	To produce graph of loading on hole.
D.6	VUSTRESS:	To produce graph of stresses around boundary of specified elements.

Table D.1 Macros used with the FESM program

For each macro a description of its use and a full specification of its parameters is given. Some indication of how the macro might be used is shown by the examples at the end of the specifications. Full details of all the options and facilities of the software and how data files are prepared for graphics and data modification are not given in this appendix, however users will find that when used interactively the programs will request the data required which may be input, generally in "free-format", at the terminal.

D.1 The Macro "NOTCH"

This macro is used to run the FESM program. The data files are assigned to input/output channels and, if graphical output is required, parameters for plotting are specified.

Parameter List:

```
NOTCH (@ literal @ DIRECTACCESSFILE = @ see below @,
       @ literal @ MESH = @ see below @,
       @ literal @ CONTROL = @ see below @,
       @ literal @ GRAPHDATA = @ see below @,
       @ literal @ PLOTFILE = @ see below @,
       @ literal @ ACTION = @ see below @,
       @ literal @ DEVICE = CALCOMP,
       @ literal @ SCALE = 1.0,
       @ literal @ IMMEDIATE = YES,
       @ literal @ JOBNAME = @ see below @,
       @ integer @ TIME = 50,
       @ response @ RESPONSE = RESULT)
```

Keyword description

Keyword: DIRECTACCESSFILE

Use: Specifies the name of direct access data file (see appendix C).

Values taken: Filename of existing direct access file.

Default: Temporary direct access file will be created.

Keyword: MESH

Use: Specifies the name of the mesh data file (see appendix C).

Values taken: Filename. Data input from file.

Default: Data taken from direct access file.

Keyword: CONTROL

Use: Specifies the name of control data file (see appendix C).

Values taken: Filename. Data input from file.

Default: Data taken from direct access file.

Keyword: GRAPHDATA

Use: Specifies the source of the plotting instructions (if required). Not applicable if "ACTION" does not include "VU".

Values taken: = Filename. Instructions input from file.
= *STDAD. Instructions input from alien data. (e.g. from terminal).

Default: No instructions are given and default values for the graph plot are assumed if required.

Keyword: PLOTFILE

Use: Specifies the name of file to contain output plot data. Not applicable if ACTION does not include "VU".

Values taken: Name.

Default: A new temporary file will be created if required.

Keyword: ACTION

Use: Specifies actions to be taken. If several actions are required the values below should be concatenated (e.g. ACTION = NEWDAF_VU_DRAW).

Values taken:

NEWDAF - A new direct access file is created. Input data is taken from file specified by the keyword DIRECTACCESSFILE and with the output data is put on the new file. Data on original direct access file is unchanged.

VU - A graph of the stresses on the boundary of the finite element is produced. The file specified by GRAPHDATA may contain instructions to the contrary but by default the output will be to the file specified by PLOTFILE and will be in "SAVE-DRAWING"pseudo code which may be interpreted by the macro "SOLOOKPLOT" or by including the value DRAW (see below). The remaining values for ACTION are only applicable if "VU" is also included.

DRAW - The plotfile is sent to the specified DEVICE for plotting.

PLOT - If the file specified by GRAPHDATA instructs a CALCOMP code to be produced (not default) and if the job is in a "batch" environment, the plot is carried out.

SAVE - The plotfile is saved.

Default: No further action.

Keyword: DEVICE

Use: Specifies the plotting device on which graph is to be produced. Not applicable unless ACTION includes "VU" and "DRAW".

Values taken:

= CALCOMP (Calcomp pen plotter).

= TEKTRONIX (Tektronix 4010 graphics terminal).

= IMLAC (Imlac graphics terminal).

Default: CALCOMP.

Keyword: SCALE

Use: Specifies required scaling factor for plotter. Not applicable unless ACTION includes "VU" and "DRAW".

Values taken:

= Positive number up to four characters long including mandatory decimal point. The size of the graph will be scaled by this factor.

= Any negative number. The size of the graph will be adjusted to fit the output device requested.

Default: 1.0 (No scaling is performed).

Keyword: IMMEDIATE

Use: Specifies if program is to be run immediately or entered into the batch job queue.

Values taken:

= YES. Program is run immediately.

= NO. Job entered into batch queue to be run later.

Default: YES.

Keyword: JOBNAME

Use: Specifies name for batch job if IMMEDIATE = NO.

Values taken: Name.

Default: Name specified by macro.

Keyword: TIME

Use: If IMMEDIATE = NO then TIME is an estimate of the time (in seconds) required for the job.

Values taken: Integer between 10 and 2000.

Default: 50.

Keyword: RESPONSE

Use: Specifies the result code variable.

Values taken: Response variable.

Default: RESULT

Example

To run the FESM program with data from the direct access file called DAF1 and the control data file called CON1 the following job could be run. A graph of the stresses is also to be produced (default plot instructions).

```
JOB(JOBNAME=:MERØØ4.KT1,TIME=1OO)
NOTCH(DAF1,CONTROL=CON1,ACTION=VUDRAW)
ENDJOB
****
```

D.2 The Macro "MESH"

This macro is used to generate or modify the finite element mesh stored on a direct access file, and/or modify other data required by the program. The macro is generally used interactively when instructions are given to the user on how to input the data. A plot of the finite element mesh may be produced if required.

Parameter list:

MESH (@ literal @ DIRECTACCESSFILE = @ mandatory @,
@ superliteral @ NEWDAFS = @ see below @,
@ literal @ PLOTFILE = @ see below @,
@ literal @ DATA = *STDAD,
@ response @ RESPONSE = RESULT)

Keyword description

Keyword: DIRECTACCESSFILE

Use: Specifies the name of direct access file containing existing data or to contain new data.

Values taken: Filename of existing direct access file.

Default: None. The parameter is mandatory.

Keyword: NEWDAFS

Use: Specifies the name of one or more direct access files. After modifications have been completed on the original direct access file the data is transferred in turn to the NEWDAFS and other modifications may be carried out.

Values taken: Names of existing direct access files connected by ampersands (&).

E.g. = DAF1&DAF2&DAF3

or = DAFO

Default: Data may be generated and modifications carried out on the file specifies by DIRECTACCESSFILE only.

Keyword: PLOTFILE

Use: Specifies the name of file to contain output plot data if required and if not directed to a graphics terminal for immediate display.

Values taken: Name

Default: A new temporary file is created.

Keyword: DATA

Use: Specifies the name of file containing instructions for data modification. Generally (and by default) instructions are input from the alien data stream - i.e. from the terminal when used interactively.

Values taken: = Filename. Instructions input from file.
Default: Alien data (*STDAD).

Keyword: RESPONSE (as for macro NOTCH above).

Example

To carry out modifications on data contained in the direct access file DAF1 or to generate a new mesh and store the data in this file, the following should be input to an interactive graphics terminal:

```
-
- MESH(DAF1)
-
```

Questions or instructions are given by the program to guide the user in entering the required data. The following functions may be carried out using the macro MESH:

* To generate a new mesh by specifying blocks of regular elements.
* To plot the existing finite element data to show the mesh.
* To add additional nodes and/or elements.
* To delete elements.
* To move the position of nodes.
* To stretch a portion of the finite element mesh to change the overall dimensions.
* To change boundary conditions.
* To modify the special region.
* To change the loading on the hole.
* To change the trial functions.
* To change other parameters such as elastic constants, titles, hole size and position, print option.

D.3 The Macro "DRAWMESHES"

This macro is used to produce a plot of the finite element mesh from one or more direct access files. The device on which the plot is produced and a scaling factor may be specified.

Parameter list:

```
DRAWMESHES
     (@ superliteral @ DIRECTACCESSFILES = @ mandatory @,
      @ literal @ DATA = @ see below @,
      @ literal @ PLOTFILE = @ see below @,
      @ literal @ ACTION = @ see below @,
      @ literal @ DEVICE = CALCOMP,
      @ literal @ SCALE = 1.0,
      @ integer @ TIME = 5.0,
      @ response @ RESPONSE = RESULT)
```

Keyword description

Keyword: DIRECTACCESSFILES

Use: Specifies names of files containing the finite element data.

Values taken: One or more direct access file names connected by ampersands.

Default: None. The parameter is mandatory.

Keyword: DATA

Use: Specifies source of plotting instructions.

Values taken:

= Filename. Instructions input from file.

= *STDAD. Instructions input from alien data stream in response to questions from program.

Default: No instructions are given and default values are assumed.

Keyword: PLOTFILE (as for macro MESH above).

Keyword: ACTION

Use: Specifies actions to be taken (the two words may be concatenated).

Values taken:

SAVE - The plotfile is saved.

DRAW - The plotfile is sent to the specified device for plotting. Only valid if "SAVE_DRAWING" option is specified by DATA (this is the default).

Default: The plotfile is produced but no further action taken.

Keyword: DEVICE (as for macro NOTCH above)

Not applicable unless action includes "DRAW".

Keyword: SCALE (as for macro NOTCH above).

Not applicable unless ACTION includes "DRAW".

Keyword: TIME

Use: Gives an estimate of time required by job to "draw" plot (in seconds). Not applicable unless ACTION includes "DRAW".

Values taken: Integer between 10 and 600.

Default: 50.

Keyword: RESPONSE (as for macro NOTCH above).

Example

The following job could be entered to produce plots of the meshes from the files DAF1, DAF2 and DAF3 on the Calcomp pen plotter.

```
JOB(JOBNAME=:MERØØ4.MESHES,TIME=50)
DRAWMESHES(DAF1&DAF2&DAF3,ACTION=DRAW)
ENDJOB
****
```

D.4 The Macro LOADLOAD

This macro is used to enter the Fourier coefficients of the loading function (see Chapter 3) for a number of standard loadings. (This function may also be carried out using the macro "MESH").

Parameter list:

```
LOADLOAD
     (@ literal @ DIRECTACCESSFILE = @ mandatory @,
      @ literal @ DATA = *STDAD,
      @ literal @ OUTPUT = *STDAD,
      @ response @ RESPONSE = RESULT)
```

Keyword description

Keyword: DIRECTACCESSFILE

Use: Specifies the name of the direct access file to which the Fourier coefficients are output.

Values taken: Filename of existing direct access file.

Default: None. This parameter is mandatory.

Keyword: DATA

Use: Specifies the source of program instructions. By default this is from alien data (at the terminal) and data is input in response to requests from the program.

Values taken:

= Filename. Instructions input from file.

Default: Alien data (*STDAD).

Keyword: OUTPUT

Use: Specifies filename to contain details of Fourier coefficients, etc.

Values taken: Filename or *STDAD.

Default: Output to terminal or job journal (*STDAD).

Keyword: RESPONSE (as for the macro NOTCH above).

Example

To enter the Fourier coefficients for a particular loading to the direct access file DAF1 the following could be input at a terminal:

```
-
- LOADLOAD(DAF1)
-
```

The following parameters may be specified:

* the type of loading (Default: cos θ loading).
* number of coefficients m_1 and m_2 (Defaults: 30 and 25).
* magnitude of the resultant P (Default: π).
* radius of the hole a (Default: 1.0).
* the ratio of resultant load transmitted by the shear tractions to that transmitted by the radial tractions (Default: 0.2).

The following distributions of radial load may be specified (see section 5.4.1):

b) radial tractions proportional to cos θ $(-\pi/2 \leq \theta \leq \pi/2)$

c) radial tractions proportional to $\cos^2\theta$ $(-\pi/2 \leq \theta \leq \pi/2)$

d) constant pressure over an arc.

The following distributions of tangential load may be specified:

g) shear tractions proportional to sin θ $(-\pi/2 \leq \theta \leq \pi/2)$

h) shear tractions proportional to sin 2θ $(-\pi/2 \leq \theta \leq \pi/2)$

j) shear tractions proportional to $\sin^3\theta \cos\theta$ $(-\pi/2 \leq \theta \leq \pi/2)$

Alternatively specific values for the Fourier coefficients may be given.

D.5 The Macro HOLE

This macro is used to produce graphs of the tractions on the hole. The type of loading on the hole may be specified by the direct access file or by the data input at the terminal (or from DATA file) by the user.

Parameter list:

```
HOLE (@ literal @ DIRECTACCESSFILE = @ mandatory @,
      @ literal @ DATA = *STDAD,
      @ literal @ ACTION = @ see below @,
      @ literal @ DEVICE = CALCOMP,
      @ literal @ SCALE = 1.0,
      @ integer @ TIME = 50
      @ response @ RESPONSE = RESULT)
```

Keyword description

Keyword: DIRECTACCESSFILE

Use: Specifies direct access file from which initial data about hole loading is taken.

Values taken: Name of existing direct access file.

Default: None. This parameter is mandatory.

Keyword: DATA

Use: Specifies source of plotting instructions.

Values taken:

= Filename. Instructions input from file.

= *STDAD. Instructions input from alien data stream as directed by program.

Default: No instructions are given and default values are assumed.

Keyword: ACTION

Use: Specifies whether "SAVE_DRAWING" code (if generated) is plotted.

Values taken:

DRAW - The plot file is sent to the specified device for plotting.

Default: No further action.

Keyword: DEVICE (as for macro NOTCH above).
Not applicable unless action includes "DRAW".

Keyword: SCALE (as for macro NOTCH above).
Not applicable unless action includes "DRAW".

Keyword: TIME (as for macro DRAWMESHES above).
Not applicable unless action includes "DRAW".

Keyword: RESPONSE (as for macro NOTCH above).

Example

To produce a plot of the tractions round the hole specified by Fourier coefficients stored in the file DAF1 the following job could be run. The plot is to be produced on the Imlac interactive terminal:

```
-
- HOLE(DAF1,DATA=*STDAD)
-
```

Data must be input to the terminal in reply to the requests from the program. In reply to the first question for example the Imlac terminal must be specified.

The following job however could be input to produce the plot on the Calcomp pen plotter at half scale with default plotting instructions.

```
JOB(JOBNAME=:MERØØ4.HOLEPLOT,TIME=50)
HOLE(DAF1,ACTION=draw,scale=0.5)
ENDJOB
****
```

D.6 The Macro VUSTRESS

This macro is used to produce a graph of stress along specified element boundaries (by default the outer boundary of the mesh). Data produced by the FESM program and stored on the direct access file is retrieved and plotted. The data from more than one direct access file may be plotted in this way with one call of the macro.

Synonym: VU.

Parameter list

```
VUSTRESS
     (@ superliteral @ DIRECTACCESSFILES = @ mandatory @,
      @ literal @ DATA = @ see below @,
      @ literal @ PLOTFILE = @ see below @,
      @ literal @ ACTION = @ see below @,
      @ literal @ DEVICE = CALCOMP,
      @ literal @ SCALE = 1.0,
      @ integer @ TIME = 50,
      @ response @ RESPONSE = RESULT)
```

Keyword description

Keyword: DIRECTACCESSFILES

Use: Specifies the direct access files containing data to be plotted.

Values taken: One or more direct access file names connected by ampersands.

Default: None. This parameter is mandatory.

Keyword: DATA

Use: Specifies source of plotting instructions.

Values taken:

= Filename. Instructions input from file.

= *STDAD. Instructions input from alien data stream in response to requests from program.

Default: No instructions are given and default values are assumed.

Keyword: PLOTFILE (as for macro MESH above).

Keyword: ACTION

Use: Specifies further actions to be taken.

Values taken: The following words may be included in the value for this parameter with identical meaning as for the macro NOTCH:

DRAW
PLOT
SAVE } (see macro NOTCH above)

Default: No further action.

Keyword: DEVICE (as for macro NOTCH above).

Keyword: SCALE (as for macro NOTCH above).

Keyword: TIME (as for macro DRAWMESHES above).

Keyword: RESPONSE (as for macro NOTCH above).

Example

To produce graphs of the stresses on the boundary of the finite element meshes from the data files DAF1 and DAF2, the following job could be run. Default plotting instructions are used and the graph will be plotted on the Calcomp pen plotter.

```
JOB(JOBNAME=MERØØ4.VUGRAPH,TIME=1OO)
VUSTRESS(DAF1&DAF2,ACTION=DRAW)
ENDJOB
****
```

APPENDIX E

Finite Element Meshes

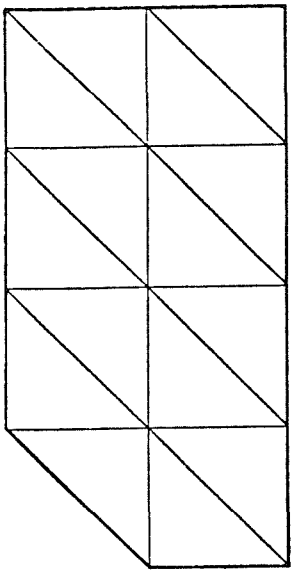

Figure E1: $N_o = 1$

$\frac{a}{w} = 0.5$, $\frac{\ell}{w} = 2.0$

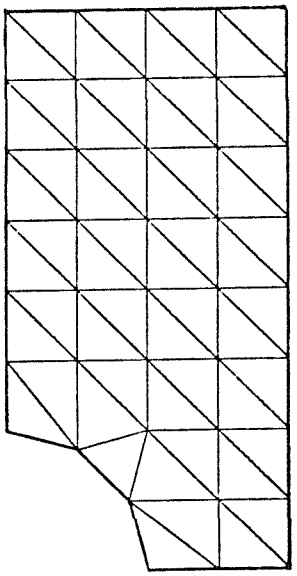

Figure E2: $N_o = 2$

$\frac{a}{w} = 0.5$, $\frac{\ell}{w} = 2.0$

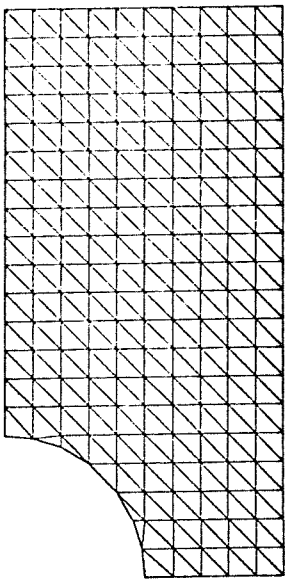

Figure E3: $N_o = 5$

$\frac{a}{w} = 0.5$, $\frac{\ell}{w} = 2.0$

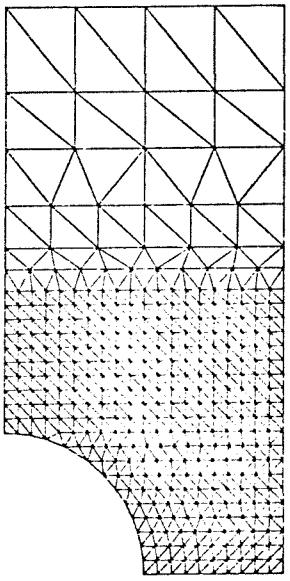

Figure E4: $N_o = 10$

$\frac{a}{w} = 0.5$, $\frac{\ell}{w} = 2.0$

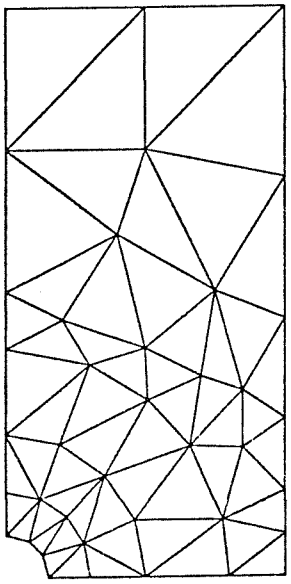

Figure E5: $\frac{a}{w} = 0.15$

$\frac{\ell}{w} = 2.0$

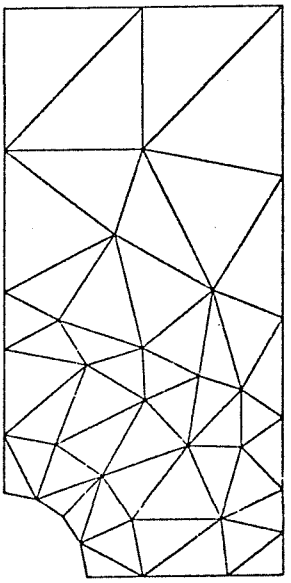

Figure E6: = 0.3

$\frac{\ell}{w} = 2.0$

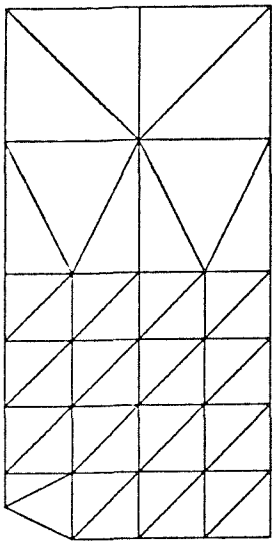

Figure E7: $\frac{a}{b} = 2.0$

$\frac{a}{w} = 0.25$, $\frac{\ell}{w} = 2.0$

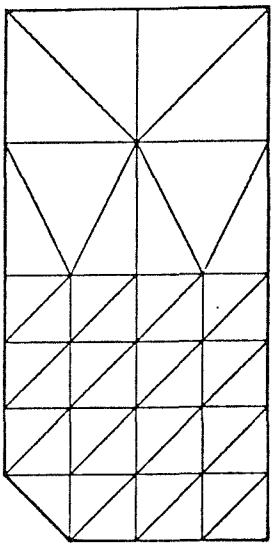

Figure E8: $\frac{a}{b} = 1.0$

$\frac{a}{w} = 0.25$, $\frac{\ell}{w} = 2.0$

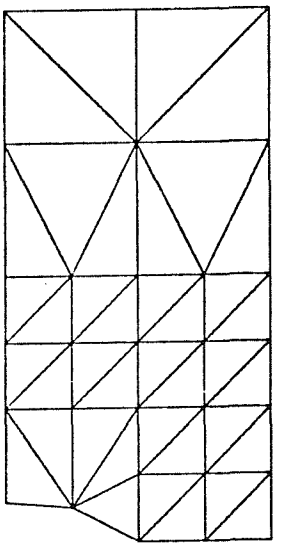

Figure E9: $\frac{a}{b} = 3.33$

$\frac{a}{w} = 0.5$, $\frac{\ell}{w} = 2.0$

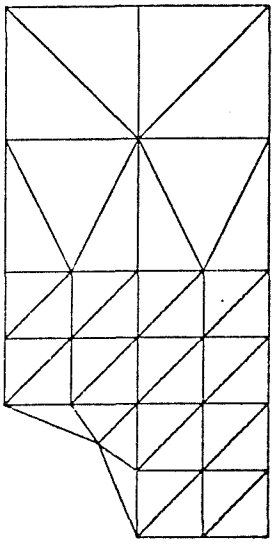

Figure E10: $\frac{a}{b} = 1.0$

$\frac{a}{w} = 0.5$, $\frac{\ell}{w} = 2.0$

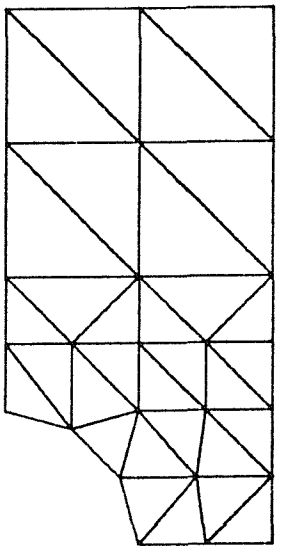

Figure E11: Mesh A

$\frac{a}{w} = 0.5$, $\frac{\ell}{w} = 2.0$

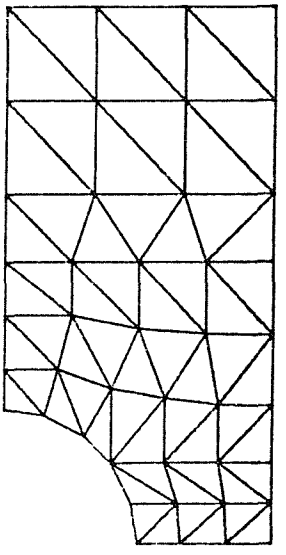

Figure E12: Mesh B

$\frac{a}{w} = 0.5$, $\frac{\ell}{w} = 2.0$

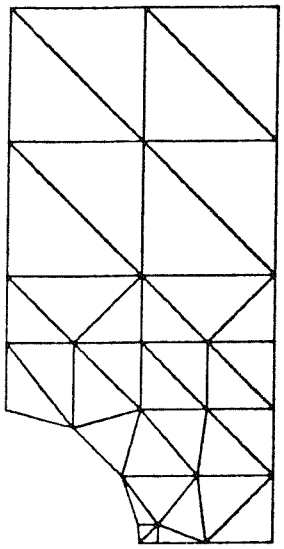

Figure E13: Mesh A(i)

$\frac{a}{w} = 0.5$, $\frac{\ell}{w} = 2.0$

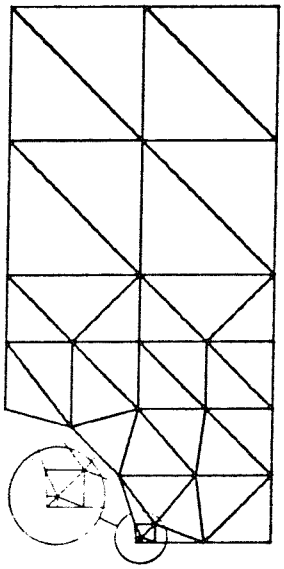

Figure E14: Mesh A(ii)

$\frac{a}{w} = 0.5$, $\frac{\ell}{w} = 2.0$

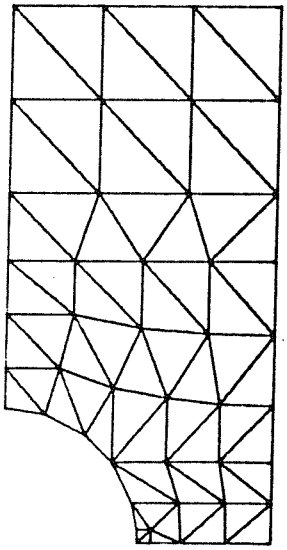

Figure E15: Mesh B(i)

$\frac{a}{w} = 0.5$, $\frac{\ell}{w} = 2.0$

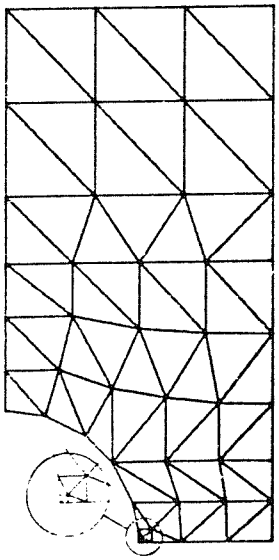

Figure E16: Mesh B(ii)

$\frac{a}{w} = 0.5$, $\frac{\ell}{w} = 2.0$

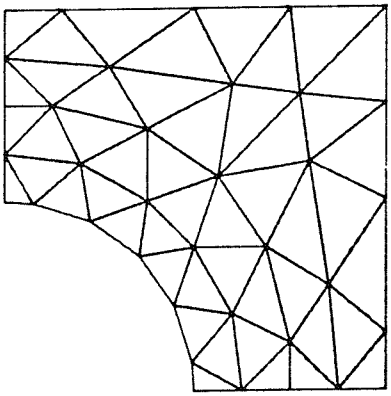

Figure E17: Mesh C

$\frac{a}{w} = 0.5$, $\frac{\ell}{w} = 1.0$

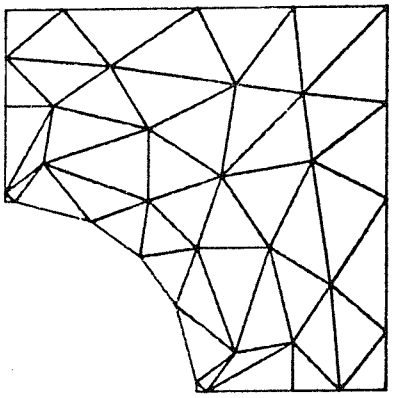

Figure E18: Mesh D

$\frac{a}{w} = 0.5$, $\frac{\ell}{w} = 1.0$

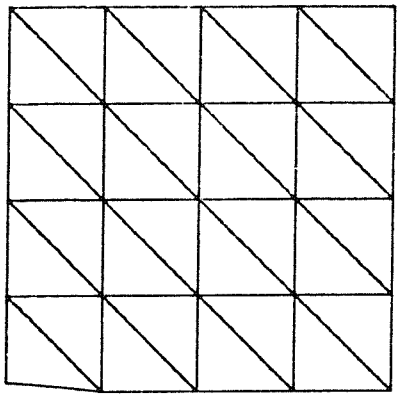

Figure E19: $\frac{a}{b} = 10.0$

$\frac{a}{w} = 0.25$, $\frac{\ell}{w} = 1.0$

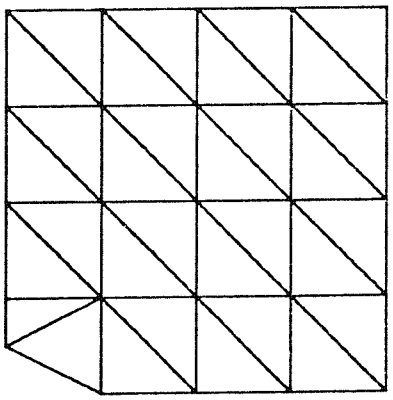

Figure E20: $\frac{a}{b} = 2.0$

$\frac{a}{w} = 0.25$, $\frac{\ell}{w} = 1.0$

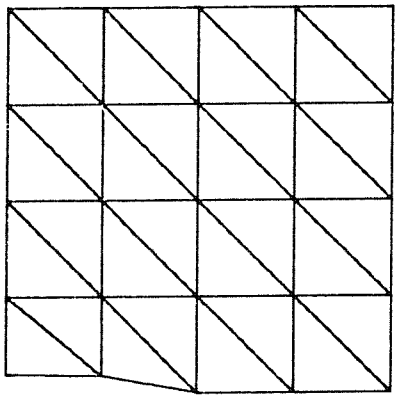

Figure E21: $\frac{a}{b} = 10.0$

$\frac{a}{w} = 0.5$, $\frac{\ell}{w} = 1.0$

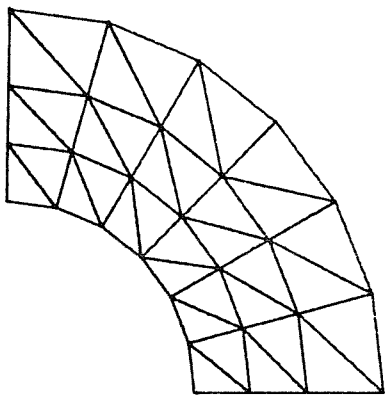

Figure E22: Annulus

$\frac{a}{w} = 0.5$

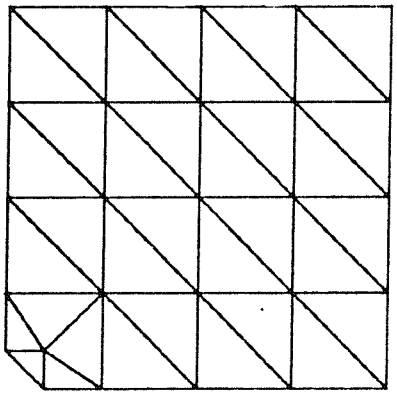

Figure E23: Square Plate

$\frac{a}{w} = 0.1$

(In the figures below the special region is shown shaded).

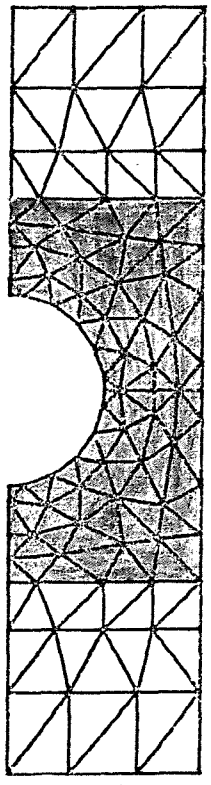

Figure E24: Symmetrical lug, $\frac{a}{w} = 0.5$, $\ell_1/w = 2.0$ $\ell_2 = \ell_1$

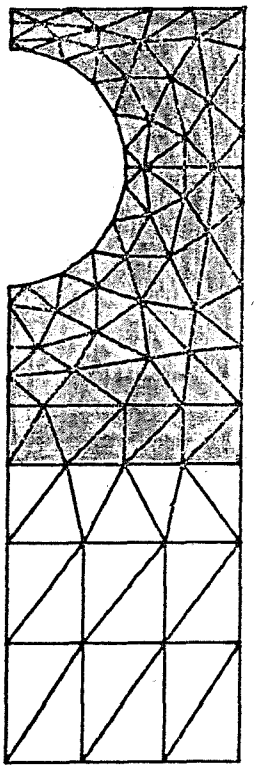

Figure E25: $\frac{a}{w} = 0.5$, $\ell_1/w = 0.75$, $\ell_2/w = 2.5$

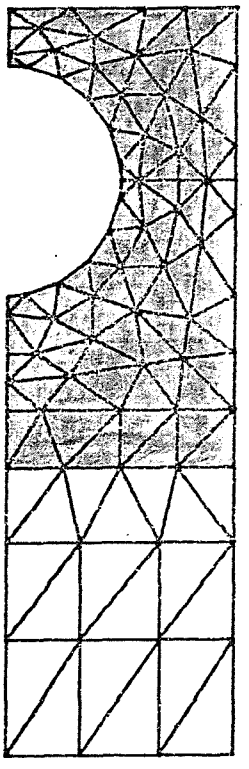

Figure E26: $\frac{a}{w} = 0.5$, $\ell_1/w = 0.8$, $\ell_2/w = 2.5$

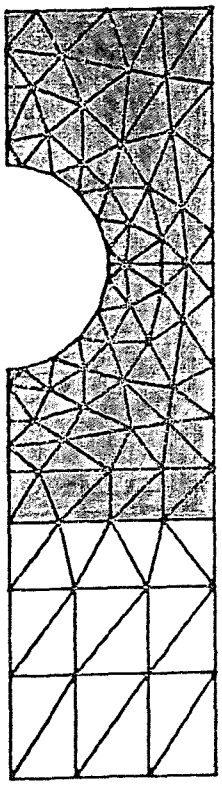

Figure E27: a/w = 0.5 $\ell_1/w = 1.25$, $\ell_1/w = 2.5$

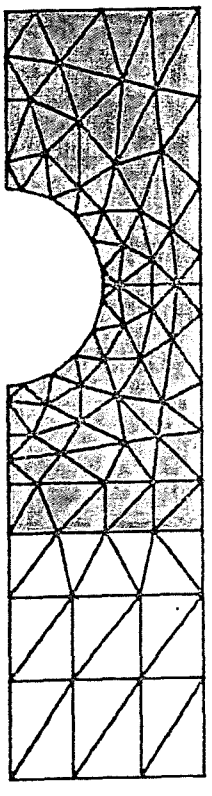

Figure E28: a/w = 0.5 $\ell_1/w = 1.5$, $\ell_2/w = 2.5$

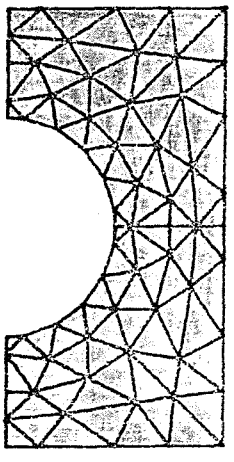

Figure E29: Symmetrical lug, a/w = 0.5, $\ell_1/w = 1.0$, $\ell_2 = \ell_1$

APPENDIX F

Kernel function for region with a circular hole

The solution is required for the tractions and displacements in an infinite region with a circular hole of radius a, at a point z in the complex plane due to a unit point force in the k direction acting at the point z_o. These may be expressed (see chapter 6) in terms of the complex potentials $\phi_k(z,z_o)$ and $\psi_k(z,z_o)$ and their derivatives. ϕ_k and ψ_k are given by Murakami and Nisitani [6.19] as:

$$\phi_k = \frac{1}{2\pi(1+\kappa)} \{- \chi_k \ell n(z-z_o) - \kappa\chi_k \ell n(1-a^2/z\,\bar{z}_o) + \frac{\bar{\chi}_k{}^2(z_o\bar{z}_o-a^2)}{\bar{z}_o{}^2(z\,\bar{z}_o-a^2)} \} \qquad (F.1)$$

$$\psi_k = \frac{1}{2\pi(1+\kappa)} \{\kappa\,\bar{\chi}_k \ell n(z-z_o) + \bar{\chi}_k \ell n(1-a^2/z\,\bar{z}_o) + \frac{\chi_k\bar{z}_o}{z-z_o} - \frac{\chi^2}{z\,z_o}$$

$$+ \frac{\kappa\chi_k a^4}{z^2(z\bar{z}_o-a^2)} + \frac{\bar{\chi}_k a^4(z_o\bar{z}_o-a^2)}{z\,\bar{z}_o(z\,\bar{z}_o-a^2)^2} \} \qquad (F.2)$$

where χ_k is given, in terms of the Kronecker delta, by:

$$\chi_k = \delta_{1k} + i\,\delta_{2k} \qquad (F.3)$$

Defining $z_{o,j}$ as:

$$z_{o,j} = \delta_{1j} + i\delta_{2j} \qquad (F.4)$$

the derivatives of ϕ_k and ψ_k are given by equations (F.5)-(F.12).

$$\phi_{k,j} = \frac{1}{2\pi(1+\kappa)} \{[\frac{\chi_k}{z-z_o} + \frac{\bar{\chi}_k a^2}{\bar{z}_o(z\,\bar{z}_o-a^2)}]\, z_{o,j} + [- \frac{\kappa\chi_k a^2}{\bar{z}_o(z\,\bar{z}_o-a^2)} + \frac{\bar{\chi}_k a^2 z_o}{\bar{z}_o^2(z\,\bar{z}_o-a^2)}$$

$$- \frac{\bar{\chi}_k a^2(z_o\bar{z}_o-a^2)(3z\,\bar{z}_o-2a^2)}{\bar{z}_o{}^3(z\,\bar{z}_o-a^2)^2}]\,\bar{z}_{o,j} \} \qquad (F.5)$$

$$\phi'_k = \frac{1}{2\pi(1+\kappa)} \left\{ -\frac{\chi_k}{z-z_o} - \frac{\kappa\chi_k a^2}{z(z\,\bar{z}_o-a^2)} - \frac{\bar{\chi}_k a^2(z_o\bar{z}_o-a^2)}{\bar{z}_o(z\,\bar{z}_o-a^2)^2} \right\} \tag{F.6}$$

$$\phi'_{k,j} = \frac{1}{2\pi(1+\kappa)} \left\{ \left[-\frac{\chi_k}{(z-z_o)^2} - \frac{\bar{\chi}_k a^2}{(z\,\bar{z}_o-a^2)^2} \right] z_{o,j} + \left[\frac{\kappa\chi_k a^2}{(z\,\bar{z}_o-a^2)^2} - \frac{\bar{\chi}_k a^2 z_o}{\bar{z}_o(z\,\bar{z}_o-a^2)^2} \right.\right.$$

$$\left.\left. - \frac{\bar{\chi}_k a^2(z_o\bar{z}-a^2)(3z\,\bar{z}_o-a^2)}{\bar{z}_o^{\,2}(z\,\bar{z}_o-a^2)^3} \right] \bar{z}_{o,j} \right\} \tag{F.7}$$

$$\phi''_k = \frac{1}{2\pi(1+\kappa)} \left\{ \frac{\chi_k}{(z-z_o)^2} + \frac{\kappa\chi_k a^2(2z\,\bar{z}_o-a^2)}{z^2(z\,\bar{z}_o-a^2)^2} + \frac{2\bar{\chi}_k a^2(z_o\bar{z}_o-a^2)}{(z\,\bar{z}_o-a^2)^3} \right\} \tag{F.8}$$

$$\phi''_{k,j} = \frac{1}{2\pi(1+\kappa)} \left\{ \left[\frac{2\chi_k}{(z-z_o)^3} + \frac{2\bar{\chi}_k a^2\bar{z}_o}{(z\,\bar{z}_o-a^2)^3} \right] z_{o,j} + \left[\frac{2(\kappa\chi_k\bar{z}_o+\bar{\chi}_k z_o)a^2}{(z\,\bar{z}_o-a^2)^3} \right.\right.$$

$$\left.\left. - \frac{6\bar{\chi}_k a^2(z_o\bar{z}_o-a^2)z}{(z\,\bar{z}_o-a^2)^4} \right] \bar{z}_{o,j} \right\} \tag{F.9}$$

$$\psi_{k,j} = \frac{1}{2\pi(1+\kappa)} \left\{ \left[-\frac{\kappa\bar{\chi}_k}{z-z_o} + \frac{\chi_k\bar{z}_o}{(z-z_o)^2} + \frac{\chi_k a^2}{z\,z_o^{\,2}} - \frac{\bar{\chi}_k a^4}{z(z\,\bar{z}_o-a^2)^2} \right] z_{o,j} \right. \tag{F.10}$$

$$\left. + \left[\frac{\bar{\chi}_k a^2}{\bar{z}_o(z\,\bar{z}_o-a^2)} + \frac{\chi_k}{z-z_o} + \frac{(\bar{\chi}_k z_o-\kappa\chi_k\bar{z}_o)a^2}{z\,\bar{z}_o(z\,\bar{z}_o-a^2)^2} - \frac{\bar{\chi}_k a^4(z_o\bar{z}_o-a^2)(3z\,\bar{z}_o-a^2)}{z\,\bar{z}_o^{\,2}(z\,\bar{z}_o-a^2)^3} \right] \bar{z}_{o,j} \right\}$$

$$\psi'_k = \frac{1}{2\pi(1+\kappa)} \left\{ \frac{\kappa\bar{\chi}_k}{z-z_o} + \frac{\bar{\chi}_k a^2}{z(z\,\bar{z}_o-a^2)} - \frac{\chi_k \bar{z}_o}{(z-z_o)^2} + \frac{\chi_k a^2}{z^2 z_o} - \frac{\kappa\chi_k a^4(3z\,\bar{z}_o-2a^2)}{z^3(z\,\bar{z}_o-a^2)^2} \right.$$

$$\left. - \frac{\bar{\chi}_k a^4(z_o\bar{z}_o-a^2)(3z\,\bar{z}_o-a^2)}{z^2\bar{z}_o(z\,\bar{z}_o-a^2)^3} \right. \qquad \text{(F.11)}$$

$$\psi'_{k,j} = \frac{1}{2\pi(1+\kappa)} \left\{ \left[\frac{\kappa\bar{\chi}_k}{(z-z_o)^2} - \frac{2\chi_k\bar{z}_o}{(z-z_o)^3} - \frac{\chi a^2}{z^2 z_o^2} - \frac{\bar{\chi}_k a^4(3z\,\bar{z}_o-a^2)}{z^2(z\,\bar{z}_o-a^2)^3} \right] z_{o,j} \right.$$

$$+ \left[- \frac{\bar{\chi}_k a^2}{(z\,\bar{z}_o-a^2)^2} - \frac{\chi_k}{(z-z_o)^2} + \frac{\kappa\chi_k a^4(3z\,\bar{z}_o-a^2)}{z^2(z\,\bar{z}_o-a^2)^3} \right.$$

$$- \frac{\bar{\chi}_k a^4(6z\,z_o\bar{z}_o - 3z\,a^2 - z_o a^2)}{z^2\bar{z}_o(z\,\bar{z}_o-a^2)^3}$$

$$\left. \left. + \frac{\bar{\chi}_k a^4(z_o\bar{z}_o-a^2)(3z\,\bar{z}_o-a^2)(4z\,\bar{z}_o-a^2)}{z^2\,\bar{z}_o^{\,2}(z\,\bar{z}_o-a^2)^4} \right] \bar{z}_{o,j} \right\} \qquad \text{(F.12)}$$

APPENDIX G

Using the modified boundary element program.

This appendix deals with preparing the data file for the boundary element program and using the three "macros" (system control commands) which were prepared for modifying the data and running the program. One data file is required for each run of the program and the information it should contain and its format is given below. It follows closely the format of the original program [6.2].

G.1 BEM data file

1. Title record. (Format 18A4) This title is printed in the heading on output.

2. Basic parameters. (Format 8I5, 3F10.4, 2I5) These parameters are in order: i) the number of boundary elements, ii) the number of internal points where the stress is calculated, iii) the number of different surfaces, iv) to viii) the last node of each different surface, ix) Young's modulus (n.b. not shear modulus as in previous versions), x) Poisson's ratio, xi) the radius of the circular hole, xii) number of Gauss points (for integration: equal to 4 or 8), xiii) ICODE which takes the values ±1 or ±2. |ICODE|=2 for plane strain (default). If ICODE<0 then additional "de-bug" data is printed.

3. Internal point coordinates.(Format 2F10.4) As many records as internal points with the x_1, x_2 coordinates on each record.

4. Coordinates of extreme points of the boundary elements. (Format 2F10.4) Each record defines the coordinates ofthe extreme point of an element, read in the counterclockwise direction for external surfaces and clockwise for internal ones.

5. Boundary condition records. (Format I5, F10.4, I5, F10.4) As many records as boundary nodes giving the values of the known variable in x_1 and x_2 directions. The integer preceding each value, KODE, defines whether the value is a displacement (KODE=0) or a traction (KODE=1). Boundary conditions may be specified in normal and tangential directions rather than x_1,

x_2 directions if required. In this case the first integer = 2 and the second integer = 0 or 1 to specify displacements or tractions respectively.

G.2 The Macro DRAWBEL

As an alternative to inputting the above data file the macro DRAWBEL may be used to generate the boundary grid (ACTION = AUTO, see below). The configuration is input as a series of arcs or straight lines with constant spacing between each node or (for straight lines) a constant ratio of lengths of adjacent elements. The basic parameters and boundary conditions are then input in free format as prompted by the program. The macro may also be used to plot the boundary grid from an existing data file.

Parameter list:

```
DRAWBEL
     (@ literal @ DATA = *STDAD,
      @ literal @ ACTION = @ see below @,
      @ literal @ OUTPUTFILE = @ see below @,
      @ literal @ DEVICE = CALCOMP,
      @ literal @ SCALE = 1.0,
      @ integer @ TIME = 50,
      @ response @ RESPONSE = RESULT)
```

Keyword description

Keyword: DATA

Use: Specifies file from which data is read.

Values taken: Filename. Data is read from existing data file.

Default: Data read from alien data. This should be used if generating new boundary grid.

Keyword: ACTION

Use: Specifies action to be taken. If two actions are to be taken the values below should be concatenated (e.g. ACTION=AUTO_SAVE)

Values taken:

AUTO - A new boundary grid is to be generated. The data is output to the file specified by OUTPUTFILE (see below).

SAVE - The file specified by OUTPUTFILE is to be saved.

DRAW - This action may only be specified if AUTO is not specified. The *OUTPUTFILE* may then contain a "SAVE_DRAWING" pseudo plot file and if ACTION includes "DRAW" this file is plotted.

Default: A DATA file, formatted as specified in section G.1 above, is input and plot data for the boundary grid is output.

Keyword: OUTPUTFILE

Use: Specifies the name of the output file. If ACTION includes "AUTO" the output file will be a boundary element data file. Else the output file is a plotfile.

Values taken: Name.

Default: A new temporary file is created.

Keyword: DEVICE

Use: Specifies the plotting device on which plot is to be produced. Not applicable unless ACTION includes "DRAW".

Values taken:

= CALCOMP (Calcomp pen plotter).

= TEKTRONIX (Tektronix 4010 graphics terminal).

= IMLAC (Imlac graphics terminal).

Default: CALCOMP.

Keyword: SCALE

Use: Specifies required scaling factor for plotter. Not applicable unless ACTION includes "DRAW".

Values taken:

= Positive number up to four characters long including mandatory decimal point. The size of the plot will be scaled by this factor.

= Any negative number. The size of the plot will be adjusted to fit the output device requested.

Default: 1.0 (No scaling is performed).

Keyword: TIME

Use: Gives an estimate of the time required to "draw" plot (in seconds). Not applicable unless ACTION includes "DRAW".

Values taken: Integer between 10 and 600.

Default: 50

Keyword: RESPONSE

Use: Specifies the result code variable.

Values taken: Response variable.

Default: RESULT.

Example

The following job could be entered to plot the boundary grid from a boundary element data file BEMDATA. The plot would be produced on Calcomp pen plotter.

```
JOB(:MERØØ4.BEMPLOT,TIME=50)
DRAWBEL(BEMDATA,ACTION=DRAW)
EJ
****
```

Alternatively if the macro is to be used to generate a boundary grid the following could be entered from the Imlac graphics terminal.

```
-
- DRAWBEL(ACTION=AUTOSAVE)
/ - 0, 2, 0, 2
/ - 4
/ - 2, 0
/ - 2, 6, 0, 0, -90
/ - 1, 4, 0, 1, 0.8
/ - 2, 6, 0, 0, 90
/ - 1, 4, 2, 0, 1.25
/ - 0/
/ - ANNULUS
/ - 2, 1.0, 0.3, 0.0, 0
/ - 1.5, 0.5
/ - 0.5, 1.5
```

```
/ - 2, 0, 1, 0
/ - /
/ - /
/ - /
/ - /
/ - /
/ - 0, 0, 1, 0
/ - /
/ - /
/ - /
/ - 2, 1, 1, 0
/ - /
/ - /
/ - /
/ - /
/ - /
/ - 1, 0, 0, 0
/ - /
/ - /
/ - /
```

The data following the DRAWBEL command specifies the parameters requested by the program (e.g. dimensions, boundary conditions, etc.). The above data produces the boundary grid shown in Figure G1.

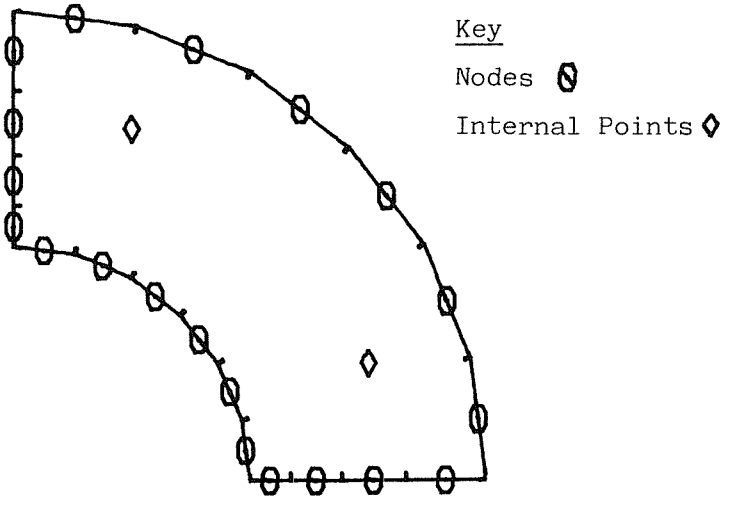

Figure G1 Boundary grid specified using the macro DRAWBEL.

G.3 The Macro BEM

This macro is used to run the modified boundary element method program. The modified (NEW) or standard (OLD) kernel functions may be used and the program may be run immediately or entered into the batch queue.

Parameter list:

```
BEM  (@ literal @ DATA = *STDAD,
      @ literal @ OUTPUT = @ see below @,
      @ literal @ KERNEL = NEW,
      @ literal @ IMMEDIATE = YES,
      @ integer @ TIME = 50,
      @ response @ RESPONSE = RESULT)
```

Keyword description

Keyword: DATA

Use: Specifies file from which data is read.

Values taken: Filename data is read from existing data file.

Default: Alien data.

Keyword: OUTPUT

Use: Specifies the name for the output file if required.

Values taken: Name. If a file of this name exists output is sent to this file. Else file is created. The file is listed after the program has run.

Default: A temporary file is created.

Keyword: KERNEL

Use: Specifies which kernel function is used for the boundary element method.

Values taken:

= NEW. The modified kernel function for a plane containing a circular hole is used.

= OLD. The standard Kelvin kernel function is used.

Default: NEW.

Keyword: IMMEDIATE

Use: Specifies if program is to be run immediately or entered into the batch queue.

Values taken:

= YES. Program is run immediately.

= NO. Job entered into the batch queue to be run later.

Default: YES.

Keyword: TIME

Use: If IMMEDIATE = NO then TIME is an estimate of the time (in seconds) required for the job.

Values taken: Integer between 10 and 2000.

Default: 50.

Keyword: RESPONSE

Use: Specifies the result code variable.

Values taken: Response variable.

Default: RESULT.

Example

The following job could be entered to run the boundary element program with data from the file BEMDATA, using the modified kernel function.

```
JOB(:MERØØ4.BEMRUN,TIME=50)
BEM(DATA=BEMDATA)
EJ
****
```

G.4 The Macro RUNNER

It is sometimes convenient when a number of runs of the boundary element program are required to use the macro RUNNER. In this case the data file is edited before the program is run (see example below).

Parameter list:

```
RUNNER     (@ literal @ FILE = @ mandatory @,
            @ literal @ EDITFILE = *STDAD,
            @ literal @ KERNEL = NEW,
            @ literal @ IMMEDIATE = YES,
            @ integer @ TIME = 50,
            @ response @ RESPONSE = RESULT)
```

Keyword description

Keyword: FILE

Use: Specifies the data file which is edited and then input to the boundary element program.

Values taken: Filename of existing data file.

Default: None. This parameter is mandatory.

Keyword: EDITFILE

Use: Specifies the file from which the edit instructions are read.

Values taken: Filename.

Default: Alien data.

Keywords: KERNEL, IMMEDIATE, TIME, RESPONSE — These keywords have the same meaning as for the macro BEM above.

Example

The following job could be entered to run the boundary element program with the datafile BEMDATA, which has a hole size specified as 5.0, followed by runs with the same data except for the hole sizes which are 3.0 and 1.0.

```
JOB(:MERØØ4.BRUNS,TIME=600)
BEM(BEMDATA)
RUNNER(BEMDATA)
----
T2, T.60,R/5.0/3.0/,E
++++
RUNNER(BEMDATA)
----
T2, T.60,R/5.0/1.0/,E
++++
EJ
****
```